
# *North Atlantic Ocean Circulation and the Onset of Northern Hemisphere Glaciation*

**Peter G. Bloxsom**

*Thesis submitted for the degree of Doctor of Philosophy.*

*September 2013*

DECLARATION 1

This work has not been submitted in substance for any other degree or award at this or any other university or place of learning, nor is being submitted concurrently in candidature for any degree or other award.

Signed …… (candidate) Date ……

STATEMENT 1

This thesis is being submitted in partial fulfillment of the requirements for the degree of ……(insert MCh, MD, MPhil, PhD etc, as appropriate)

Signed …… (candidate) Date ……

STATEMENT 2

This thesis is the result of my own independent work/investigation, except where otherwise stated.

Other sources are acknowledged by explicit references. The views expressed are my own.

Signed …… (candidate) Date ……

STATEMENT 3

I hereby give consent for my thesis, if accepted, to be available for photocopying and for inter-library loan, and for the title and summary to be made available to outside organisations.

Signed …… (candidate) Date ……

STATEMENT 4: PREVIOUSLY APPROVED BAR ON ACCESS

I hereby give consent for my thesis, if accepted, to be available for photocopying and for inter-library loans after expiry of a bar on access previously approved by the Academic Standards & Quality Committee.

Signed …… (candidate) Date ……

# Abstract

Since the early Cenozoic, the Earth's climate has been gradually cooling. Large ice sheets have expanded on several occasions in the past 5000 kyr (50 Ma), with the last major expansion being the onset of major ice sheets in the Northern Hemisphere between 3600 and 2500 ka. This period was characterised by a prolonged increase in ice volume, modulated by orbital forcing. At the same time, major tectonic changes were taking place, with the closure of the Central American Seaway most significant.

This thesis aims to address the issue of what caused the onset of major Northern Hemisphere glaciation through an in depth study of samples from North Atlantic ODP Site 982 (57° 31' N, 15° 51' W; 1145 m water depth). Multi-species benthic foraminifera composite trace metal records (Mg/Ca, B/Ca, Li/Ca, Cd/Ca) were produced, and the composite Mg/Ca record was used to develop a new regional temperature calibration for the Pliocene. Paleoceanographic records of bottom water temperature and saturation state were produced, as well as bottom water flow speed records using the Sortable Silt ($\overline{SS}$) proxy. Bottom water temperature (BWT) records showed an abrupt, ~2°C cooling at 2800-2700 ka, consistent with other previously published records.

These data are combined with previously published benthic stable isotope ($\delta^{18}O_b$) records to reconstruct seawater oxygen isotope reconstructions ($\delta^{18}O_{sw}$) across the period of study, and this is found to predominately reflect changes in global ice volume. A major and prolonged increase in ice volume (3500-3000 ka) is identified, equivalent to up to ~55m sea level decrease. The response of the North Atlantic region to this ice sheet growth was tested using previously published sea surface temperature (SST) and $\delta^{18}O_b$ records from ODP Site 982, in addition to the new $\overline{SS}$ record from this study. The ice volume was found to have influenced the response of SST, $\delta^{18}O_b$, and $\overline{SS}$, to orbital forcing from changing insolation. Prior to the ice sheet growth, bottom water flow speed varied proportionally with sea surface temperatures, with increased deep water formation during periods of high seasonality. The growing ice sheets responded more slowly to insolation changes, and the presence of this ice sheet increased deep

water formation by further cooling saline surface waters. This resulted in feedback loops that intensified deep water flow, leading to a significant increase in North Atlantic Deep water penetration to the southern ocean. A major decrease in $\delta^{18}O_{sw}$ at 2800-2700 ka was interpreted as either a loss of Antarctic ice mass, or a reorganization of North Atlantic water masses.

Comparison of ice volume records with orbital spectra and reconstructions of the closure of the Central American Seaway suggest the immediate cause of Northern Hemisphere glaciation was a period of orbital conditions favourable to ice sheet growth. Another underlying cause was a series of tectonic shifts, including the closure of the Central American Seaway from 4200 ka, which changed heat and moisture transport patterns to the high latitudes.

# Acknowledgements

Firstly, I would like to thank my supervisors Carrie Lear and Ian Hall for their tireless help, direction and encouragement throughout this project. They have been of great assistance to me during this project, and have improved my understanding of my work immensely.

Secondly, I would like to thank my colleagues in the Palaeoceanography office at Cardiff University, for being always motivational, funny, and encouraging at the right times. Particular thanks are due to the members of the quiz team 'Universally Challenged', for proving a much needed change of pace and direction on a Monday night at the pub quiz.

Thank you to Ana Morte Rodenas for tireless assistance with trace metal cleaning and analysis, in particular for coming back into work on a Friday night when the Mass Spectrometer broke down. Thank you to Helen Medley for assistance with washing samples and Sortable Silt analysis, and Sindia Sosdian for valuable discussions and encouragement. Thanks are due to both my parents and also to Elaine Mawbey and David Wallace, for providing food and shelter during the final weeks of work.

Finally, I would like to thank Kirstie Fagan, for her infinite support and encouragement – I couldn't have done this without you.

# Table of Contents

# 1 Introduction

The general climatic trend throughout the Cenozoic has been towards cooler global temperatures and increasing ice sheet volume (Zachos et al. 2001; Miller et al. 2005; Shackleton & Kennett 1975), along with an increased meridional temperature gradient. This trend began in the early Eocene, when temperatures were high enough to support large scale forests at high latitudes (78° N) (Francis 1988). Since then, major episodes of ice sheet growth occurred in the earliest Oligocene, early Miocene, middle Miocene and Plio-Pleistocene (Lear et al. 2000). The current paradigm is that the three earlier events were centred around the development of major ice sheets on Antarctica (Miller et al. 2005; Zachos et al. 2001; Zachos et al. 2008), whereas the Plio-Pleistocene glaciation resulted in the expansion of Northern Hemisphere Ice sheets after 2.7 Ma.

The long term cooling over the Cenozoic is thought to be the response to a combination of factors including the opening and closing of tectonic gateways, changing continental configuration including mountain building events, and levels of atmospheric greenhouse gases superimposed on orbital variability (Haug & Tiedemann 1998; DeConto et al. 2008; Foster et al. 2010; Raymo & Ruddiman 1992; Zhisheng et al. 2001). Declining atmospheric $pCO_2$ is a key feature of the Cenozoic, with Eocene $pCO_2$ levels as high as 1000-1500ppm, over three times preindustrial levels (Pagani et al. 2005). Rhythmic changes in orbital parameters such as the eccentricity and tilt of the Earth's orbit, combined with internal climate system feedbacks such as changing albedo can act as amplifiers of tectonic changes in the Earth's major boundary conditions.

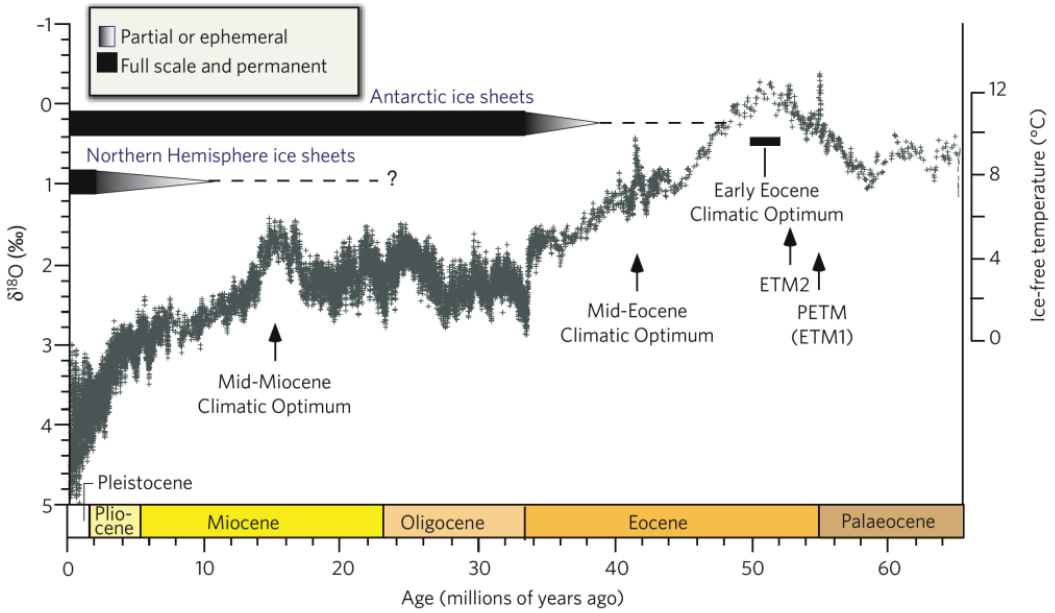


*Figure 1-1 Global oxygen isotope stack from Zachos et al (2008). Major periods of ice sheet are shown by black bars. The figure clearly shows the long term cooling trend from the Early Eocene Climatic Optimum to the modern.*

This study covers the period 5200-1900 ka, during which time the global climate shifted from a warmer Pliocene world to a colder Pleistocene world with significant glacial/interglacial cycles. This study will investigate the nature of this transition, and evaluate potential causes.

## 1.1 Chronology of the late Neogene and Quaternary

The period covered by this study (5100-1900 ka) comprises the majority of the Plicoene and the first 600 kyr of the Pleistocene. Recent revisions of the boundary between the Pliocene and Pleistocene have moved the Gelasian age (2588-1806 ka) from the Pleistocene to the Pliocene, shifting the boundary between the two backwards by ~800 kyr (Gibbard et al. 2010). This was done to better reflect the major climatic transitions which occurred around 2588 ka. At the same time, the Quaternary Period was defined as encompassing the entire post-Pliocene period, with the Pleistocene and Holocene subsidiary to it. These revisions divide the climatic evolution into clear pre- and post-glacial worlds at the Period and Epoch levels.

This study will use the most recent timescale, and any data referred to from prior to this revision will be updated to reflect this.

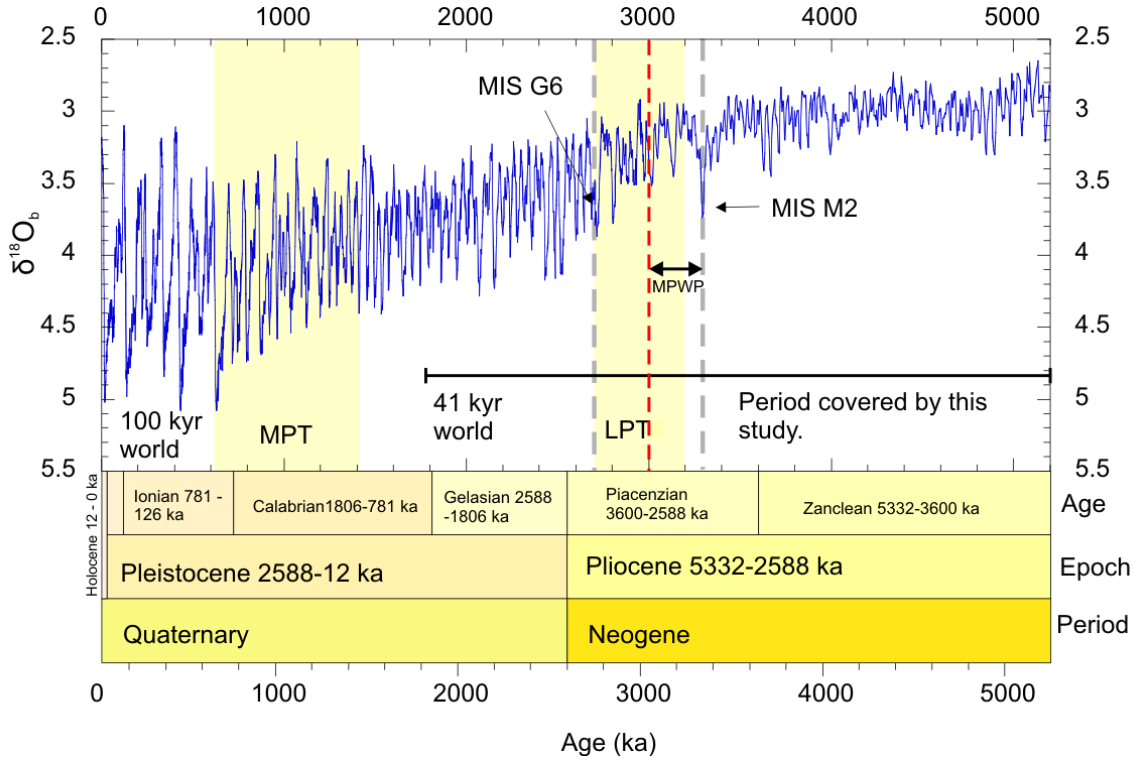


*Figure 1-2 Cooling climate 5200 ka to present. Global benthic δ18O stack ( Lisiecki & Raymo 2005) with major climatic transitions annotated. MPT: Mid Pleistocene Transition LPT: Late Pliocene Transition. MIS M2, (~3300 ka) marks the first major input of Ice Rafted Debris (IRD) into the North Atlantic, but persistent IRD does not occur until MIS G6, ~2700 ka. Red dashed line represents the end of the Mid Pliocene Warm Period.*

## 1.2 Climate of the Plio-Pleistocene

The Pliocene is generally considered to be a period of greater warmth than today, particularly at higher latitudes, where average temperatures were up to 8-12 °C warmer than present (Brigham-Grette et al. 2013). Glacial sediments in the Transantarctic Mountains show evidence for wet-based marine glaciation (Webb & Harwood 1996) and even tundra-like environments on the margin of the East Antarctic ice sheet (Francis et al. 2007). In the northern hemisphere, evergreen taiga forest reached as far north as 82°, approximately 10° further north than the modern extent (Salzmann et al. 2008). Global average temperatures were as much as 3.5 °C warmer

than present (Raymo et al. 1996), however in the western equatorial Pacific, sea surface temperatures were not dissimilar to the modern (Wara et al. 2005).

The Pliocene has been long put forward as an analogue for a world affected by global warming. Reduced continental ice volumes, significantly higher high latitude temperatures combined with good sample availability and age control have made it a tempting period for detailed study into the dynamics of a warmer world. The Pliocene Research Interpretation and Synoptic Mapping (PRISM) project defined a period known as the Mid-Pliocene Warm Period (3300-3000 ka) for the purposes of providing detailed boundary conditions for a series of climatic models designed to simulate the Pliocene as an analogue for a warmer, post-industrial world (Dowsett et al. 2009). This 'MPWP' was defined as the last period of low oxygen isotopic values prior to the expansion of Northern Hemisphere ice sheets at approximately 3000-2500 ka. The global extent of the PRISM dataset allows regional differences in temperature to be compared to the modern ocean. Pliocene low latitude sea surface temperatures were not dissimilar to modern values, however high latitude North Atlantic sea surface temperatures are thought to be as much as 8°C warmer than modern (Dowsett et al. 2009).

The modern equatorial Pacific is characterised by a distinct SST gradient with the equatorial waters of the western Pacific being approximately 6 °C warmer than waters at the same latitude in the east Pacific (Cane 1998). The exception to this is during the El Nino climate system, which decreases longitudinal temperature gradients on a period of several years. In non El Nino years, the gradient is driven by easterly trade winds driving warmer water to pool in the west, and causes a shoaling of the thermocline in the east Pacific region. However, the Pliocene (4000-3000 ka) was characterised by a much reduced temperature gradient of approximately 1.5 °C, which has been interpreted as a 'permanent El Nino' state (Wara et al. 2005). Positive feedbacks associated with the maintenance of this gradient against the prevailing winds include increased incidence/intensity of tropical storms (Fedorov et al. 2010).

Deep ocean temperature reconstructions are limited, but Ostracod derived Mg/Ca bottom water temperature (BWT) estimates from the mid Pliocene Atlantic suggest temperatures similar to today (Dwyer & M. A. Chandler 2009). Longer term BWT reconstructions also exist across the period 3300-2500 ka, and show general cooling trends (Sosdian & Rosenthal 2009; Bartoli, Sarnthein & Weinelt 2005).

Major ice rafted debris first appears in the North Atlantic 2720 ka (Bailey et al. 2013; Flesche Kleiven et al. 2002), closely linked to the increase in amplitude of benthic $\delta^{18}O$ isotope values to a maximum (prior to the Late Pleistocene transition) at 2500 ka (Shackleton et al. 1984). This is has been interpreted as increasingly large changes in ice volume controlled by the obliquity period of the Earth's orbit (41 ky period) (Tiedemann et al. 1994). Over the same time period, cooling of surface and bottom water temperatures in the North Atlantic (Sosdian & Rosenthal 2009; Lawrence et al. 2009), a decline in the strength of NADW (Raymo et al. 1990) and an increase in stratification in the North Pacific all point to a change in the global climate around 2700 ka. This has commonly been termed the onset of Northern Hemisphere Glaciation.

However, IRD was present in the North Atlantic from as far back as 3300 ka, and in the Norwegian sea from 3600 ka (Flesche Kleiven et al. 2002). Similarly, SSTs from the North Atlantic decreased in a stepwise fashion from 3500 ka (Lawrence et al. 2009), with major cooling steps at 3300 and 2700 ka. Glacial deposits from the Hudson Bay region in modern north America are dated to approximately 3500 ka (Menzies et al. 2013; Gao et al. 2012) Statistical analysis of globally distributed $\delta^{18}O_b$ records shows a significant increase in ice volume from 3600 ka (Mudelsee & Raymo 2005), also suggesting an early start to the Northern Hemisphere glaciation. The apparent paradox between clear evidence for warm climates in the high northern latitudes at the same time as significant ice sheet growth remains a pressing question in Neogene palaeoclimatology, and one this study aims to investigate.

## 1.3 Insights into Pliocene paleoclimate from a modelling perspective

Computer modelling of the Pliocene has tended to focus around two major targets – testing the influence of changing tectonic gateways on the circulation system (Nisancioglu et al. 2003; Maier-Reimer et al. 1990), and testing climate models against palaeo-data from the mid Pliocene (Haywood et al. 2000). Model-data comparisons reveal significant failings in the models' ability to transport heat effectively to the Northern Hemisphere high latitudes (Dowsett et al. 2011), with models showing a cool patch in the middle of what is, according to SST proxies, a consistently warm section of the North Atlantic. However, recent improvements to the boundary conditions of the models have improved this somewhat by changing the orography of the Rocky Mountains (Hill et al. 2011).

Modelled changes in the Central American Seaway (CAS) highlight the importance of the closure in the high latitude formation of deep water masses and the strength of thermohaline overturning (Schneider & Schmittner 2006; Heydt & Dijkstra 2008), a hypothesis first proposed by Keigwin (1982). However the impact of the CAS closure on the initiation of northern hemisphere glaciation is somewhat less clear. Lunt et al. (2008) use a high resolution ice sheet model to suggest that despite the increased overturning and moisture transport to the high latitudes, the major control on ice sheet formation in the northern hemisphere was declining $pCO_2$. Reconstructions of Pliocene $pCO_2$ do not show major changes in atmospheric carbon dioxide at the time of ice sheet growth, so the contribution of declining $pCO_2$ is still uncertain (Seki, Gavin L. Foster, et al. 2010; Pagani et al. 2009; Pearson & Palmer 2000).

## 1.4 Closure of the Central American Seaway

Today, the region that used to be called the Central American Seaway (CAS) is now occupied by southern Central America (Coates et al. 2004). The final closure of this seaway took place at the far south of the Isthmus, close to modern South America. The Isthmus of Panama forms a land bridge between North and South America, and the Panama Isthmus blocks the flow of Pacific surface waters into the Atlantic. However in the Miocene, an island arc spanned the gap between the South American and Central

American continents (Coates et al. 1992), allowing the exchange of water. Continued uplift of this mountain belt took place throughout the Miocene and early Pliocene, and the final sedimentary evidence for a connection between the Caribbean and the Pacific appears in what is now northern Columbia at approximately 4800 ka (Duque-Caro 1990). This is the earliest date at which the closure could be considered complete, as the sedimentary record is limited. Oceanographic records show the impact of CAS closure 600 kyr later.

From 4200 ka onwards, sea surface salinity gradients between the East Pacific and Caribbean began to develop, an indication of restricted water mass exchange on the surface (M Sarnthein et al. 2009; Groeneveld 2005), and represents a shoaling of the CAS to <100m (Haug et al. 2001). The increasing salinity of the Caribbean surface water was due to intense evaporation and westward transport of water vapour from the Caribbean into the Pacific (Broecker & Denton 1989). The modern $\delta^{18}O_{sw}$ gradient of 0.5 ‰ was established by 3600 ka, 1000 kyr prior to major terrestrial faunal exchange at 2700 ka (Marshall et al. 1982).

The Central American Seaway was likely closed to deep ocean circulation from at least 8000 ka (Frank et al. 1999), forcing proto-North Atlantic Deep Water to enter the Southern Atlantic, instead of entering the deep Pacific through the CAS (Wright & Miller 1996). CAS closure has also been hypothesised to impact surface water circulation by increasing the salinity of the Caribbean water mass, and hence the salinity of the North Atlantic Current (Haug et al. 2001), and intensity of deep water formation in the North Atlantic.

## 1.5 Ocean circulation and climate in the modern, glacial and Neogene world.

The global ocean circulation system transports heat and moisture from the low latitudes to the high latitudes (Broecker & Denton 1989), and plays an important role in the transfer of carbon between the atmosphere and oceans on glacial-interglacial timescales during the late Pleistocene (Oppo et al. 1990). In the modern ocean, the

ocean circulation system is driven by deep water formation in the North Atlantic Ocean and the Southern Ocean around Antarctica. The cooling and sinking of surface water at high latitudes in the North Atlantic and Norwegian Seas draws relatively warm and saline water northward (Raymo 1994). The cooling of this warm surface water releases heat to the North Atlantic region equivalent to 25% of incoming solar radiation (Broecker & Denton 1989), significantly warming the region compared to other regions at the same latitude.

During glacial periods in the Pleistocene, the formation of North Atlantic Deep Water (NADW) was greatly decreased (Boyle & Keigwin 1982), and increased stratification of the oceans contributed to drawdown of atmospheric $CO_2$ by limiting the interaction between upwelling water masses and the atmosphere (Sigman et al. 2004, Boyle & Keigwin 1985). The decrease in production and shoaling of NADW allowed bottom water masses from the Southern Ocean to fill much of the North Atlantic basin (Venz et al. 2000a). Increased extent of ice sheets during glaciations also resulted in an increased amount of ice rafted debris (IRD) input to the Atlantic oceans during these colder periods (Jansen et al. 2000; Ruddiman 1977). Entry into and exit from the Pleistocene glaciations is governed by a complex interaction of feedbacks involving ocean circulation, atmospheric $pCO_2$, ice sheet size, and changes in insolation due to orbital periodicities (Ridgwell et al. 1999; Raymo 1997).

Ocean circulation has not always followed the North-South deep water flow pattern that exists in the modern Atlantic Ocean. Prior to 15 Ma, deep water formation was concentrated around the Southern Ocean, and the deep waters in the North Pacific and Atlantic were the oldest (the most depleted $\delta^{13}C$ signal, see section 1.4) water masses (Woodruff & Savin 1989). Increasing amounts of NADW were formed after 9 Ma, with $\delta^{13}C$ gradients between Atlantic and Pacific sites suggesting a modern style circulation regime with deep water formation in the North Atlantic present since at least the Middle Miocene, and potentially as long ago as the Eocene-Oligocene (Hodell & Venz-Curtis 2006; Davies et al. 2001). During the Pliocene, decreased North-South Atlantic $\delta^{13}C$ gradients suggest greater penetration of NADW into the South Atlantic than much of the Pleistocene, and hence a stronger conveyor.

How the ocean circulation – climate system responded to the climatic changes across the initiation of Northern Hemisphere Glaciation (3600-2500 ka) is not yet fully understood, and this study aims to improve that understanding via reconstruction of water mass parameters (temperature, carbonate saturation state, bottom water flow speed) for a key site in the Northern Hemisphere.

## 1.6 The use of trace metals, stable isotopes, and physical proxies to reconstruct past climate and circulation

### 1.6.1 Stable isotopes

$\delta^{18}O$

Since the discovery that the oxygen isotope ratio in marine carbonates through the Pleistocene primarily reflected changes in the oxygen isotope composition of seawater, driven by changes in global ice volume (Shackleton, 1967), stable isotopes of marine carbonate have been a staple of the paleoclimatologists toolbox (Pearson 2012). $\delta^{18}O$ is defined as the ratio of the two most common stable isotopes ($O^{16}$ and $O^{18}$) to an internationally agreed standard (Equation 1-1).

$$\delta^{18}O\ sample\ ‰ = 1000 \times \frac{\left[\frac{^{18}O}{^{16}O} sample - \frac{^{18}O}{^{16}O} standard\right]}{\frac{^{18}O}{^{16}O} standard} \quad \text{(Equation 1-1)}$$

While $\delta^{18}O$ ratios in foraminifera are not controlled solely by ice volume but rather a combination of temperature and the isotopic composition of seawater ($\delta^{18}O_{sw}$) from which they were formed, the use of independent water temperature proxies such as foraminiferal Mg/Ca ratios allows the deconvolution of temperature and isotopic signals.

Foraminiferal $\delta^{18}O$ measurements are made with reference to the Vienna Pee Dee Bee standard, based on a calcite standard ratio, whereas $\delta^{18}O$ values of seawater are made with reference to the Vienna Standard Mean Ocean Water, defining the isotopic composition of fresh water. To convert between the two standards, a standard correction is applied: VPDB = VSMOW – 0.27‰

$\delta^{13}C$

$\delta^{13}C$ of foraminifera is commonly used as a water mass tracer (Shackleton 1987), with bottom water mass $\delta^{13}C$ values determined by the initial $\delta^{13}C$ of the water mass when it was formed at the surface, combined with the input of dissolved inorganic carbon from export of isotopically light organic material to the deep ocean, along with mixing between water masses with different $\delta^{13}C$ values. Similarly to $\delta^{18}O$, $\delta^{13}C$ is defined in relation to the VPDB calcite standard. (Equation 2)

$$\delta^{13}C\ sample\ ‰ = 1000 \times \frac{\left[\frac{^{13}C}{^{12}C} sample - \frac{^{13}C}{^{12}C} standard\right]}{\frac{^{13}C}{^{12}C} standard} \qquad \text{(Equation 2)}$$

The whole ocean $\delta^{13}C$ value is controlled by shifts in carbon between different resevoirs. On the tectonic scale, this can include the wholesale burial and subsequent erosion of carbonate or organic carbon (Raymo & Ruddiman 1992). On shorter scales, exchanges in storage of carbon in the atmosphere and ocean, as well as within interacting water masses are responsible for local shifts in $\delta^{13}C$ (eg. Raymo et al. 1990). Biological processes can also affect $\delta^{13}C$ (Mackensen et al. 1993), which can result in anomalously low $\delta^{13}C$ values as a result of increased organic carbon export to the sediment.

### 1.6.2 Trace metals

Cd/Ca

In a similar fashion to $\delta^{13}C$, foraminiferal Cd/Ca are also used as water mass tracers (Boyle 1986). Cd behaves similarly to phosphate, a key nutrient, and therefore is found in elevated concentrations in regions with high nutrient levels. This causes it to be concentrated in water masses that have not been exposed to high organic productivity, such as old deep-water masses like the Antarctic Bottom Water. There is evidence that Cd/Ca in planktonic foraminifera is correlated with temperature, not nutrient concentration (Rickaby & Elderfield 1999), however benthic Cd/Ca is in good agreement with $\delta^{13}C$ for water mass reconstructions (Marchitto & Broecker 2006).

Mg/Ca

Perhaps the most significant trace metal proxy for palaeoceanographic purposes is the Mg/Ca ratio of organically precipitated carbonate. The increasing proportion of Mg included in the calcite lattice with increasing temperature has been used in planktonic foraminifera for some time (Lea et al. 1999, Mashiotta et al. 1999, Delaney, 1985), but has been increasingly applied to benthic foraminifera as well, (Lear et al. 2000; Billups & Schrag 2003; Martin & Lea 2002). While core-top studies demonstrate that temperature is the dominant influence on benthic foraminiferal Mg/Ca (Lear et al. 2002), carbonate saturation state ($\Delta[CO_3^{2-}]$)also exerts a secondary control (Elderfield et al. 2006; Yu & Elderfield 2008; Martin et al. 2002; Lear & Rosenthal 2004). Multiple temperature calibrations exist for benthic foraminiferal Mg/Ca, with differing sensitivities to temperature.

Carbonate saturation state ($\Delta[CO_3^{2-}]$) is the difference between the *in situ* carbonate ion concentration - $[CO_3^{2-}]$ - and $[CO_3^{2-}]$ required for seawater to be at saturated with dissolved carbonate. The carbonate saturation point -$[CO_3^{2-}]_{SAT}$ - is controlled by pressure, and hence water depth in the oceans. There is evidence for a threshold on the $[CO_3^{2-}]$ effect on Mg/Ca, above which the influence of $\Delta[CO_3^{2-}]$ is minimal (Elderfield et al. 2006), and so at intermediate depth sites like ODP Site 982, this should be less of an issue compared to deeper sites.

B/Ca

Benthic foraminiferal B/Ca appears to be linearly related to the degree of carbonate saturation state, thus providing a method of evaluating the saturation state effect on Mg/Ca (J. Yu et al. 2008). The relationship between B/Ca and $\Delta[CO_3^{2-}]$ has been used in down core records of the Holocene and Pleistocene and LGM (J. M. Yu et al. 2008; Raitzsch et al. 2011), and is known to vary between species (Jimin Yu & Elderfield 2007).

Another approach to deal with the secondary carbonate saturation state effect on downcore benthic foraminiferal Mg/Ca records is to assume a zero or constant relative contribution of $\Delta[CO_3^{2-}]$ to the record. For example, Sosdian and Rosenthal (2009) determined an apparent temperature sensitivity by comparing the core-top to Last

Glacial Maximum (LGM) offset in benthic foraminiferal Mg/Ca from a North Atlantic Site with estimates of temperature change derived from benthic foraminiferal $\delta^{18}O$ assuming a 0.8‰ change in $\delta_{\omega}$. This sensitivity was then applied to their 3150-0 ka record, assuming constant relative contributions of temperature and $\Delta[CO_3^{2-}]$ to the Mg/Ca record. There are several uncertainties regarding choice of temperature calibration, which will be evaluated in Chapter 3.

### 1.6.3 Sortable silt bottom water flow speed proxy

The sortable silt mean grain size (hereafter $\overline{SS}$) – the mean grain size of the 10-63μm of terrigeneous sediment – has been used as a proxy for the strength of near-bottom currents. Coarser values represent higher flow speed, and vice versa. Although it is presently uncalibrated to absolute velocity, $\overline{SS}$ has been used in conjunction with chemical measures of the strength of circulation (such as $\delta^{13}C$) and has given consistent results (Hall et al. 1998; Hodell et al. 2009). In this study, it will be used to compare the strength of near bottom currents to global changes in climate as well as other palaeohydrographic proxies.

## 1.7 Research aims

The primary aims of this thesis are to investigate the timing and nature of the climatic cooling across the Plio-Pleistocene and determine whether possible oceanographic and tectonic changes at the time are linked to the cooling as a cause or a response. In achieving these aims, sediment samples from the key North Atlantic Site 982 were analysed to fulfil the following key objectives:

1. Use Mg/Ca analysis of benthic and planktonic foraminifera to reconstruct sea surface and bottom water temperatures at North Atlantic ODP Site 982 across the period 5200-1900 ka and compare these to other Mg/Ca records for the period with the intent of determining regional and global trends.
2. To use Mg/Ca derived bottom water temperatures in common with benthic $\delta^{18}O$ records to reconstruct changes in the isotopic composition of seawater and to determiner regional and global trends. If it is possible, link

$\delta^{18}O_{sw}$ records to global ice volume and investigate changes in global ice volume across the initiation of Northern Hemisphere Glaciation.

3. To use the Sortable Silt bottom water flow speed proxy to reconstruct relative changes in the strength of the bottom water currents at ODP Site 982 across the initiation of Northern Hemisphere Glaciation, and to investigate possible relationships to changes in Atlantic deep ocean circulation and the climatic changes of the North Atlantic region during the study period.
4. Integrate the conclusions from this study with previously published information on global climatic evolution during the Plio-Pleistocene to try and determine the primary cause of the trend towards global cooling and ice growth during the Plio-pleistocene.

## 1.8 Thesis Layout

The methods and calibration aspects of this research are presented in Chapters 2-4, while the main scientific results are described in Chapters 4-7. The chapters are as follows:

**Chapter 1**: Introduces the palaeoceanography and climate of the Pliocene

**Chapter 2**: Details the methodology used to analyse benthic and planktonic foraminifera, collect trace metal records and collect physical records.

**Chapter 3:** Presents initial trace metal records and discusses their combination into higher resolution stacked records. Presents records of physical processes, i.e. $\overline{SS}$, coarse fraction weight percent, and ice rafted debris abundance.

**Chapter 4**: Sets out a novel approach to determining a regional benthic foraminiferal Mg/Ca-temperature calibration for the Pliocene, and compares trends in BWT at Site 982 to other regional BWT records as well as Sea Surface Temperatures.

**Chapter 5:** Uses BWT and previously published $\delta^{18}O_b$ records to determine the evolution of $\delta^{18}O_{sw}$ at Site 982, and interprets this in the context of changing global ice volume. Potential locations for continental ice are also assessed.

**Chapter 6:** Assesses the relationship between orbitally controlled insolation, ice volume and intensity of bottom water circulation in the North Atlantic region. Changes in ice volume are put into the context of changing boundary conditions of the Pliocene world (orbital, tectonic, $pCO_2$).

**Chapter 7:** Summarises and integrates the main findings of this study. Potential further work suggested by this study is discussed.

**Chapter 8:** Appendices

# 2 Material and Methods

## 2 Study site and samples

### 2.1.1 Site location and oceanographic setting

Ocean Drilling Program (ODP) Site 982 is located in the north-eastern Atlantic (57° 31' N, 15° 51' W; 1134 m water depth) on the Rockall Plateau (Figure 2.1). The plateau rises 1500m above the surrounding basins to a depth of around 1000m below modern sea level and is interpreted as a continental fragment or micro-continent isolated during the sea floor spreading evolution of the North Atlantic Ocean (Roberts, 1975). ODP Site 982 is sited in a depression between two topographic highs – the Hatton Bank to the northwest and the Rockall Bank to the southeast. The Rockall Bank rises above the modern sea level at a single point, Rockall Island. It is likely that during periods of lower sea level, larger areas of the plateau were subaerially exposed.

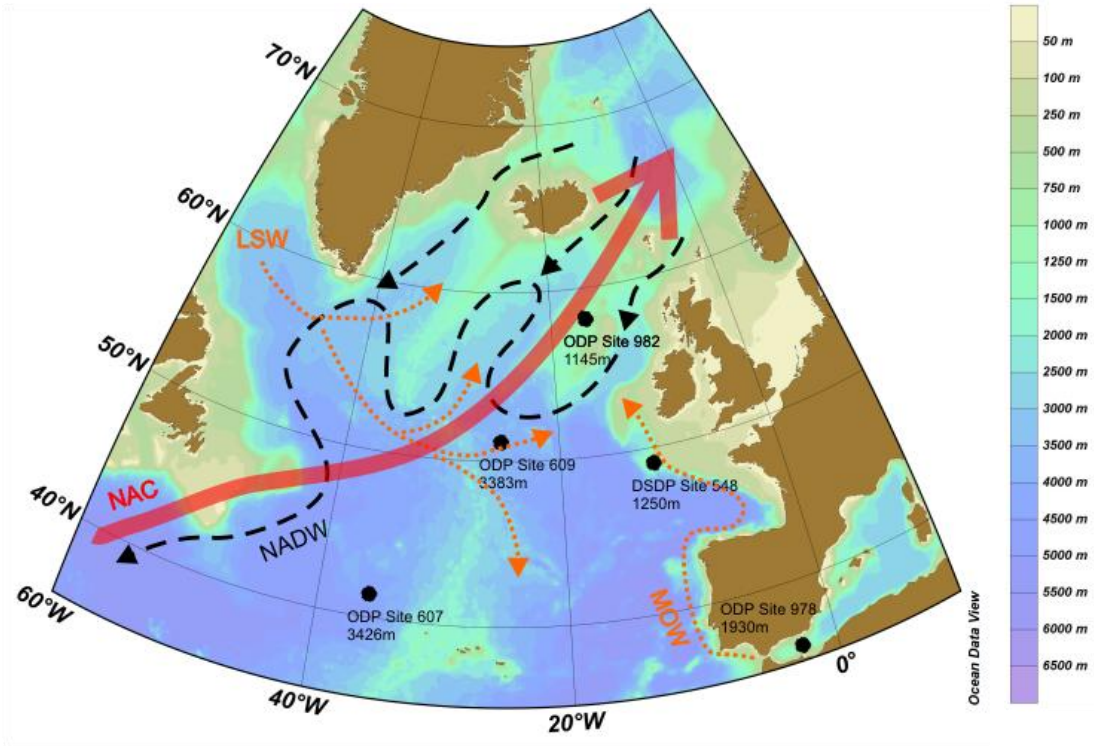


*Figure 2-1. Bathymetric map of the North Atlantic showing the major surface, intermediate and deep water currents. Surface water currents are shown in red (NAC – North Atlantic Current), intermediate water currents are shown in orange (LSW – Labrador Sea Water and MOW – Mediterranean Ocean Water), and deep currents in black (NADW – North Atlantic Deep Water). Certain sites used in this study are shown. Circulation scheme modified after Bartoli, M Sarnthein & Weinelt (2005).*

The site was drilled during ODP Leg 162 with the aim to investigate the Neogene evolution of thermohaline circulation in the North Atlantic. In the modern ocean, ODP Site 982 lies under the North Atlantic Current, the higher latitude surface extension of the Gulf Stream, that transports warm saline water from the low latitudes to the north-eastern Atlantic (Schmitz and McCartney 1993 Diester-Haass et al. 2009). The site is situated close to the modern source region of North Atlantic Deep Water (NADW) (Kroopnick, 1985), and the intermediate water mass influencing the site today is primarily a mixture of Labrador Sea Water (LSW) mixed with Mediterranean Outflow Water (MOW), with a small contribution of Antarctic Intermediate Water (AAIW) (Kawase and Sanniento, 1986) This intermediate water mass is known as the Upper North Atlantic Deep Water (UNADW). The admixture of some overflow water from the Nordic Seas also contributes to the water mass at ODP Site 982. The main Lower North Atlantic Deep Water (LNADW) flow comprising overflow water from the Nordic Seas and admixed Atlantic water passes around the Rockall plateau at a greater depth than ODP Site 982, and is responsible for significant drift formation at nearby deeper sites such as ODP Site 980.

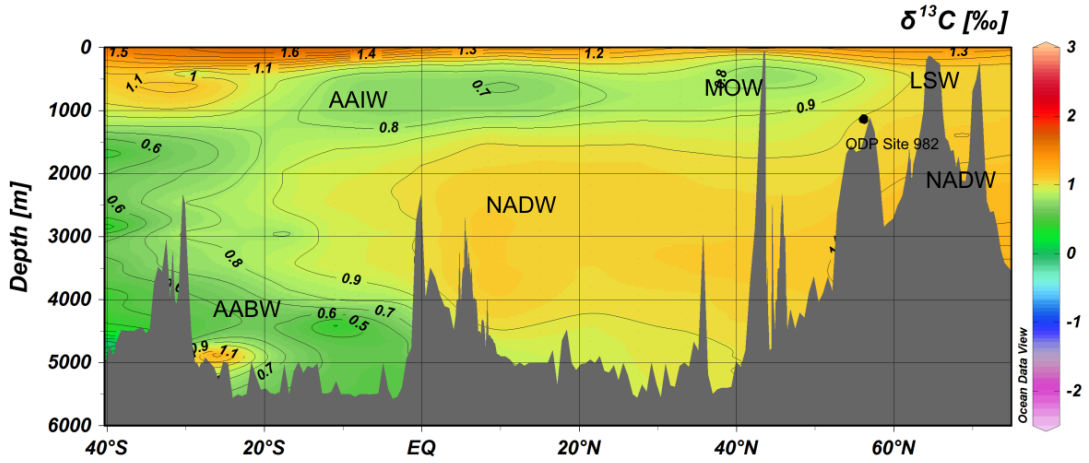


*Figure 2-2. Modern meridional section of seawater $\delta^{13}C$ showing the major deep water masses in the Atlantic Ocean (Schlitzer 2013). NADW is sandwiched between AABW (Antarctic Bottom Water) and AAIW (Antarctic Intermediate Water) in the South Atlantic. ODP Site 982 is situated on the upper limb of the NADW water mass, between the MOW (Mediterranean Outflow Water) and LSW (Labrador Sea Water).*

### 2.1.2 Sedimentological setting and sampling of ODP Site 982

Over 600m of sediment was recovered from ODP Hole 982B, spanning the early Miocene through to the Holocene. The lithology is dominated by carbonate sedimentation, primarily nannofossil ooze, with variable amounts of clay and silt. The sediment recovered was divided into two units by the shipboard party, each with subunits based upon physical properties including colour, natural gamma ray measurements, and magnetic susceptibility measurements. Unit 1 extends from the surface to around 57 metres below sea floor (mbsf) and is comprised of highly variable amounts of calcareous nannofossils, clay, silt and foraminifera. Unit 1 is subdivided into two subunits based on the relative proportions of terrigeneous and biogenic material. Subunit 1A is the most compositionally variable, with cyclic alteration between siliciclastic-rich and biogenic-rich sediment. Subunit 1B is dominated by nannofossil ooze with foraminifera, with only small amounts of siliciclastic material. Unit 2 is much more homogenous, with consistently high percentages of biogenic carbonates. The mean carbonate content of Unit 1 is 57.7%, with a standard deviation of 29.8%, whereas the mean and standard deviation of Unit 2 are 90% and 3.7% respectively. Dropstones or Ice Rafted Debis (IRD) are only present in Unit 1 (Flesche Kleiven et al. 2002). Samples were taken for this study across both lithological units.

Samples were selected from ODP Site 982 Hole B between 39 and 135.3 mbsf (43.08 and 149.3 metres composite depth (mcd)). Samples were initially taken every 40 cm; however this was subsequently increased to every 20 cm in the upper half of the record (above 86.2 mcd) to improve resolution. Where possible, 40 $cm^3$ of material were taken from the working half of the core with a 2 cm sampling interval. In some cases due to a heavily sampled core section, this interval was extended to a maximum of 4 cm. 40 $cm^3$ were required to provide sufficient non-biogenic material for 'Sortable Silt' mean grain size analysis (Section 2.4) and sufficient numbers of benthic foraminifera for trace metal analysis (Section 2.7). This sampling includes the majority of the Pliocene and the early Pleistocene, from 1912.94 – 5081.01 ka.

## 2.2 Age model

Initial age models for this site were developed by Channel and Lehmann (1999) using magneto- and biostratigraphy, and were subsequently adjusted by Venz et al. (1999) and Venz & Hodell (2002) using stable oxygen isotope ($\delta^{18}O$) stratigraphy. This formed the basis of the record that was incorporated into the global benthic $\delta^{18}O$ LR04 stack (L. E. Lisiecki & Raymo 2005). The 3200 and 2700 ka portion of the LR04 derived age model (hereafter LR04-982) was subsequently challenged by Khélifi et al. (2012) who used revised magnetostratigraphic datums and an alternative interpretation of the $\delta^{18}O$ stratigraphy to propose a 130 kyr hiatus between 3190 and 3106 ka (approximately 68-70 mcd) at ODP Site 982. In addition, Khélifi et al. (2012) altered the timing of three benthic $\delta^{18}O$ stages that were previously attributed to Marine isotope Stages (MIS) K2, G4, and G2 to MIS G20, G2, and 104.

The resulting Khélifi et al (2012) age model has recently been criticised for introducing a hiatus for which there is no sedimentary evidence (such as an abrupt change in sediment composition or colour), and for requiring extremely variable sedimentation rates in comparison to the Venz et al. (2000) standard age model (Lawrence et al. 2013). In addition, the Khélifi et al. (2012) age model requires IRD deposition at Site 982 to begin at a different MIS stage to other nearby sites such as DSDP Sites 610 (Flesche Kleiven et al. 2002) and 611 (Bailey et al. 2010), and ODP Site 984 (Bartoli, Sarnthein & Weinelt 2005). The LR04-982 age model shows a significant increase in IRD deposition occurred at MIS G6, in concert with nearby sites; however the Khélifi et al. (2012) age model requires IRD deposition to increase at MIS G2, ~80kyr later. Given these significant problems with the Khélifi age model, the LR04-982 age model will be used in this study in common with previous work.

## 2.3 Bulk sediment processing

Samples had a small (1 $cm^3$) section archived, and were then weighed and put into 60 ml glass jars with 15 mΩ deionised (DI) water. These jars were placed on a spinner for several days to disaggregate the sediment before the samples were washed over a 63µm sieve using pressurised 15mΩ DI water. Sieving continued until the runoff from

the retained coarse fraction was clear, indicating no fine (<63 μm) material present. The coarse (>63 μm) and fine fractions were placed in a 40°C oven to dry. Their respective dry masses were used to calculate the percentage by weight of the coarse fraction (cfwt%) using the following equation.

$$cfwt\% = \frac{coarse\ fraction\ weight}{(coarse\ fraction\ weight + fine\ fraction\ weight)} \times 100$$

This assumes that the entire fine fraction was completely washed through the sieve, which is not necessarily true – some sediment may be retained within foraminifera. However, fine sediment retained in the washed coarse fraction would be a very small proportion, and can reasonably be ignored.

## 2.4 Sortable Silt Mean Grain Size

The sortable silt mean grain size (hereafter $\overline{SS}$) - the mean grain size of the 10-63 μm fraction of terrigenous material – is a proxy for the vigour of near bottom currents, with coarser values recording faster flow speeds and vice versa (e.g. Hall et al. (1998) and Praetorius et al. (2008). The proxy can be used where a broad range of grain sizes characterizes the source sediment and the distance to the depositional (sediment core) site is sufficient for a sorted signal to develop (McCave et al. 1995; Bianchi 2001; McCave & Hall 2006). The $\overline{SS}$ proxy indicates relative current speed but is presently uncalibrated in terms of velocity. Some idea of actual current speed can be gained by comparison with critical erosion and deposition curves (McCave et al. 1995). The $\overline{SS}$ proxy has given results consistent with other palaeohydrographic proxies in a number of studies (Hall et al. 1998; Hodell et al. 2009).

### 2.4.1 Removal of biogenic material

The biogenic material (carbonate and biogenic silica) was removed from the fine fraction in two stages. Carbonate was removed by the addition of excess 2M acetic acid ($CH_3COOH$) to the dry sediment following the method of Bianchi (2001). Following the initial vigorous reaction between the carbonate and the acid, the sediment was stirred to ensure all carbonate had reacted. The sample was then left to settle (>24

hours) and the acetic acid siphoned off, and the sediment rinsed with DI water several times. Approximately 2000 mL of acetic acid was added to ensure complete removal of carbonate.

Biogenic silica was removed using a modified leaching method from Mortlock & Froelich (1989) using the addition of 0.002M sodium carbonate ($Na_2CO_3$) to the remaining sediment. The mixture was placed in an 85°C water bath for 5 hours and stirred vigorously every 2 hours to ensure that any reaction between $Na_2CO_3$ and the biogenic silica was not buffered. Following this step, it was observed that some biogenic silica, predominately sponge spicules, had not been successfully removed. To test the efficacy of the silica removal procedure, a series of samples were placed in the water bath for 8 hours and stirred hourly, resulting in a more intensive silica removal process. No significant change in the mean grain size of these samples was observed, suggesting that the incomplete silica removal did not impact the mean grain size.

The samples were then rinsed in DI water and placed on a spinner until analysis. Significant delay in analysis can result in particles within the processed sortable silt samples aggregating, so constant agitation, combined with brief ultra-sonication directly prior to analysis was required.

### 2.4.2 Grain Size Analysis

Grain size analyses of the terrigenous samples were carried out using a Beckman-Coulter Multisizer 3 coulter counter. The so called 'electrical sensing zone' method infers the Equivalent Spherical Diameter (ESD) of the particles from measurable changes in electrical resistance produced by the nonconductive particles suspended in an electrolyte. An aperture between electrodes forms a 'sensing zone' through which suspended particles pass. In the sensing zone each particle displaces its own volume of electrolyte. Volume displaced is measured as a voltage pulse; the height of each pulse being proportional to the volume of the particle, reported as ESD. This method of analysis avoids problems that laser particle sizers have with overestimating the diameter of platy minerals such as clays, which are commonly seen in palaeoceanograpic situations (McCave et al. 2006). The Coulter Counter measures the

distribution of grain sizes between 10 and 63µm. Due to repeated fouling of the aperture by particles with a diameter <63µm but a length greater than the aperture diameter (140µm), samples were added to the working fluid of the Coulter Counter through an additional 63µm sieve. Up to 70000 particles between 8-63 µm were counted, but only the 10-63 µm fraction was analysed. Repeat analyses of individual samples show a standard deviation of 1.16µm, equivalent to a relative standard deviation (r.s.d.) of 5.2%

Long term consistency was assessed using repeated analysis of a 20 µm Teflon standard (Teflon beads of a known average diameter were analysed using the same procedure as the lithic samples). This returned a standard deviation of 0.58 µm, equivalent to an r.s.d. of 2.9%

## 2.5 Ice rafted debris counts

Ice rafted debris (IRD) was operationally defined as the number of lithic grains >150 µm per gram of dry sediment. Following splitting of the >150 µm fraction using a riffle splitter, counts were made using optical microscope examination of the split material. Only grains >150 µm were counted to avoid potential problems with current deposition of the finer sand fraction (Flesche Kleiven et al. 2002). At least 300 individual grains were counted per sample, with larger samples being split multiple times and then one split counted. Volcanic tephra shards were observed, but not included in the definition of IRD.

## 2.6 Calculation of % Northern Component Water (%NCW)

As discussed in Section 1.5.1 the $\delta^{13}C$ gradients measured in benthic foraminifera from different locations in the ocean can be used to trace deep water masses with distinct isotopic signatures. The relative proportion of NCW – water derived from regions of deep water formation in the high latitudes of the North Atlantic/Norwegian Sea – can be defined as the relative proportions of two end members. One end member represents the unmixed $\delta^{13}C$ value of the NCW, while the other represents the $\delta^{13}C$ value of the unmixed Southern Component Water (SCW). These can be compared to

the $\delta^{13}C$ value of a site on the mixing line between the two end members using the equation of Oppo and Fairbanks (1987):

$$\%NCW = \frac{\delta^{13}C_x - \delta^{13}C_{SCW}}{\delta^{13}C_{NCW} - \delta^{13}C_{SCW}}$$

Using absolute isotopic values to infer circulation changes in deep water assumes that the $\delta^{13}C$ values of the end members do not change significantly, something that is not necessarily the case (Hodell and Venz-Curtis, 2006). During the Pleistocene, Southern Ocean waters have a lower $\delta^{13}C$ than those of the Pacific, possibly as a result of increased stratification in the Antarctic SCW formation area inhibiting the equilibration of deep water masses with the atmosphere. Reconstructing the Pleistocene %NCW at ODP Site 607 using South Atlantic ODP Site 1090 as the SCW endmember and comparing it to the %NCW at site 607 using Pacific ODP Site 849 as the SCW endmember, Venz & Hodell (2002) found the %NCW reconstructions were not changed significantly, suggesting that for the period 0-1300 ka, the end-members have been relatively stable, and the same assumption was made for the Pliocene. In this study, ODP Site 982 is taken as the North Atlantic endmember, ODP Site 1090/704 as the Southern Ocean mixing point, and Pacific ODP Site 849 as the Pacific endmember.

## 2.7 Trace metal analysis

### 2.7.1 Benthic and planktonic foraminifera species selection and taxonomy

Benthic foraminifera were picked from the 250-315 µm size fraction to minimise possible ontogenetic effects on B/Ca and Mg/Ca ratios (Raitzsch et al. 2011). The samples were crushed between clean glass slides to open all chambers to the cleaning procedure. Obvious detrital fragments were removed under binocular microscope with a fine paintbrush. Between 4 and 10 individual tests were used per sample and if more than 10 tests were available, these were crushed, homogenised and split into two or more samples to test cleaning methods (Section 2.7.2). *Globigerina bulloides* was picked from 46 samples between 2500 and 3300 ka. Between 25 to 30 individuals from the 250-315µm size fraction were picked, crushed and cleaned following the same procedure as the benthic foraminifera.

Six species/morphotypes of benthic foraminifera were selected for trace metal analysis (*Table 2-1*). These include both epifaunal and infaunal species, as the environment of the infaunal species is buffered against major changes in the saturation state of the surrounding water, and they can therefore be used in combination with epifaunal species to assess the impact of the changing saturation state of bottom waters on benthic foraminifera. Where possible all six species were picked, however in many samples only one species had sufficient individuals for analysis.

| **Species** | **Reference** | **Water depth habitat** | **Habitat** | **Stratigraphic range** |
|---|---|---|---|---|
| *Cibicidoides wuellerstorfi* | Holbourn & Henderson (2002) | Mainly bathyal and abyssal | Epifaunal | Miocene - Recent |
| *Cibicidoides mundulus* | Holbourn & Henderson (2002) | Bathyal to abyssal | Epifaunal | Oligocene - Recent |
| *Cibicidoides mundulus var.* | Rae et al. (2011) | Assumed bathyal to abyssal | Epifaunal | Oligocene - Recent |
| *Melonis barleeanum* | Van Morkhoven et al. (1986) | Bathyal | Infaunal | Miocene - Recent |
| *Oridorsalis umbonatus* | Van Morkhoven et al. (1986) | Bathyal to abyssal | Shallow Infaunal | Cretaceous - Recent |
| *Pyrgo murrhina* | Van Morkhoven et al. (1986) | Bathyal to abyssal | Infaunal | Miocene - Recent |
| *Globigerina bulloides* | Kennet and Srinivasan (1983) | | Planktonic | Miocene - Recent |

*Table 2-1. Benthic and planktonic foraminifera used in this study.*

The species selected were identified using the taxonomy of Van Morkhoven et al. (1986) and Holbourn & Henderson (2002) with additional information from Rae et al. (2011).

*Identification of morphotypes of* C. mundulus*.*

*C. mundulus* has had a somewhat convoluted taxonomic history, with *C. kullenbergi* being considered both a junior synonym of *C. mundulus* and vice versa. In this study *C. mundulus* is considered the superior synonym, to remain consistent with previous Pliocene studies using this species .

Two morphotypes *of C. mundulus* were defined*. C. mundulus* can be distinguished from *C. mundulus var* by a more pronounced umbonal boss that almost resembles that of *O. umbonatus*, clearer and straighter sutures on the spiral side and a generally glassier appearance*.* Additionally, *C. mundulus* has a clear keel, whereas in *C. mundulus var.* this is not present. Both morphotypes exhibit the characteristic coil of coarse perforations on the spiral side (Holbourn & Henderson 2002), however neither clearly show the biconvex character used to differentiate this species from *C. pachyderma.* In this study, the characteristic 'lip' on the outer edge of the spiral side of *C. pachyderma* (causing the spiral side to appear similar in profile to an old air raid helmet) was used to help differentiate the two species. These morphotypes have previously been identified as having distinct offsets in trace metal ratios (Rae et al. 2011 and pers. comm. 2012), and the glassy form has also been noted in Khélifi et al. (2009).


*Figure 2-3. Composite natural light images of the major benthic foraminifera species used in this study. Scale bar is common to all images.*

*A-B* Cibicidoides wuellerstorfi

*C-D* Cibicidoides mundulus

*E-F* Cibicidoides mundulus var.

*G-H* Melonis barleeanum

*I-J* Oridorsalis umbonatus.

*Original images were acquired using a Leica MZ 16 optical microscope and inline Leica camera. To produce a fully focused image, each foram was imaged repeatedly at different focal plane depths and then the sequence of images was combined using Helicon Focus software (http://www.heliconsoft.com/heliconsoft-products/helicon-focus/). Standard digital processing techniques (sharpening, colour and*

### 2.7.2 Trace metal cleaning procedures

Following crushing, foraminifera were cleaned to remove contaminants. The method was adapted from Boyle and Keigwin (1985/86) and is described in detail in Appendix 1. Briefly, it comprises four steps:

1. Clay removal with 18.2mΩ DI water, methanol and ultrasonication.
2. Reductive removal of metal oxide coatings.
3. Oxidising removal of remnant organic material.
4. Final removal of adhered material with a weak acid leach.

Where sufficient material was available, homogenised samples of crushed benthic foraminifera were split into two samples to quantify the effect of the reducing step on trace metal composition. Exactly the same procedure was followed aside from the omission of the reductive cleaning step. In all species, the majority of replicates showed lower Mg/Ca in samples that were reductively cleaned (Table 2-2 and Figure 2-4). This is consistent with the findings of Yu et al. (2007) and Barker et al. (2003), and further suggests that the reducing step affects the trace metal ratios in two infaunal species not covered in those studies; *M. barleeanum* and *O. umbonatus*. The mechanism for this reduction is believed to be partial dissolution of calcite enriched in Mg, Mn, Cd, and U by the Citrite component of the reducing reagent (Yu et al. 2007).

All element/Ca ratios that were observed to decline in Yu et al. 2007 also did so in this study, but by a smaller percentage. This may reflect different concentrations of Citrate used in the reducing reagent and hence a different effectiveness of the cleaning procedure, different initial concentrations of the Mg, Mn, Cd, and U in the calcite, or different proportions of contaminant phases such as metal oxide coatings. Yu et al. 2007 also note a slight difference in the ratio decrease of analysed samples downcore, so it is possible that post-burial processes such as diagenesis may change the susceptibility of calcite to the reducing step. B/Ca and Li/Ca are unaffected by the reducing step, which suggest either that the distribution of B and Li in the calcite of the test is more homogenous, or that metal oxide coatings are rich in Mg but not B or Li.

| | Li/Ca | B/Ca | Mg/Ca | Mn/Ca | Sr/Ca | Cd/Ca | U/Ca | Fe/Ca |
|---|---|---|---|---|---|---|---|---|
| *C. wuellerstorfi* (n=6) | 1.63 | 7.24 | -5.85 | -18.08 | 0.87 | -24.75 | -37.07 | -37.25 |
| *C. mundulus* (n=4) | -1.37 | 2.14 | -5.20 | -25.77 | -0.14 | -30.66 | -38.49 | -23.05 |
| *C. mundulus var*.(n=6) | 3.41 | 4.45 | -7.99 | -17.54 | -0.31 | -29.18 | -39.35 | -24.16 |
| *M. barleeanum* (n=9) | -5.05 | -0.57 | -6.59 | -20.25 | 0.12 | -18.96 | -35.55 | -7.41 |
| *O. umbonatus* (n=7 ) | 0.39 | 3.97 | -5.91 | -10.10 | -0.14 | -17.35 | -21.59 | -15.59 |
| Mean change for all species. | -0.20 | 3.44 | -6.31 | -18.35 | 0.08 | -24.18 | -34.41 | -21.49 |
| Change observed by Yu et al. 2007 for *C. wuell* and *C. mund*. (n=26) | No change | No change | -10 | -69 | No change | -51 | -45 | No data |

*Table 2-2 Mean offset in trace metal ratio between the two cleaning procedures (see text for details). Negative values indicate that reductive cleaning decreases ratio. N = number of paired specimens examined.*

All thirty samples of *Pyrgo murrhina* responded to the cleaning procedure by disintegrating completely. Initially, it was assumed that *P. murrhina* was particularly

susceptible to the corrosive effects of the reducing step. However, a second batch of cleaning with the reducing step omitted exhibited the same behaviour. This species has a very thin test wall, and appears to be easily fragmented by the repeated ultrasonication required particularly in the clay removal step. Additionally, the tests of *Pyrgo murrhina* are made up of randomly oriented calcictic needles, unlike the *Cibicidoides* species. As such, *P. murrhina* is more susceptible to dissolution (Corliss & Honjo 1981). It is suggested that future work minimises ultrasonication and perhaps even omits crushing of the foraminifera test. It is likely that cleaning would still be effective, as *P. murrhina* is often seen in dry samples as a 'half bowl' – very open to the cleaning process when compared to the chambered *Cibicidoides* species.

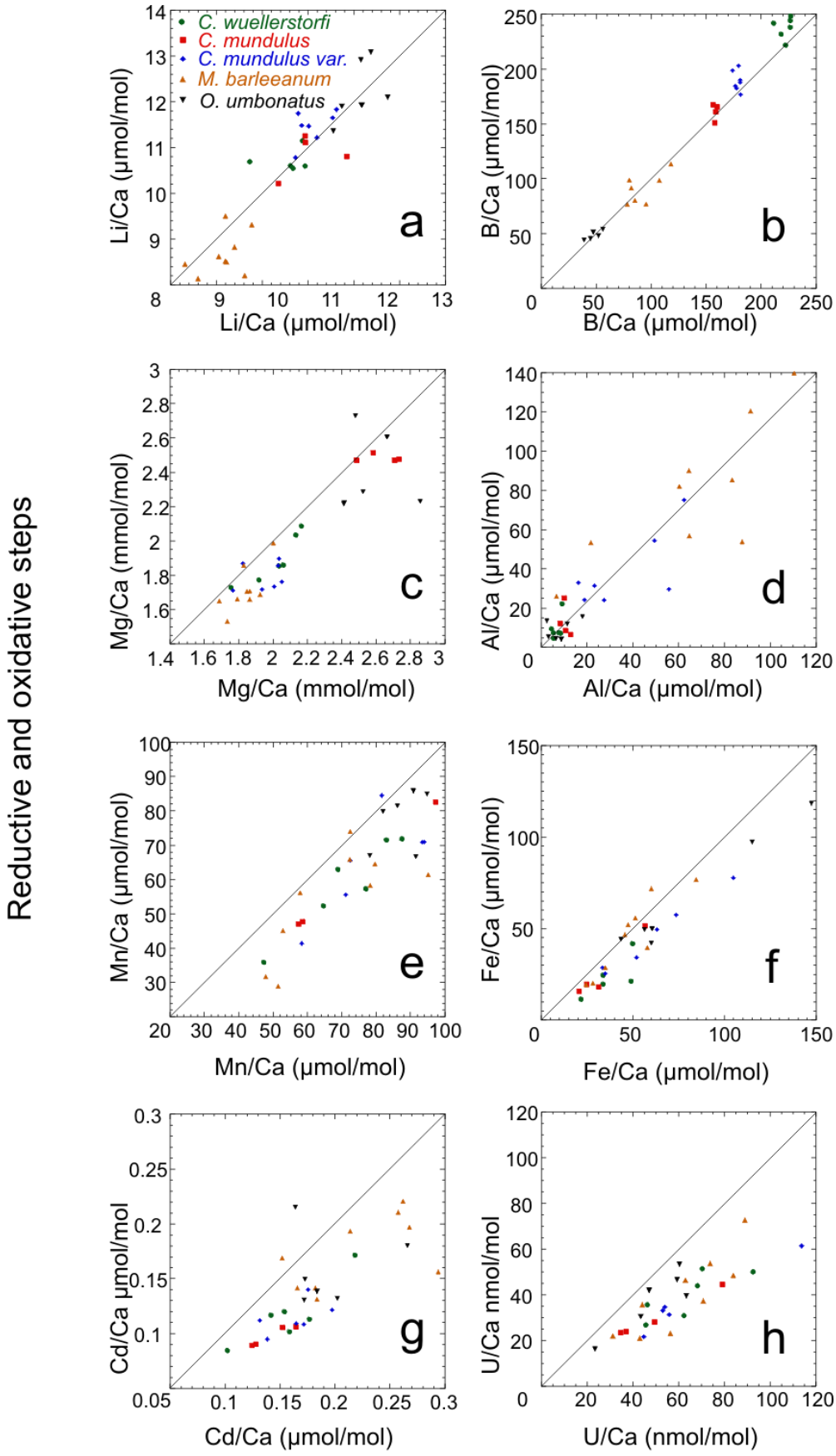
C. wuellerstorfi
C. mundulus
C. mundulus var.
M. barleeanum
O. umbonatus
a
Li/Ca (µmol/mol)
Li/Ca (µmol/mol)
b
B/Ca (µmol/mol)
B/Ca (µmol/mol)
c
Mg/Ca (mmol/mol)
Mg/Ca (mmol/mol)
d
Al/Ca (µmol/mol)
Al/Ca (µmol/mol)
e
Mn/Ca (µmol/mol)
Mn/Ca (µmol/mol)
f
Fe/Ca (µmol/mol)
Fe/Ca (µmol/mol)
g
Cd/Ca µmol/mol
Cd/Ca (µmol/mol)
h
U/Ca nmol/mol
U/Ca (nmol/mol)
Reductive and oxidative steps
Oxidative step

*Figure 2-4 (Overleaf) Comparison of results for five benthic foraminifera species cleaned with and without the reductive procedure. Solid line, y=x.*

### 2.7.3 Analysis of samples and long term precision.

Samples were analysed on the Thermo Element XR ICP-MS at Cardiff University. Samples were run against matrix-matched standards of similar [Ca]. These inline standards were used to calibrate samples, and long term precision was assessed using repeated analysis of two in-house standards with different trace metal composition (CS1 and CS2) at the beginning and end of each run. The two consistency standards are designed to span the range of trace metal compositions typically observed in benthic and planktonic foraminifera (Rosenthal et al. 1999).

| Ratio | CS1 | r.s.d (n=44) | CS2 | r.s.d (n=44) |
|---|---|---|---|---|
| Mg/Ca (mmol/mol) | 1.24 | <1% | 7.15 | <1% |
| Li/Ca (µmol/mol) | 6.09 | 2.4% | 45.12 | 3.1% |
| B/Ca (µmol/mol) | 13.04 | 6.5% | 221.95 | 2.9% |
| Cd/Ca (µmol/mol) | 1.25 | 2.6% | 1.56 | 2.7% |
| U/Ca (nmol/mol) | 4.49 | 2.9% | 27.21 | 3.1% |

*Table 2-3 Long-term precision based on repeat analyses of two consistency standards (CS1 and CS2) in 22 runs over the course of a year (2/2/12 to 31/1/13). Standards were taken from a parent batch produced at Cardiff University and were only used by this study.*

For both the CS1 and CS2 standards, Mg/Ca variability was <1% r.s.d. (percent relative standard deviation) based on 44 analyses. As part of the uncertainty in the

temperature calibration, this is an extremely small component – much less than the calibration error. The minor trace elements exhibited higher variability, which is partly a result of the lower concentrations. Li/Ca, B/Ca and Cd/Ca all occur in the μmol/mol concentration, whereas Mg/Ca has a much higher concentration. U/Ca was lower again, being measured in the nmol/mol range. The r.s.d of B/Ca CS1 is of note, as it is roughly double the variability of the other ratios. The variability is a result of elevated B/Ca ratios in the analyses made after the end of the main sequence in 8 runs carried out between 2/2/12 and 2/8/12. During these runs, the end standards were uncovered for several hours in the autosampler. While the samples waiting for analysis were in theory protected from environmental contamination by a perspex cover, it appears that some amount of boron contamination occurred. Uncapping samples immediately prior to analysis in the remaining runs reduced variability in the B/Ca to 3.28% r.s.d – similar to the other element ratios and the CS2 B/Ca standard. The CS2 standard does not exhibit the same trend as the CS1 standard, as the much higher B/Ca ratio means it is much less sensitive to environmental contamination. The B/Ca ratio of the foraminiferal species analysed is much closer to that of CS2 than CS1, and therefore the influence of external boron is not thought to have affected them significantly.

### 2.7.4 Data integrity

Following analysis, the data were examined for potential sample contamination and analytical errors. Several steps were used to screen anomalous data.

Firstly, all samples with isotope intensities less than 5 times the blank concentration were discarded for that element. This was only an issue with Li and B in 5 samples of *O. umbonatus*. Only samples with [Ca] between 90 and 110% that of the corresponding matrix matched standard were used. Due to the magnification of matrix effects at low [Ca], the data were also discarded if the sample [Ca] concentration was below 1.5 mM. The final quality control was the magnitude of the % r.s.d of the trace metal intensity ratio. Data with a % r.s.d of >3.8 were discarded.

The next step identified samples that were correctly analysed, but which remained contaminated following the cleaning procedure. Three indicators of contamination

were used, the Al/Ca ratio, the Mn/Ca ratio and the Fe/Mg ratio. Al is present in clay minerals, as is Mg so elevated levels of Al were taken to indicate unsuccessful cleaning and hence untrustworthy Mg values. While Al/Ca and Mg/Ca did not in general covary, all data for a sample were rejected when Al/Ca ratios exceeded 150 µmol/mol. All data for a sample was also rejected if Mn/Ca exceeded 140 µmol/mol. While this threshold is higher than that used for other published studies (J. M. Yu et al. 2008; Boyle 1983), long term trends in Mn/Ca and Fe/Ca in all species of benthic foraminifera at this site(Figures 2-5 to 2-9) suggest that changing bottom water conditions, and not sample contamination were responsible for increased Fe/Ca and Mn/Ca ratios. See Section 2.8 for a discussion of relative trends in Fe/Ca and Mg/Ca. Similar to Barker et al. (2003), all data for a sample was rejected if the Fe/Mg ratio was >0.1mol/mol, which is indicative of significant contamination of the sample. Other studies have used the Fe/Ca ratio (e.g. Lear et al. 2010), however almost exactly the same samples are rejected using either method.

Several samples from the early part of the ODP 982 record were inadvertently analysed with the ICP-MS incorrectly calibrated in medium resolution. As such, Fe/Ca data for these samples were not obtained. However, correctly analysed samples adjacent in the core show consistently low Fe/Ca ratios, so it is assumed that the partially analysed samples were also correctly cleaned.

During analysis, samples were blank corrected using a blank consisting of 0.5M $HNO_3$. The composition of the preceding blank was subtracted from each sample to remove the contribution of the diluting 0.5M $HNO_3$ from the analytical signal. In some cases, the blank analysed prior to the first sample was contaminated by a memory effect following analysis of CS2, resulting in an anomalously high lithium and boron intensities and negative intensity ratios for the sample. These errors were corrected manually using a drift-corrected blank. This problem persisted even with deliberately increased wash times, and in future several blank analyses should be run between the first set of consistency standards and the samples.

## 2.8 Temperature calibration of benthic foraminifera

A site specific temperature calibration was defined for ODP Site 982 and compared to other potential calibrations. The effect of $\Delta[CO_3^{2-}]$ changes on benthic Mg/Ca were quantified by using B/Ca to reconstruct $\Delta CO_3^{2}$. The development of the temperature calibration is detailed in Chapter 4.

## 2.9 Temperature calibration of planktonic foraminifera

The temperature calibration of Elderfield and Ganssen (2000) was used to produce SST estimates from planktonic species *G. bulloides.* This calibration was chosen because it was based on core top sediments from the North Atlantic region.

$$Mg/Ca = 0.81exp^{\,0.0081*SST} \textit{(Equation 2-1)}$$

## 2.10 Production of $\delta^{18}O_{sw}$ records from trace metal and stable isotope data

Due to low abundance of benthic foraminifera, production of paired Mg/Ca and $\delta^{18}O$ records was not possible. Therefore, in order to obtain a first order estimate $\delta^{18}O_b$ *Cibicidoides spp*. $\delta^{18}O_b$ values were linearly interpolated from previously published high resolution records (Lisiecki & Raymo 2005 and references therein). The high resolution (average sample spacing 5 cm) of the $\delta^{18}O$ record means that interpolated values were based on data points no more than 2.5 cm (equivalent to ~2 ky) away from the nearest Mg/Ca sample. As such, no significant error is thought to be introduced by this process. The palaeotemperature equation of Shackleton (1974) was used to determine the $\delta^{18}O$ composition of seawater ($\delta^{18}O_{sw}$) from BWT and $\delta^{18}O_b$ . Conversion between VSMOW and VPDB was carried out by the addition/subtraction of 0.27‰ as required, in common with previous Pliocene studies (Sosdian & Rosenthal 2009).

$$T = 16.9 - 4.0\left(\delta^{18}O_b - \delta^{18}O_{sw}\right) \textit{(Equation 2-2)}$$

The rationale behind the selection of this particular equation is discussed further in Chapter 4. Propagation of analytical and calibration errors results in a ±0.25 ‰ uncertainty on $\delta^{18}O_{sw}$ estimates.

## 2.11 Statistical methods

Time series analysis, including power spectra, filtering, coherency and phase analysis was carried out using the Analyseries software, developed by D. Paillard et al 1996. Specific procedures are described in detail in Chapter 5. All smoothed records were generated by resampling at the average resolution of the record, and then a tricubic Gaussian smoothing was applied using Kaleidegraph v4.0 software. This is a form of weighted average that highly weights the data points nearest to it, and then rapidly decreases their influence with distance.

# 3 Results

In this chapter the data produced as part of this study is presented. First, the raw trace metal results are presented and briefly summarised, then select trace metal records are compiled into stacked records to increase the temporal resolution. These stacked records are referred to in subsequent chapters. Also presented are records of physical properties: cfwt%, ird and SS.

## 3.1 Multi-element plots

Shown below are multi-element plots for each benthic species analysed (Figures 3-1 to 3-5). In *C. mundulus, C. mundulus var,* and *M. barleeanum*, there is a pronounced drop in Mg/Ca (panel A in all plots) ratios of ~0.2mmol/mol at 2800-2700 ka. The drop is not seen in *O. umbonatus,* and there are no specimens of *C. wuellerstorfi* at this time period. The Mg/Ca drop does not correlate with a shift in any other trace metal. There are gradual increases in Fe/Ca and Mn/Ca in all benthic records from 3600 ka, with a larger increase in Fe/Ca at 2500 ka. Some research has suggested that non-contaminant Fe/Ca (panel H) and Mn/Ca (panel E) may reflect changes in the oxygenation level of the bottom water (Glock et al. 2012), however at this stage no further interpretations are made. The Mg/Ca drop at 2800-2700 ka also does not correlate with shifts in Li/Ca, B/Ca, Al/Ca, or Cd/Ca. There may be a slight increase in U/Ca (panel G in all plots) in all species except *M.* barleeanum between 3000-2600 ka, possibly related to changes in sediment redox conditions (Boiteau et al. 2012). Irregardless, there is no correlation between Mg/Ca and U/Ca, so at this stage no further interpretations are made.

Also shown below (Figure 3-6) is the multi element plot for planktonic species *G. bulloides*. It should be noted that this record spans a shorter range than the benthic records – between 3300 and 2500 ka. The planktonic record shows different trends to the benthic records. There is a declining trend in Mg/Ca across the record , and in addition a sudden decrease of 0.8 mmol/mol between 2800-2700 ka. The gradual increase in Fe/Ca and Mn/Ca seen in all of the benthic species is not reflected in the

planktonic species, which suggests these trends are not diagenetic in nature, or the trend would be seen in *G. bulloides* as well.

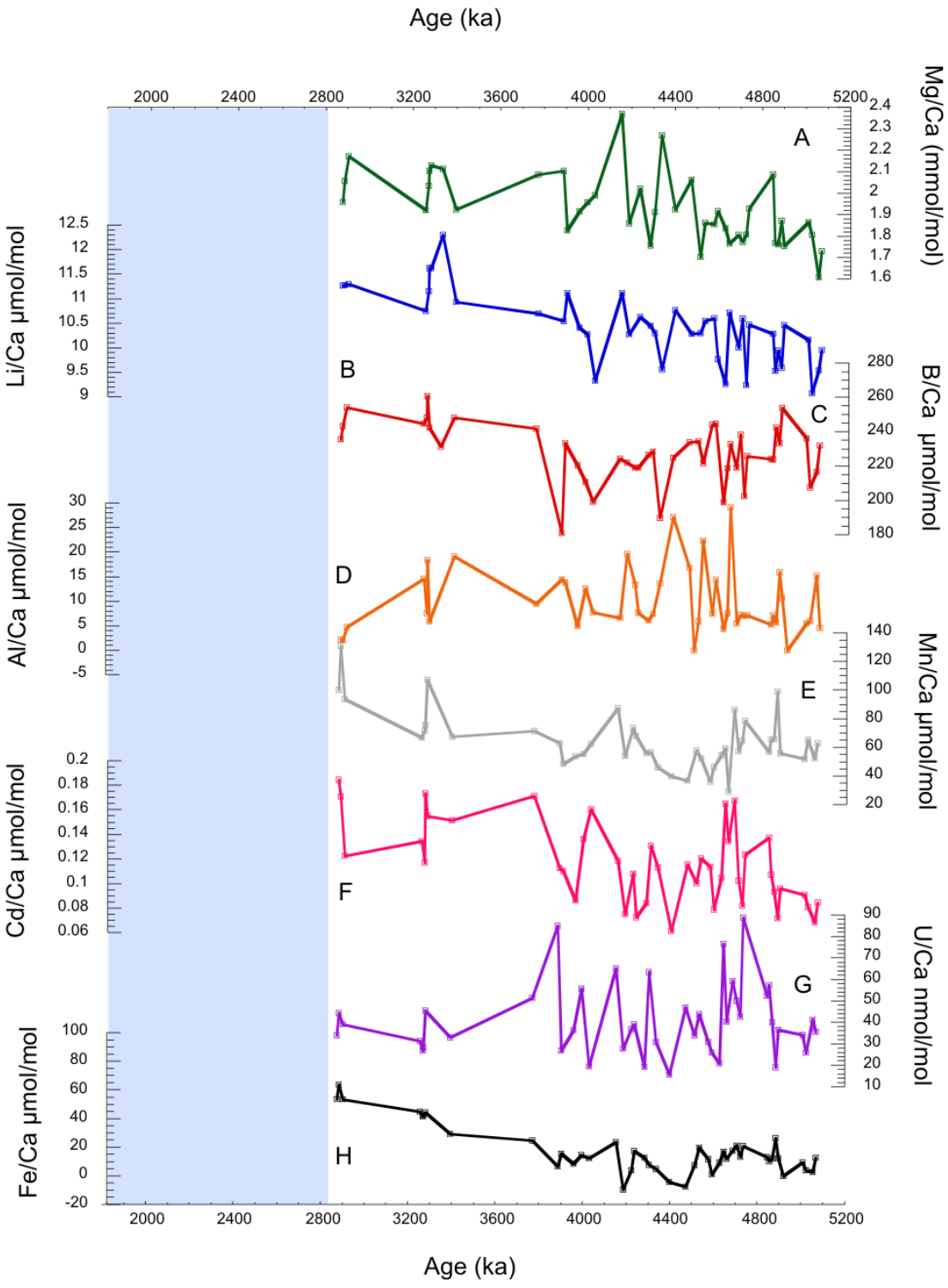


*Figure 3-1 Trace metal ratios for C. wuellerstorfi. There are no specimens from later than 2800 ka at this Site. Blue box highlights the timing of the Mg/Ca decrease seen in C. mundulus, C. mundulus var and M. barleeanum*

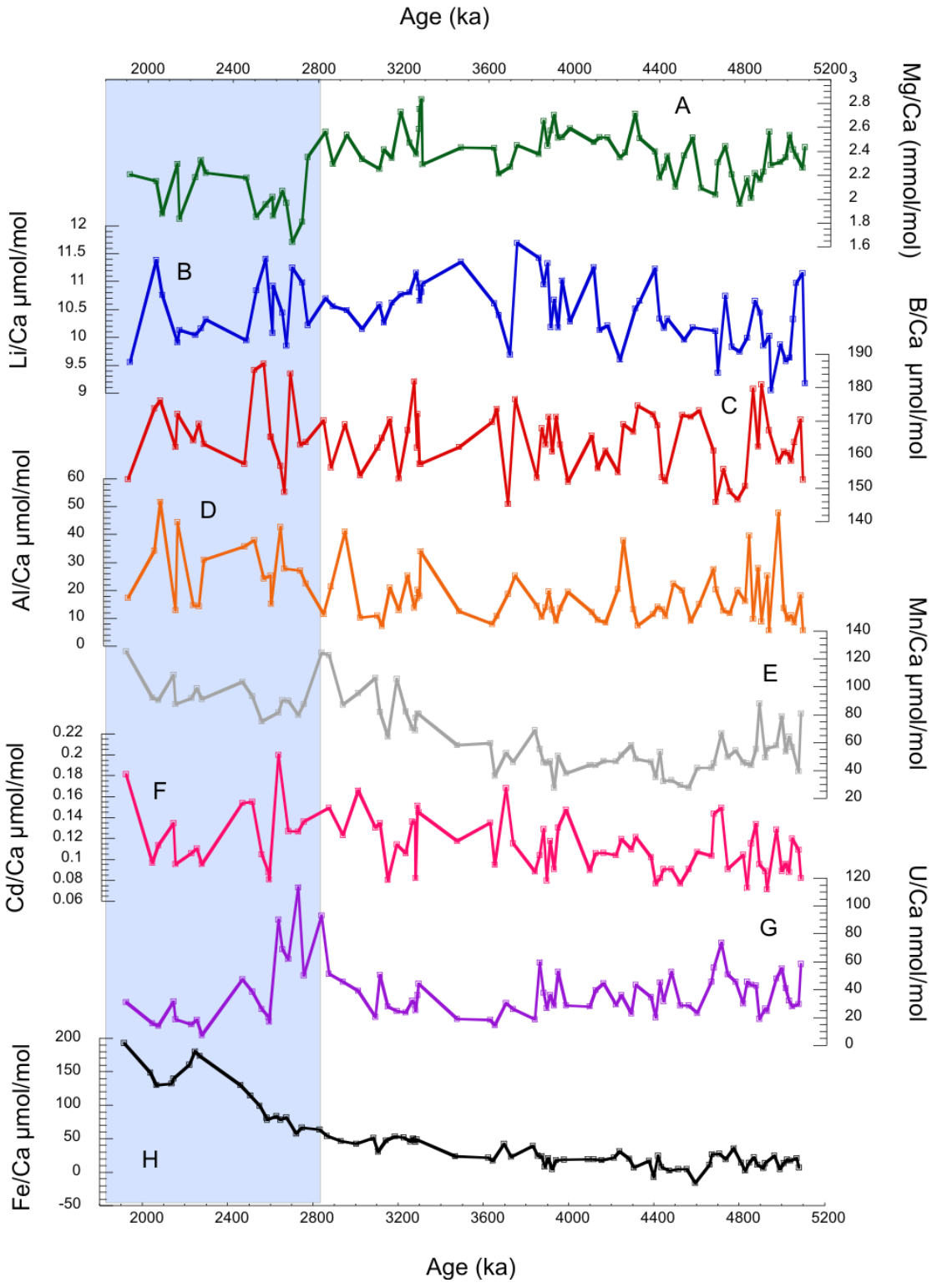


*Figure 3-2 Trace metal ratios for C. mundulus between 5200-1900 ka*

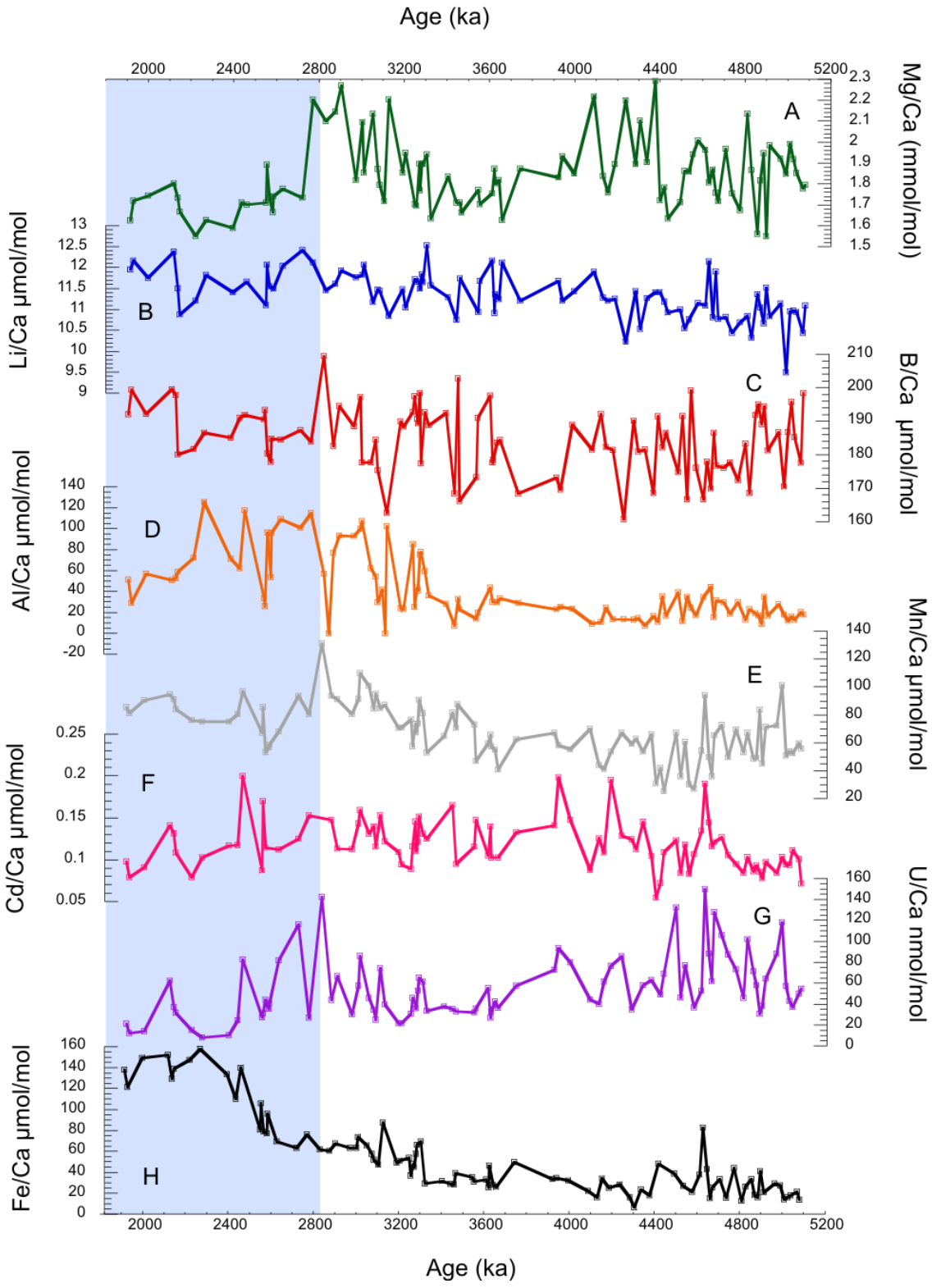


*Figure 3-3 Trace metal ratios for C. mundulus* var. *between 5200-1900 ka*

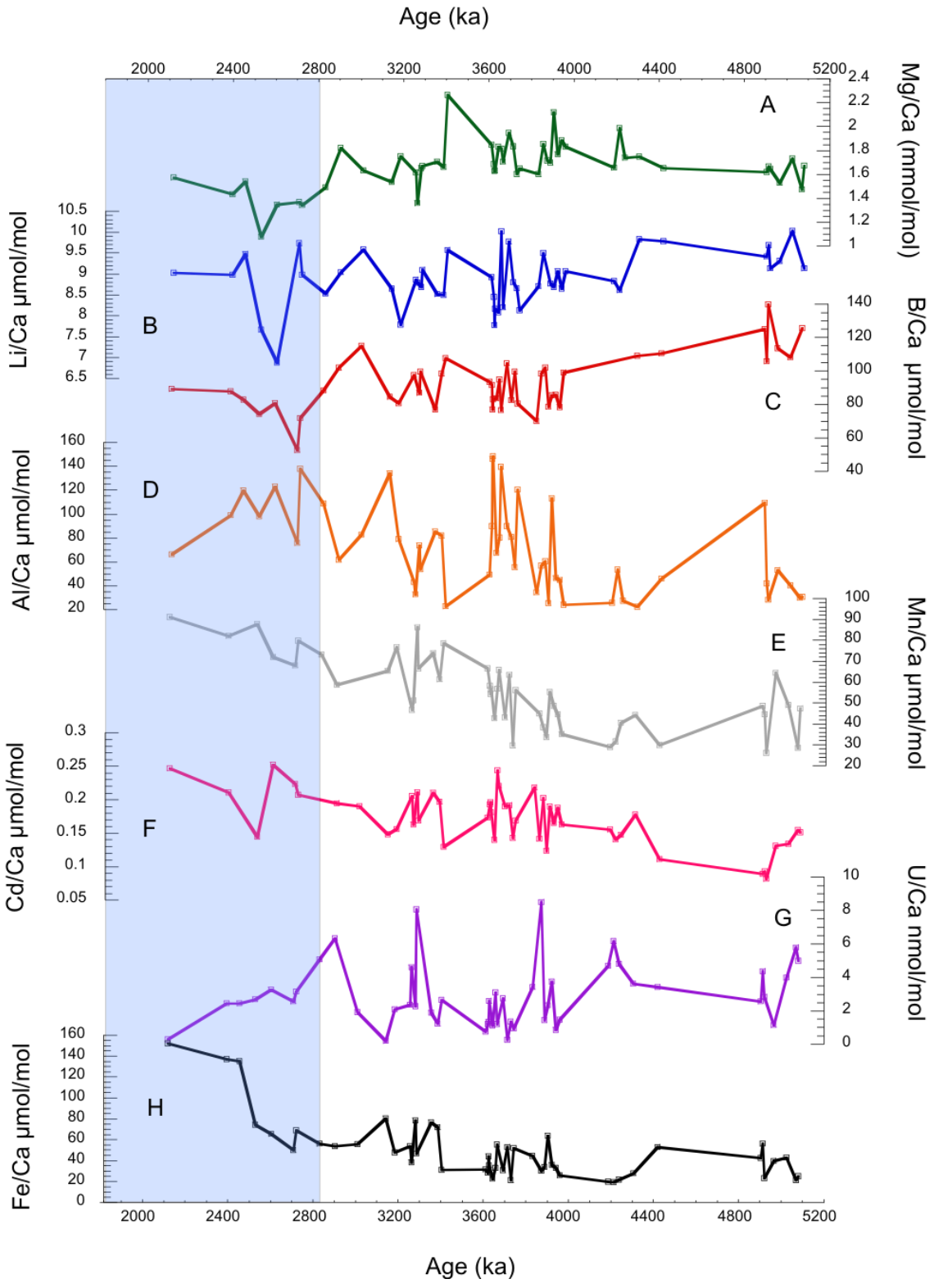


*Figure 3-4 Trace metal ratios for M. barleeanum between 5200-1900 ka*

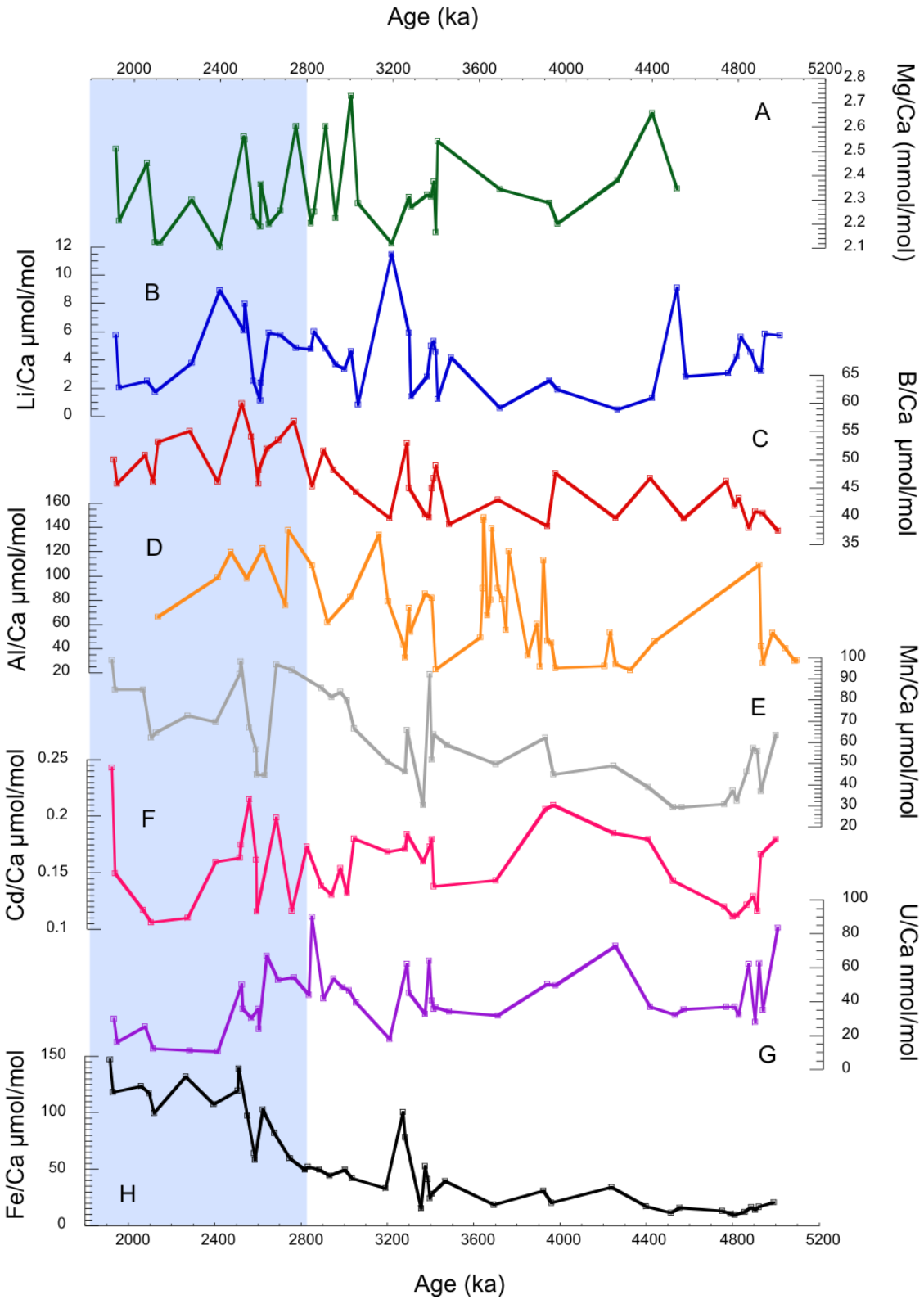


*Figure 3-5 Trace metal ratios for O. umbonatus between 5200-1900 ka. Cooling shift at 2800-2700 ka in Cibicidoides spp. (blue shading) is not mirrored in O. umbonatus.*

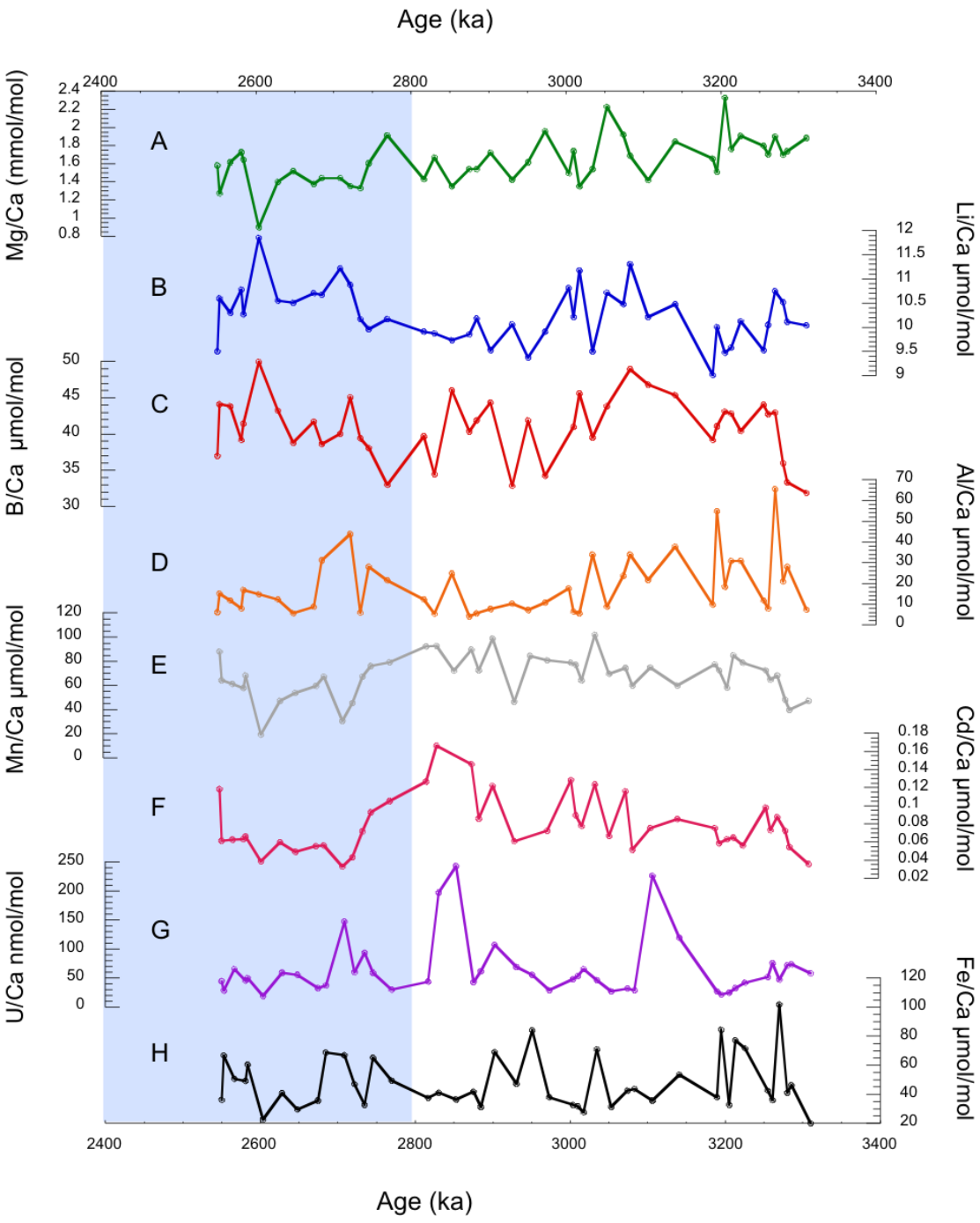


*Figure 3-6 Trace metal ratios from planktonic species G. bulloides between 3300 and 2500 ka.*

## 3.2 Compilation of multispecies records into composite trace metal stacks.

Previous studies that have combined samples from different benthic foraminifera species into composite trace metal records have used mean downcore Mg/Ca to generate constant offsets to correct each sample (Lear et al., 2000), or have applied

individual temperature calibrations and then combined the different species into one record (Bartoli et al. 2005; Lear et al. 2003). Here, a modified version of the procedure used by Lear et al. (2000) was followed. Samples with multiple species present were used to calculate a ratio of each species to the 'target' species, and then all other species were normalised to this target using the mean ratio (*Table 3-1*). Following this, the normalised values were averaged wherever multiple species were present.

The uncertainty of the offsets was assessed using the r.s.d. of the ratio variability. With the *Cibicidoides* species, the r.s.d. of the ratio between paired species was between 5-10 %, except for the Mg/Ca offset between *C. wuellerstorfi* and *C. mundulus*. This higher variability is likely a result of the lower number of 'tie points' with *C. mundulus*. A similar trend is seen with *M. barleeanum*, which has the same number of tie points as *C. wuellerstorfi*. Variation in the offset is generally <10 % for all species except *O. umbonatus*.

Composite stacks were produced for Mg/Ca, Li/Ca and B/Ca. Mg/Ca records were normalised to *C. wuellerstorfi* to allow direct comparison of Mg/Ca values with those previously published for the North Atlantic Pliocene (Sosdian & Rosenthal 2009; Bartoli et al., 2005). B/Ca records were normalised to *C. mundulus* to allow the use of the *C. mundulus* specific B/Ca - $\Delta CO_3^{2-}$ calibration of Yu & Elderfield (2007) throughout the study time period. Not all trace metal records produced were combined into the stacks, as one species (*O. umbonatus*) did not exhibit the same long term trends in Mg/Ca. See *Figure 3-5*. In addition, another species (*M. barleeanum*) was not included in the composite stacks as it was only present in a few samples that included other more numerous species, as well as it is not a member of the same genus. Furthermore, its infaunal habit precludes its inclusion due to potential differences in sensitivity to the carbonate saturation state effect. Since the number of unique data points potentially included in the stack by *M. barleeanum* was minimal (<10), the additional uncertainty from adding a species from a different genus with potentially different sensitivity was considered undesirable.

| Species | Mg/Ca (relative to *C. wuell*) | r.s.d (%) of offset | Li/Ca (relative to *C. wuell*) | r.s.d (%) of offset | B/Ca (relative to *C. mund*) | r.s.d (%) of offset |
|---|---|---|---|---|---|---|
| ***C. mundulus*** | 1.23 n=24 | 11.2 | 1.02 (n=24) | 7.18 | x | x |
| ***C. wuellerstorfi*** | x | x | x | x | 0.73 (n=24) | 8.72 |
| ***C. mundulus var*** | 0.97 (n=30) | 10.7 | 0.92 (n=48) | 5.77 | 0.89 (n=51) | 7.69 |
| ***M. barleeanum*** | 0.87 (n=12) | 10.5 | 1.17 (n=24) | 9.45 | 1.77 (n=24) | 16.7 |
| ***O. umbonatus*** | 1.20 (n=11) | 8.72 | 0.85 (n=22) | 7.62 | 3.70 (n=20) | 13.05 |

*Table 3-1 Offsets between species of benthic foraminifera determined in this study. Offsets given are normalised to the target species given in the top row.*

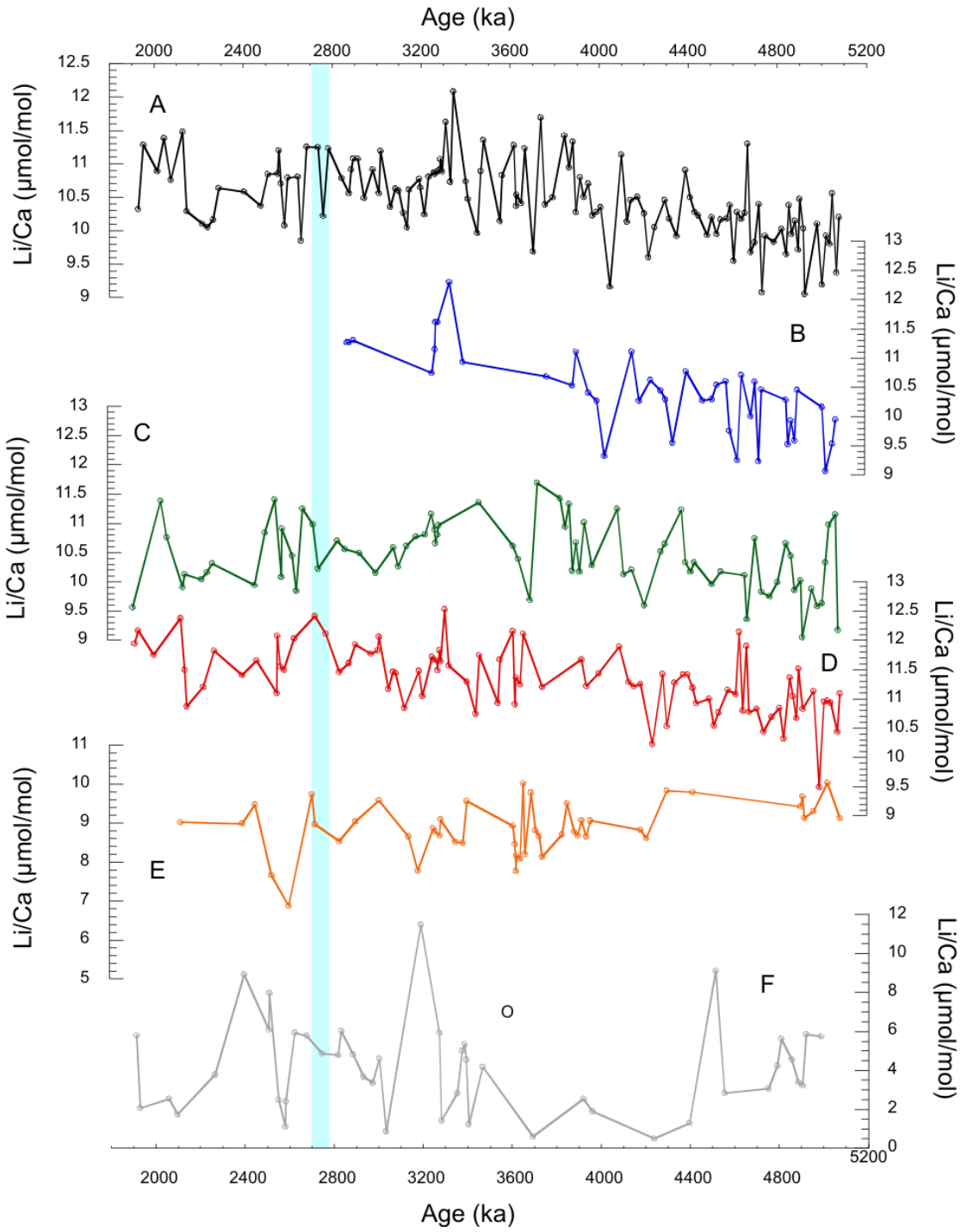


*Figure 3-7 Long term trends in Li/Ca: Stack record A) comprises all Cibicidoides species.B) C. wuellerstorfi, C) C. mundulus D) C. mundulus var. E) M. barleeanum and F) O. umbonatus. Blue band represents drop in Mg/Ca at 2800-2700 ka.*

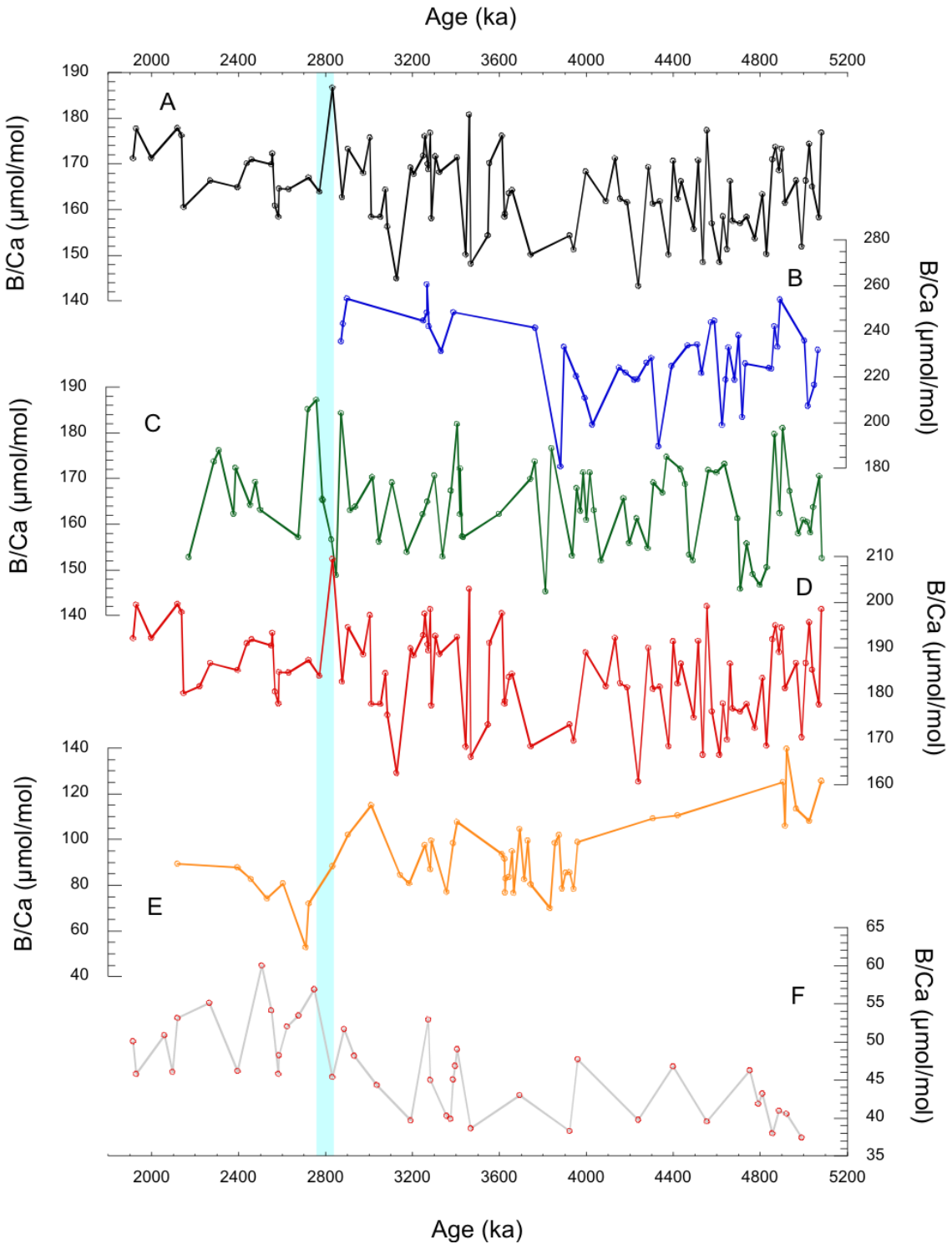


*Figure 3-8 Long term trends in B/Ca: Stack record A) comprises only C mundulus and C mundulus var B) C. wuellerstorfi, C) C. mundulus D) C. mundulus var. E) M. barleeanum and F) O. umbonatus.. Blue band represents drop in Mg/Ca at 2800-2700 ka.*

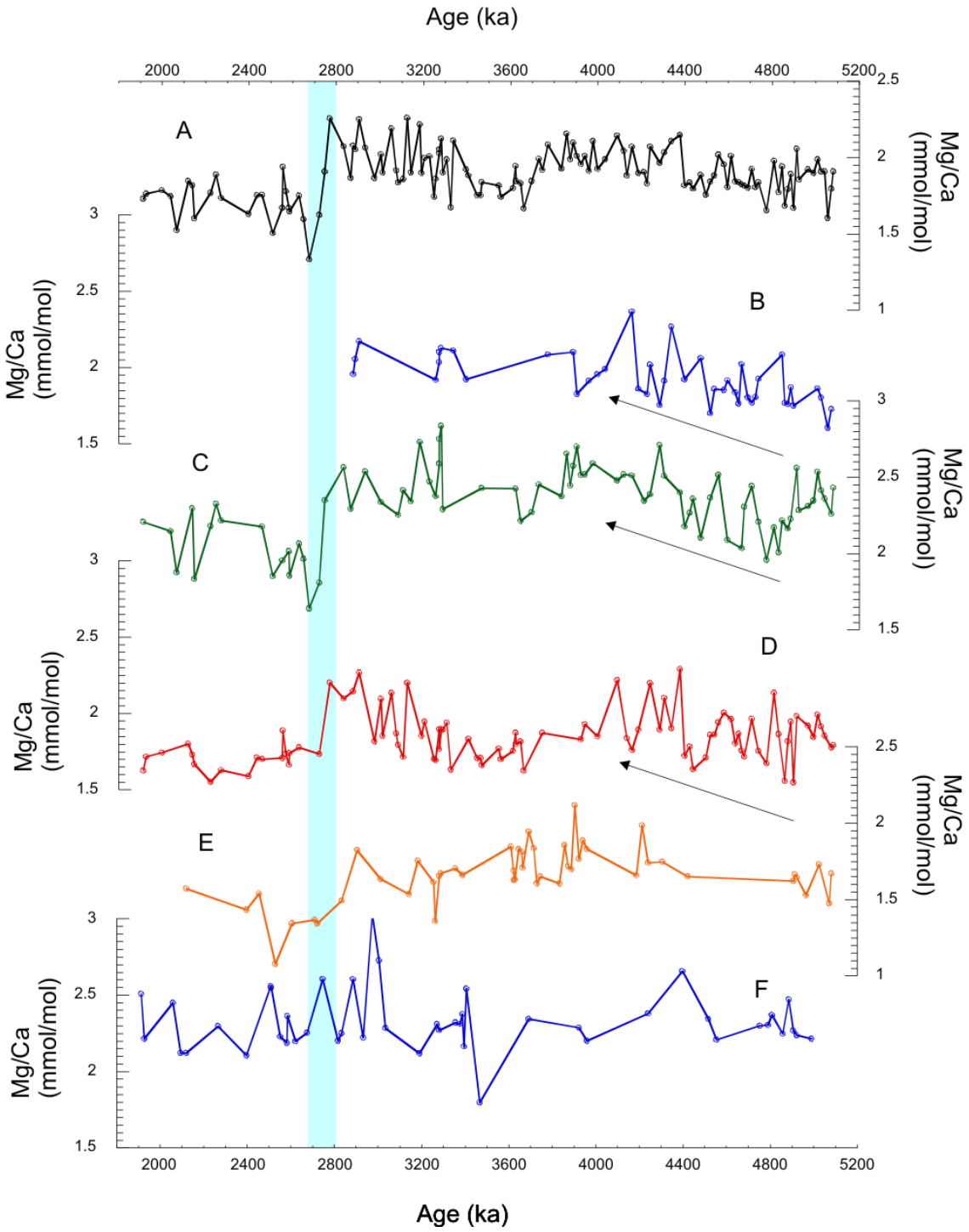


*Figure 3-9 Long term trends in Mg/Ca: Stack record A) comprises only C mundulus and C mundulus var.B) C. wuellerstorfi, C) C. mundulus D) C. mundulus var. E) M. barleeanum and F) O. umbonatus. Blue band represents drop in Mg/Ca at 2800-2700 ka. Arrows on records B) C) and D) highlight the increasing Mg/Ca value 5000-4000 ka.*

## 3.3 Physical measurements from Site 982

Shown in Figure 3-10 are the three physical parameters measured from Site 982. Sortable silt mean grain size, the coarse fraction weight percent, and ice rafted debris abundance. The sortable silt record exhibits rapid variability and a mean of around 22 µm. A potential increase starts at ~2800 ka, nearly coincident with the onset of IRD deposition. IRD abundance repeatedly peaks from 2800 ka to the end of the record. Independent of the trends in SS and IRD, the cfwt% appears to increase in mean percentage and variability from ~3500 ka.

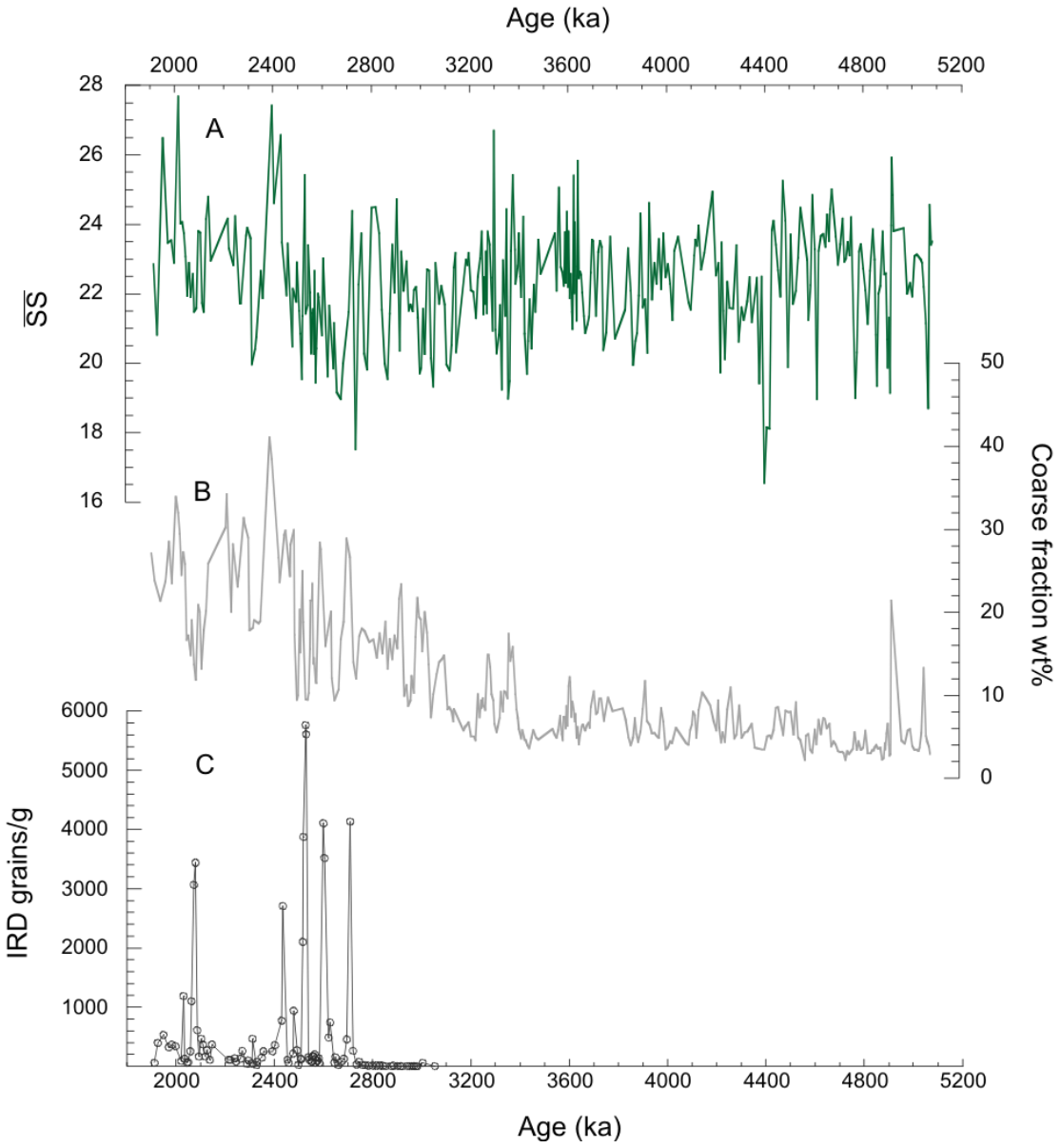


*Figure 3-10 A) Sortable silt mean grain size, B) Coarse fraction weight percent, and C) IRD abundance*

# 4 Temperature calibration

## 4.1 Benthic foraminiferal Mg/Ca temperature calibrations

The ratio of magnesium to calcium in the calcite of benthic foraminifera (i.e. shell Mg/Ca) is an important tool to reconstruct past bottom water temperatures (BWT). However, the exact relationship between Mg uptake in benthic foraminifera and temperature remains ambiguous. The following chapter provides a short review of the published temperature calibrations and it is shown that existing Mg/Ca-temperature calibration based on Late Pleistocene BWT variations (e.g., Sosdian and Rosenthal (2009)) or a modern depth transect (e.g., Lear et al., 2002 Yu and Elderfield 2008, Tisserand et al. 2013 ) are not suitable for the Pliocene section of ODP Site 982. In order to robustly estimate BWT variability in the Pliocene section of ODP Site 982 details of an alternative calibration are outlined and are used throughout this study.

## 4.2 Previously published temperature calibrations

Laboratory experiments demonstrate that the partition coefficient of $Mg^{2+}$ into inorganic calcite increases with increasing temperature (e.g., Katz 1973; Nürnberg et al. 1996). An exponential sensitivity of Mg/Ca of planktonic foraminiferal calcite to temperature has also been well documented in core-top, sediment trap and culture experiments (Anand et al. 2003; Lea et al. 1999; Elderfield & Ganssen 2000). In contrast, the sensitivity of benthic foraminiferal Mg/Ca to temperature is less well-constrained, and multiple empirical temperature calibrations exist which yield very different temperature histories when applied to downcore Mg/Ca records (*Table 4-1 Figure 4-4*, and references therein). There are several potential reasons for the wide range of empirical calibrations (Table 1). The first is the so-called “vital effect”, as each species appears to respond differently to temperature, which underscores the value of using species-specific calibrations (e.g., Lear et al., 2002). The extent to which these “vital effects” evolve through time and between morphotypes is unknown. A relatively minor complication may result from the cleaning method used prior to analysis, as the inclusion of a reductive step has been shown to reduce foraminiferal Mg/Ca through a dissolution effect (see Barker et al., 2003 Elderfield et al. 2006). Perhaps the most

significant source of uncertainty regarding the benthic foraminiferal Mg/Ca-temperature calibrations is that Mg/Ca is not solely affected by BWT. Core-top benthic foraminifera from cold yet highly carbonate saturated waters of the Norwegian Sea lie above the "global" Mg/Ca-temperature relationship, while those from warm, less well-saturated waters of the Caribbean lie below this curve (Martin et al. 2002; Elderfield et al. 2006; Rosenthal et al. 2006; Yu and Elderfield, 2008). These obvious outliers have led to the identification of a carbonate saturation state control on benthic foraminiferal Mg/Ca (Elderfield et al., 2006; Rosenthal et al., 2006; Yu and Elderfield, 2008), which post-date the publication of the early "global" Mg/Ca-temperature calibrations (e.g., Lear et al., 2002).

Assuming constant $[Ca^{2+}]$ the degree of carbonate saturation in ambient seawater may be expressed as $\Delta[CO_3^{2-}]$, the difference between *in situ* $[CO_3^{2-}]$ and $[CO_3^{2-}]$ required for calcite to be at saturation ($[CO_3^{2-}]_{SAT}$), which is a function of pressure, and hence water depth in the oceans (Broecker and Peng, 1982). It has been proposed that the carbonate saturation state effect on benthic foraminiferal Mg/Ca operates below a $\Delta[CO_3^{2-}]$ threshold of 25μmol/kg (Elderfield et al., 2006), and that in warm, more saturated waters (e.g., above ~3˚C in the majority of the modern ocean basins) the effect is insignificant. However, later work has questioned the notion of an upper threshold for the carbonate saturation state effect (Yu and Elderfield, 2008).

There are currently two approaches that have been adopted to deal with this complication in benthic foraminiferal Mg/Ca palaeothermometry. The first approach is to use an independent proxy for changes in bottom water saturation state (e.g., B/Ca or Li/Ca) and "correct" the downcore Mg/Ca record (e.g., Yu and Elderfield, 2008; Lear et al., 2010). This is potentially the optimal approach, but in practise suffers from current uncertainties surrounding sensitivities and threshold levels of trace metals to $\Delta[CO_3^{2-}]$ (Lear et al., 2010). The second approach is to assume either a zero or constant relative contribution from $\Delta[CO_3^{2-}]$ changes to the downcore Mg/Ca record, and to use an appropriate regional Mg/Ca-temperature calibration that adequately reflects this assumption. For example, this latter approach has been used by Sosdian and Rosenthal

(2009) in their interpretation of the downcore Plio-Pleistocene benthic foraminiferal Mg/Ca record from ODP Site 607 (North Atlantic; 41°N, 32°W; water depth 3427 m).

Sosdian and Rosenthal (2009) generated a regional temperature calibration for ODP Site 607 by comparing *C. wuellerstorfi* core-top and Last Glacial Maximum Mg/Ca from a nearby core (Chain 82-24-23PC; 43°N, 31°W, 3406 m depth) with modern and LGM BWT estimates at the site. The authors derived their BWT for the LGM by subtracting the ice-volume driven Glacial/Interglacial change in deep water $\delta^{18}O_{sw}$ estimated from pore water measurements (Adkins et al. 2002), from the benthic $\delta^{18}O$ . This resulted in a two-point calibration with a temperature sensitivity of 0.15 mmol/mol per ˚C, which is higher than that published by Marchitto et al. (2007) (0.12 mmol/mol per ˚C). They attributed this difference in sensitivity to a ~30% influence on the Mg/Ca values from the $\Delta[CO_3^{2-}]$ effect. They tested their calibration by comparing derived Glacial/Interglacial $\delta^{18}O_{sw}$ or and hence global ice volume values from ODP Site 607, which were found to be in good agreement with Pleistocene ice sheet models. However, by applying this calibration to their downcore Mg/Ca record the authors assume that BWT and $\Delta[CO_3^{2-}]$ co-varied with a similar proportional influence on benthic foraminiferal Mg/Ca for the duration of the record (3150 ka to present). Recent ice volume modelling (de Boer et al. 2010) suggests that while the reconstruction of Sosdian and Rosenthal (2009) is accurate after the mid Pleistocene transition, it overestimates ice volume during glacial periods in the late Pliocene. This would be expected if the Pliocene Mg/Ca data were less influenced by a $\Delta[CO_3^{2-}]$ effect (for example if bottom waters were above the proposed ~25µmol/kg threshold during this interval).

| Reference | Species | Cleaning Method | Mg/Ca – BWT relationship | Temperature Range °C | Calculated temp decrease for a hypothetical Mg/Ca change of 2.5 to 2.0 mmol/mol |
|---|---|---|---|---|---|
| C. H. Lear et al. 2002 | *C. wuellerstorfi* | Reductive | Mg/Ca = 0.867exp(0.109*BWT) | 0.8-18 | 2.04 |
| Martin et al. 2002 | *C. wuellerstorfi* | Reductive | Mg/Ca = 0.85exp(0.11*BWT) | 1.1-18 | 2.02 |
| Elderfield et al. 2006 | *C. wuellerstorfi* | Oxidative | Mg/Ca = 0.9exp(0.11*BWT) | 1.1-18 | 2.02 |
| Marchittoet al. 2007 | *C. pachyderma* | Reductive | Mg/Ca = (0.116*BWT)+1.2 | 5.8-18.6 | 4.3 |
| Yu & Elderfield 2008 | *C. wuellerstorfi* | Oxidative | Mg/Ca = 0.59exp(0.28*BWT) | 0.98-4.26 | 0.79 |
| Healey et al. 2008 | *C. wuellerstorfi* | Reductive | Mg/Ca = 0.652exp(0.28*BWT) | 0.95-3.8 | 0.79 |
| Tisserand et al. 2013 | *C. wuellerstorfi* | Oxidative | Mg/Ca = 0.82exp(0.19*BWT) | 0-6 | 1.17 |
| Sosdian & Rosenthal 2009 | *C. wuellerstorfi* | Reductive | Mg/Ca = 0.15*BWT + 1.16 | -0.5-2.6 | 3.33 |
| C. H. Lear et al. 2002 | *M. barleeanum* | Reductive | Mg/Ca = 0.982exp(0.101*BWT) | 0.8-18.4 | 2.75 |

*Table 4-1.(Overleaf)A selection of previously published calibrations for Mg/Ca – BWT relationships. These calibrations are produced graphically in Figure 4-44.*

ODP Site 982 occupies a shallower position in the water column (1145m water depth) than ODP Site 607, and therefore is bathed within more saturated bottom waters today. However, Mg/Ca published for the Rockall Plateau near to ODP Site 982 (Yu & Elderfield 2008) are higher during the LGM than the Holocene, which has been interpreted to reflect a strong $\Delta[CO_3^{2-}]$ effect in intermediate waters in the late Pleistocene (Yu and Elderfield, 2008). This prompts the question of whether the Pliocene Mg/Ca record at ODP Site 982 has also been affected by changes in saturation state.

## 4.3 Evaluating a carbonate saturation state effect at ODP Site 982

In order to evaluate the contribution of changes in $\Delta[CO_3^{2-}]$ to benthic foraminiferal Mg/Ca during the Pliocene at ODP Site 982 co-registered B/Ca ratios are used to reconstruct $\Delta[CO_3^{2-}]$ trends and absolute values. Benthic foraminiferal B/Ca exhibits a linear relationship with $\Delta[CO_3^{2-}]$ in *Cibicidoides spp*., (J Yu & Elderfield 2007).

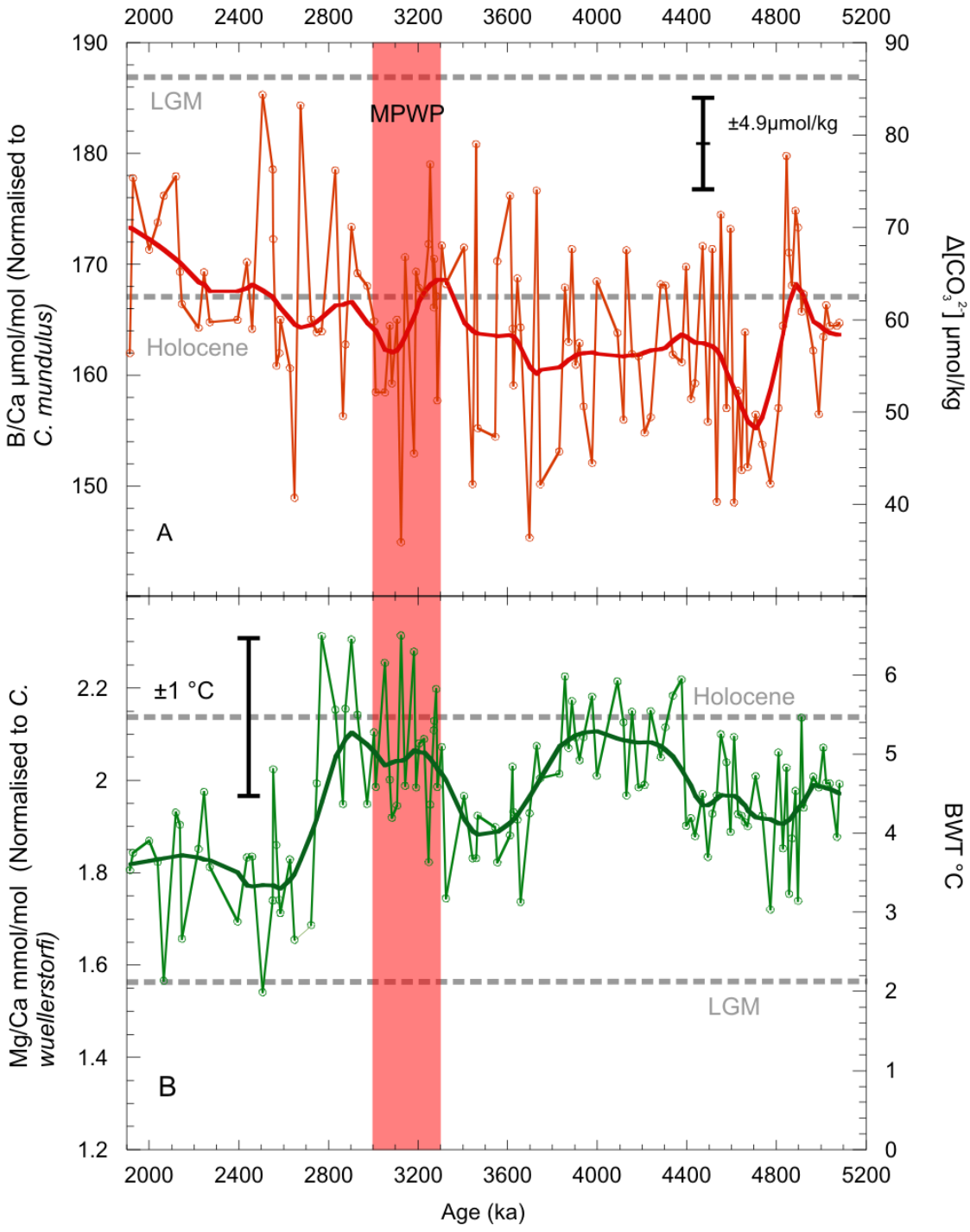


*Figure 4-1. Long term trends in A) B/Ca and B) Mg/Ca. Decrease in B/Ca through the MPWP and subsequent increase not reflected in Mg/Ca which remains stable through the MPWP and sharply decreases from 2900 ka. Grey dashed lines show the Holocene-LGM change in B/Ca and inferred $\Delta[CO_3^{2-}]$(Yu & Elderfield 2008) and BWT (inferred from pore water modelling after (Adkins et al. 2002)). Mg/Ca record is produced as described in section 2.8 from records of C. wuellerstorfi, C. mundulus and C. mundulus var. B/Ca record is produced using the same methods from C. mundulus and C. mundulus var. Heavy lines denote a 12% weighted smoothing, equivalent to a 100kyr window. Error bar in A) represents uncertainty of $\Delta[CO_3^{2-}]$ calibration from (Yu & Elderfield) Error bar in B) represents uncertainty of BWT derived from equation (4-2), Section 4-4.*

Measured B/Ca ratios in ODP Site 982 vary between 144-185 µmol/mol throughout the study interval, with a secular increase in B/Ca apparent throughout much of the record, starting around 4700 ka. This trend may reflect a sampling bias caused by the decreased abundance of benthic foraminifera during glacial stages (where B/Ca might be expected to be lower) aliasing the record towards higher values. Nonetheless, using the benthic foraminiferal B/Ca to $\Delta[CO_3^{2-}]$ relationship of Yu and Elderfield (2007), and assuming modern seawater B/Ca, the ODP Site 982 B/Ca values correspond to a $\Delta[CO_3^{2-}]$ range of between 40-80 µmol/kg. Taking $[CO_3^{2-}]_{SAT}$ as that of the modern deep water at ODP Site 982 (52.5 µmol/kg ) indicates that bottom water $[CO_3^{2-}]$ varied between 100-140 µmol/kg throughout the Pliocene record. Given the published error of the $\Delta[CO_3^{2-}]$ calibration of ±10 µmol/kg, this is similar to that seen at ODP Site 982 in the modern ocean (124 µmol/kg). If $\Delta[CO_3^{2-}]$ did influence the Pliocene benthic foraminiferal Mg/Ca record from ODP Site 982, the Mg/Ca-$\Delta[CO_3^{2-}]$ sensitivity of 0.0086 mmol/mol per µmol/kg (Elderfield et al., 2006) would suggest a maximum contribution of up to 0.3 mmol/mol, equivalent to ~1.6˚C using the global calibration of Lear et al., (2002). While variability of such a magnitude is seen in the Mg/Ca stack (normalised to *C. wuellerstorfi*), B/Ca and Mg/Ca records do not covary consistently throughout the study interval on either long or short timescales (*Figure 4-1*A, B), unlike the similar late Pleistocene downcore records presented by Yu and Elderfield (2008) (their Figure 4). Therefore, it seems reasonable to assume that the Pliocene benthic foraminiferal Mg/Ca from ODP Site 982 do not contain a significant signal of varying $\Delta[CO_3^{2-}]$. The corollary of this observation is that a Mg/Ca-temperature calibration based on Late Pleistocene BWT variations (e.g., Sosdian and Rosenthal (2009)) or a modern depth transect (e.g., Lear et al., 2002 and (Tisserand et al. 2013)) would not be appropriate for the Pliocene section of ODP Site 982, and an alternative means of determining the appropriate Mg/Ca-temperature sensitivity is required.

## 4.4 Independent temperature calibration for ODP Site 982

The initial assumption made in constructing a new temperature calibration for the Pliocene Mg/Ca record from ODP Site 982 is that it has an exponential form, similar to the relationships determined for inorganic calcite and planktonic foraminiferal calcite.

While the majority of (but not all) published benthic foraminiferal Mg/Ca-temperature calibrations have an exponential form there is often no statistical basis for choosing this form in preference to a linear relationship (Marchitto et al. 2007). Exponential calibrations are controlled by two constants, the exponential constant (A) and the pre-exponential constant (B) as shown in eq. 3.1.

$$Mg/Ca = B\ exp^{\ A*BWT} \text{ (}\textit{Equation 4-1}\text{)}$$

(A) defines the temperature sensitivity of the Mg/Ca ratio (increase in Mg/Ca per °C) and hence the amplitude of the BWT variability for a given change in Mg/Ca, while (B) defines the absolute BWT value.

| | **BWT °C** | **$\delta^{18}O_{benthic}$ ‰ Modern** | **Salinity (Modern)** | **$\delta^{18}O_{benthic}$ ‰ Pliocene** |
|---|---|---|---|---|
| Site 982 | 5.38 | 2.88 | 34.95 | 3.33 |
| Site 607 | 2.58 | 3.58 | 35.00 | 3.63 |
| Gradient 982-607 | 2.8 | -0.7 | -0.05 | -0.30 |

*Table 4-2. Bottom water properties for Site 982 and Site 607. Modern BWT and salinity are from the eWoce data set. Pliocene $\delta^{18}O_b$ are the average value for each core for the period 1900 – 2700 ka.*

The second assumption made in constructing the new temperature calibration is that the salinity difference between Pliocene bottom waters at ODP Site 982 and ODP Site 607 was the same as modern (0.05; Table 2). This assumption enables the residual inter-site offset in benthic foraminiferal $\delta^{18}O$ ($\Delta\delta^{18}O_b$) to be interpreted purely in terms of BWT, as it can be reasonably assumed that both Sites record an identical global ice volume signal.

### 4.4.1 Selection of $\delta^{18}O_b$ palaeotemperature equation

Similar to the Mg/Ca temperature calibrations, there are multiple palaeotemperature equations (documented in Pearson 2012) which yield differing relationships between $\delta^{18}O$ and temperature. This discrepancy is due to various factors. Firstly, different calibrations are derived from a variety species of foraminifera both planktonic and benthic; or not from foraminifera at all in the case of Shackleton (1974), which is derived from synthetic calcite. It is possible that different species fractionate $^{18}O$ differently, and a calibration derived from one species is not applicable to others. Secondly, the calibration ranges listed vary from 10-500 °C. Calibrations using planktonic foraminifera are commonly based on warmer temperatures and smaller ranges than those derived from benthic foraminifera. Again, it is probable that these different calibrations are not interchangeable. The most commonly used temperature calibration in benthic paleoceanography is that of Shackleton, (1974) however Pearson, (2012) suggests that the calibration of Cramer, (2011) is more appropriate, as it is based on a large data set of in-situ foraminifera, not synthetic calcite.

Previous Pliocene North Atlantic studies have used the equation of Shackleton (1974) (Sosdian & Rosenthal 2009; Khelifi et al. 2009). The modern $\Delta\delta^{18}O$ between site 982 and 607 is 0.7‰, which using the palaeotemperature equation of Shackleton (1974) modified for colder waters (Equation 4-2) is in excellent agreement with the observed 2.8 °C BWT difference (Table 4-2). The calibration of Cramer (2011) overestimates the temperature difference by ~ 0.5 °C and will therefore not be used in this study.

$$T = 16.9 - 4.0(\delta^{18}O_b - \delta^{18}O_{sw}) \text{ (Equation 4-2)}$$

### 4.4.2 Bootstrapping approach to temperature calibration development

Comparing $\delta^{18}O_b$ records from ODP Site 982 and ODP Site 607 (Venz & Hodell 2002; L. E. Lisiecki & Raymo 2005; Raymo et al. 1992) during the Pliocene suggests that the $\Delta\delta^{18}O_b$ was less than half the modern value, at around 0.3‰. This implies a reduced temperature gradient between sites during the Pliocene of ~1.2°C. Indeed, between 3300 and 2800 ka, the $\delta^{18}O_b$ gradient was reversed, so this interval was not included in the calculation of the temperature gradient (possible reasons for this reversal are

discussed further in Chapter 4). For the interval 3150 – 1900 ka benthic Mg/Ca are available from ODP Site 607 (Sosdian & Rosenthal 2009) to compare with the ODP Site 982 Mg/Ca record. This shows a broadly consistent inter-site offset of 0.2 mmol/mol Therefore, the temperature sensitivity (the value of (A) in Equation 4-1.) was determined by assuming that the total inter-site offset in Mg/Ca is the result of 1.2˚C cooler bottom water being present at ODP Site 607 relative to ODP Site 982.

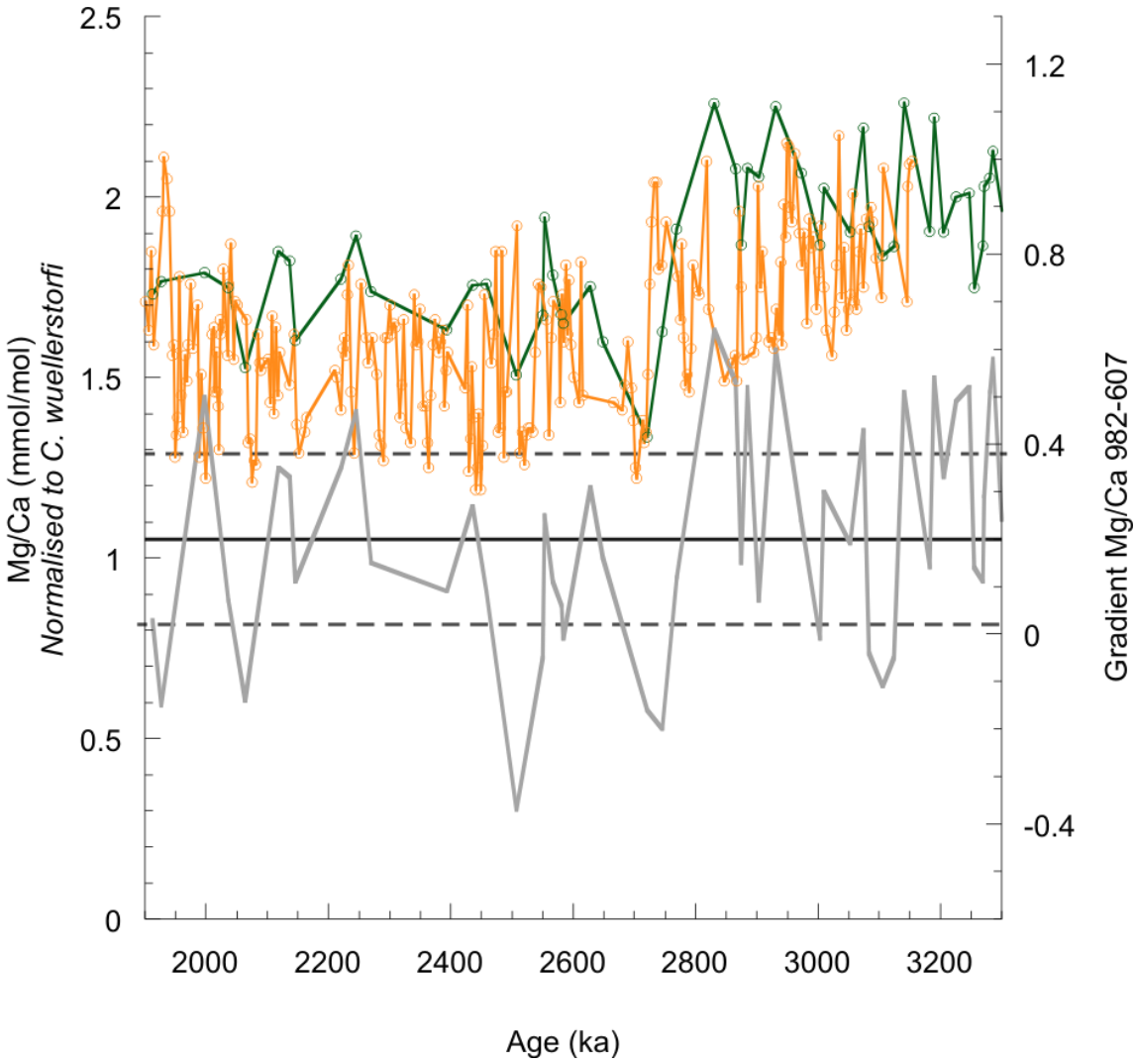


*Figure 4-2 Relative Mg/Ca values at ODP Site 982 (green) and 607 (orange). Gradient (grey) calculated by interpolating 607 record to 982 resolution. ODP Site 607 record from Sosdian et al. (2009) measured on C. wuellerstorfi and O. umbonatus (normalised to C. wuellerstorfi). Horizontal -solid line shows the mean gradient used in Section 3.4, and horizontal dashed lines represent the uncertainty included in the calibration error from the Mg/Ca gradient.*

While the exponential constant (A) is critical for determining downcore BWT variations, the preexponential constant (B) determines absolute BWT. There are many

factors that could lead to variations in B, including benthic foraminiferal vital effects and changing seawater Mg/Ca. It should also be noted that due to the long residence time of Mg and Ca in the ocean, it was assumed that the Mg/Ca ratio of seawater was constant across the record. However, seawater Mg/Ca was lower prior to the Neogene (e.g., Horita et al., 2002; Coggon et al. 2010). While this may affect absolute values for BWT reconstruction, relative changes on shorter timescales will still be accurate.

In order to estimate (B) a bootstrapping approach is adopted in which the calculated $\delta^{18}O_{sw}$ (equation 1, Chapter 2.9) based on ODP Site 982 Mg/Ca BWT and $\delta^{18}O_b$ for the early Pliocene (4000-5000 ka) is constrained to the independent estimates of $\delta^{18}O_{sw}$ using the global 1-D ice-sheet model of de Boer et al. (2010). The constraint was limited to the early Pliocene as there was very little ice sheet variability at this time (Mudelsee & Raymo 2005), thus reducing associated uncertainties. For the early Pliocene, the de Boer et al. (2010) ice-sheet model simulation produces an average $\delta^{18}O_{sw}$ of ~ 0.1‰ lower than modern, consistent with the absence of major northern hemisphere ice sheets.

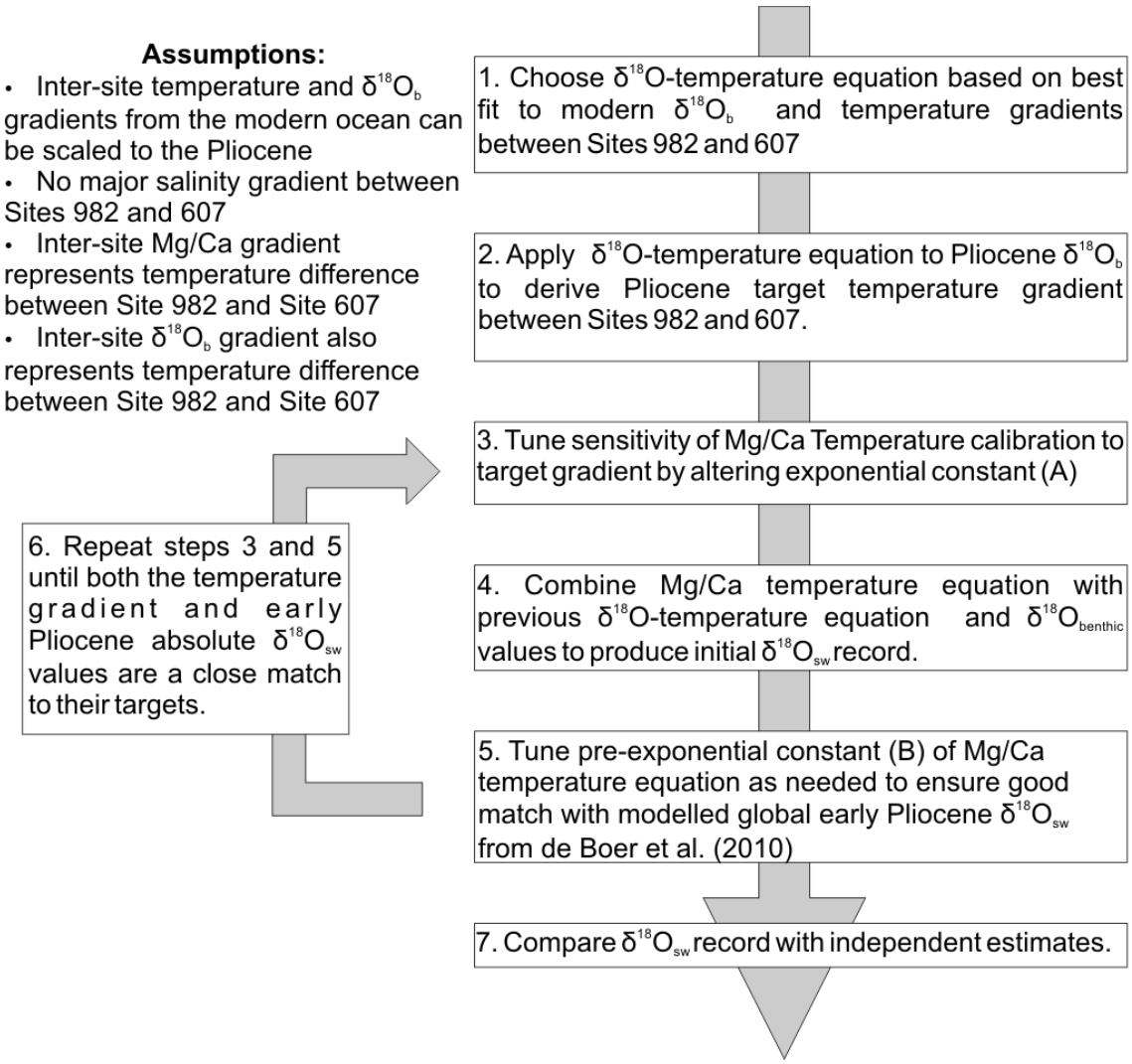


*Figure 4-3. Summary flowchart of key assumptions and stages in development of temperature calibration.*

The resulting *Cibicidoides*-based Mg/Ca-temperature calibration for the Pliocene record from ODP Site 982 is:

$$Mg/Ca = 1.26\ exp^{\,0.09*BWT} \quad \text{(Equation 4-3)}$$

Assuming a negligible $\Delta[CO_3^{2-}]$ effect on Mg/Ca, propagation of errors including analytical error and calibration error yields 1σ uncertainties of temperature of ±1.0°C. This is consistent with previous calibrations with an uncertainty of approximately ±1.1°C (Sosdian & Rosenthal 2009). Calibration error was determined by including the variability of the Mg/Ca and $\delta^{18}O$ used to define the temperature gradient between

ODP Site 607 and 982 (Figure 4-2), along with error introduced as part of the stacking procedure in a standard error propagation equation.

Compared to other published calibrations, the new ODP Site 982 temperature calibration used in this study has a similar sensitivity to those based on samples from a large BWT range (*Figure 4-4*). Calibrations utilising samples from smaller BWT ranges tend to be a) from colder waters, and b) much more sensitive to temperature. (eg. Yu & Elderfield 2008). This apparent high sensitivity to changes in BWT may be a result of $\Delta[CO_3^{2-}]$ also controlling the Mg/Ca ratio, the effect of which is more significant at colder temperatures (Elderfield et al. 2006).

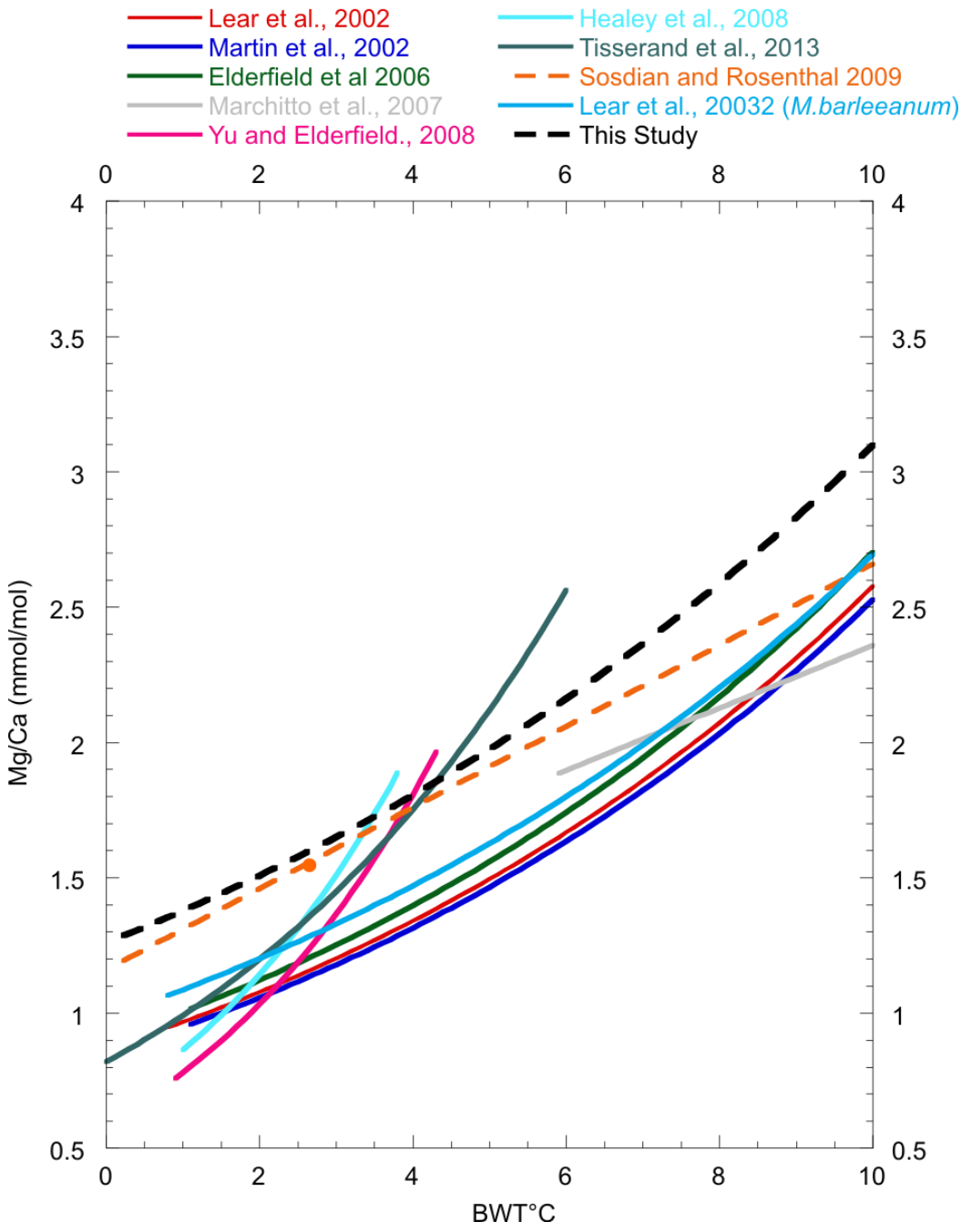


*Figure 4-4. Temperature calibrations for Mg/Ca from this study and previous studies. Regional calibrations for Site 607 (Sosdian and Rosenthal, 2009) and Site 982 (this study) are shown with dashed lines. All calibrations are for C. wuellerstorfi except for the single calibration for M. barleeanum (Lear et al. 2002). Where listed, temperature ranges are as shown in Table 4-1 except for Sosdian and Rosenthal (2009), which is based on two data points (-0.5 and 2.6°C) - one of which is shown on this graph as a solid orange circle - and is extended across the figure for clarity.*

## 4.5 Comparison of the new ODP Site 982 Pliocene temperature calibration with an infaunal Mg/Ca record

Recent work has suggested that infaunal benthic foraminiferal Mg/Ca records may be more robust BWT proxies as pore waters are to some extent buffered against changes in bottom water $\Delta[CO_3^{2-}]$ (Elderfield et al. 2010; Mawbey and Lear 2013). *Melonis* is an infaunal genus (Jain & Collins 2007) present in the ODP Site 982 Pliocene samples, and thus presents an opportunity to test the new *Cibicidoides* calibration, which has been constructed assuming minimal contribution from changes in $\Delta[CO_3^{2-}]$ on Mg/Ca. Unfortunately, the existing core-top *Melonis* Mg/Ca-temperature calibration is based on mixed species from a range of ocean basins (Lear et al., 2002). For this reason, the ODP Site 982 *M. barleeanum* Mg/Ca record is translated into temperature using both the *Melonis spp.* calibration and an empirical exponential relationship between *M. barleeanum* and BWT (equation 3, data from Little Bahama Banks sites in Lear et al., 2002 (n=9)) (*Figure 4-5*).

$$\textit{Melonis barleeanum}\ \text{Mg/Ca} = 1.64e^{0.065 \times BWT} \quad \text{(Equation. 4-4)}$$

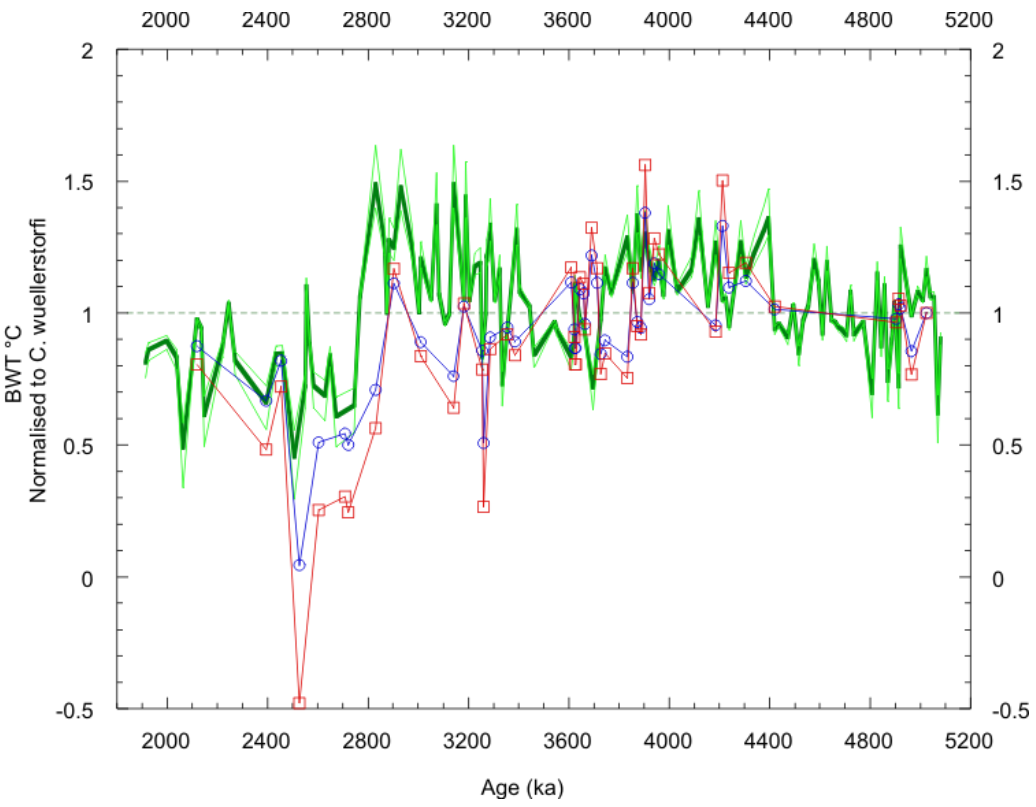


*Figure 4-5 ODP Site 982 bottom water temperatures based on* Melonis barleeanum *Mg/Ca using both the* Melonis *spp. temperature calibration (Lear et al., 2002) – blue line, and a calibration based solely on core-top* Melonis barleeanum *Mg/Ca data from the Bahamas – red line, and* Cibicidoides *spp. Mg/Ca – Dark green green line. Additional pale green lines represent the ±1°C uncertainty envelope for the* Cibicidioides *calibration. All temperatures normalised to the mean of the* C. wuellerstorfi *stacked record.*

The *Cibicidoides* Mg/Ca-BWT record derived using the *Cibicidoides* calibration is in relatively good agreement with the *Melonis barleeanum* Mg/Ca-BWT record derived using the global *Melonis* calibration of Lear, (2002) (Figure 3-4). This supports the notion that there is a minimal $\Delta[CO_3^{2-}]$ influence on the Pliocene Mg/Ca record from ODP Site 982. Observed *M. barleeanum* outlier data (from both calibrations) at 2500 ka are not paired directly with samples from the *Cibicidoides* record, which may explain the offset. Paired samples at 2000 and 2400 ka are in better agreement with the *Cibicidoides* record. The calibration derived solely from *Melonis barleeanum* from the Little Bahama Banks appears to produce larger downcore BWT variations, but the calibration is based on more scattered core-top data, with a greater associated calibration uncertainty.

## 4.6 Bottom water and sea surface temperature trends at Site 982.

The calibration derived in Section 4-4 allows the evaluation of bottom water temperature (BWT) changes at Site 982 during the Plio-Pleistocene, and the comparison of these trends to Sea Surface Temperature records from this location and BWT records from other sites. The relationship between ice rafted debris and water temperatures is also examined.

### 4.6.1 Bottom water trends at Site 982

*Long term trends*

The Mg/Ca records from ODP Site 982 show long-term changes in BWT throughout the Pliocene (Figure 4-6). The event most immediately significant is a sharp (<100 ka in length) 1.5 °C cooling between 2800 and 2700 ka, however there are also significant changes earlier in the Pliocene. The smoothed BWT record shows an 0.8 °C increase in temperature from 5000-4200 ka, followed by a period of stable temperatures. This warming is an abrupt step at 4400 ka, approximately the same time as the initial restriction of the Central American Seaway to surface water exchange (Steph, Tiedemann, Prange, Groeneveld, Schulz, Timmermann, Nürnberg, Rühlemann, Saukel, Haug, et al. 2010).

Maximum temperatures at this time approach Holocene levels, but minimum temperatures remained warmer than LGM temperatures, consistent with a less extreme glacial-interglacial cycle than compared to the late Pleistocene. Between 3700 and 3300 ka there was a transient 400 kyr cooling of ~1.2 °C, and in general Pliocene bottom water temperatures were stable until approximately 2800 ka. During the Mid Pliocene Warm Period (MPWP), bottom waters at Site 982 were around 5 °C, which is in good agreement with independent BWT estimates from Ostracod Mg/Ca (Thomas M. Cronin et al. 2005), and is similar to the modern BWT. The meridional temperature gradient of the deep Atlantic therefore appears similar to the modern, consistent with reconstructions of the Pliocene deep water circulation as being similar to or more intense than today (Raymo et al. 1996, Mudelsee & Raymo 2005). Between 2800 and 2700 ka, an abrupt cooling lowered average temperatures by ~ 1.7 °C with

temperatures after the cooling as low as 1.4 °C during glacial periods, and during warm periods as high as 1.9 °C. This cooling appears to span at least MIS stages G8-G6 (2777-2804 ka), and may begin as early as MIS G10 (2810 ka), however the relatively low resolution of the Mg/Ca record means this conclusion is uncertain.

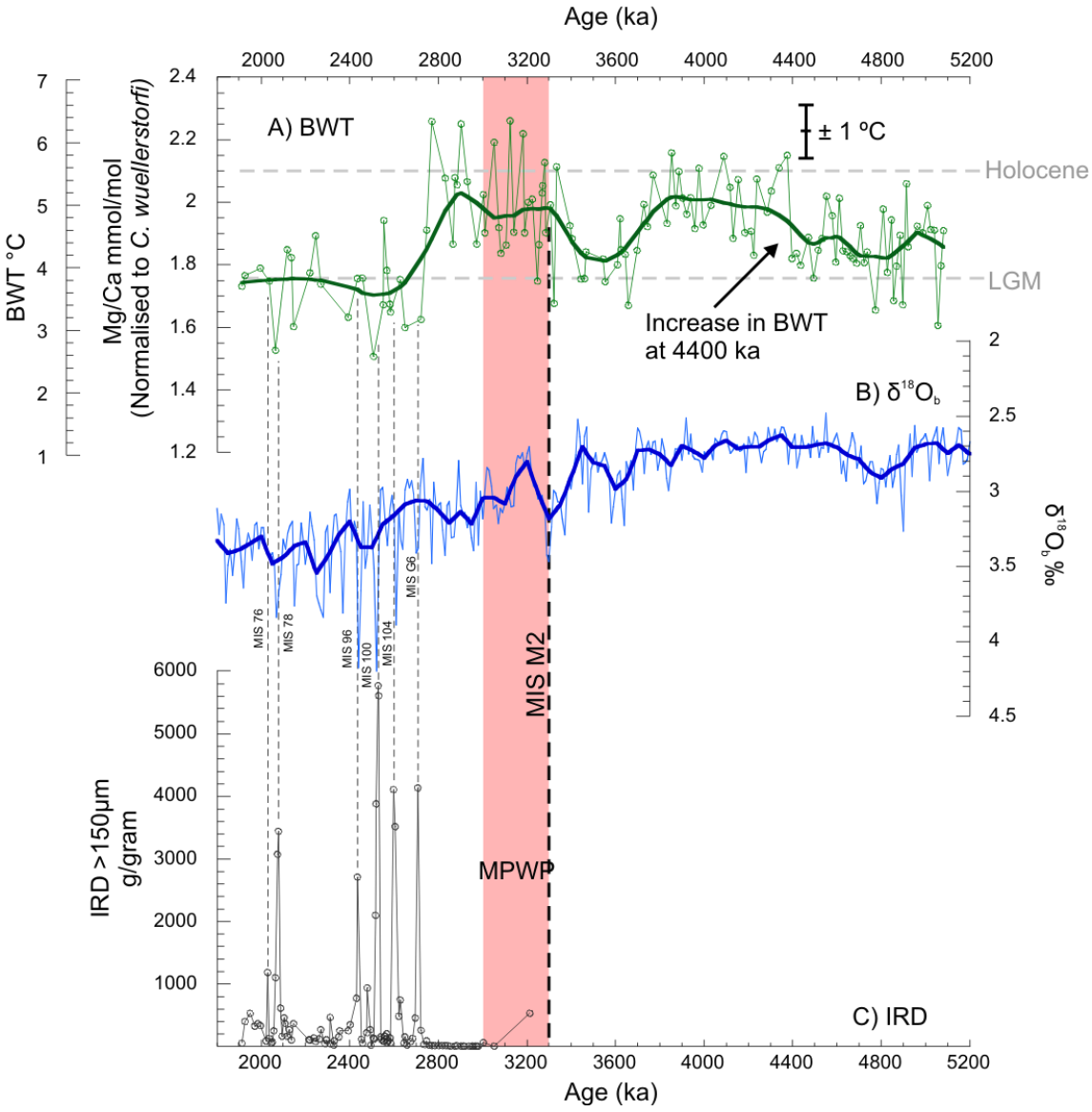


*Figure 4-6 A) BWT, B) $\delta^{18}O_b$, C) Ice rafted debris records for Site 982. Heavy lines on A and B mark 100kyr smoothing. Vertical dashed lines mark major IRD input to Site 982 and are labelled with the corresponding MIS stage. Mid Pliocene Warm Period (MPWP) based on bounds set by* (Harry J Dowsett, Robinson, et al. 2009).

The cooling at 2800 ka also coincides with the first occurrence of persistent IRD at Site 982. The first transient occurrence was 500 ky prior to this, at 3300 ka during MIS M2. This is consistent with other sites in the North Atlantic region, and is believed to be the

first glacial event where IRD was input to the North Atlantic region. IRD was visible in low amounts prior to this time in the Norwegian Seas (Kleiven et al. 2002). After 2750 ka, IRD was a permanent presence at Site 982, with major spikes at MIS stages 104, 100 and 96.

The $\delta^{18}O_b$ record for Site 982 (Figure 4-1B) shows different long-term trends to the bottom water temperature record. An initial decrease in $\delta^{18}O_b$ values in the early Pliocene coincides with the BWT increase from 5100-4400 ka. Thereafter, the $\delta^{18}O_b$ record exhibits a prolonged trend towards heavier values starting at 4000 ka and continuing into the early Pleistocene. Mudelsee & Raymo (2005) used a simple parametric model of a climate change, a ''ramp'' (Mudelsee 1999) to infer the start, end, and amplitude of the increase in mean $\delta^{18}O_b$ from 2000 – 4000 ka. Superimposed on the long term $\delta^{18}O_b$ increase are increasingly large oscillations about the mean, which reflect 41 kyr obliquity forcing of $\delta^{18}O_b$, in particular after 2700 ka (Sosdian & Rosenthal 2009).

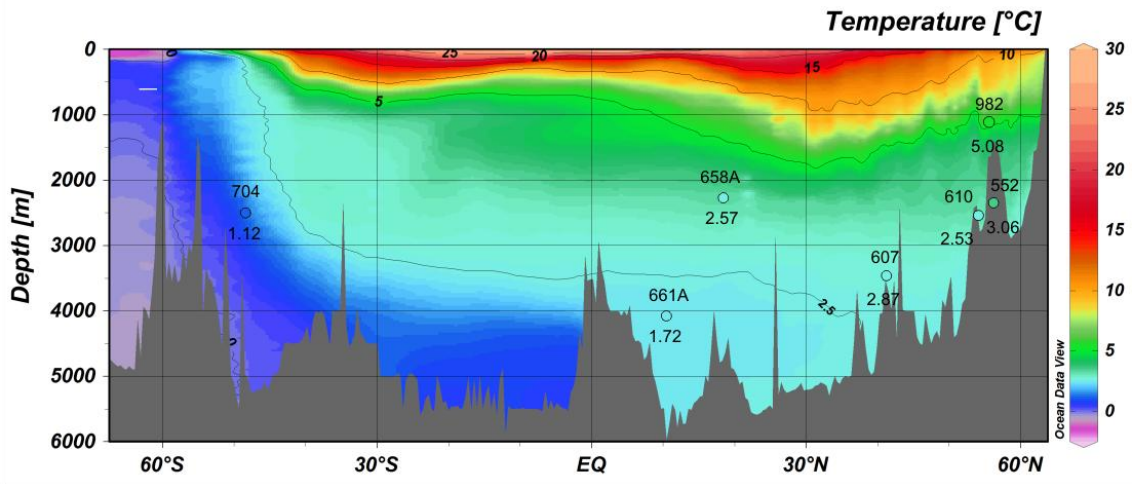


*Figure 4-7 Bottom water temperatures derived from MPWP (3300-3000 ka) Mg/Ca measurements overlain against a modern BWT transect (data from eWOCE). Site 982 data is from this study and is the average for the time period. All other data is based on Ostracod Mg/Ca from* (Thomas M. Cronin et al. 2005)*. Fill colour of site markers corresponds to analysed BWT plotted on the same spectrum as the modern BWT.*

The bottom water trend at Site 982 can also be compared to that at Site 607, where a benthic Mg/Ca record already exists (Sosdian & Rosenthal 2009). In this study, the temperature calibration derived in this Chapter will be used for all North Atlantic

benthic Mg/Ca records, as it is specifically calibrated for use in the Pliocene. This is in contrast to other calibrations, including the site specific calibration developed by Sosdian and Rosenthal (2009) which rely on modern data.

Long term trends for Site 607 are generally similar to that at Site 982 (Figure 4-8), with an average cooling of ~1.3 °C at approximately 2800 ka, and BWT varying about a stable mean of 2.5 °C after that point. This cooling at Site 607 appears more abrupt than at Site 982, however this may be a result of the higher resolution of the Site 607 record. Prior to the cooling at 2800 ka, the Site 607 trend shows a different trend. Mean bottom water temperatures at Site 607 for the period 3150-2800 ka remain generally stable, however the range of the BWT between cooler and warmer periods increases progressively from 2 °C to 3 °C. This is driven by a decrease in BWT minima, and these temporary excursions may suggest increased influence of dense and cold bottom waters at Site 607 that are not present at the much shallower Site 982. Despite these differences, BWT comparisons between the two sites confirm that the cooling at Site 982 at 2800 ka is at least a regional phenomenon, and is therefore likely related to the changing global climate.

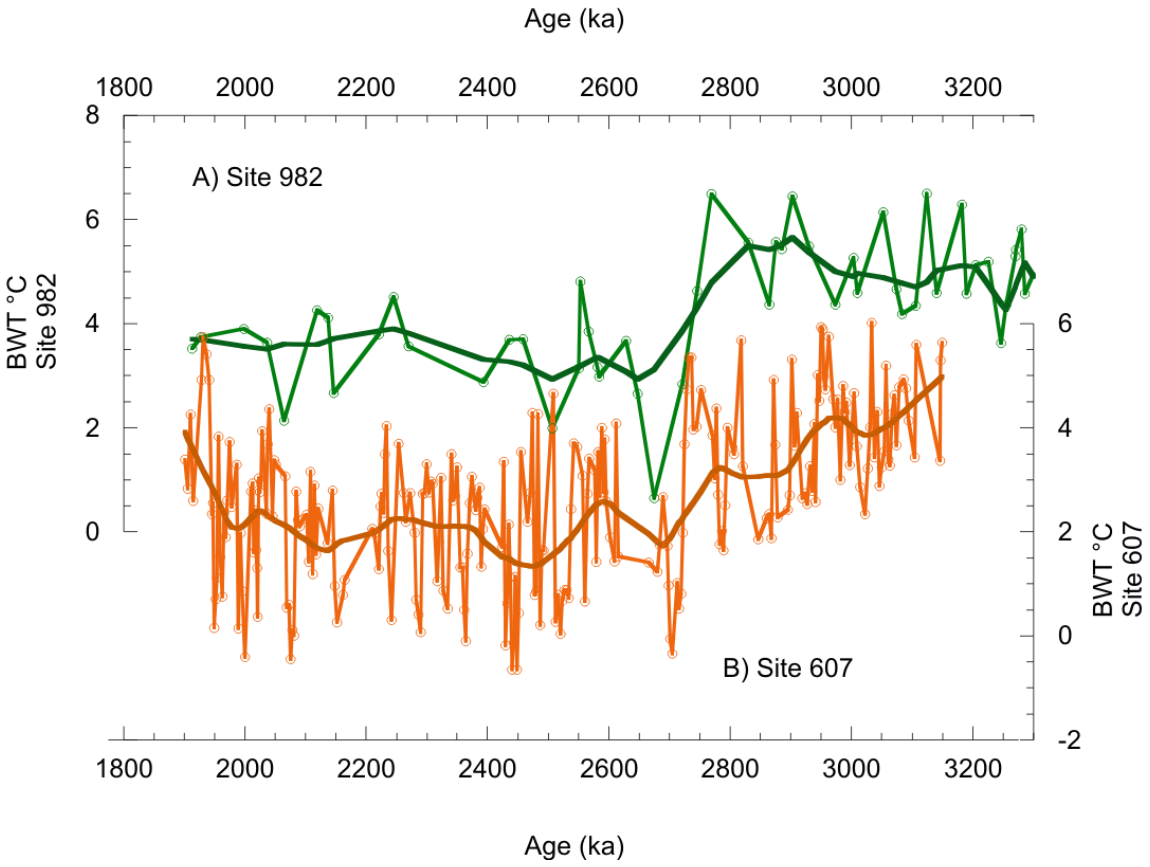


*Figure 4-8 Comparison between BWT derived from benthic Mg/Ca at A) Site 982 and B) Site 607. Heavy lines denote 100 ky weighted smoothing. Original Site 607 Mg/Ca data from Sosdian and Rosenthal 2009, using temperature calibration from this study.*

*Short term variability at Site 982*

Between 5200 and 4600 ka, a series of bottom water temperature lows occur synchronously with $\delta^{18}O_b$ highs, suggesting BWT variability as the dominant control on $\delta^{18}O_b$ at this time. This is consistent with expected lower ice sheet volume and variability in the early Pliocene compared to the late Pliocene/Pleistocene (de Boer et al. 2010). During this period, $\delta^{18}O_b$ has a mean of 2.78 ‰ and a range of 0.4 ‰. BWT for the same time period has a mean of 4.26 and a range of 0.8 °C. Ideally, these ranges would be ascribed to Glacial-Interglacial variability in BWT and $\delta^{18}O_b$, however the relatively low resolution of the Mg/Ca record precludes this level of detail. While lower BWT does corresponds with higher $\delta^{18}O_b$ (and vice versa) throughout the record as expected, a significant proportion of samples throughout the record are not

precisely at the $\delta^{18}O_b$ maximum or minimum, and so the full G-IG variability cannot be accurately stated. Nevertheless, the temperature ranges discussed in this section do reflect repeated warming and cooling cycles.

MIS M2 - a period of confirmed ice growth in the Northern Hemisphere (Kleiven et al. 2002) - is not characterised by a significant decrease in BWT at the same time as the positive $\delta^{18}O_b$ excursion (Figure 4-6). However, sea surface temperature records for the time indicate a prolonged regional cooling of ~ 3 °C between 3330 ka and 3283 ka (Lawrence et al. 2009; Naafs et al. 2010), and ostracod Mg/Ca derived BWT from the Atlantic show a smaller 1 °C cooling (Dwyer & Chandler 2009). A lack of bottom water cooling could suggest that during MIS M2, BWT and ice volume are not linked at site 982, or that this particular cold period was driven by different mechanisms than others where BWT cooling is seen.

During the Mid Pliocene Warm Period (3300-3000 ka), BWT and $\delta^{18}O_b$ variability are both higher than the early Pliocene, varying by 1.7 °C and 0.5 ‰ respectively. This would be consistent with a more variable climate than the early Pliocene, albeit one with a higher mean BWT of ~5 °C at Site 982. Immediately prior to the major cooling at 2800 ka, there is no trend towards cooling of BWT during warm periods or cold periods, indicating a variable but fundamentally static BWT. The increased variability suggests a destabilising climate prior to 2800 ka.

The variability in BWT and $\delta^{18}O_b$ does not change after the abrupt BWT cooling at 2800 ka, but remains the same. This is despite the decrease in mean BWT and the continued progressive increase in mean $\delta^{18}O_b$ values. The sudden decrease in BWT could therefore be considered a shift in global mean deep ocean temperatures that did not greatly affect G-IG variability. However, at the same time as this the BWT range at Site 607 did increase from 2 °C prior to the cooling, to 3.3 afterwards (Sosdian & Rosenthal 2009), which may mean Site 982 is not representative of variability in the whole ocean.

### 4.6.2 Sea surface temperature trends at Site 982

Sea surface temperatures for the period 2500-3300 ka were derived from Mg/Ca ratios of foraminifera G. bulloides (Section 2.10), covering the major cooling of the bottom

water at Site 982. Above 40 °N, this species records the April-June mean temperature signal (Elderfield & Ganssen 2000). A long term cooling of 3 °C is seen across the period, culminating in a 0.5 °C drop at the same time as the BWT cooling seen at Site 982 (2800-2700 ka).

Previously published SST estimates for Site 982 include the $Uk_{37}$ alkenone SST record of Lawrence (2009). At this latitude, this proxy is believed to reflect summer-early autumn SST, and the two records provide a way to compare the seasonality of the surface water temperature record. While the absolute value of G. bulloides derived SST is calibration dependent, the calibrations listed in Anand (2009) all give SST lower than that of $Uk_{37}$, consistent with a spring/summer signal, when sea temperatures are expected to be lower than summer/autumn. Both the *G. bulloides* and $Uk_{37}$ records show a general decrease in temperature across the period, and a sharper 3 °C decrease in SST at 2750 ka. The $Uk_{37}$ record shows an increase of 2 °C between 3000 and 2800 ka, which diverges from the steady decrease of the *G. bulloides* record. This may point to increasing seasonality and increasingly warm summer temperatures immediately prior to the cooling event at MIS G^, which is seen in both records at 2750 ka. Both SST records also show significant cooling at same time as the BWT record, suggesting SST and BWT are responding to similar forcings, however the SST decrease is roughly twice as large as the BWT decrease.

### 4.6.3 Links between IRD deposition and Sea Surface Temperatures

Ice rafted debris first occurs at Site 982 immediately after the SST and BWT cooling at 2800 ka, during MIS G6. Thereafter it is a constant presence, however significantly increased fluxes occur at several MIS stages. The presence or absence of IRD at this site is not directly indicative of the presence or absence of ice sheets in the North Atlantic region, as IRD is deposited as a result of melting icebergs. The position of this melting is dependent on their size and the temperature of the surrounding water, as well as the circulation patterns at the time. During the last glaciation, the zone of IRD deposition was just north of the polar front (Ruddiman 1977), and it is possible that during some cold periods the circulation patterns did not allow iceberg melting in the vicinity of Site 982. Aside from the initial IRD pulse at MIS G6, no IRD pulse occurs

when the SST is above 13 °C. This suggests a thermal threshold for IRD deposition at this site, but does not distinguish between if this temperature is linked to the location of the IRD deposition belt or regional iceberg production.

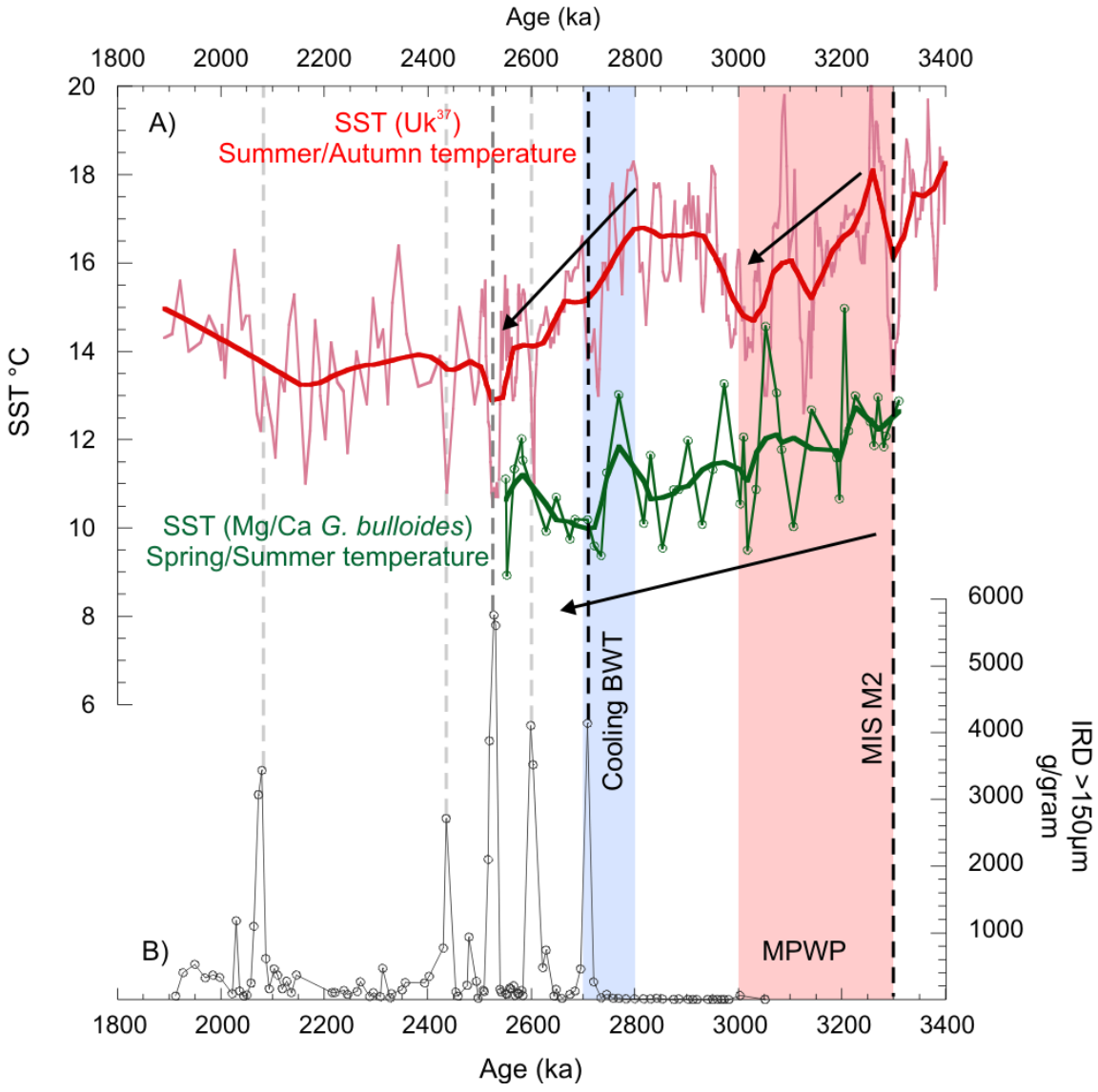


*Figure 4-9 SST trends for Spring/Summer and Summer/Autumn at Site 982, derived from $Uk_{37}$ (Lawrence et al. 2009) and Mg/Ca proxies respectively. B) IRD deposition at Site 982. Dashed lines extend IRD peaks across SST records. Mid Pliocene warm period is highlighted in pink, and the BWT cooling in blue. Arrows denote major trends in SST. Heavy line is a 100 ky weighted smoothing.*

## 4.7 Conclusion

The new Mg/Ca temperature calibration derived for the North Atlantic region produces BWT values in good agreement with previous independent studies of Mid Pliocene Warm Period BWT (Thomas M. Cronin et al. 2005; Dwyer et al. 1995) . These together confirm that the temperature of the MPWP bottom waters was similar to today, and that the deep Atlantic meridional temperature gradient was also similar. The larger temporal range of the record from Site 982 allows longer term evolution of BWT to be determined, and shows a warming trend towards the late Pliocene followed by a sudden bottom water cooling, coincident with the onset of IRD deposition. The cooling was preceded by increased variability in BWT, at the same time as cooling SSTs and increasing seasonal contrasts in the surface waters. This points towards a destabilising climate prior to the BWT cooling and IRD deposition at approximately 2800 ka, and suggests that while ice rafted debris may have appeared after 2800 ka, it may be possible that ice sheet growth began as far back as 3400-3600 ka.

# 5 Changes in global ice volume 5200-1900 ka.

## 5.1 Introduction

Previously published global ice volume reconstructions derived from combined Mg/Ca derived BWT and benthic foraminiferal ($\delta^{18}O_b$) estimates have been interpreted to show a gradual increase in global ice volume and hence decrease in eustatic sea level across the Late Pliocene Transition (LPT – 3000-2500 ka) (Sosdian & Rosenthal 2009). Comparison of global $\delta^{18}O_b$ records from Lisiecki & Raymo (2005) shows that the deep North Atlantic $\delta^{18}O_b$ records used by Sosdian and Rosenthal (2009) from ODP Site 607 are not representative of global trends in $\delta^{18}O_b$ during the key time period 3200-2800 ka (Section 4.3.2-3), leading to an underestimation of the magnitude of long term changes in the $\delta^{18}O$ value of seawater ($\delta^{18}O_{sw}$). This chapter presents long term (5200-1900 ka) $\delta^{18}O_{sw}$ records from ODP Site 982 in the North Atlantic which better record the global signal, and show a transient maxima in global ice volume at 2900 ka. This is then followed by an abrupt (~100 kyr) decrease in global ice volume to average levels consistent with previous reconstructions from 2700 ka onwards into the Pleistocene, such as Sosdian & Rosenthal, (2009). Evidence for ice sheet variability is assessed for both the Northern and Southern hemisphere ice sheets in an attempt to determine the location of the increased volume of continental ice and the cause of the subsequent decrease.

## 5.2 Pliocene changes in BWT, $\delta^{18}O_b$ and $\delta^{18}O_{sw}$ at Site 982

Independent proxies of BWT such as Mg/Ca ratios are required to deconvolve the changes in $\delta^{18}O_b$ associated with temperature and thus allowing $\delta^{18}O_{sw}$ to be estimated and ice volume variations to be assessed.

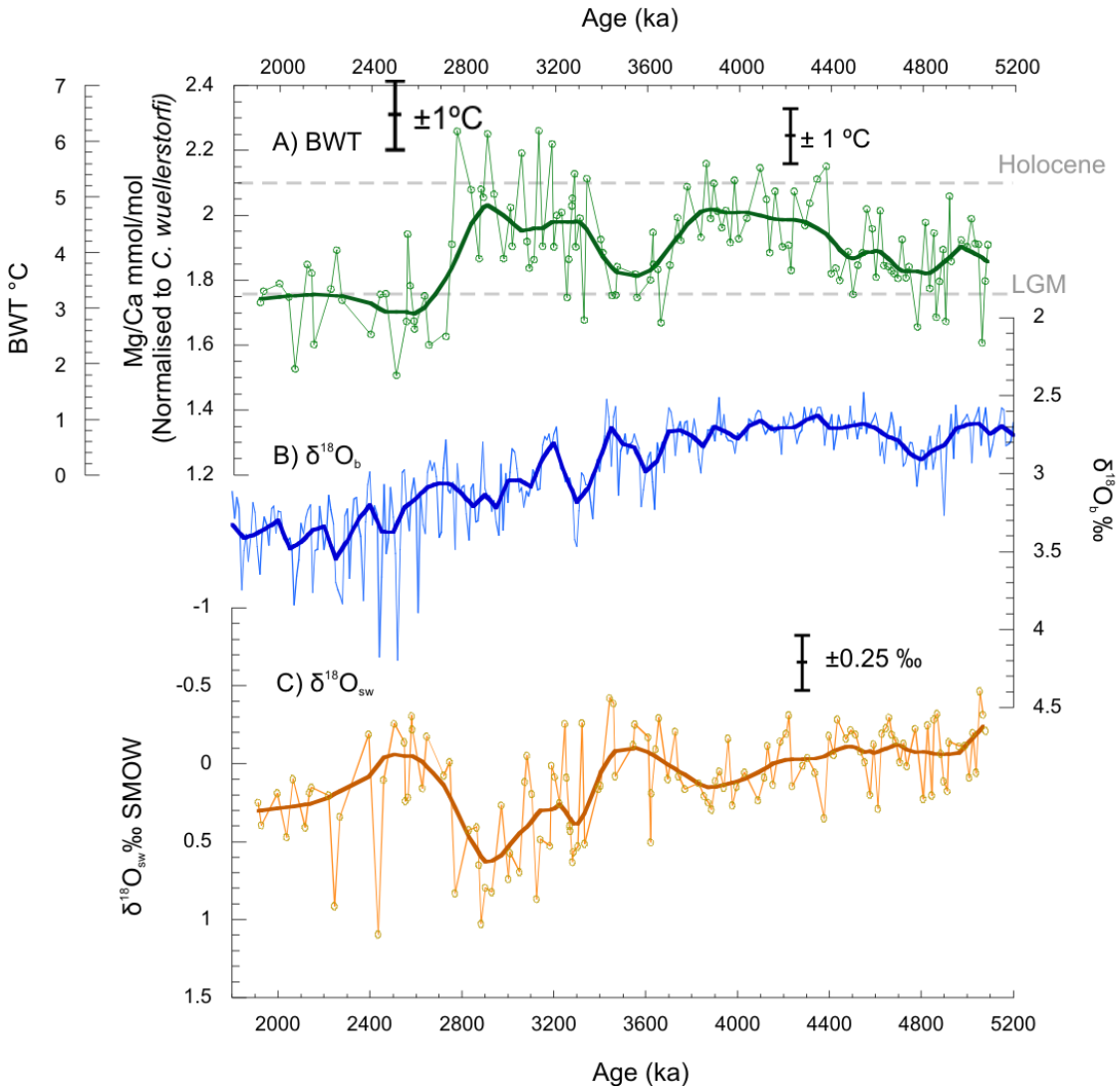


*Figure 5-1 Long term trends in bottom water temperature, δ18O and δ18Osw. A) Mg/Ca and BWT for Site 982. Calibration error (black bar) is approximately ±1°C. Dashed lines represent Holocene and LGM bottom water temperatures for Site 982 from Schlitzer (2013) and inferred from Adkins et al. (2002) respectively. B) Benthic δ18O for Site 982 from Venz & Hodell 2002; Lisiecki & Raymo 2005. C) Calculated δ18Osw for Site 982. Heavy line seen on all records is a ~100kyr weighted smoothing.*

The estimated $\delta^{18}O_{sw}$ using the above Mg/Ca BWT and $\delta^{18}O_b$ (Venz and Hodell 2002; Lisiecki and Raymo 2005) from ODP Site 982 show that prior to 3500 ka (Figure 5-1B) there was little long-term change in $\delta^{18}O_{sw}$, suggesting that the variations in $\delta^{18}O_b$ between 5000-4000 ka were controlled predominately by BWT, and any extant ice sheets exhibited small variability. After 3500 ka the $\delta^{18}O_{sw}$ increases from a background early Pliocene value of ~0.0 ‰, reaching a long term maximum of around ~0.55 ‰ at between 2750 and 3050 ka. In addition to the long term increase in $\delta^{18}O_{sw}$, short term variability increases to a maximum of ±0.4 ‰ about the long term trend.

The long term trend is of an amplitude greater than the uncertainty derived from the temperature and $\delta^{18}O_{sw}$ calibrations (± 0.25 ‰). There is then an <100 kyr decrease in $\delta^{18}O_{sw}$, from ~0.55 ‰ to an average of ~0.14 ‰ between 2700-1900 ka. The maximum potential $\delta^{18}O_{sw}$ decrease is a drop of up to 1 ‰ across a period of ~100 kyr. The average $\delta^{18}O_{sw}$ decrease of around 0.40 ‰, if entirely the result of changing ice volume, equates to an approximately 35m sea level increase. It is commonly held that the period 3000-2500 ka is a time of global cooling and ice sheet expansion in the northern hemisphere (Haug et al. 2005; Naafs et al. 2010; Flesche Kleiven et al. 2002), which is consistent with BWT cooling seen at ODP Site 982 and other North Atlantic sites, but not with a major decrease in ice volume that is potentially suggested by the ODP Site 982 $\delta^{18}O_{sw}$ record at this time.

## 5.3 Comparison of Site 982 $\delta^{18}O_{sw}$ to that of other sites – a global or local signal?

To determine whether the observed long-term trends observed in the ODP Site 982 $\delta^{18}O_{sw}$ are recording a global or local signal, the record is compared to other existing Pliocene reconstructions of $\delta^{18}O_{sw}$. ODP Site 548 (48°54'N, 12°09'W, 1250 m water depth) is located in the northeast Atlantic on the continental margin. Combined high resolution Mg/Ca based BWT and $\delta^{18}O_b$ records from this site suggest an increase in $\delta^{18}O_{sw}$ between 3500 and 3300 kyr (Khelifi et al. 2009) (Figure 5-3), which the authors suggest reflects the influence of an increasingly saline Mediterranean Outflow Water (MOW). This is because the ODP Site 548 BWT and $\delta^{18}O_{sw}$ records show similar trends to those observed in Western Mediterranean ODP Site 978 (Khelifi et al. 2009). Furthermore, the bottom water neodymium signal ($\varepsilon_{nd}$) values for the Pliocene Site 548 (-10) more closely resemble that of modern Western Mediterranean Deep Water (-9) than that of North Atlantic water masses such as the Labrador Sea Water (-12).

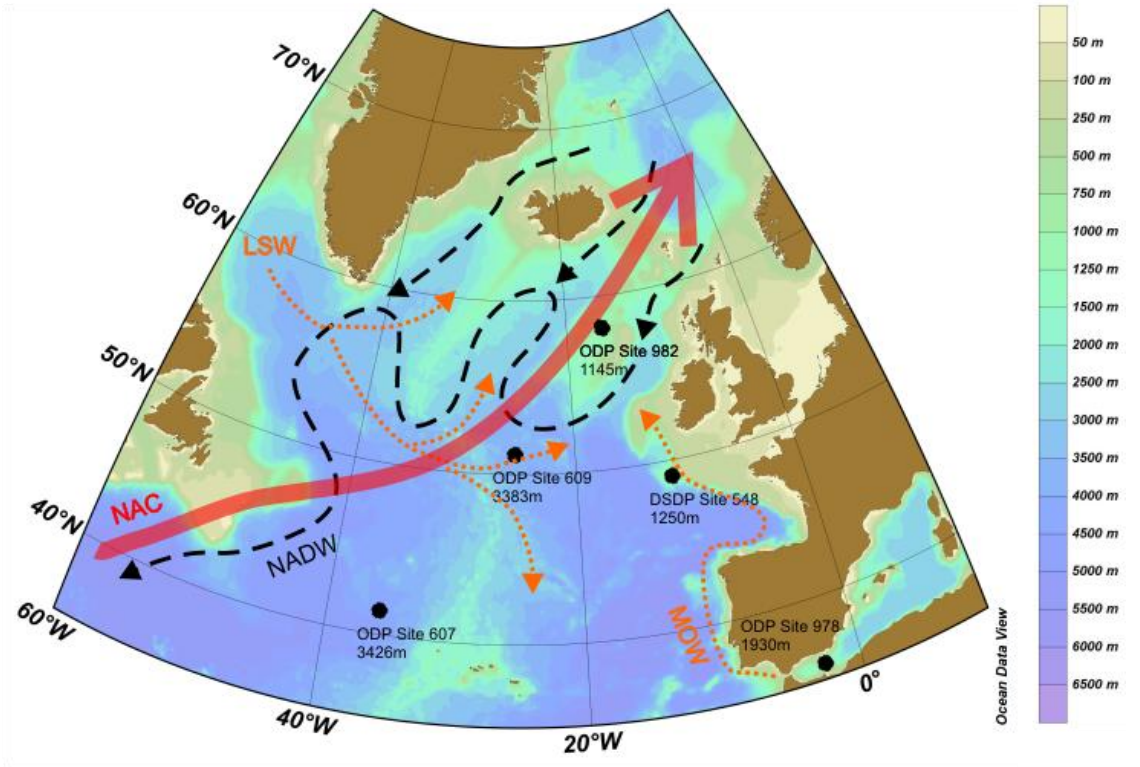


*Figure 5-2 North Atlantic sites with high resolution Mg/Ca bottom water records. Major North Atlantic Water masses are shown. Surface water mass North Atlantic Current (NAC) in red, intermediate depth water masses Labrador Sea Water (LSW) and Mediterranean Outflow Water (MOW) in orange, and North Atlantic Deep Water in black. Map made using Ocean Data View.*

While the Mg/Ca values at ODP Sites 982 and 548 are similar, the absolute temperatures reconstructed in this study and by Khelifi et al. (2009) respectively are quite different due to the differing calibrations employed. Khelifi et al. (2009) used the calibration of Elderfield et al. (2006) as it estimates BWT that are very similar to that of modern MOW (8-10°C), and this is the dominant water mass they believe was influencing ODP Site 548. However, recalibrating the ODP Site 548 Mg/Ca data from Khelifi et al. (2009) using the calibration developed in this study for ODP Site 982 (see Chapter 3), which is believed to be representative of the Pliocene North Atlantic, gives a BWT of ~4.5 °C for the period 3300-3000 ka, which is close to those observed at ODP Site 982, and absolute values and trends of $\delta^{18}O_{sw}$ that are in general agreement with those from ODP Site 982 (Figure 5-3).

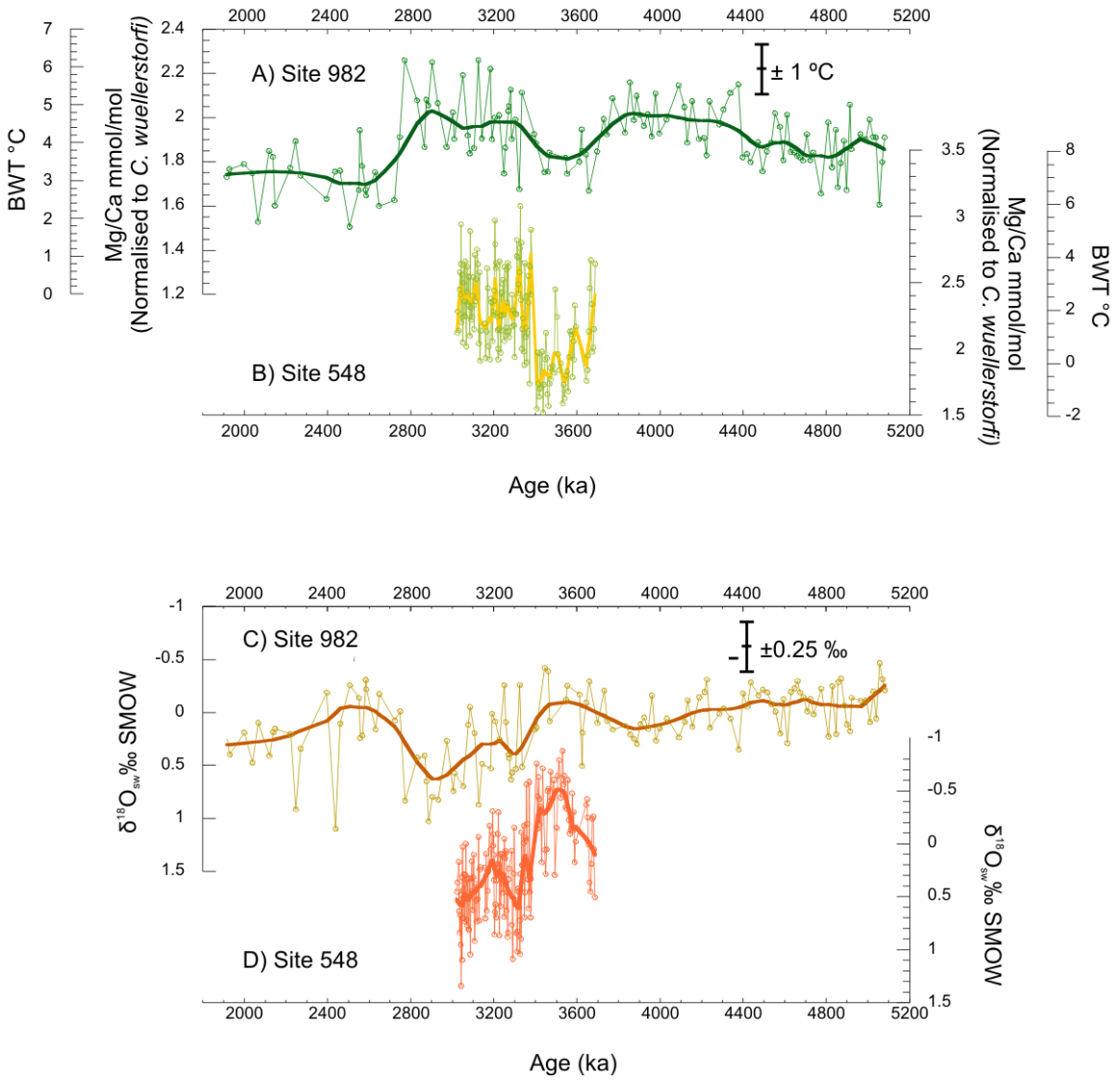


*Figure 5-3. Mg/Ca and $\delta^{18}O_{sw}$ for Sites 982 and 548. A) Mg/Ca and BWT for Site 982 B) Mg/Ca and BWT for Site 548, using the temperature calibration derived in Chapter 3. C) $\delta^{18}O_{sw}$ for Site 982 D) $\delta^{18}O_{sw}$ for Site 548. North East Atlantic Site 548 Mg/Ca and $\delta^{18}O$ for calculation of $\delta^{18}O_{sw}$ taken from Khélifi et al. (2009). Heavy line seen on all records is an ~ 100kyr weighted smoothing.*

The $\delta^{18}O_{sw}$ increase between 3500 and 3000 ka observed at ODP Site 982 is therefore also seen at ODP Site 548. As Khelifi et al. (2009) suggest for ODP Site 548, both sites could simply be recording relative proportions of the regional North Atlantic response to changes in MOW salinity and not related to a global $\delta^{18}O_{sw}$ shift, which would imply a change in global ice volume. While this is possible, it should also be noted that the Site 548 record clearly shows an increase in $\delta^{18}O_{sw}$ concurrent with MIS M2, the global $\delta^{18}O_b$ isotope excursion associated with the first occurrence of ice rafted debris in the

North Atlantic (Flesche Kleiven et al. 2002; Jansen et al. 2000). Therefore, at least part of the $\delta^{18}O_{sw}$ shifts seen at Site 548 and Site 982 reflects global trends in $\delta^{18}O_{sw}$. In order to determine the global magnitude of the 3300-3000 ka $\delta^{18}O_{sw}$ shift seen in ODP Sites 548 and 982 it is necessary to further compare the records with far-field Sites that are removed from any potential MOW influence.

There are currently only two other high resolution Mg/Ca derived BWT records for the Pliocene, and both are from the deep North Atlantic, beyond the direct influence of the MOW, which currently only ventilates the intermediate depth water mass in the northeast Atlantic (Reid 1979). Mg/Ca BWT values from ODP Site 607 (41°N, 32°W; water depth 3427m) (Sosdian & Rosenthal 2009) and ODP Site 609 (49.528N, 24.148W, water depth 3883m) (Bartoli et al. 2005) both show a similar trend of warmer early Pliocene BWT and a significant cooling after 2800 ka. The BWT decrease in ODP Site 609 starts at approximately 3000 ka, around 200 kyr earlier than observed in ODP Site 982 and 607 (which are synchronous), and is much less abrupt. The BWT record for ODP Site 609 was constructed using a suite of species-specific temperature calibrations for the multiple species employed in the reconstruction of the composite record. In comparison both ODP Sites 982 and 607 BWT estimates are based on mono-specific benthic foraminiferal reconstructions. The estimate of $\delta^{18}O_{sw}$ from the BWT and $\delta^{18}O_b$ of the deep Sites ODP 607 and 609 shows that neither record exhibits the clear increase in $\delta^{18}O_{sw}$ seen at the intermediate depth sites between 3500 and 3000 ka, or the abrupt decrease at 2800-2600. Indeed, ODP Site 607 shows more stable $\delta^{18}O_{sw}$, with average values for the mid-Pliocene Warm Period (3150-3000 Ka) of ~0.23‰. The $\delta^{18}O_{sw}$ for the post-cooling period is lower by around 0.1‰, at 0.33‰.

Aside from the period 3500-3000 ka, the average $\delta^{18}O_{sw}$ increase at site 982 from 5000-4000 ka to 2700-1900 ka is approximately 0.21‰. The average increase in $\delta^{18}O_{sw}$ of 0.1‰ at Site 607 between 3150 and 2700 ka is significant when compared to that of the longer term increase at Site 982. It is possible that if the record of Site 607 were extended back past 3150 ka, it would record a larger increase in $\delta^{18}O_{sw}$, similar to that seen at Site 982. In that case, the start and end points of the two contradicting records would be in agreement, and the period 3500-3000 ka at site 982 could be considered a

local anomaly and not representative of global $\delta^{18}O_{sw}$ values. The 3150 - 2800 period of the Site 607 record is particularly important to this study as it may represent the global long term deep ocean $\delta^{18}O_{sw}$ trend.

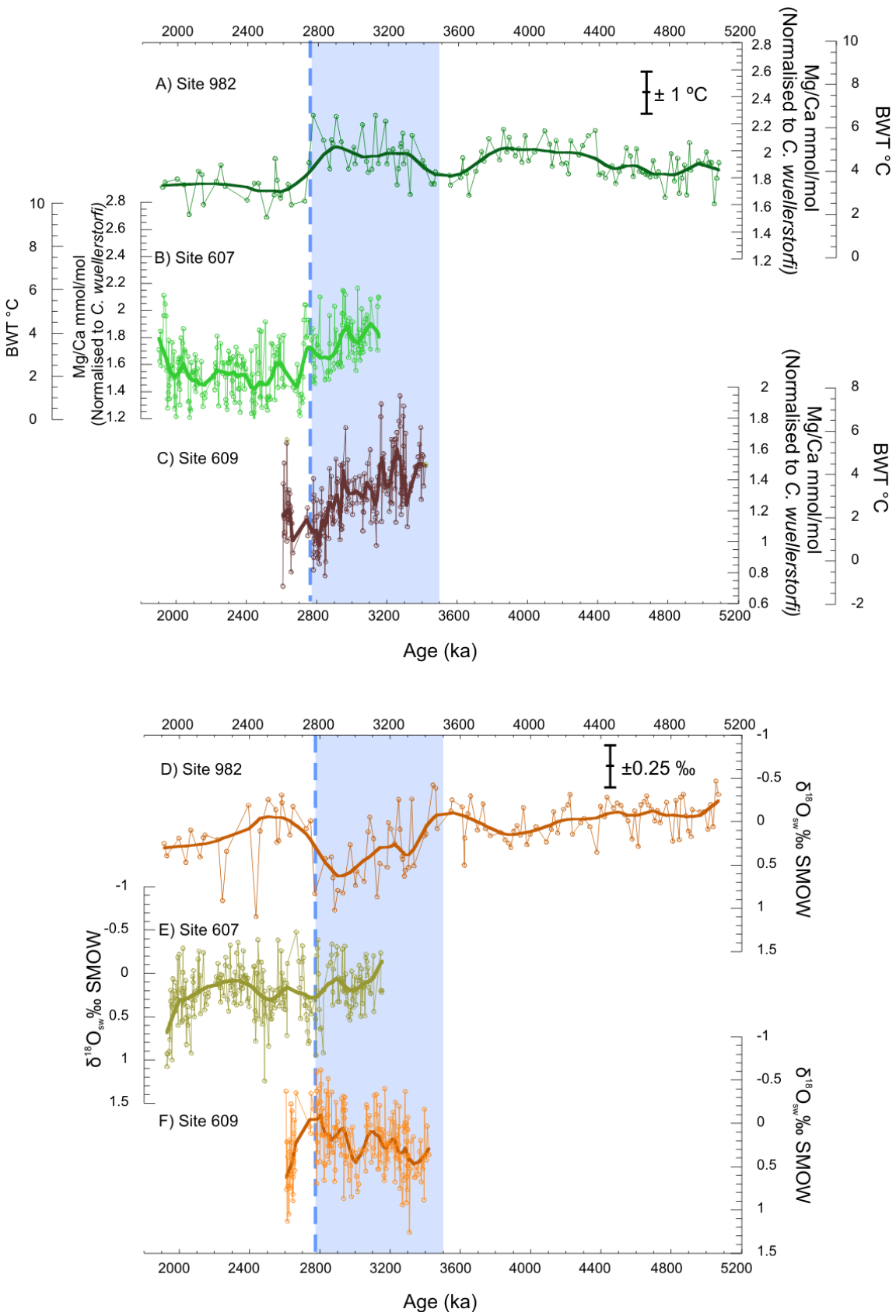


*Figure 5-4 Mg/Ca and $\delta^{18}O_{sw}$ for Sites 982, 607 and 609. A) Mg/Ca and BWT for Site 982 B) Mg/Ca and BWT for Site 607 C) Mg/Ca and BWT for Site 609 D) $\delta^{18}O_{sw}$ for Site 982. E) $\delta^{18}O_{sw}$ for Site 607 F) $\delta^{18}O_{sw}$ for*

*Site 609. BWT for all sites is calculated from Mg/Ca using calibration derived in Chapter 3. Mg/Ca and $\delta^{18}O_b$ for calculation of $\delta^{18}O_{sw}$ taken from Sosdian & Rosenthal (2009) for Site 607, and Bartoli et al. (2006) for Site 609. Heavy line seen on all records is an ~100kyr weighted smoothing.*

### 5.3.1 Determining the global extent of the $\delta^{18}O_{sw}$ shifts seen in the North Atlantic

During the period 3500-2800 ka, Pliocene deep North Atlantic reconstructions of $\delta^{18}O_{sw}$ (ODP Sites 607 and 609) do not show similar trends to those from the intermediate depth North Atlantic (ODP Sites 982 and 548), or the Western Mediterranean (ODP Site 978). Therefore, one or both of these sets of records do not accurately reflect global changes. Global changes in ice volume affect all parts of the deep ocean equally, resulting in geographically distant $\delta^{18}O_b$ records that covary throughout the glacial-interglacial changes of the past 3 million years (Lisiecki and Raymo 2005). Site specific deviations from the global average $\delta^{18}O_b$ record indicate changes in $\delta^{18}O_b$ driven by local changes in temperature or salinity. Without global records of temperature or $\delta^{18}O_{sw}$ to provide absolute values, comparison of globally distributed $\delta^{18}O_b$ records allows an initial examination of whether the records of Site 982 can be considered globally representative.

Although the global stack of $\delta^{18}O_b$ records produced by Lisiecki and Raymo (2005) (the LR04 stack) could be used as a comparison for the North Atlantic sites it would be rather circular as (i) ODP Sites 982 and 607 are both key sites in the Pliocene section of the LR04 Stack and (ii) there are fewer sites comprising the Pliocene section in comparison to the Holocene/late Pleistocene. Therefore, ODP Sites 982 and 607 exert a significant influence on the global average $\delta^{18}O$ composition as recorded in LR04. In comparison, ODP Site 846 is situated in the East Pacific (3°06`S, 90°49`W, 3296 m water depth) and is not affected by water masses from the North Atlantic, (Hodell & Venz-Curtis, 2006). As such, any regional influences on North Atlantic Sites such as changes in the salinity of the MOW will have no impact on this site. Therefore, a consistent $\delta^{18}O_b$ gradient ($\Delta\delta^{18}O$) between the East Pacific and the North Atlantic would suggest that the regions were responding equally to global shifts in $\delta^{18}O_{sw}$, whereas a change in the $\Delta\delta^{18}O_b$ would suggest either local temperature or $\delta^{18}O_{sw}$ changes were affecting one or both records.

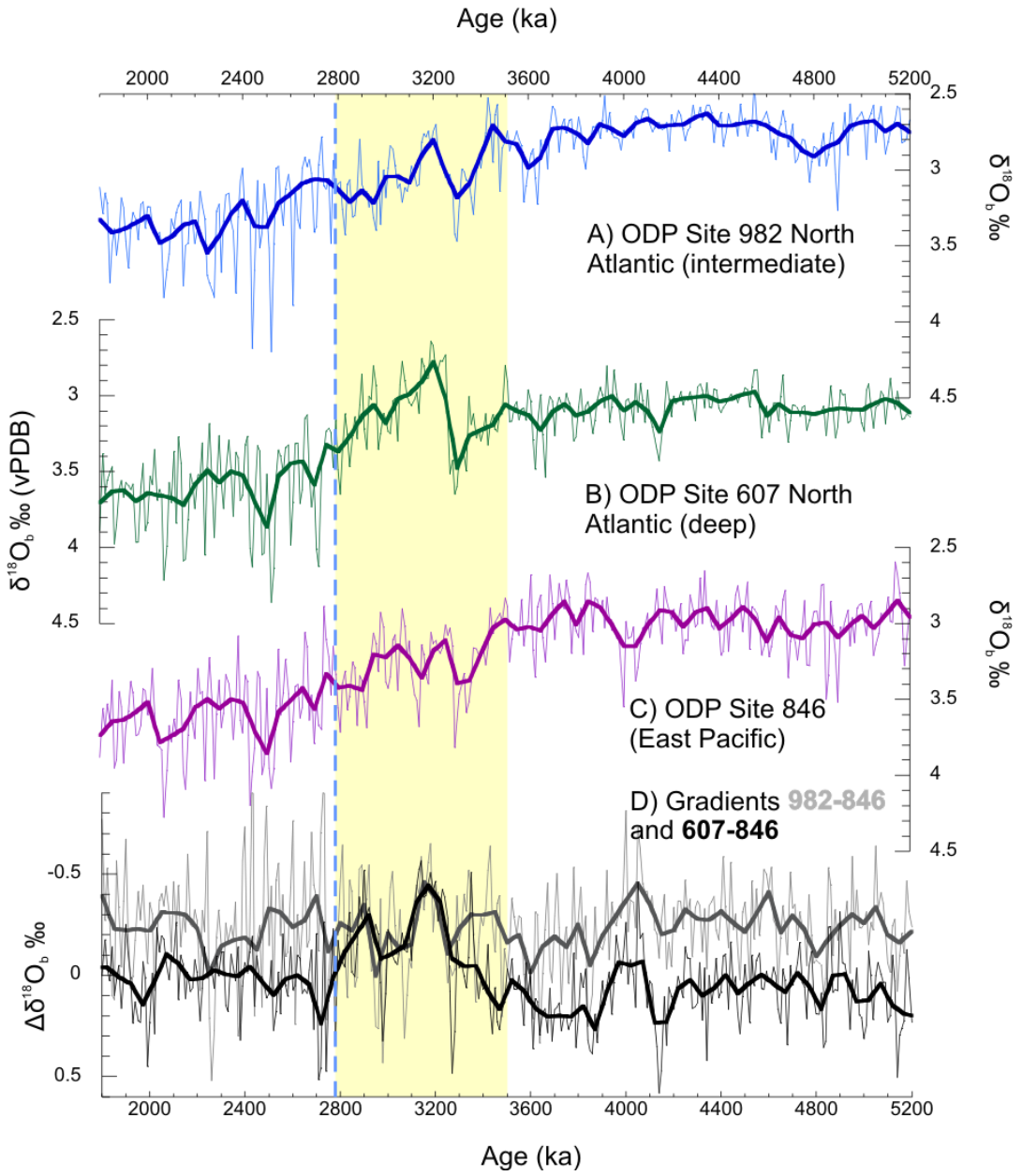


*Figure 5-5. Benthic $\delta^{18}O_b$ and $\Delta\delta^{18}O_b$ between Atlantic and Pacific sites for North Atlantic Site 607 and 928, and East Pacific Site 846. A) $\delta^{18}O_b$ for 982 B) $\delta^{18}O_b$ for Site 607 C) $\delta^{18}O_b$ for Site 846 All $\delta^{18}O$ data from Lisiecki & Raymo (2005) and references therein D) Gradient 982-846 and 607-846. Yellow area highlights $\delta^{18}O_{sw}$ anomaly, blue line BWT cooling at 2800 ka. Heavy line seen on all records is a ~100kyr weighted smoothing.*

The long-term $\Delta\delta^{18}O_b$ gradient between ODP Sites 982 and 846 (Figure *5-5*) has a relatively constant offset of around -0.18‰ between 5000 and 2000 ka, consistent with Site 846 being colder than Site 982, similar to the modern ocean. This offset is occasionally punctuated by decreases in the gradient, driven by higher $\delta^{18}O_b$ values in the Atlantic, however these are transient and in some cases mirrored in the ODP Site

607-846 $\Delta\delta^{18}O_b$. After 2000 ka, the gradient becomes less consistent, as a result of an increasingly variable North Atlantic $\delta^{18}O_b$.

The $\Delta\delta^{18}O_b$ between ODP Site 607 and Site 846 does not exhibit a constant offset throughout the record. Between 5000-3500 ka, the gradient is near zero, and the short term changes in the gradient mirror those in the ODP Site 982-846 $\Delta\delta^{18}O_b$. However, at 3300 ka, the gradient drops by ~0.3‰ to overlap with that of the ODP Site 982-846 gradient, before returning to the previous offset at around 2750 ka. This is caused by a prolonged 300 ky decrease in $\delta^{18}O_b$ at ODP Site 607, relative to both ODP Sites 982 and 846. This shift is also unseen at other sites in the deep North Atlantic, including Site 609 (3383m water depth) or Site 610 (2420m), both sites that should be affected by similar water masses to Site 607. Similarly, the pattern continues in the South Atlantic where intermediate Site 1088 (2082m) and deep Sites 1090 (3702), 925 (3040m), and 927 (3330m) do not show the shift.

### 5.3.2 Cause of the $\delta^{18}O_b$ shift at ODP Site 607

The $\delta^{18}O_b$ value of any given data point is a result of two factors – bottom water temperature and the $\delta^{18}O$ value of seawater. $\delta^{18}O_{sw}$ is in turn controlled by the salinity of the water mass (Urey, 1948). Sites 607 and 982 have very similar BWT profiles but different $\delta^{18}O_{sw}$ profiles during the period of concern (3500 - 2800 ka). The period of high $\delta^{18}O_{sw}$ at Site 982 between 3500 and 2800 ka increases $\delta^{18}O_b$ values across this time period, in contrast with the absence of high $\delta^{18}O_{sw}$ at Site 607, which lowers $\delta^{18}O_b$ values by approximately 0.5‰ (Sosdian & Rosenthal 2009). The result of this is an apparently significant shift in the $\delta^{18}O_b$ record at Site 607, whereas the major change in water mass properties is in fact an increase and subsequent decrease in $\delta^{18}O_{sw}$ at Site 982. The increase and subsequent decrease in $\delta^{18}O_{sw}$, combined with the stable BWT of the period cancel each other out, resulting in a smooth $\delta^{18}O_b$ trend, in contrast to that of Site 607.

The period of lowered $\delta^{18}O_b$ at Site 607 is shorter by 200 ky than that of the increase in $\delta^{18}O_{sw}$ at Site 982 (3300-2800 ka compared to 3500-2800 ka), and starts at its greatest extent immediately after MIS M2. The total decrease from the middle of MIS M2 to

the maximum extent of the period immediately after is 0.77 ‰. This period is not covered by the Mg/Ca BWT record from Site 607, so it is not possible to directly determine what proportion of this is a temperature or a $\delta^{18}O_{sw}$ derived effect. If the whole shift was driven by temperature changes, the shift would be equivalent to around 3 °C of warming. While deep ocean warming is not unexpected after a glacial period, no increase in BWT approaching this size is seen at sites where BWT records exist. These sites – North Altantic Sites 609, 982, and 548 - as well as distant sites such as Site 1090 in the South Atlantic and Sites 846 and 1143 in the Pacific also show a smaller $\delta^{18}O_b$ decrease of ~0.5‰. The water mass at Site 607 appears to have either warmed or freshened more than the general trend seen at other sites. This leads to the conclusion that in the case of the exit from MIS M2, Site 607 is considered not representative of the global trend, and that Site 982 is considered to more accurately represent global changes in $\delta^{18}O_{sw}$ during the period of this study. The reason for the apparent warming/freshening at Site 607 is not known, but may be the result of the water at Site 607 being temporarily sourced from a region that has significantly different $\delta^{18}O_{sw}$ values to the source water of the other sites. This would alter the preformed $\delta^{18}O_{sw}$, and result in an apparent shift.

### 5.3.3 Hypothetical global trends in BWT and $\delta^{18}O_{sw}$

For the global $\delta^{18}O_b$ trend in the LR04 stack to reflect that of Site 982 as observed, one of two scenarios must have occurred:

1. *The evolution of BWT and $\delta^{18}O_{sw}$ globally must have followed that of Site 982, with BWT remaining stable across the period 3500-2800 ka then cooling, and $\delta^{18}O_{sw}$ increasing from 3500-2800 ka then decreasing at 2800 ka. This scenario is consistent with the $\delta^{18}O_{sw}$ increase and decrease at Site 982 representing a global excursion and an inferred increase in ice volume from 3500 ka to 2800 ka followed by a smaller decrease from 2800-2700 ka.*

Or, conversely

2. *The global evolution of BWT and $\delta^{18}O_{sw}$ must significantly differ from that of Site 982, but in such a way that maintains the generally stable inter site $\delta^{18}O_b$ gradients. This would be characterised by a gradual increase in local salinity at each site balanced with a gradual decrease in BWT throughout the period 3500-2800 ka. This scenario suggests that the $\delta^{18}O_{sw}$ record at 982 between 3500 and 2800 ka is dominated by MOW waters and is not globally representative.*

The hypothesis introduced by Scenario 2 - of a gradual, globally consistent decrease in BWT at different sites - implies that water masses in the southern hemisphere Atlantic ocean would show a gradual decline in bottom water temperature between 3500-2800 ka, in contrast to the relatively abrupt decline seen at North Atlantic site 607 and 982 at 2800 ka.

Reconstructions of NADW based on $\delta^{13}C$ records suggest a particularly strong NADW during the mid-late Pliocene between 3500 and 2800 ka (Discussion in Chapter 5 and Hodell & Venz-Curtis 2006; Kwiek & Ravelo 1999; Billups et al. 1998), and southward penetration of NADW similar to or greater than the modern system. Therefore, latitudinal temperature gradients in the Atlantic basin would also appear similar to the modern system, as Southern Atlantic locations were sited in NADW sourced waters. This is supported by Ostracod Mg/Ca derived bottom water temperatures from 3300-2970 ka, which show similar values to modern records (Cronin et al. 2005 and discussion in Chapter 3). This reconstruction of the temperature structure of the deep Atlantic requires Southern Atlantic sites to follow the same temperature evolution as that of the Northern Atlantic sites throughout the Pliocene, and supports Scenario 1 in that Site 982 could be considered representative of a global trend.

The hypothesis introduced by Scenario 2 - of a gradual, globally consistent decrease in BWT at different sites – further implies that deep water masses in the Pacific and Indian ocean would also show a gradual decline in bottom water temperature, as well as in the Atlantic. Distant deep water masses such as those at Site 846 show the same $\delta^{18}O_b$ profile as Site 982. However, outside the Atlantic there are no high resolution Pliocene BWT reconstructions meaning it is not possible to directly reconstruct the

trend in the interbasinal BWT gradient if any, or to determine whether the Pacific sites show a $\delta^{18}O_{sw}$ evolution similar to Site 982. Some Pacific deep water Ostracod derived Mg/Ca BWT data are included within the PRISM3D global data set of (H. J. Dowsett et al. 2009), and suggest a Atlantic - Pacific inter site temperature gradient of approximately 2 °C

BWT reconstructions across the Mid Pleistocene transition do show a different response to the Pliocene climate: Atlantic sites show a 1 degree cooling while the Pacific shows no temperature change during a period of intensification of glaciation (Elderfield et al. 2012; Sosdian & Rosenthal 2009). Similarly, BWT trends between the LGM – Modern are significantly different in the Atlantic and Pacific basins (Adkins et al. 2002). North Atlantic water masses are ~ 4 C cooler during the LGM whereas the Pacific site water mass only cools by ~ 2.5 C. This may suggest that the water mass in the North Atlantic is more sensitive to climatic shifts than that of the Pacific.

Both of these examples demonstrate a different BWT response to climatic change in the Pacific to that of the Atlantic, which would suggest that Atlantic BWT cannot be used to infer global BWT trends. However, the initial conditions of the situation 3500-2800 ka are significantly different to those of the Modern-LGM transition or the Mid-Pleistocene transition. In particular, the Mid-Pleistocene transition marks a major change in the dominant periodicity of ice sheets from low-amplitude 41 ky cycles to higher amplitiude 100 ky cycles, (Sosdian & Rosenthal 2009) possibly as a result of interactions between the ice sheet and the bedrock (Bailey et al. 2010); a distinctly different situation than during the late Pliocene when ice sheets were first forming, and so the situations are not necessarily comparable.

*Inferring Atlantic-Pacific BWT and $\delta^{18}O_{sw}$ gradients.*

Modern values for BWT, $\delta^{18}O_{sw}$ and $\delta^{18}O_b$ are shown in Table 5-1. The Pliocene $\delta^{18}O_b$ gradient is smaller than the modern (0.18‰ and 0.5‰ respectively), suggesting a smaller temperature/$\delta^{18}O_{sw}$ contrast between the two sites, but with Site 846 remaining cooler. Dividing the period 5200-1900 ka into three sub-periods (5200-3500, 3500-2800, and 2800-1900) and scaling the modern gradients in temperature, salinity

and $\delta^{18}O_{sw}$ to the observed Pliocene $\delta^{18}O_b$ gradient allows hypothetical values for Site 846 to be inferred from average values at Site 982 for each time period (Table 5-2 and Figure 5-6). The 5200-3500 ka (A) and 2900-1900 ka (C) solutions are the start and end points, and two different solutions for the period 3500-2800 ka are shown on Figure 4-6 (B and B') based on the different scenarios for global evolution of BWT outlined at the start of this section.

| | **Site 982** | **Site 846** | **Gradient 982-846** |
|---|---|---|---|
| **BWT °C** | 5.38 | 1.79 | 3.59 |
| **Salinity (psu)** | 34.95 | 34.68 | 0.27 |
| **$\delta^{18}O_b$ ‰** | 2.88 | 3.38 | 0.5 |

*Table 5-1 Measured modern BWT, Salinity and $\delta^{18}O_b$ for Site 982 and Site 846. Data from eWOCE data set.*

The inferred Site 846 values shown as 'ABC' on Figure 5-6 assume a constant inter site gradient in temperature across the period 5200-2800 ka, as derived from the stable $\delta^{18}O_b$ gradient and assumed stable pattern of global circulation (Kwiek & Ravelo 1999). To maintain the $\delta^{18}O_b$ gradient therefore requires a change in $\delta^{18}O_{sw}$ at Site 846 that matches that at Site 982. They also assume no changes in the inter site temperature gradients across the global cooling and decrease in NADW production seen at 2800 ka (Hodell & Venz-Curtis 2006). This last point is not necessarily an accurate assumption, as decreased NADW input to the Pacific would likely result in different inter-basinal gradients. The absolute values of Site 846 point C are therefore not certain. Nevertheless, in the absence of any direct records they provide a useful starting point.

*Figure 5-6 (Overleaf) Top: Hypothetical bottom water temperature trends and Bottom: inferred BWT and $\delta^{18}O_{sw}$ solutions for Pacific site 846 relative to Site 982. The $\delta^{18}O_b$ isolines calculated for Site 846 assume a constant 846-982 $\delta^{18}O_b$ gradient of 0.18 ‰, and plot the range of temperature and $\delta^{18}O_{sw}$/Salinity values that fulfil this gradient. They use the paleotemperature equation of Shackleton (1974) and a $\delta^{18}O_{sw}$:S relationship of $\delta^{18}O_{sw}$ = 0.49xS-17.126, derived from the modern Pacific $\delta^{18}O_{sw}$:S relationship. Density isolines are calculated for a depth of 3300m. Site 982 data is represented by circles, and is the mean BWT and $\delta^{18}O_{sw}$/Salinity for the marked periods.*

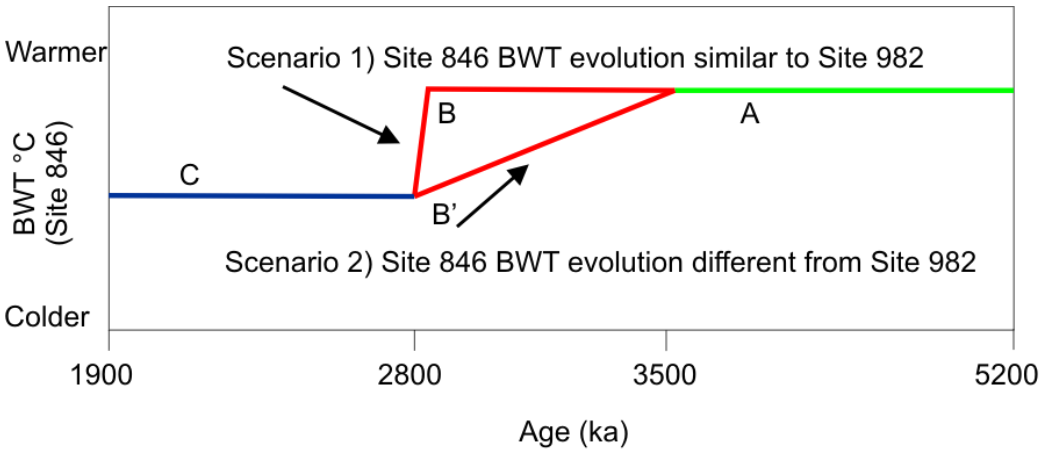
Warmer
Scenario 1) Site 846 BWT evolution similar to Site 982
B
A
C
B'
BWT °C (Site 846)
Scenario 2) Site 846 BWT evolution different from Site 982
Colder
1900
2800
3500
5200
Age (ka)

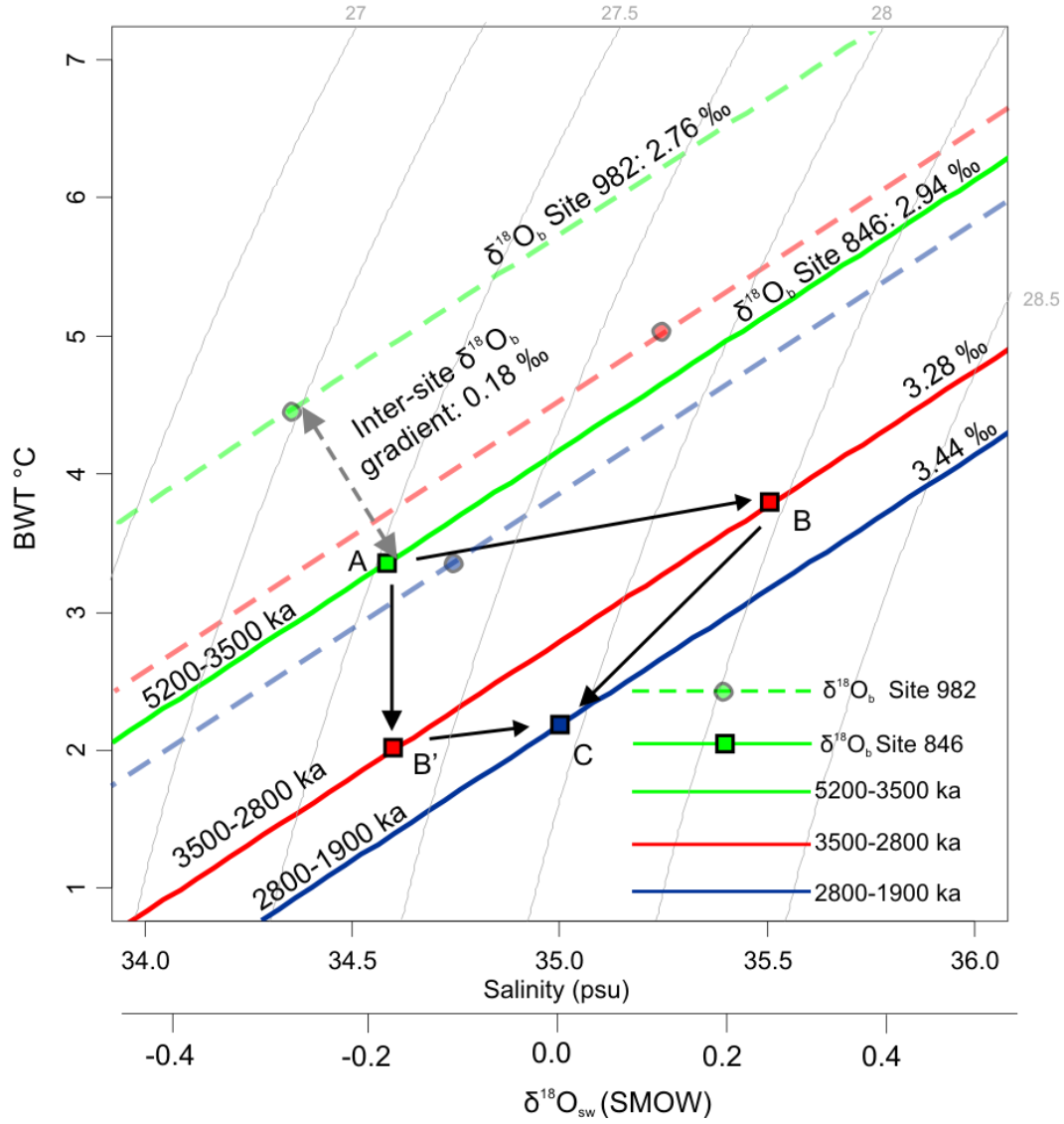
27
27.5
28
28.5
δ18Ob Site 982: 2.76 ‰
δ18Ob Site 846: 2.94 ‰
Inter-site δ18Ob gradient: 0.18 ‰
3.28 ‰
3.44 ‰
5200-3500 ka
3500-2800 ka
2800-1900 ka
A
B
B'
C
δ18Ob Site 982
δ18Ob Site 846
5200-3500 ka
3500-2800 ka
2800-1900 ka
BWT °C
1
2
3
4
5
6
7
34.0
34.5
35.0
35.5
36.0
Salinity (psu)
-0.4
-0.2
0.0
0.2
0.4
δ18Osw (SMOW)

| | | | Scenario 1) Site 846 follows Site 982 at a constant gradient. | | Scenario 2) Site 846 does not follow Site 982. | |
|---|---|---|---|---|---|---|
| | | **Site 982 (mean for period)** | **Site 846 (ABC)** | **Gradient between 982-846** | **Site 846 (AB'C)** | **Gradient between 982-846** |
| **5200-3500 ka** | **BWT °C** | 4.51 | 3.22 | 1.29 | - | - |
| | **Salinity (psu)** | 34.35 | 34.25 | 0.10 | - | - |
| | **$\delta^{18}O_b$ ‰** | 2.76 | 2.94 | 0.18 | - | - |
| | **$\delta^{18}O_{sw}$ ‰** | -0.07 | 0.04 | 0.11 | - | - |
| **3500-2800 ka** | **BWT °C** | 5.08 | 3.79 | 1.29 | 2.05 | 3.00 |
| | **Salinity (psu)** | 35.24 | 34.14 | 0.10 | 34.25 | 0.99 |
| | **$\delta^{18}O_b$ ‰** | 3.10 | 3.28 | 0.18 | 3.28 | 0.18 |
| | **$\delta^{18}O_{sw}$ ‰** | 0.41 | 0.52 | 0.11 | 0.04 | 0.37 |
| **2800-1900 ka** | **BWT °C** | 3.35 | 2.06 | 1.29 | - | - |
| | **Salinity (psu)** | 34.74 | 34.64 | 0.10 | - | - |
| | **$\delta^{18}O_b$ ‰** | 3.26 | 3.44 | 0.18 | - | - |
| | **$\delta^{18}O_{sw}$ ‰** | 0.14 | 0.25 | 0.11 | - | - |

*Table 5-2 Average of data (Site 982) and inferred (Site 846) BWT, Salinity, $\delta^{18}O_b$ and $\delta^{18}O_{sw}$ for 3 time periods of the Plio-Pleistocene. 5200-3500 and 2800-1900 periods assume constant offset in BWT and $\delta^{18}O_{sw}$ between Site 982 and Site 846 and have same values for both Scenarios.*

Also shown on Figure 5-6 is an alternative solution for Site 846 during the Pliocene that *does not* require a $\delta^{18}O_{sw}$ increase of the same size as at Site 982 (AB'C). This refers to Scenario 2, and provides an example of global trends where the $\delta^{18}O_{sw}$ increase and subsequent decrease at Site 982 is a phenomenon local to the intermediate depth NE Atlantic. In this scenario, BWT at Site 846 cools gradually from around 3.86 °C at 3600 ka to 2.13 °C by 2700 ka, which requires an increase of the temperature gradient between the persistently warm Atlantic and the 'cooling' Pacific of at least 3 °C*(Table 5-2*). This is not consistent with the estimated Atlantic-Pacific temperature gradient for the period 3300-3000 ka of at most 2 °C (H. J. Dowsett et al. 2009). AB'C suggests there is no increase in $\delta^{18}O_{sw}$ until 2800 ka, when there is a ~0.2 ‰ increase, consistent with ice sheet expansion at around 2800 ka. $\delta^{13}C$ derived reconstructions of Pacific deep ocean circulation suggest enhanced North Pacific intermediate water formation along with enhanced NADW input prior to 2700 ka (Kwiek & Ravelo 1999), which would supply relatively warm and saline water to the majority of the Pacific basin – incompatible with an increased temperature gradient between the Pacific and Atlantic.

Given the previously discussed limitations of the models, the two scenarios of potential $\delta^{18}O_b$ solutions shown in Figure 5-6 cannot offer any absolute constraints as to Pliocene evolution of the $\delta^{18}O_{sw}$ signal. However, the limits posed by maintaining a plausible thermal gradient between the Atlantic and Pacific between 3500 and 2800 ka suggest that a significant proportion of the $\delta^{18}O_{sw}$ increase seen at Site 982 during that period has to be a global record of increasing ice volume. It is still possible that some of the increase is the result of local salinity increases in the North Atlantic. Less certain is the $\delta^{18}O_{sw}$ decrease at 2800-2700 ka, which coincides with major changes in global ocean circulation (Chapter 5). The stable ocean structure which allows the inference of global temperature and salinity trends breaks down, meaning that any conclusions about the period 2800-2700 ka are limited.

To test the hypothesis that global ice volume significantly increased and then decreased, the following section examines the implications of the maximum possible $\delta^{18}O_{sw}$ shift being a direct record of ice volume changes.

## 5.4 Increased global ice volume 3500-2900 ka

The implied global nature of the $\delta^{18}O_{sw}$ shifts seen at ODP Site 982 suggests a major increase and subsequent decrease in global ice volume during between 3500 and 2900 ka. Assuming a $\delta^{18}O_{sw}$ shift of 0.11‰ equates to a change in sea level of approximately 10m (Fairbanks 1989), the maximum potential $\delta^{18}O_{sw}$ increase of 0.6‰ observed from 3500-2900 ka indicates a sea level decrease of ~55m. This is some 45% of the $\delta^{18}O_{sw}$ shifts seen between glacial and interglacial periods during the late Pleistocene to Holocene, which are dominated by eccentricity forcing on the 100 kyr timescale and indicate a sea level decrease of ~ 120 m at the LGM. While the glacial global ice volume increases during the Pleistocene were accommodated predominately through the expansion of the circum-North Atlantic ice sheets, such as the Laurentide, Scandinavian and Greenland ice sheets, which in turn exported large amounts of Ice Rafted Debris (IRD) to the North Atlantic and Norwegian sea, there is no evidence for significant IRD input into the Norwegian Sea prior to 3300 ka (Flesche Kleiven et al. 2002). This represents the first major expansion of glaciation on Greenland, although small amounts of IRD are present at least as far back as 3600 ka (Flesche Kleiven et al. 2002) and possibly long ago as the late Miocene (Jansen & Sjøholm 1991). Regional IRD deposition across the North Atlantic region from Greenland, Scandinavia and the North-eastern Laurentide Ice Sheet did not commence until at least 2700 ka (Bailey et al. 2013), however small amounts of IRD was being deposited at a much lower rate from 3100 ka (Flesche Kleiven et al. 2002). Similarly, in the North Pacific, IRD is not deposited in significant amounts until ~2740 ka (Haug et al. 2005).

The expansion of the Greenland ice sheet at 3300 ka is associated with a major $\delta^{18}O$ decrease of approximately 0.5 ‰ at MIS Stage M2, and this interval is also seen in the $\delta^{18}O_{sw}$ records from ODP Site 982 (*Figure 5-7*) as an increase in $\delta^{18}O_{sw}$ of approximately 0.5 ‰, consistent with the lack of a clear cooling in BWT seen at ODP Site 982 at that time. This 0.5 ‰ increase is equivalent to approximately 45m of sea level drop, which is far in advance of the current capacity of the Greenland ice sheet (~6m r.s.l). The long term average of the $\delta^{18}O_{sw}$ record shows a 0.3-0.4 ‰ ice volume increase between the start of the $\delta^{18}O_{sw}$ trend at 3500 ka, and MIS M2 at ~3300 ka. This is still far in excess

of the carrying capacity of the Greenland ice sheet, and therefore significant expansion in other ice sheets (i.e. either the Laurentide, Scandinavian, West or East Antarctic Ice Sheets) must have occurred between 3500-2900 ka.

### 5.4.1 North American glaciation – 3500-2900 ka

While there is no major IRD input into the North Atlantic prior to 2700 ka, minor deposition from 3100 ka suggests the presence of at least some continental ice after that period. However, there remains no IRD evidence for major Northern Hemisphere ice sheets prior to 3300 ka. IRD in the North Atlantic is formed when icebergs from the ice sheets of the Northern Hemisphere break off from sections of the continental ice sheet that have reached the sea. These bergs then melt in the warmer waters of the North Atlantic, depositing their entrained terrigenous material. During the last glaciation, this zone of IRD deposition was just north of the polar front (Ruddiman 1977, Robinson 1995). Therefore, the production of an IRD signal in the North Atlantic is dependent on two factors – coastal ice sheets producing icebergs, and the relative temperature of the surface water in the high latitudes, which controls the melting of the icebergs.

Evidence for early continental ice on the North American continent is seen as far back as 3500 ka, with glacial tills preserved from erosion by subsequent glaciation by deposition and subsequent burial in a bedrock trench (Gao et al. 2012; Menzies et al. 2013). These are situated in a lowland and relatively low latitude region (52° N, 83° W), and the tills show evidence of sediments emplaced under rapidly moving glacial ice, similar to surging or ice stream conditions (Menzies et al. 2013) and there is also pollen evidence for the proximity of deciduous forests (Gao et al. 2012). When contrasted with the lack of IRD evidence for the presence of North American glaciation until the later stages (2640 ka) of the initiation of Northern Hemisphere Glaciation, ~80 kyr after the expansion of Greenland and Scandinavian ice sheets at 2720 ka (Bailey et al. 2013), the sensitivity of the late Pliocene/early Pleistocene Atlantic IRD record to continental glaciation, particularly on the North American continent, must be questioned. The above evidence shows that it is certainly possible to accommodate significant ice sheet growth on the North American without significant IRD deposition in the Atlantic,

suggesting that the ice sheets of the early Pliocene did not extend to the continental shelf until ~2700 ka.

The volume and extent of the North American ice sheets during the period 3500 – 2900 kais not currently known, and neither is the volume and extent at which expanding North American ice sheets begin to contribute IRD to the North Atlantic. While it is possible that the majority of the global 55m sea level drop seen in the $\delta^{18}O_{sw}$ record was accommodated in the Northern Hemisphere, expansion of the Antarctic ice sheet is another possible explanation.

### 5.4.2 Carrying capacity of the Antarctic continent

The Mg/Ca temperature calibration used to derive the ODP Site 982 $\delta^{18}O_{sw}$ record was tuned to the global ice volume model of de Boer et al. (2010) for the period 4000-5000 ka (See Chapter 3). This model was forced by insolation and the benthic global $\delta^{18}O$ stack, and simulated three northern hemisphere ice sheets (European, Greenland and North American) and two Antarctic ice sheet (EAIS and WAIS). The model accurately reflects the differing contributions of the Antarctic and Northern Hemisphere ice sheets to the LGM increase in global ice volume (Miller et al. 2005; Shackleton & Kennett 1975), but it does not recreate the amplitude of ice volume changes implied for the early Pliocene by this study. Nonetheless, the early Pliocene (5000-4000 ka) was selected as the tuning target for the $\delta^{18}O_{sw}$ estimates from ODP Site 982 as changes in ice volume were smaller during this time period than the late Pliocene, despite the evidence for ice sheet instability detailed in Section 2.1.

The average modelled (and hence reconstructed in the records of this study) $\delta^{18}O_{sw}$ for the early Pliocene was similar to that of the modern ocean: ~0‰ SMOW. Therefore, the ice volume shifts reconstructed between 3500-3000 ka would have been in addition to ice volumes that were similar to today. Antarctic ice volume at the LGM is assumed to be close to the maximum 'carrying capacity' of the continent, as the grounding line of the continental ice expanded towards the break in the slope of the continental scarp (Waitt, 1983). Despite the increased areal extent of Antarctic ice, estimates of the change in ice volume on Antarctica from the LGM to the present vary

considerably - from as little as 6.1m to as much as 37m relative sea level (r.s.l.). The significant variability is due in part to the complexity of glacioisostatic modelling and the lack of continuous local records spanning the LGM to the present (Lambeck et al. 2000). As yet, sheet specific ice volume estimates do not sum to the globally seen 120m r.s.l. difference, suggesting either unaccounted for ice or inaccurate estimates (Bentley 1999).

### 5.4.3 Antarctic ice sheet stability and growth in the Pliocene

There is a long-standing geomorphological debate about the stability of the Antarctic ice sheet in the Pliocene. Early evidence from biostratigraphy, based on diatoms reworked into glacial sediments from the Transantarctic Mountains, suggest a warmer Antarctic climate as recently as the late Pliocene (Webb & Harwood, 1996). This evidence has been more recently supported by discovery of fossilised wood within Pliocene glacial debris deposited within glaciolacustrine environments (Hambrey et al. 2003).

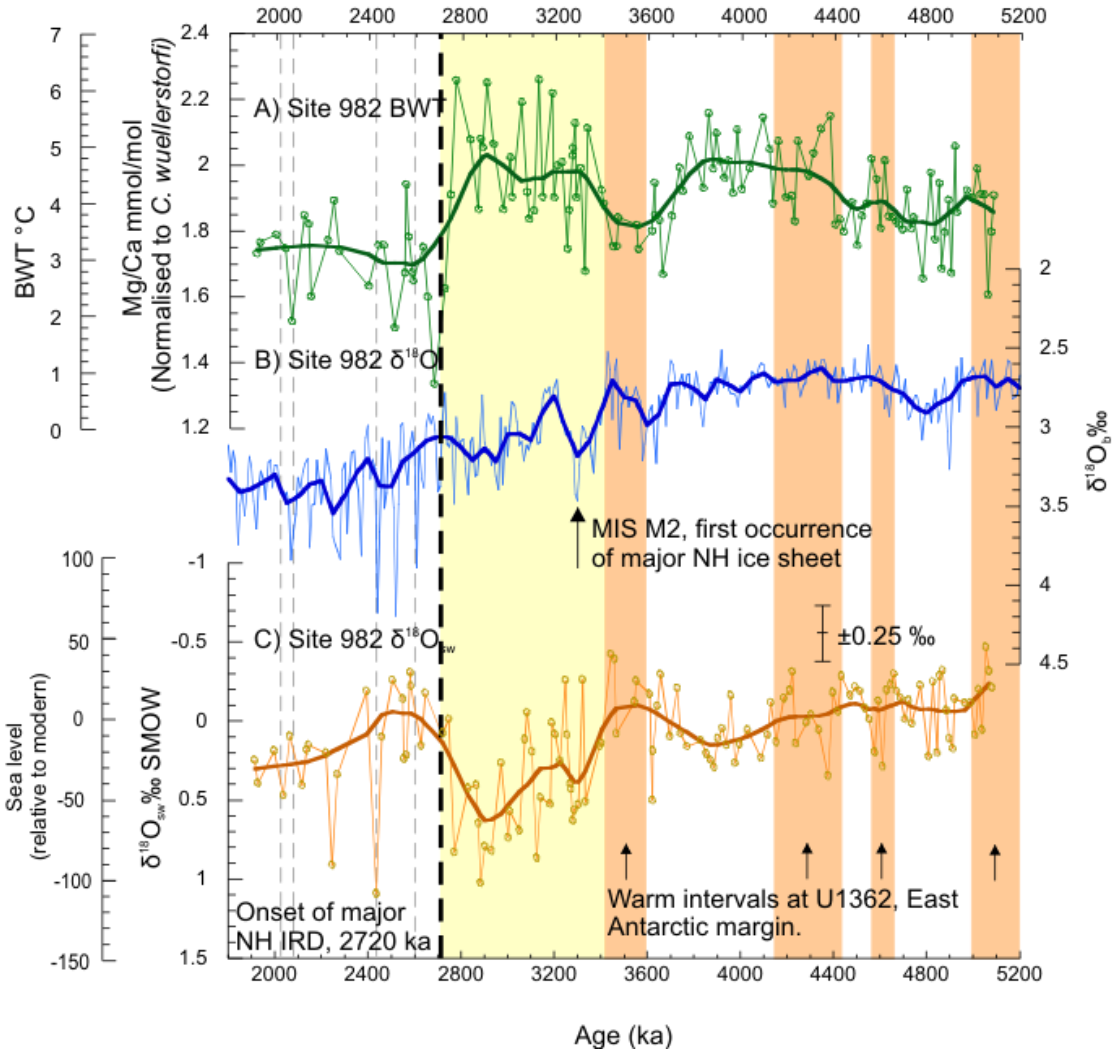


*Figure 5-7. A) North Atlantic BWT and B) $\delta^{18}O$ used to generate C) global $\delta^{18}O_{sw}$ changes throughout the Pliocene and early Pleistocene. Key climatic events are marked in black text. Initial Northern Hemisphere (NH) IRD marked by black dashed line, subsequent major IRD events in grey.* Heavy line on all records is a ~ 100kyr weighted smoothing.

Recent modelling of the Antarctic ice sheet using a high resolution nested ice sheet model has succeeded in simulating a West Antarctic Ice Sheet (WAIS) that when forced by insolation and global $\delta^{18}O_b$ records from the Pleistocene through to the recent, grows and collapses in good agreement with Ross Shelf sedimentary records of ice sheet instability from the ANDRILL project (Pollard & DeConto 2009; Naish et al. 2009). However, the ice sheet model is forced using Pleistocene parameterisations and does not successfully reproduce a variable East Antarctic Ice Sheet during the Pliocene.

Sediment cores from the Ross Sea region show that the WAIS exhibited repeated ~40 kyr cyclic patterns of advance and retreat throughout the Pliocene, as well as long

term shifts in the underlying position of the ice sheet. In the early Pliocene (~5000-4500 ka), the ANDRILL site on the Ross Ice Shelf shows repeated beds of diamictites, consistent with an advancing and retreating WAIS. These sediments are replaced between ~4500-3400 ka by diatom rich sediments indicative of prolonged open water, with little to no contribution from nearby ice sheets (Naish et al. 2009). Terrigenous material reappears at approximately 3400 ka, and is interbedded with marine diatomites throughout the remainder of the Pliocene and the Pleistocene. However, repeated hiatuses in the ANDRILL cores, due to glacial scouring, do not allow a continuous high-resolution record across the 3500-2700 ka period of ice sheet growth and decrease as defined by ODP Site 982 $\delta^{18}O_{sw}$ records, and preclude precise age dating. A ~400 kyr interval of predominately diamictite deposition at the ANDRILL Site indicating the influence of a proximal ice sheet ends at ~2950 ka, and is followed by period of open water sedimentation. This in turn is replaced by subglacial dimictites after about 2700 ka. This evidence of potential changes in the ice volume on Antarctica is consistent with the interpretation of the Pliocene $\delta^{18}O_{sw}$ shifts recorded in ODP Site 982 Figure 5-7) which suggest a prolonged increase in ice volume until approximately 2900 ka, then a brief deglaciation immediately prior to the onset of persistent Northern Hemisphere glaciation ~2700 ka.

Marine sediments recovered from the East Antarctic margin record repeated periods of increased surface water productivity during the early-mid Pliocene, consistent with elevated circum-Antarctic water temperatures (Cook et al. 2013). In addition, the geochemical provenance of detrital material deposited during these warm intervals suggests erosion of the Antarctic interior and a retreat of a significant part of the EAIS several hundred kilometres inland on at least four prolonged occasions (Cook et al. 2013). This instability of the ice sheet is seen at multiple locations along the East Antarctic margin, with at least three geographically separate basins known to be source regions of large amounts of IRD during the Pliocene (Williams et al. 2010). ODP Site 1165 near to Prydz Bay in exhibits a sudden increase in deposition of IRD and terrigeneous clays from 3450 ka through to 3000 ka, consistent with an increasingly proximal and unstable ice sheet in that area (S. Passchier 2011). This lithological

evidence is in contrast to modelling studies that predict a stable East Antarctic ice sheet (Pollard & DeConto 2009).

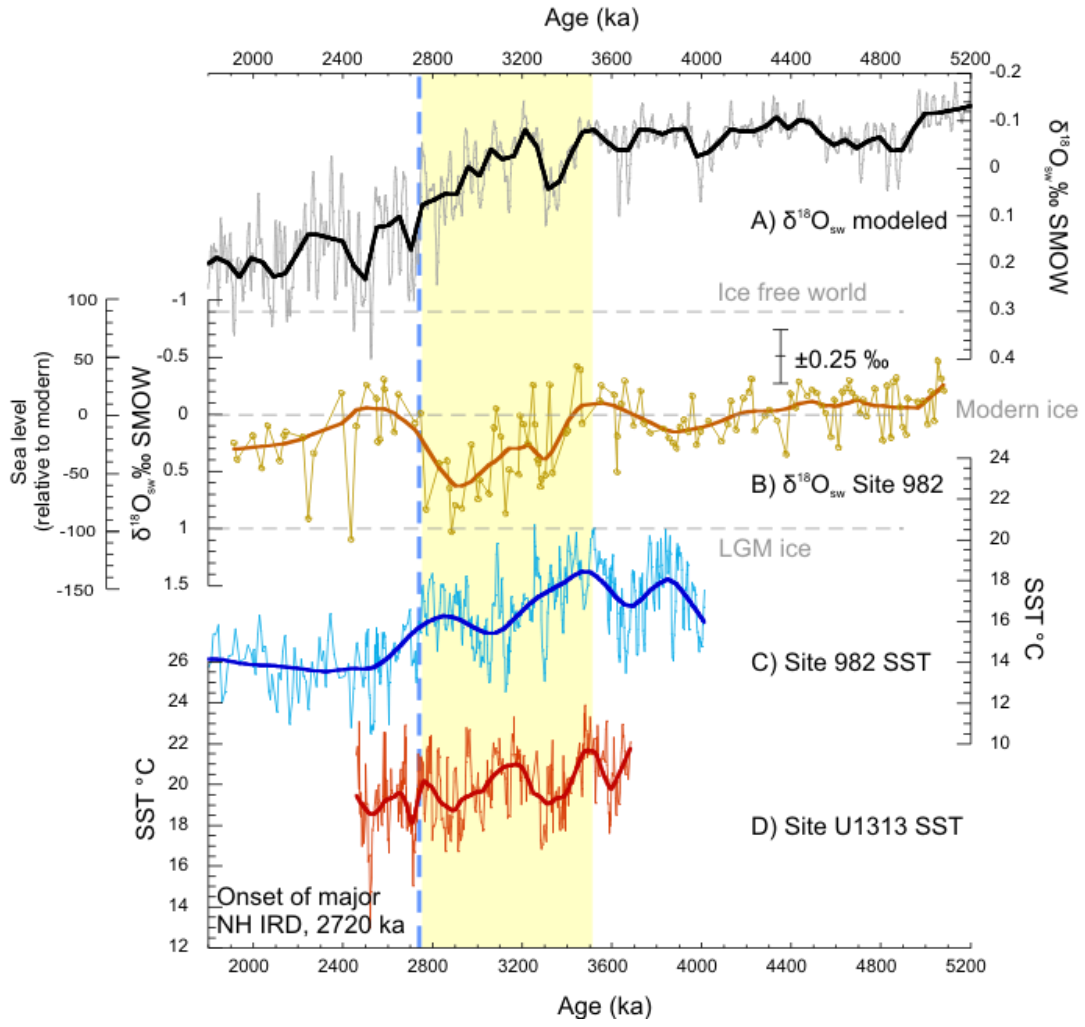


*Figure 5-8. A) Modelled δw from de Boer et al. (2010) resampled to 1kyr resolution. B) $\delta^{18}O_{sw}$ Site 982. Grey dashed lines represent maximum and minimum values for $\delta^{18}O_{sw}$ given an ice free world or a LGM world. C) Site 982 SST from $Uk^{37}$ records (Lawrence et al. 2009). D) Site U1313 SST from $Uk^{37}$ records (Naafs et al. 2012)* **.** Heavy line on all records are~ 100kyr weighted smoothing.

### 5.4.4 Where was the ice volume increase 3500-3000 ka located?

As previously discussed, evidence for the presence of ice sheets in the Northern Hemisphere during the Pliocene is compatible with the absence of major IRD deposition at that time. It is possible that up to 55m of r.s.l. decrease could have been accommodated on the North American continent, but evidence of occupation of the

high latitudes by taiga forests (Salzmann et al. 2008; Salzmann et al. 2011) suggests a reasonably small or highly variable ice sheet.

Given the errors in the $\delta^{18}O_{sw}$ reconstruction, and the significant uncertainties surrounding the carrying capacity of Antarctica, it is also possible that the majority of the implied late Pliocene sea level decrease could have been accommodated by increased ice volume on Antarctica, even starting from an ice volume similar to the modern. There is some evidence to suggest a West Antarctic Ice Sheet smaller than the modern prior to 3500 ka, and a subsequent expansion (Naish et al. 2009). However, the significant scale of the required ice volume increase means it is also plausible that some proportion of the $\delta^{18}O_{sw}$ is an artefact of increasing salinity of Mediterranean Outflow Water entering the NADW system. It is not possible as yet to determine the relative contributions of local salinity and global ice volume.

### 5.4.5 Sea Surface Temperature (SST) evidence for increased ice volume during the Pliocene.

Alkenone based SST reconstructions from ODP Site 982 (Lawrence et al. 2009) and U1313 (41°N, 33°W, 3426 m water depth (Naafs et al. 2010) in the North Atlantic both show long-term cooling trends starting at around 3500 ka, coincident with the $\delta^{18}O_{sw}$ increase seen at ODP Site 982. SSTs at Site 982 decrease by approximately 2°C between 3500-3200 ka, followed by a 2.5°C cooling at ~2700 ka (Lawrence et al. 2009). A brief warming of SST by approximately 1.5 °C (3100-2800) occurs between cooling periods, which coincides with the ice volume maxima at. This may indicate a stronger North Atlantic Current (NAC) warming the surface water mass at ODP Site 982, and hence a potential connection between the strength of the NAC and growth of the ice sheet (maxima at ~2900) during the same time period. The mechanism for this is thought to be increased transport of moisture northwards by the intensified NAC assisting in the growth of northern hemisphere ice sheets (Bartoli et al., 2005), however the opposite trend – declining SST and increasing ice volume - is seen for the earlier period 3500-3100 ka.

The 3500 ka cooling event is mirrored in ODP Site U1313 (Naafs et al. 2012)., some 17° further south of ODP Site 982, suggesting a regional surface cooling in North Atlantic Ocean at this time. (*Figure 5-8*). Apart from a cooling at 3500 ka, the longer term major coolings (3500-3200 and 2700-2500 ka) seen at Site 982 are not as significant at Site U1313, suggesting that colder waters did not regularly reach this far south. This is interpreted in this study as the result of the subpolar front (essentially the northward side of the North Atlantic Current) shifting further south in response to increased ice volume in the Northern Hemisphere freshening the high latitude North Atlantic surface waters, in a similar fashion to that seen during glacial periods in the Pleistocene.

## 5.5 Paradox of the 2700-2800 ka 'deglaciation'

At Site 982, the period 2800-2700 ka exhibits a significant decrease in $\delta^{18}O_{sw}$ values from 0.6 to 0.05 ‰. If interpreted solely as a change in global continental ice volume this is a major deglaciation at precisely the same time as the onset of IRD deposition in the Northern Hemisphere. This is the first time Northern Hemisphere ice sheets have reached the coastline to produce IRD since the brief period during MIS M2 (Jansen et al. 2000); is also coincident with a cooling of surface (Lawrence et al. 2009) and deep (Sosdian & Rosenthal 2009 and this study) water temperatures, and increased amplitude of $\delta^{18}O_b$ oscillations (L. E. Lisiecki & Raymo 2005). All of the above is consistent with global cooling and a sustained increase in ice volume, and therefore other possible explanations for the observed decrease in $\delta^{18}O_{sw}$ need to be examined.

### 5.5.1 Issues with the Mg/Ca proxy

The similarity in Mg/Ca trends between deep and intermediate depth sites in the Atlantic (Section 4.3.1) do not support a fundamental problem with the Mg/Ca proxy at Site 982. In addition, B/Ca records presented in Chapter 3 also show no potential saturation state effects on Mg/Ca. Therefore, Mg/Ca can be said to represent the evolution of BWT accurately.

### 5.5.2 Potential changes in North Atlantic circulation

While the majority of the Pliocene prior to 2800 ka is characterised by sustained intense NADW formation and stepped cooling of sea surface temperatures (Chapter 5), there was a significant alteration in circulation patterns at 2800 ka. In addition to further SST cooling (Lawrence et al. 2009; Naafs et al. 2010), NADW penetration into the Southern Atlantic was greatly reduced, suggesting that the intensity of NADW production was reduced (Hodell & Venz-Curtis 2006). In the Pleistocene, reduced NADW formation was seen during glacial periods, and was linked to southward shifts in the North Atlantic Current, similar to what is observed at 2800 ka (Venz & Hodell 2002; Venz et al. 2000a). This combination of trends means the possibility of different water masses being present at Site 982 before and after 2800 ka requires investigation.

The most likely change in water masses at Site 982 is a shift in the location of the MOW. It has already been established that this water mass is present in the intermediate depth North East Atlantic during the Mid-Pliocene (Khelifi et al. 2009), and that while the $\delta^{18}O_{sw}$ changes seen at Site 982 are believed to be global in nature (Section 5.3), it is still possible that some part of that change is due to changing strength or position of the MOW.

BWT trends at Site 982 follow the same pattern as at Site 607, and Site 607 is likely independent of the direct impact of the MOW – being far beneath the stable depth of 1000-2000m the MOW currently affects (Reid, 1979). Therefore, the cooling of Site 982 at 2800-2700 ka is not a response to the MOW moving away from Site 982, but reflects a general ocean cooling. Mid Pliocene MOW $\delta^{13}C$ is significantly more negative than Atlantic $\delta^{13}C$, which can be seen in lower values at Site 548 (Khelifi et al. 2009). Prior to 2800 ka, Site 982 $\delta^{13}C$ values lie between those of Site 548 and Site 607, consistent with a water mass comprising a mixture of MOW and Atlantic water (Figure 5-9). Records from Site 982 do show an increase in $\delta^{13}C$ values towards those of Site 607, but this is a long term trend that bears no resemblance to trends in $\delta^{18}O_{sw}$. Therefore, neither BWT or $\delta^{13}C$ trends support an alteration in the position or strength of the MOW.

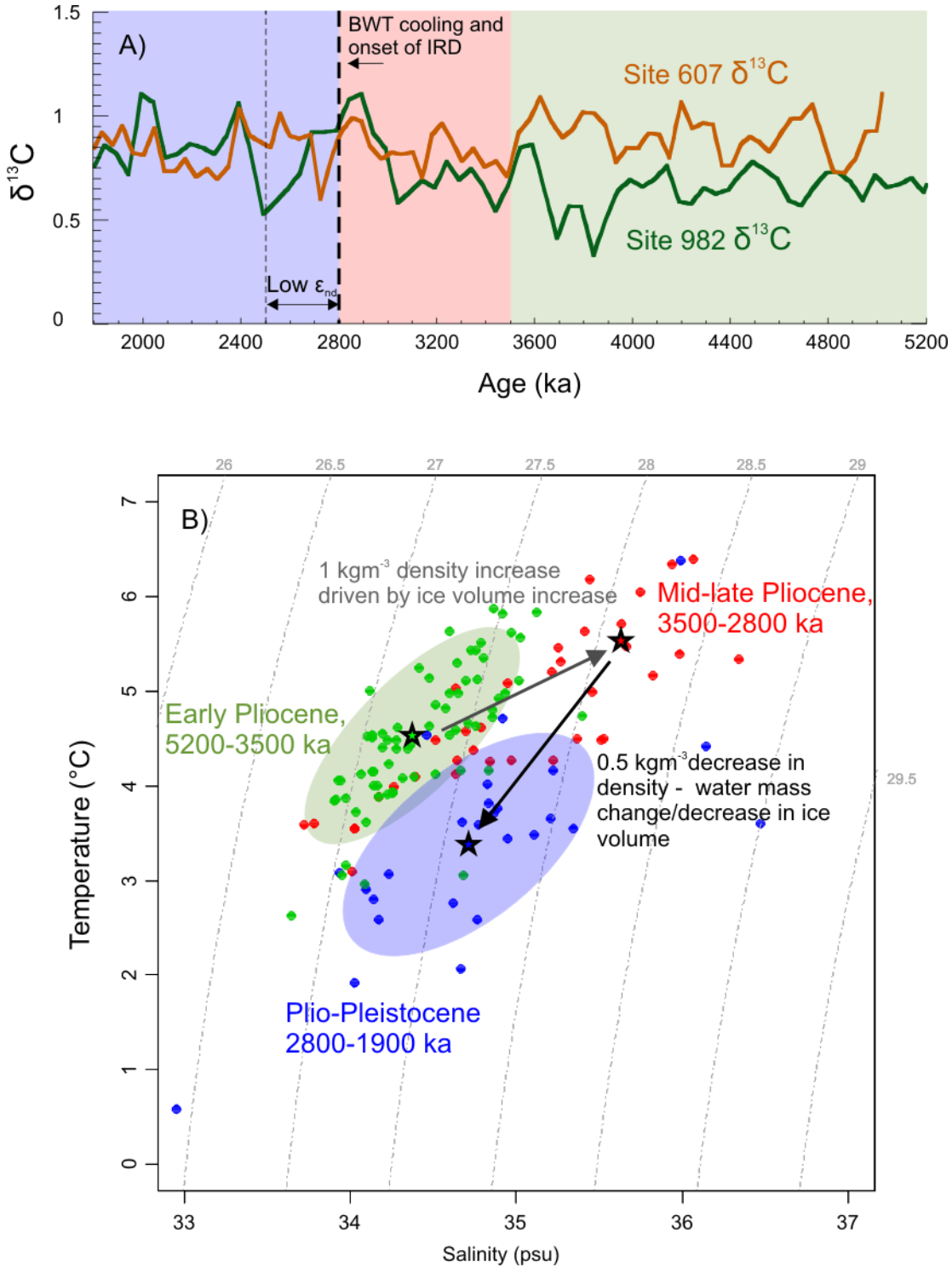


*Figure 5-9 A) $\delta^{13}C$ and B) Temperature-Salinity evolution of water mass at Site 982. Stars in B) show mean BWT and Salinity for each time period. Shaded areas in B) show general T-S field for early Pliocene and Plio-Pleistocene periods. Salinity was derived from the general North Atlantic $\delta^{18}O_{sw}$ – S relationship $\delta^{18}O_{sw}$ = 0.0.551xS-19 Density isolines are calculated for a depth of 1100m. $\delta^{13}C$ in A) from Hodell & Venz-Curtis (2006)*

$\varepsilon_{Nd}$ values from the modern and Pliocene Site 982 both lie between the more negative 'Atlantic' values and the less negative 'MOW' values seen at Site 548 (Khélifi et al. 2014). This is again consistent with a proportional influence of MOW on Site 982. Around the time of the 2800-2700 ka decrease in $\delta^{18}O_{sw}$, a temporary decrease in $\varepsilon_{Nd}$ suggests a reduction in MOW input to the North Atlantic (Figure 5-9), however no such trend is seen in the record at Site 548 (Khélifi et al. 2014). This period of inferred 'low MOW' does coincide with a period of minimum $\delta^{18}O_{sw}$ at Site 982 immediately after the BWT cooling, which would be a consequence of reduced salinity waters.

In the modern ocean MOW persists as a salinity anomaly into the Norwegian Sea where it shoals and mixes with proto-NADW (Reid, 1979). The Pliocene cooling of the subsurface water masses (which is independent but contemporaneous of MOW salinity changes) and surface water (Lawrence et al. 2009; Naafs et al. 2010) could have caused a change in the density structure of the North Atlantic. This may have been enhanced by increases in the density of the MOW as a result of increased aridity in the Mediterranean (Fauquette et al. 1998). Shifting the input of MOW away from the high latitude deep water forming regions is predicted to have an effect on NADW production in the present (Reid 1979), and the same effect could be expected to occur in the past as well.

This hypothesis would explain the changes in $\varepsilon_{Nd}$ values seen at Site 982 and possibly the changes in global circulation, and the replacement water would be less dense to fit with the observed decrease in density at Site 982 between 2800-2700 ka. A deepening of the MOW flow away from Site 982 and its replacement by cooler less dense waters from above would fit, however as previously discussed this is inconsistent with the $\delta^{13}C$ record from Site 982, which shows no significant changes in the water mass at the site.

### 5.5.3 Changes in Antarctic Ice Volume

At present there is little evidence for an Antarctic deglaciation that could account for some of the observed decrease in $\delta^{18}O_{sw}$ between 2800-2700 ka. There is a tentative period of open water in the Ross Sea, suggesting a period of WAIS retreat (Naish et al.

2009). However, age control on that site is limited. There is also a brief period of IRD deposition at ODP Site 1090 (Southern Ocean 46.2°S, 7.4°W) during the Marine Isotope Stage G11 (2830 ka), an interglacial period. It has been hypothesised that this represents rising sea levels destabilising the Antarctic margin and causing large numbers of icebergs to enter the Southern Ocean (Murphy et al. 2002), a situation similar to that proposed for the Pleistocene (Kanfoush 2000). In contrast to the relatively long (~100kyr) and unidirectional nature of the 2800 ka shift, these interactions are inherently transient and on a much shorter timescale than the resolution of the records from this study at Site 982. Nevertheless, they serve to illustrate potential connections between Northern Hemisphere circulation and Southern Hemisphere ice volume.

## 5.6 Conclusions

Long term $\delta^{18}O_{sw}$ from derived from previously published Site 982 $\delta^{18}O_b$ and BWT records from this study show a significant increase and subsequent decrease in $\delta^{18}O_{sw}$ between 3500-2800 ka.

Using global $\delta^{18}O_b$ and estimated interbasinal temperature gradients, it was possible to determine that North Atlantic $\delta^{18}O_{sw}$ records reflected a global trend, which suggests a long term increase in global ice volume equivalent to 55m r.s.l decrease between 3500 and 2800 ka. While it is possible that some of this 'ice volume' is caused by a local increase in salinity from the Mediterranean, a significant proportion of the shift has to be the result of ice sheets developing in either the Northern or Southern hemisphere. At 2800 ka, a decrease in $\delta^{18}O_{sw}$ of 0.4 ‰ at Site 982 may indicate a loss of continental ice volume equivalent to ~35 m sea level rise, at a time of global cooling. It is also possible that this decrease is the result of a reorganisation of the North Atlantic circulation system and the incursion of cooler and fresher waters to Site 982. Evidence regarding possible water mass changes is contradictory, and it is not possible to confirm the cause of the decrease in $\delta^{18}O_{sw}$ as yet.

Possible relationships between sea surface temperatures, global ice volume and deep water circulation are discussed in more detail in Chapter 6.

# 6 Global changes in deep ocean circulation and high latitude climate response to changes in orbital forcing, 5200-1900 ka.

Given the potential increase in global ice volume discussed in the previous chapter, this chapter first assesses the impact of such an increase on global trends in deep ocean circulation. The potential link between high latitude processes (such as surface water productivity and the changing location of deep water source regions), and global circulation intensity is highlighted by re-examining the previously published %NCW records of Hodell & Venz Curtis in the light of new Cd/Ca and coarse fraction weight percent records from Site 982. Spectral analysis of Sortable Silt ($\overline{SS}$), SST, and $\delta^{18}O_b$ records establishes an early Pliocene link between orbitally controlled sea surface temperature variations and deep water flow speeds at Site 982, then the breakdown of this connection as a result of the increasing regional impact of global ice volume from 3600 ka. Finally, potential long term causes of the increase in global ice volume are examined, concluding that a combination of orbital conditions favourable to ice sheet inception were preconditioned by tectonic changes.

## 6.1 Modern and LGM circulation regime of the Atlantic basin

The modern Atlantic basin is dominated by three major water masses. North Atlantic Deep Water (NADW), forming in the high northern latitudes fills the majority of the deep North Atlantic with well-ventilated high $\delta^{13}C$ and low nutrient water (Oppo & Fairbanks 1987). The southern Atlantic hydrography comprises a tongue of NADW sandwiched between Antarctic Intermediate Water (AAIW) above and Antarctic Bottom Water (AABW) below (Kroopnick 1985). These two water masses are more nutrient rich than NADW, and less well ventilated - lower $\delta^{13}C$ (Kroopnick 1985). NADW is also warmer and more saline than AABW, which is characterized by decreasing temperatures and salinities towards the bottom (Orsi et al. 1999; Rhein et al. 1998) It is evident that the bottom topography plays an important role in the flow and distribution of NADW (Roden 1987) and AABW in the Atlantic and the resulting

mixing of these waters results in the bottom waters at any location being an admixture of waters made up of differing proportions of these end-member water masses (Martínez-Méndez et al. 2008). During the glacial periods of the Pleistocene and Holocene, the relative strength and penetration of the water masses changed (Boyle & Keigwin 1982; César Negre et al. 2010). As the North Atlantic circulation regime shifted from a interglacial to a glacial state, NADW became less saline/dense and shoaled, forming GNAIW, while the deep water masses of the Antarctic penetrated much further north in the deep basin of the Atlantic (Venz et al. 2000b; Martínez-Méndez et al. 2008; Cesar Negre et al. 2010).

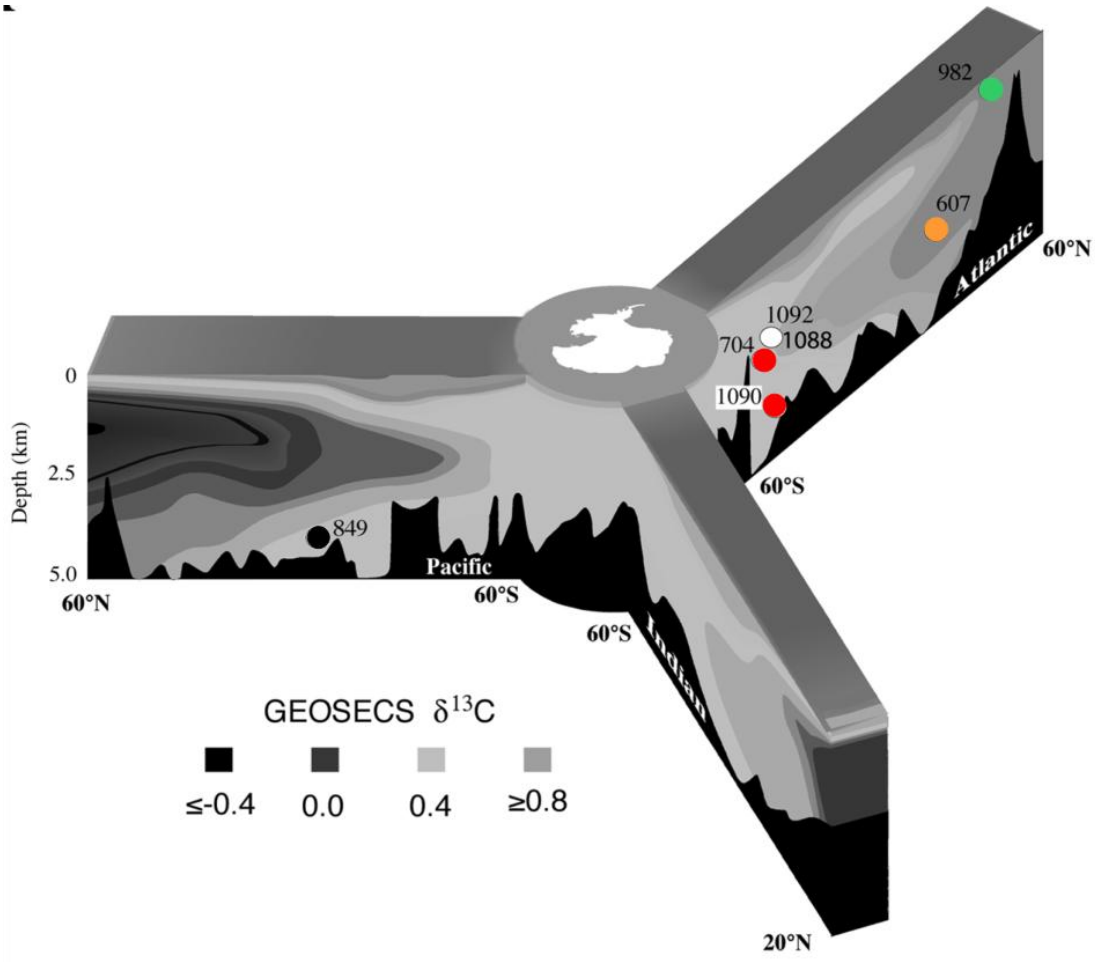


*Figure 6-1 Schematic of the major ocean basins showing the sites used in the reconstruction of the relative strength of the water masses in the Atlantic. Figure after Hodell & Venz-Curtis (2006), with vertical $\delta^{13}C$ distribution after Kroopnick (1985)*

## 6.2 Long term trends in bottom water flow speed ($\overline{SS}$) at Site 982

The Sortable Silt record ($\overline{SS}$) generated for Site 982 spans the transition from the stable and warm early Pliocene to the much more variable climate of the early Pleistocene. It offers a direct record of relative flow speed variability, independent of chemical tracers such as $\delta^{13}C$, something currently unique in Pliocene palaeoceanography.

While it is not possible to ascribe absolute flow speed values to $\overline{SS}$ records (McCave & Hall 2006), the general stability of the record is not thought to be the result of a limited sediment supply. Increases or decreases in flow rate (resulting in increases or decreases in $\overline{SS}$) that ran up against a physical limit in sediment would be shown as approaching a threshold beyond which no $\overline{SS}$ could pass. This is not seen in the record, suggesting that the trends seen are an accurate reflection of changes in bottom water flow speed at Site 982.

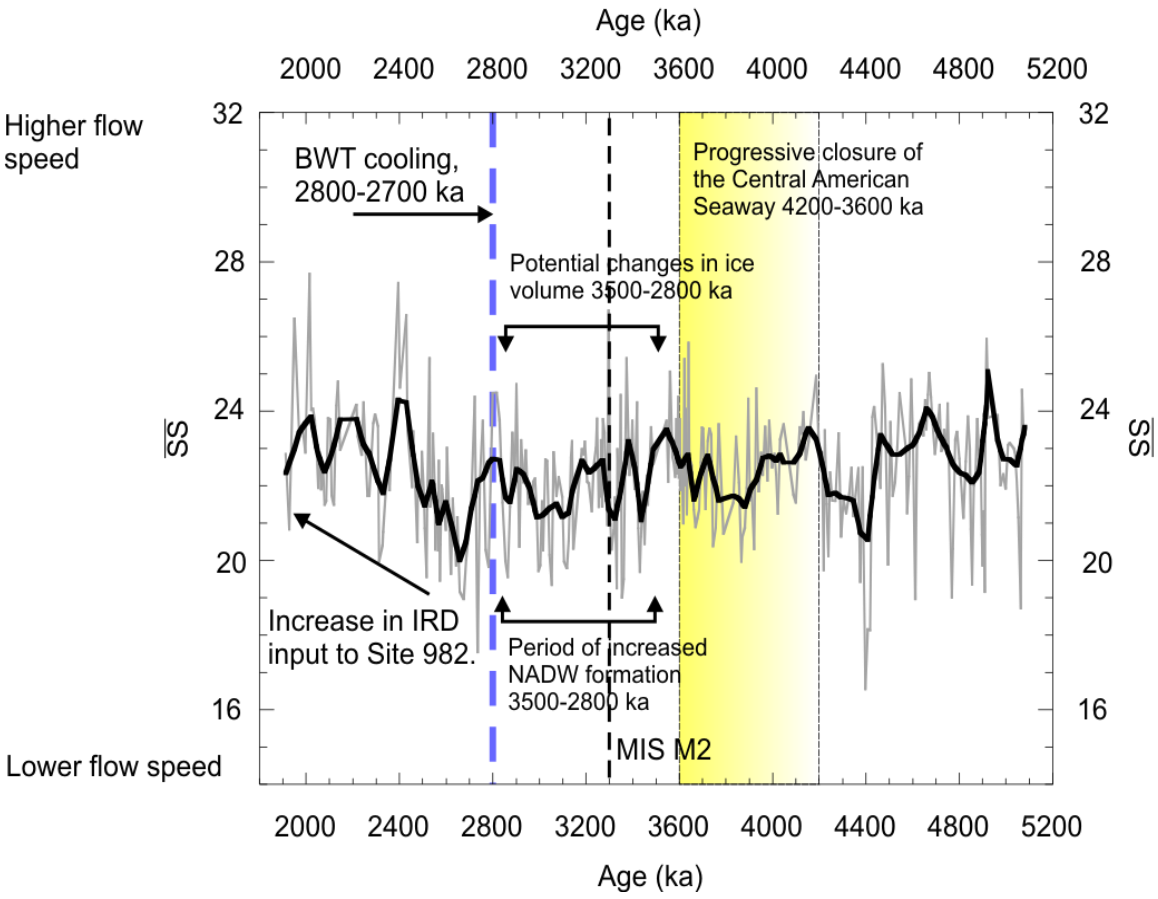


*Figure 6-2 Long term trends in* $\overline{SS}$ *during the Plio-Pleistocene. Significant climatic events are highlighted with reference to the* $\overline{SS}$ *record. Heavy black line is a 100 kyr weighted cooling.*

There is no permanent shift in $\overline{SS}$ that could be ascribed to the BWT cooling at 2800 ka, which would suggest the cooling had no long term effect on high latitude deep water formation. A brief decrease immediately after 2800 ka may be linked to the BWT cooling event. Following this there was an increase in $\overline{SS}$ between 2600 ka and 1900 ka, which may indicate increased bottom water flow speed. However, this is coincident with the onset of IRD at Site 982 and as the grain size distribution of IRD is not known, the possible influence of IRD on the $\overline{SS}$ record means this trend must be considered suspect. There also appears to be no long term trend across the period 3500-2800 ka, when an ice volume increase/decrease and potential NADW maxiumum both occur. Throughout the Pliocene, long term trends in bottom water flow speeds at Site 982 seem to have been generally independent of major global climatic events.

The likely causes of the clear short term variability in the $\overline{SS}$ record are assessed in Section 6.4.

## 6.3 Changes in Atlantic circulation throughout the Neogene.

### 6.3.1 Relative NADW strength

Reconstructions of the late Neogene (10 - 0 Ma) global circulation regime - most recently D. A. Hodell & Venz-Curtis (2006) but also Raymo et al. (2004); Raymo et al. (1996) - have put forward a broadly similar picture to the modern, with deep water formation in the high latitude North Atlantic and Southern Ocean. NADW was first produced in the late Miocene, and has continued with varying strength throughout the Neogene (Kouwenhoven & van der Zwaan 2006). Increased benthic foraminiferal $\delta^{13}C$ values from the Southern Ocean and Caribbean (Hodell & Venz-Curtis 2006; Haug & Tiedemann 1998) approach the values of the North Atlantic, along with increasing carbonate preservation in the Caribbean suggest a maximum in NADW production between 3600-2750 ka. This increased Atlantic overturning has been linked to the final restriction of the Central American Seaway (Haug & Tiedemann 1998) increasing the salinity (and density) of North Atlantic surface waters, thereby enhancing high latitude deep water formation (Bartoli, Sarnthein & Weinelt 2005)

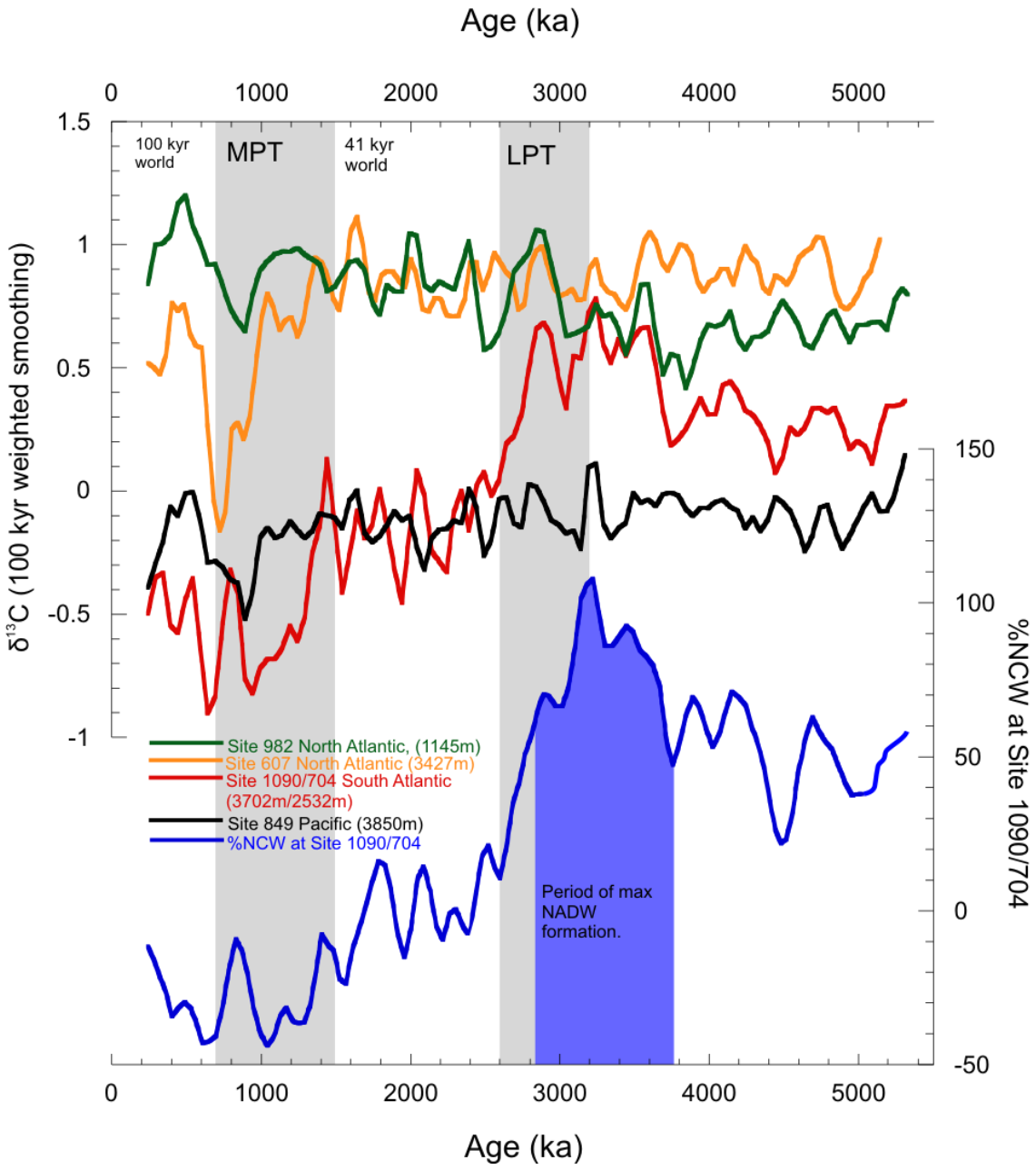


*Figure 6-3 Benthic foraminiferal based $\delta^{13}C$ records for the last 5200 kyr. Benthic $\delta^{13}C$ records from Hodell and Venz Curtis (2006) and references therein. The percentage Northern Component Water (%NCW) was determined using the equation in Section 2-6. All data was interpolated to 10 kyr resolution and smoothed with a 100kyr weighted mean. Late Pliocene Transition (LPT) and Mid Pleistocene Transition (MPT) are highlighted in grey.*

Following the climate transition at 2700 ka, the benthic $\delta^{13}C$ values of South Atlantic ODP Site 1090/704 decline rapidly away from the North Atlantic end members ODP Sites 607 and 982, to closely resemble values of the Pacific ODP site 849 (Figure 6-3).

After 1500 ka, the 1090 $\delta^{13}C$ value shifts again, to a value more negative than the Pacific water mass, typically the least ventilated water mass in the global ocean (Shackleton et al. 1988; Mix et al. 1995). This shift can be interpreted as some combination of two different scenarios: a decline in the relative input of Northern Component Water (NCW) to the mixing point at ODP Site 704/1090, or a change in the preformed value of the Southern Component Water (SCW). The preformed SCW value is controlled by Southern Ocean surface export productivity and air/sea gas exchange (Broecker and Peng, 1989; Charles and Fairbanks, 1990). Increased sea ice and stratification limit both of these parameters (Marchitto & Broecker 2006), lowering the $\delta^{13}C$ value of the deep water mass (Boyle & Keigwin 1985). Recently, evidence for increased stratification in the Southern Ocean has been reported across the Mid-Pleistocene transition (Rodríguez-Sanz et al. 2012) and in the Early Pliocene from 2700 ka (Sigman et al. 2004). Despite this mechanism for a preformed control on Southern Ocean $\delta^{13}C$, late Pleistocene combined $\delta^{13}C$ - Cd/Ca data from when South Atlantic $\delta^{13}C$ was significantly lower than that of the Pacific still suggest the penetration of low $\delta^{13}C$ /high nutrient Southern Component Water significantly further into the deep Atlantic during glacial periods (Marchitto et al. 2002). This suggests that changes in the preformed $\delta^{13}C$ value of the SCW end-member during glacial periods throughout the Pleistocene were in addition to changes in relative water mass at site 1090.

Given that the $\delta^{13}C$ value of SCW in the Pliocene/Early Pleistocene does not decrease below Pacific values, this study assumes that the $\delta^{13}C$ gradient between North Atlantic ODP Sites 607 and 982 and South Atlantic ODP Site 704 at least qualitatively reflects the relative strength of NCW/SCW in the Atlantic Basin. As such, the equation defined in Section 2-6 is used to estimate a relative strength of the end-member water masses at the mixing site ODP 1090/704 (*Figure 6-3*).

### 6.3.2 Nutrient and isotopic evolution of $\delta^{13}C$ composition of North Atlantic end members.

Long term benthic $\delta^{13}C$ records from ODP sites 607 and 982 (Hodell & Venz-Curtis 2006) show predominately similar values (~0.8 **‰**) for the period 3600-1500 ka. After 1500 ka ODP Site 607 becomes increasingly influenced by low $\delta^{13}C$ SCW during glacial

periods, with $\delta^{13}C$ values approximately halfway between Atlantic and Pacific end-members. Prior to 3600 ka, ODP Site 982 has lower $\delta^{13}C$ than Site 607, which would appear to suggest a less well ventilated water mass at this site. $Cd/Ca_{sw}$ $\delta^{13}C$ proxy-proxy plots for ODP Site 982 show values similar to modern NADW values throughout the whole period of this study (5100-1900 ka) (*Figure 6-4*). The slight increase in $\delta^{13}C$ values at 3600 ka is not mirrored by a decrease in $Cd/Ca_{sw}$, suggesting decreased stratification in the surface source water of Site 982, consistent with the stronger NAC/NADW at that time inferred by the North Atlantic/South Atlantic $\delta^{13}C$ gradient.

The $\delta^{13}C$ record of ODP Site 607 prior to 3600 varies inversely to that of Site 982 – i.e. when Site 982 exhibits low $\delta^{13}C$ values, Site 607 exhibits higher. This inverse relationship suggests two separate water masses with differing preformed values of $\delta^{13}C$, and the persistent offset between the two sites suggests an older water mass at Site 982. Sortable Silt bottom water flow speed proxy and $\delta^{13}C$ covary at Site 982 from as far back as 4500 ka (Figure 6-4), showing increased bottom water flow speed with increased ventilation, so changes in flow strength (physical ventilation) at ODP Site 982 at 3600 ka are not the cause of the changes in $\delta^{13}C$ (chemical ventilation) at ODP Site 982. Changes in air-sea gas exchange at the source region of either 982 or 607, implying two somewhat different water masses with different controls on chemical ventilation prior to 3600 ka and one water mass afterwards, would account for the end of the inverse relationship between ODP Site 982 and 607.

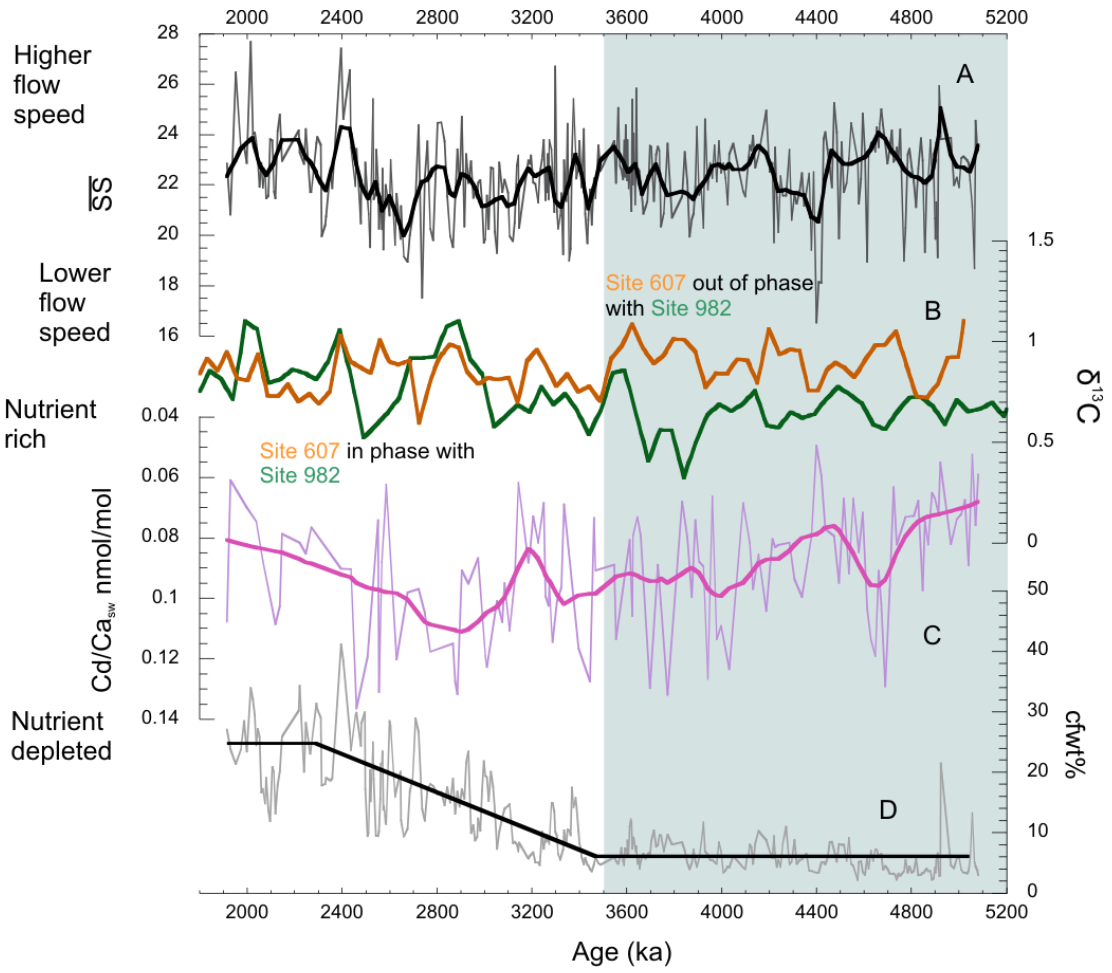
Higher flow speed
Lower flow speed
Nutrient rich
Nutrient depleted
SS
Cd/Ca$_{sw}$ nmol/mol
δ$^{13}$C
cfwt%
A
B
C
D
Site 607 out of phase with Site 982
Site 607 in phase with Site 982
Age (ka)

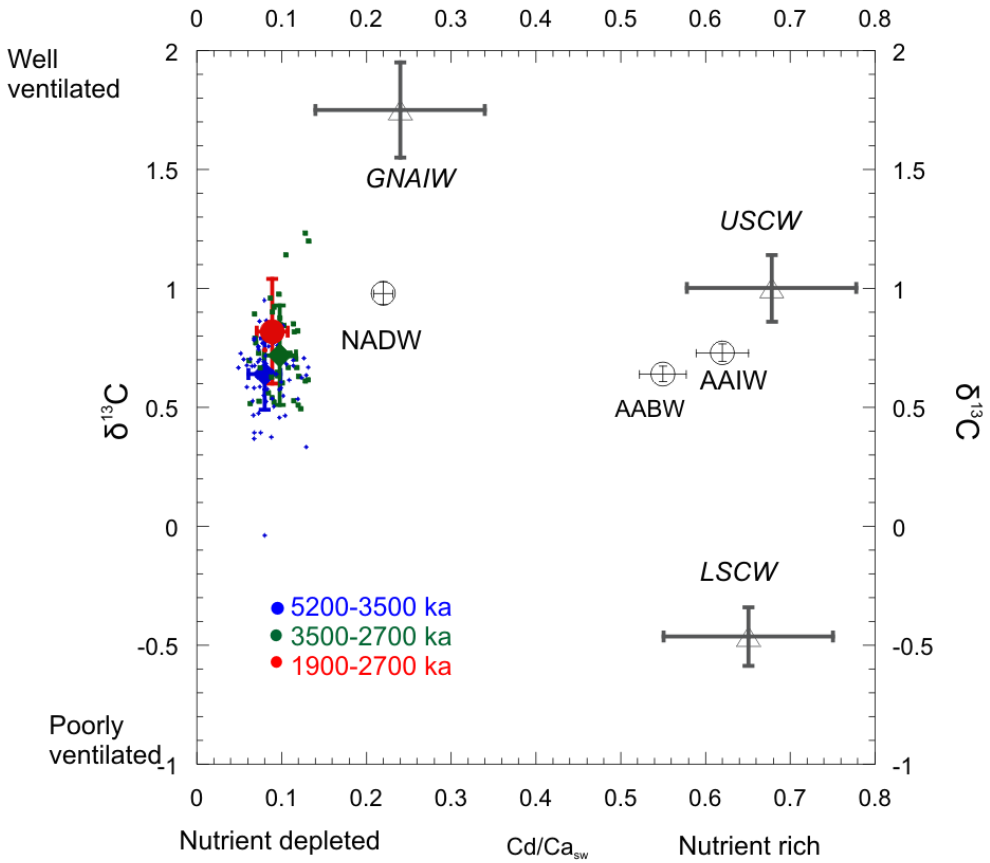
Well ventilated
Poorly ventilated
GNAIW
NADW
USCW
AAIW
AABW
LSCW
5200-3500 ka
3500-2700 ka
1900-2700 ka
δ$^{13}$C
Nutrient depleted
Cd/Ca$_{sw}$
Nutrient rich

*Figure 6-4 (overleaf) Upper panel: a) $\overline{SS}$ record from ODP Site 982. b) δ13C for the North Atlantic ODP Sites 607 and 982. Grey shading highlights the period during which ODP Site 607 and 982 are not reflecting the same water mass, as defined by differing benthic δ13C trends. Data from Hodell et al (2006) c) Cd/Casw from ODP Site 982. d) Coarse fraction weight % inflection points (stepped black line) determined using RAMPFIT program (Mudelsee 1999) with inflection points specified between 1900-2700 and 2800-3400 ka. a) b) and c) data smoothed using a ~100kyr weighted mean. Lower panel: δ13C-Cd/$Ca_{sw}$ proxy proxy plot for ODP Site 982. Modern end-member values (North Atlantic Deep Water - NADW, Antarctic Intermediate Water - AAIW, and Antarctic Bottom Water - AABW) from Boyle (1986), and glacial period end-member values from Martínez-Méndez et al. (2008). Error bars are all given to 1σ.*

At approximately 3600 ka, the average benthic $\delta^{13}C$ value of ODP Site 982 increases by ~0.2 ‰, approaching that of ODP Site 607. This may represent a declining contribution of advected Mediterranean Outflow Water (MOW) to the water mass at ODP Site 982 after 3600 ka, as the MOW has a $\delta^{13}C$ value ~0.4 ‰ lower than that of the NADW water masses (Khélifi 2010) in the Pliocene. This is in contrast to the Holocene, where MOW has a $\delta^{13}C$ ~0.1-0.2 ‰ higher than the $\delta^{13}C$ at ODP Site 982 (Kroopnick 1985). ODP Sites 982 and 607 then exhibit very similar trends and absolute $\delta^{13}C$ values throughout the remainder of the record. The covariance between $\delta^{13}C$ and $\overline{SS}$ at ODP Site 982 along with the similarity of the $\delta^{13}C$ recorded at ODP Site 607 strongly suggests a well-ventilated and homogenous North Atlantic basin, which would be consistent with increased NADW formation from 3600 ka.

### 6.3.3 Increase in surface water productivity from 3500 ka

A prolonged increase in the weight percent of the coarse (>63 μm) sediment fraction (Cfwt%) at ODP Site 982 occurs between ~3500 and 2300 ka (*Figure 6-4*). This shift largely reflects an increase in the proportion of planktonic foraminifera forming the sediment at ODP Site 982. This is not believed to be a result of an increase in the preservation of carbonate, as no significant changes are seen in previously published $\delta^{13}C$, $\overline{SS}$ records from this study, or the visual appearance of benthic foraminfera at this location. There is also no significant decrease in $\Delta[CO_3^{2-}]$ at this time (Chapter 3, Figure 1), again suggesting no changes in preservation as a result of waters undersaturated in $[CO_3^{2-}]$. The increase in Cfwt% does not reflect an increased IRD input, as IRD is not evident at ODP Site 982 until ~2700 ka, and peaks in cfwt% occur without synchronous IRD events. Therefore, the increase in Cfwt% is interpreted as being driven by an increase in surface water productivity following ~3500 ka, and

subsequent export of biogenic carbonate. Sea surface temperature reconstructions at ODP Site 982 decline from a maxima of ~20° C at 3500 ka to a Pleistocene average of ~14°C by 2500 ka (Lawrence et al. 2009). This is mirrored by similar though much less marked declines at IODP Site U1313 (a redrill of ODP Site 607) (Naafs et al. 2010) across the same time period. The decrease in SST and associated increase in surface water productivity as seen in the Cfwt% at ODP Site 982 from 3500 ka occurs prior to major IRD input to the North Atlantic region (~2700 ka). Lawrence et al. (2009) suggest the decrease in SST observed at ODP Site 982 results from orbitally forced changes in the latitude and intensity of the westerlies that control the position of the North Atlantic Current. This would potentially increase mixing of the surface waters at Site 982, enhancing productivity.

## 6.4 Changes in SST, $\delta^{18}O_b$ and $\overline{SS}$ response to orbital forcing at ODP Site 982

To examine the potential contribution of a change in response of SST to orbital forcing, cross-spectral analyses of SST ($Uk_{37}$ alkenone proxy; Lawrence et al., 2009), $\delta^{18}O_b$ (Venz & Hodell 2002; L. E. Lisiecki & Raymo 2005) and $\overline{SS}$ (this study) were compiled for three different time intervals (*Figure 6-5*). The lower resolution of the $\overline{SS}$ record, combined with significant (up to 60kyr) gaps in the record as a result of core breaks, precluded the use of evolutionary spectra across these records. The three time-sliced intervals 1900-2700, 2500-3500, and 3500-4100 ka were selected based on a visual comparison of the ODP Site 982 $\overline{SS}$ and $\delta^{18}O_b$ are records, which showed apparent changes in phasing between the two records. The time-slice 1900-2700 ka was extended to overlap the late Pliocene window 2500-3500 ka by 200 kyr, to increase the number of data points in the $\overline{SS}$ record. All cross-spectral analyses from this study were generated using the AnalySeries package (Paillard et al. 1996). The results presented here for SST and $\delta^{18}O_b$ are similar to those reported by Lawrence et al., (2009) who used the Arand software with iterative spectral analysis across the 4100 ka - present interval. Therefore, the time-slice spectral method used here appears not significantly influence the interpretation.

Following paleoceanographic convention, $\delta^{18}O_b$ records were inverted prior to analysis, to orient increasing $\delta^{18}O_b$ BWT with increasing alkenone SST. Confidence intervals were located at the 90% level, except for one record, which additionally used the 95% confidence level. Confidence intervals were defined using a red noise spectrum. Prior to coherency and phase analysis, all records were interpolated to evenly spaced intervals of 3kyr. Due to the lower resolution of the $\overline{SS}$ record (<10 kyr sample spacing), no spectral peaks below the 41 kyr peak are discussed in this section. SST, $\delta^{18}O_b$ and $\overline{SS}$ are compared to the orbital solutions of Laskar et al. (2004)

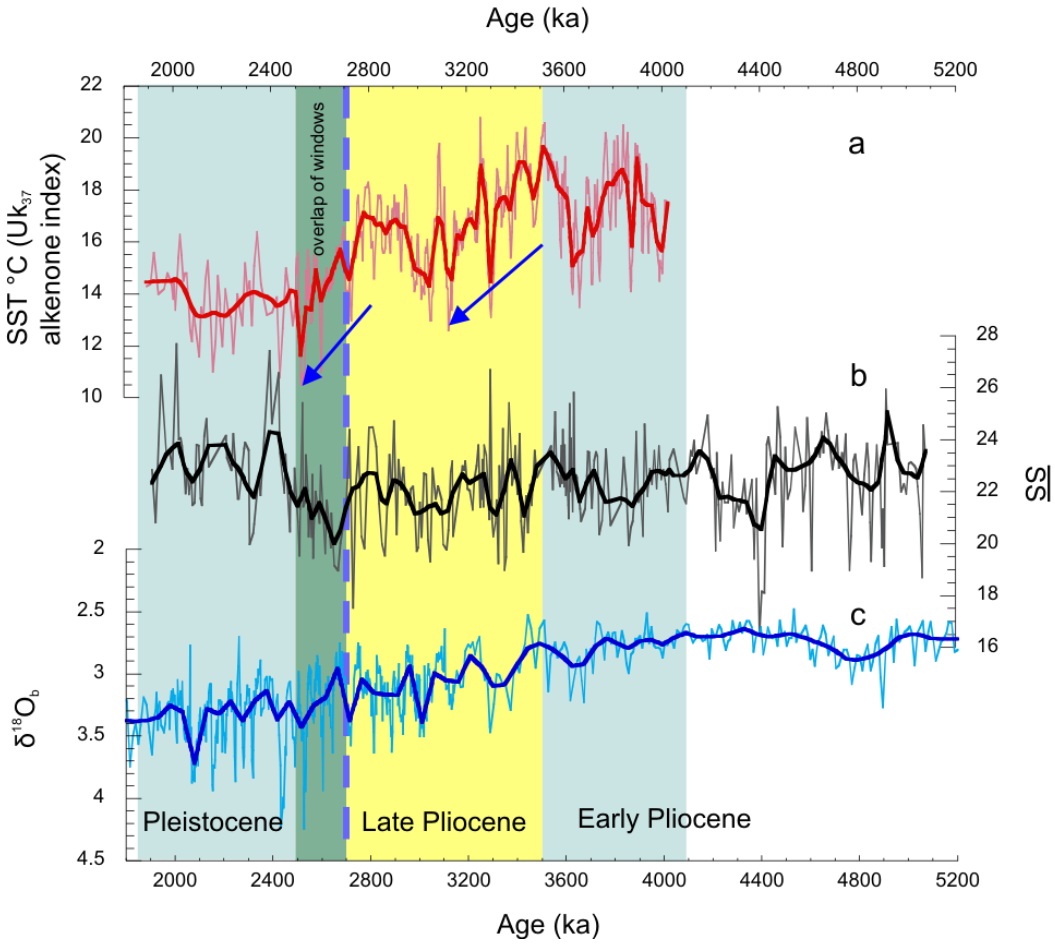


*Figure 6-5 a) SST (Lawrence et al. 2009), b) $\overline{SS}$ bottom water flow speed (this study) and c) $\delta^{18}O_b$* (Venz & Hodell 2002; L. E. Lisiecki & Raymo 2005) *for Site 982 across the period 5200-1900 ka. All records are smoothed with an approximately 100 kyr weighted mean. The three windows used for spectral analysis are highlighted in grey and yellow. Note the overlap between the Pleistocene and Late Pliocene windows of approximately 200 kyr. Periods of declining SST are highlighted with blue arrows at 3500-3100 and 2800-2600 respectively. Blue dashed line at 2700 ka highlights the cooling of bottom waters.*

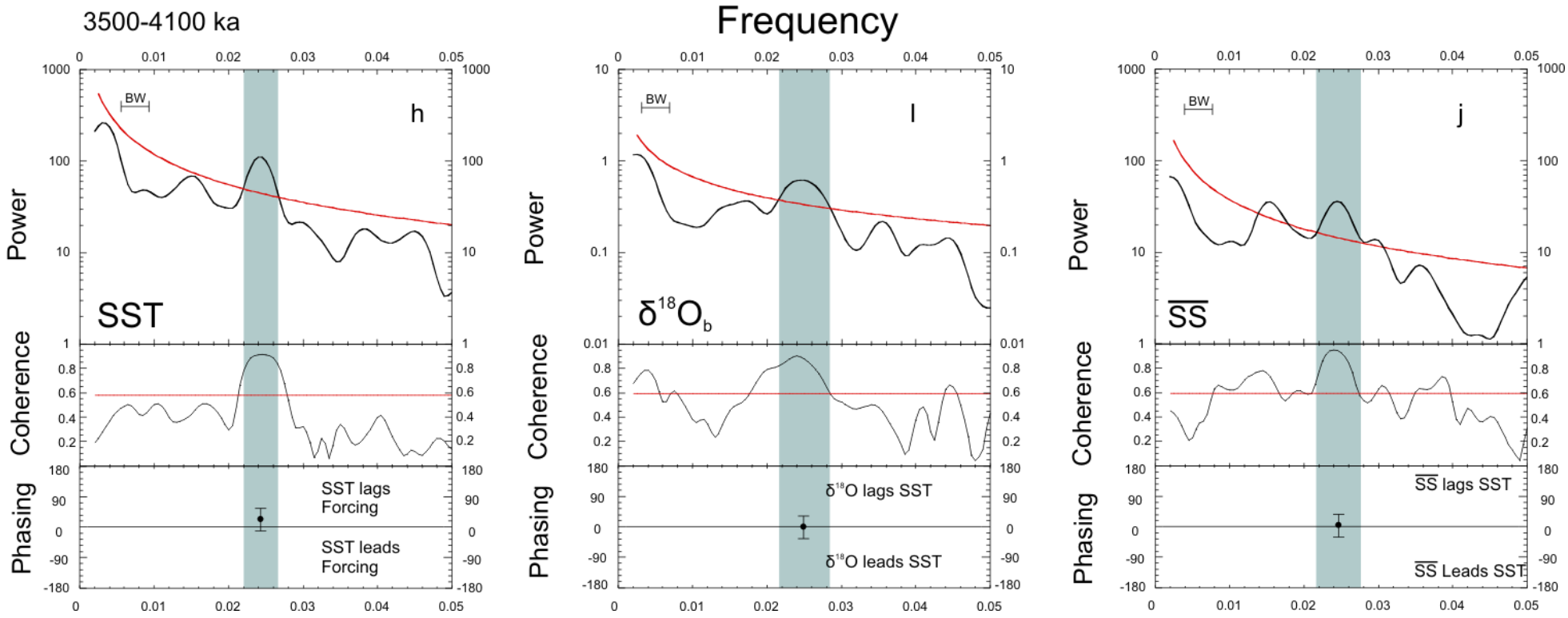


*Figure 6-6 Early Pliocene (5100-3500 ka)*

*This period is characterised by all three records showing similar peaks in the power spectra. All records show a significant 41kyr signal (grey band). Both $\overline{SS}$ (j) and $\delta^{18}O_b$ (i) are coherent with SST, and both show a minimal phase lag of 1kyr to when compared to SST. SST lags obliquity forcing by approximately 3kyr, beneath the significance level. Red lines are the 90% confidence interval.*

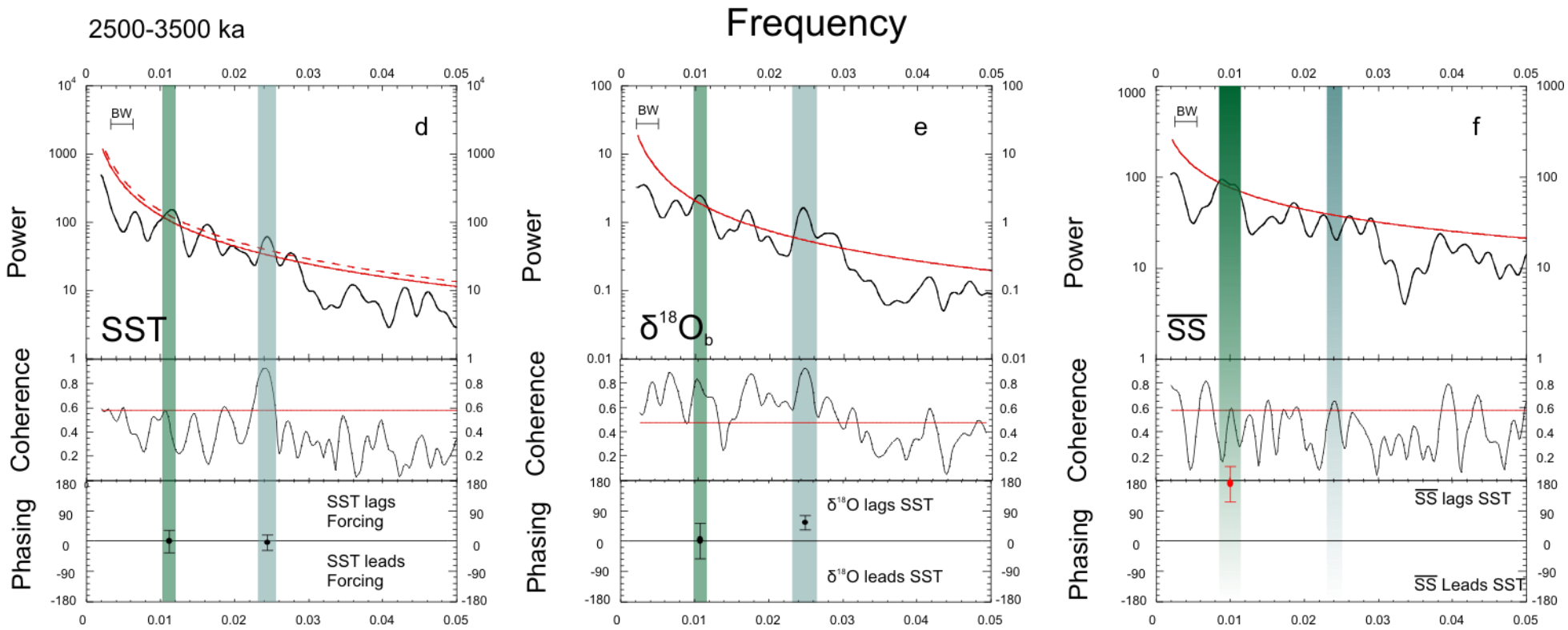


*Figure 6-7 Late Pliocene (3500-2500 ka)*

*SST (d) exhibits weak distinct but still significant spectral peaks at 100 and 41 kyr. The 95% confidence interval was included on this record to emphasise that these peaks are still significant. SST also shows little to no lag with respect to obliquity forcing (grey band). $\delta^{18}O_b$ (e) shows significant peaks in the 100kyr and 41kyr periods, while $\overline{SS}$ (f) only shows weakly significant peaks in the 100kyr period, but both exhibit coherence with the eccentricity solution (e and f, green band). $\delta^{18}O_b$ is in phase with eccentricity, while $\overline{SS}$ is 180 degrees out of phase. In the 41kyr band, $\delta^{18}O_b$ lags the SST record by 44°, or approximately 9kyr. Red lines are the 90% confidence interval.*

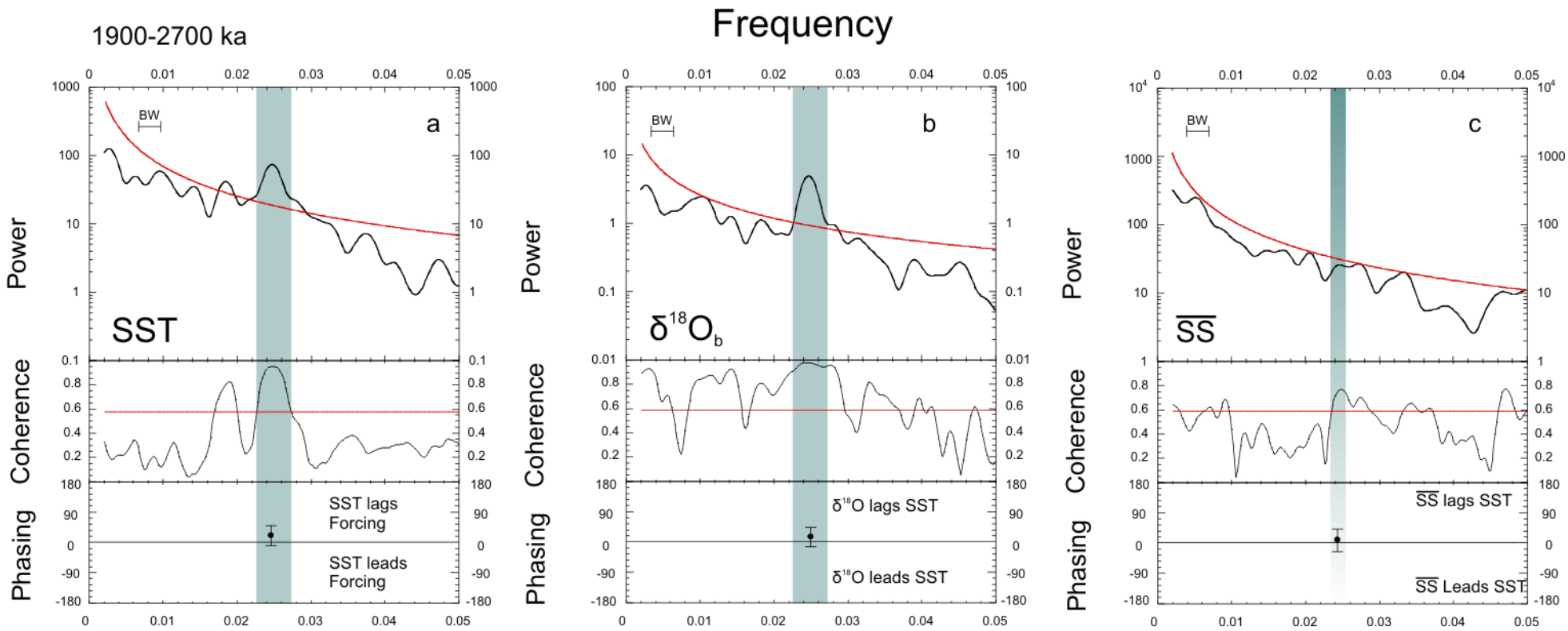


*Figure 6-8 Early Pleistocene (1900-2700 ka) Both SST (a) and $\delta^{18}O_b$ (b) exhibit strong 41kyr cyclicity and are coherent to the 90% confidence level, with $\delta^{18}O_b$ lagging forcing by approximately 5.8 kyr. SST lags obliquity forcing by approximately 3.4 kyr. $\overline{SS}$ exhibits no strong spectral peaks or coherency with either SST or $\delta^{18}O_b$. Red lines are the 90% confidence interval.*

To briefly summarise the major phase relationships:

*Early Pliocene 4100-3500 ka*

Sortable silt and $\delta^{18}O_b$ are strongly in phase with each other and SST at the 41 kyr period, and all three show no significant lag to obliquity forcing. There is no significant 100 kyr periodicity evident in this time-slice.

*Late Plicoene 3500-2500 ka*

SST remains strongly in phase with obliquity forcing, with an insignificant lead/lag. $\delta^{18}O_b$ develops a lag of up to 9 kyr with respect to SST at the 41 kyr periodicity. $\overline{SS}$ shows no significant 41 kyr periodicity. All three records show weak but significant 100 kyr periodicities at this time. SST and $\delta^{18}O_b$ are in phase with the eccentricity forcing, whereas $\overline{SS}$ is 180° out of phase.

*Plio- Pleistocene 2700-1900 ka*

SST lags obliquity forcing by ~3.4 kyr. $\delta^{18}O_b$ lags SST by 2.4 kyr, and obliquity by 5.8 kyr $\overline{SS}$ shows no relationship to orbital forcing.

### 6.4.1 Early Pliocene response to orbital forcing

The changing relationship of the three proxies between the early and late Pliocene demonstrates the increasing influence of ice sheets on the $\delta^{18}O_b$ signal, which is then reflected in the deep water masses at ODP Site 982. In the early Pliocene, the $\delta^{18}O_b$ and $\overline{SS}$ record largely reflect the North Atlantic alkenone-based SST record. North Atlantic SSTs show significant variability at the obliquity frequency during the early Pliocene, with temperatures being 2–4 °C lower when Earth's obliquity and high-latitude insolation were reduced (*Figure 6-6*). Changes in obliquity drive synchronous changes in SST and $\delta^{18}O_b$, which is interpreted at this stage of the Pliocene, prior to any major shifts in $\delta^{18}O_{sw}$, as largely reflecting bottom water temperature. The significant cross-spectral coherence between SST and $\overline{SS}$ deep water flow speeds at the obliquity period also implies a link between SST and the vigour of the intermediate depth circulation in the North Atlantic Ocean, although perhaps surprisingly, no

connection between benthic $\delta^{13}C$ and SST is seen with the same periodicity. This would suggest that at the eccentricity and obliquity periods, processes that control the vigour of the bottom water flow (as measured by $\overline{SS}$), are not the same as those which control the chemical ventilation (as measured by $\delta^{13}C$).

During periods of high obliquity, SST's at Site 982 are warmer, suggesting the increased seasonality of high obliquity drove the flow of warm and saline surface waters to high latitude deep water forming regions. The correspondence with maxima in $\overline{SS}$ suggests that these warm surface waters enhanced deep water formation in the early Pliocene. Intense evaporative cooling of the surface water would have increased its density and allowed the sinking of surface water. The opposite cycle would have occurred in periods of low obliquity, with cooler and less saline surface waters failing to sink as readily.

### 6.4.2 Late Pliocene response to orbital forcing

Following 3500 ka, a lag of 9 kyr develops between SST and $\delta^{18}O_b$ at ODP Site 982, as previously determined using a windowed approach by Lawrence (2009). During periods when the Earths obliquity and high latitude insolation were reduced, SST responds with immediate cooling, whereas the combined BWT/ice volume signal of the $\delta^{18}O_b$ record lags behind by up to 9 kyr. This is interpreted (again, following Lawrence et al. 2009) as increasing global ice volume (*Figure 6-10*c) responding more slowly to the changes in forcing than SST, and causing the $\delta^{18}O_b$ signal to be delayed in its response. This 'inertia' of the ice sheet is seen in modern data from Greenland (Hanna et al. 2008), and ice sheet models of the Antarctic continent (Pollard & DeConto 2005). The study of Lawrence et al. (2009) shows that the lag between SST and $\delta^{18}O_b$ reaches a maximum of 9 kyr at approximately 2800 ka, immediately prior to the onset of major IRD deposition in the Northern Hemisphere.

The $\overline{SS}$ record during this period does not exhibit any consistent variability at the obliquity period, and this is not likely to be due to poor sampling/low resolution data, as the average sample spacing across the time period 2500-3500 ka is <10kyr. Furthermore, a visual comparison shows little apparent link between the $\overline{SS}$ record

and the obliquity solution of Laskar et al., (2004) (*Figure 6-9*). The opposite is true of the 100 kyr cyclicity in SST and $\delta^{18}O_b$. The 100kyr cyclicity was noted in the SST record for this time period by Lawrence et al (2009), and was interpreted as spurious multiples (60, 80 and 120 kyr) of the 41kyr band. In this study, 100 kyr cyclicity is also observed in the $\delta^{18}O_b$ and $\overline{SS}$ records, which show no multiple peaks surrounding the 0.01 frequency band, but exhibit coherence with the eccentricity solution (*Figure 6-7* e and f, green band). $\delta^{18}O_b$ shows no lag with respect to eccentricity, whereas $\overline{SS}$ is 180 degrees out of phase (a lag of 50 ky).

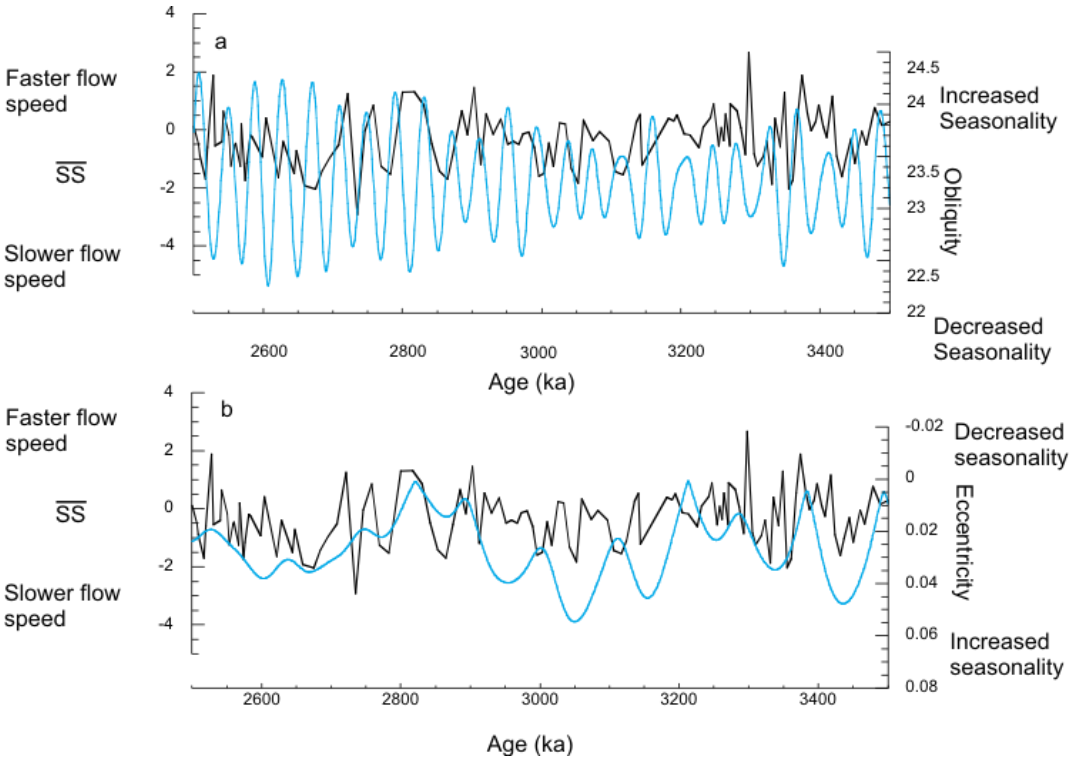


*Figure 6-9 The relationship between $\overline{SS}$ and orbital forcing in the late Pliocene. $\overline{SS}$ is normalised to the variance of the data. There is no clear correlation between a) $\overline{SS}$ and obliquity forcing. However, there is weak correlation b) between the inverse of the eccentricity solution and $\overline{SS}$. Orbital forcing from Laskar et al., 2004*

In the '100kyr world' of the late Pleistocene and Holocene (0-900 ka) the relatively weak eccentricity forcing is partially amplified by changes in the storage of $CO_2$ in the deep ocean to cause major ice volume shifts, resulting in $\delta^{18}O_b$ oscillations of up to 2.7 ‰ (Shackleton 2000); however the 100kyr variations in eccentricity in the Pliocene $\delta^{18}O_b$ record are of similar magnitude to the contemporaneous obliquity oscillations -

around 0.5 ‰. A similar transition from obliquity dominated $\delta^{18}O_b$ to eccentricity dominated $\delta^{18}O_b$ occurred in the Miocene (14.7-12.7 Ma), where a shift to eccentricity-dominated $\delta^{18}O_b$ variability was not accompanied by an increase in the amplitude of the $\delta^{18}O_b$ variation (Holbourn et al. 2005). Periods in the Miocene and Pliocene that were influenced by the 100kyr cyclicity were clearly not subject to the same feedbacks that drove the major 100 kyr paced Pleistocene glaciations.

While SST continued to respond to obliquity forcing in the same way as during the early Pliocene – with warmer waters dominating during periods of high obliquity – the $\overline{SS}$ response is completely different. Instead of increased flow speeds during periods of high obliquity, there is no relation between obliquity and $\overline{SS}$. It is important to note that there is no evidence for a decrease in deep water formation at this time. On the contrary, at the same point the link between SST and $\overline{SS}$ breaks, there is a significant increase in the relative contribution of NADW to the Southern Ocean (Section 6.3.1). The consequence of the breakdown was in fact an increase in penetration of deep water into the southern ocean. This breakdown of the link between SST and deep water flow speed also occurs at the same time as the increase in global ice volume at 3500 ka (Figure 6-10) .

Given the developing lag seen in the Site 982 $\delta^{18}O_b$ records in relation to SST and obliquity, it is possible that the increase in ice volume is the cause for the disconnect between SST and $\overline{SS}$. With any increase in ice volume in the northern hemisphere likely including ice sheets on the North American continent and Greenland, (see chapter 5), there would be an associated local cooling effect out of sync with the obliquity forcing and input of warm waters to the high latitudes. During periods of both high and low obliquity (and high and low regional SSTs), this cooling effect may have allowed deep water formation in new locations such as the Labrador Sea independent of the strength of the obliquity forcing, increasing the volume of NADW exported southwards. This would also have the added feedback of increasing the thermal isolation of the new ice sheets, further encouraging their growth (M. Sarnthein et al. 2009).

While different water masses are in some cases distinguishable using tracers such as $\delta^{13}C$, this relies on the source waters for these masses having distinct $\delta^{13}C$ values. At present, there are no records of sufficiently high resolution from potential source water regions such as the Labrador and Norwegian seas to test this. Nevertheless, a long term $\delta^{13}C$ increase at Site 982 does begin at 3500 ka, which may point to a new source water.

It is also important to emphasise that the local nature of the proposed interactions between ice sheet, deep water formation and sea surface temperatures requires that significant continental ice was present around the deep water forming regions of the North Atlantic from as early as 3500 ka. This answers a question outstanding from the previous chapter, where it was not possible to determine the location of the ice volume increase.

### 6.4.3 Plio-Pleistocene responses to orbital forcing

The dominant influence of the 100 kyr eccentricity cycle on $\delta^{18}O_b$ and $\overline{SS}$ during the late Pliocene lasts for approximately 1000 kyr until 2500 ka (*Figure 6-7e*). After that time, the power of the 41kyr cyclicity in the $\delta^{18}O_b$ record was greater than before, reflecting the marked expansion of the obliquity controlled ice sheets that dominate the 41kyr world (*Figure 6-8*). This is not reflected in the $\overline{SS}$ record for the period 2500-1900 (*Figure 6-8*c), which may imply that the intensity of the formation of deep water had become insensitive to orbital forcing. However, it may also be a combination of occasional IRD influence on the grain size distribution overwhelming the current sorted signal, low resolution, and sampling gaps in key locations.

The relatively small lag (~2 kyr) between $\delta^{18}O_b$ and SST during the period 1900-2700 ka suggests that SST at ODP Site 982 and $\delta^{18}O_b$ were both responding to the obliquity forcing at the same time - similarly to the situation in the early Pliocene. However, in contrast to that time period, they both now lag the obliquity forcing; SST by 3.6 kyr, $\delta^{18}O_b$ by 5.8 kyr (*Figure 6-8*). The persistence of the ice volume 'inertia' effect (Hanna et al. 2008; Pollard & DeConto 2005) also influences the SST record, whereas throughout the period 2500-4100, SST was essentially in phase with the obliquity

forcing (*Figure 6-6 Figure 6-7*). At ODP Site 607, BWT leads $\delta^{18}O_b$ throughout the early Pleistocene (2400-2600 ka) (Sosdian & Rosenthal 2009), much like the relationship between SST and $\delta^{18}O_b$ at ODP Site 982. The similar relationship between BWT and $\delta^{18}O_b$, along with the low $\delta^{13}C$ gradient between the sites suggests that the deep ocean water mass at ODP Site 607 was predominantly sourced from convective activity in the North Atlantic for the majority of the Pliocene.

The delayed response of SST at ODP Site 982 to obliquity forcing between 2500-1900 ka suggests a change in the controlling influence on SST in the high latitude North Atlantic. Previous studies have suggested a change in the position of the sub-polar front at various times throughout the Pliocene (Naafs et al. 2010; Lawrence et al. 2009), and this study confirms that increased lag exhibited by ODP Site 982 SST relative to obliquity following 2700 ka suggests that the SST at ODP Site 982 was being influenced to a greater extent by the proximity of the regional ice volume, as would be consistent with a sub-polar water mass. This is in direct contrast to the situation in the Pliocene 3500-2700 ka, when the tropically sourced surface water mass at ODP Site 982 was unaffected by changing ice volumes, consistent with a stronger NAC controlling the surface water at this site, and implicitly stronger overturning.

## 6.5 Cause of global changes in climate response at 3500 ka.

In order to examine the cause of observed changes in the climate response at 3500 ka the benthic $\delta^{18}O_b$ record of ODP Site 982 was filtered at the central frequencies of the eccentricity and obliquity cycles observed in the power spectra. The records shown in Figure 6-10 exhibit a clear shift in the response of the $\delta^{18}O_b$ signal to orbital forcing at 3500 ka. At that time there is a transient decrease in the strength of the 41 kyr component of the record, coincident with a prolonged increase in the power observed in the 100 kyr cycle. This change in response occurs at the beginning of a reduction in the power of the obliquity cycle (3500-3200 ka) that would suggest a decrease in high latitude seasonality. The shift also occurs at the same time as the first of a series of repeated lows in eccentricity (~3500 ka, ~3400 ka, ~3200 ka), which when combined would provide favourable conditions for the growth and survival of ice sheets, similar

to the situation in the Miocene (Holbourn et al. 2005). Therefore, combined with the $\delta^{18}O_{sw}$ inferred 60m (±25m) sea level decrease from 3500 ka, this provides a potential mechanism for the growth of significant ice sheets prior to the increase in $\delta^{18}O_b$ variability seen at ~2700 ka. However, similarly favourable orbital conditions existed at 4800 and 4500 ka, but are not associated with an increase in ice volume or SST cooling (Haug & Tiedemann 1998; Driscoll & Haug 1998). Consequently, while the orbital configuration at 3500 ka may have been the direct cause for the initiation of late Pliocene ice sheet growth, longer term changes in the sensitivity of the climate system must have taken place in the early Pliocene to allow the orbital configuration to have an effect.

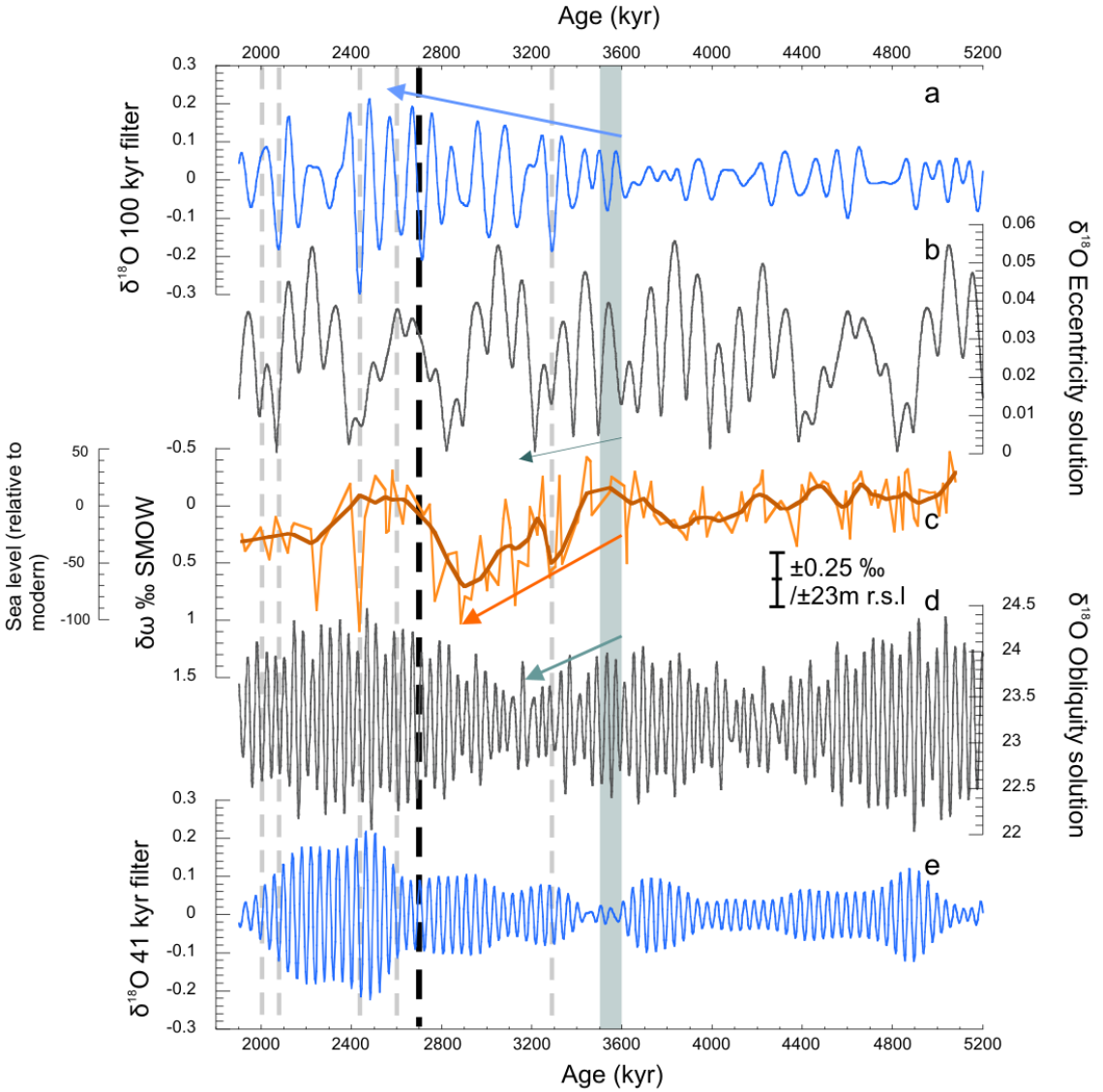

*Figure 6-10 Filtered $\delta^{18}O_b$ time series and the orbital solutions for eccentricity and obliquity forcing are compared to δw reconstructed from ODP Site 982. a) 100kyr filter of $\delta^{18}O_b$ at Site 982 . b) Eccentricity solution of Laskar (2004) c) ice volume reconstructions of this study d) Obliquity solution of Laskar (2004) e) 41kyr filter of $\delta^{18}O_b$ at Site 982. Filters were applied at the frequency of the spectral peak for that time period based on a whole core power spectrum. 100kyr filter: frequency - 0.0102 bandwidth 0.003 41kyr filter: frequency – 0.0246, bandwidth 0.005. Black and grey dashed lines represent periods of IRD depositon at Site 982. Arrows highlight increasing 100 kyr cyclicity in the $\delta^{18}O_b$ record a), declining seasonality in the eccentricity and obliquity orbital cycles b) and d), and increasing ice volume c)*

The sharp increase in the 41kyr component of the $\delta^{18}O_b$ record after 2600 ka (*Figure 6-10*e) represents increasingly large coherent variations in the BWT and global ice volume components of the $\delta^{18}O_b$ record, paced by changes in obliquity cycle. This defines the establishment of the 41kyr world, a feature that persists until the Mid-Pleistocene Transition when increasing climatic sensitivity triggered the 100kyr cyclicity that dominates until the Holocene. As demonstrated in Chapter 5, this is not necessarily a reflection of increased ice volume in the Pleistocene as compared to the Pliocene, but rather an increased sensitivity to solar forcing in already extant ice sheets (Ravelo et al. 2004), combined with an expansion of the ice sheets in the Northern Hemisphere as documented by SST cooling and IRD deposition in the Northern Atlantic region (Bailey et al. 2013; Flesche Kleiven et al. 2002; Lawrence et al. 2009). More specifically to the North Atlantic Ocean, this transition heralds the abrupt cooling of the NADW from a relatively warm Pliocene habit, to a Pleistocene like glacial/interglacial system.

### 6.5.1 Orbital influences on $\delta^{18}O_{sw}$ decrease at 2800-2700 ka

The above discussion has been based on the paradigm of a one way increase in ice volume between 3500-2800 ka. However, as discussed in the previous chapter there is also an apparent decrease in ice volume between 2800-2700 ka. Whether this is an accurate reflection of changing ice volume or rather changing water masses at Site 928 is discussed in some detail in Chapter 5. The evidence presented in this chapter also needs to be evaluated in terms of a potential loss of ice volume.

The changing of SST, $\overline{SS}$ and $\delta^{18}O_b$ to orbital forcing in the period 3500-2800 ka is consistent with an increase in ice volume. If a deglaciation did take place between 2800-2700 ka, it would be expected that relationships between these records would

return towards their pre 3500 ka Pliocene relationships. In particular, the $\overline{SS}$ would be expected to follow more closely the 41ky obliquity forcing. This is not seen, and neither is a warming of SST which would be expected to occur with the removal of the chilling ice sheet. The controls on these two records are inherently local to the North Atlantic region, however, and it may be possible that some or all of the $\delta^{18}O_{sw}$ decrease is produced by a loss of ice volume from Antarctica. Records from nearer to Antarctica are required to confirm this hypothesis.

## 6.6 Long term causes of the initiation of ice sheet growth at 3500 ka.

Assuming that the changes in orbital forcing alone are not sufficient to have caused the growth of ice sheets at 3500 ka, an additional, longer term influence is also required to precondition the climate system and allow the initiation of ice sheet growth. Major trends in the Neogene that are commonly cited as potential causes include:

1. Changing tectonic gateways such as the closure of the Central American Seaway (Haug & Tiedemann 1998) or the Indonesian throughflow (Cane & Molnar 2001), altering ocean circulation pathways and heat/moisture transfer to the high latitudes;
2. Other tectonic events such as rapid uplift of the Tibetan plateau causing aridification of central Asia and a large increase in dust deposition across the North Pacific (Rea et al. 1998);
3. Declining $pCO_2$, either as a result of longer term Cenozoic trends (Raymo et al. 1988) or shorter term responses changes in deep ocean carbon storage or high latitude ocean stratification (Sigman et al. 2010; Haug et al. 1999).

Most studies examining potential causes of Northern Hemisphere Glaciation have focused on the period 3200-2700 ka, as it is at this time that glacial-interglacial $\delta^{18}O_b$ amplitudes increase for the first time (see previous discussion). Haug et al. (1999) demonstrate an increased stratification of the North Pacific and increased sequestration of atmospheric $pCO_2$ below the halocline after 2700 ka, much like the situation in the Southern Ocean during recent glacial periods. However, with the current understanding that significant ice sheets have been growing in the Pliocene

since at least 3500 ka (Mudelsee & Raymo 2005 and this study), these abrupt changes at 2700 ka must be considered threshold responses to a cooling climate, and not causative factors in themselves.

### 6.6.1 Changes in pCO2 during the Pliocene

Atmospheric $pCO_2$ is believed to have remained relatively constant at or around 300-350ppm, from the Miocene (Foster et al. 2012; Badger et al. 2013) until the mid-Pleistocene transition. During the Plio-Pleistocene, alkenone and $\delta^{11}B$ derived $pCO_2$ estimates indicate a drop of around 50 ppm at the 2700 ka climate transition (Seki et al. 2010) (Figure 6-11). As previously discussed, this is likely a result of increased stratification of the high latitude ocean sequestering atmospheric $pCO_2$ in the deep ocean. There is no evidence from either the Seki et al. (2010) record or other pCO2 reconstructions (Pagani et al. 2005; Tripati et al. 2009; Bartoli et al. 2011) from the Pliocene for a $pCO_2$ driven increase in global ice volume at 3500 ka. Indeed, ice volume records from this study show a major increase in ice volume at a period of apparently very stable $pCO_2$ (Figure 6-11)

### 6.6.2 Tectonic changes and intensified ocean circulation

Changes in the bathymetry of Greenland-Iceland-Scotland (GIS) ridge driven by mantle plume uplift of Iceland exercise some control over the strength of North Atlantic overturning, by controlling the entrance into the open North Atlantic of water from the Norwegian Seas (Frank et al. 2002). Today the Norwegian Sea is a major site for deep water formation - the saline bottom water forms a significant component of the NADW (Kroopnick 1985). In both modelling experiments (Robinson et al. 2011) and reconstructions of the Neogene tectonic history of the GIS ridge (Poore et al. 2006), a deeper ridge increases the strength of the bottom water formation. However, it is unclear how sensitive the deep water flux is to changes in the ridge depth, as it was only ~300m deeper in the late Pliocene (Jones et al. 2002).

The closure of the Central American Seaway (CAS) began in the Miocene, with the collision of the Central American Arc into Mexico and subsequently South America (Sykes et al. 1982). The deep ocean connection between the Caribbean and the Pacific

was cut off by approximately 7000 ka, but the surface water connection persisted until around 4400 ka, when a salinity gradient began to develop across the isthmus of Panama (Steph et al. 2010). This restriction of water exchange between the Caribbean and the Pacific is significant for the climate of the high latitude North Atlantic, as it increased the poleward transport of warm salty water (Bartoli, Sarnthein & Weinelt 2005). The progressive closure of the CAS coincides broadly with a strengthening of NADW as seen in the %NCW reconstruction at ODP Site 1090, which may in turn have increased moisture supply to the high latitudes to help initiate ice sheet formation (*Figure 6-11).*

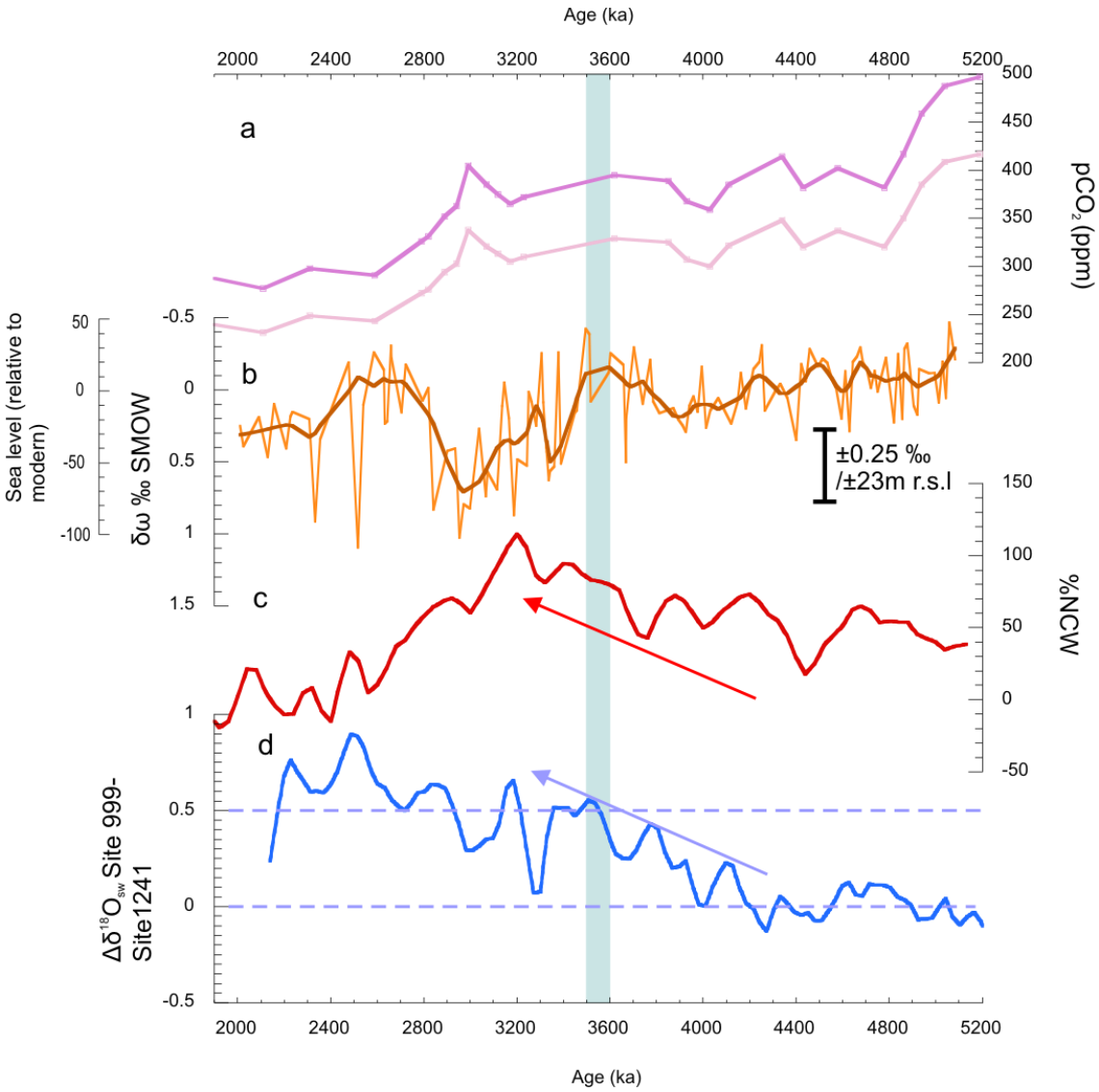


*Figure 6-11 a) Alkenone derived $pCO_2$ reconstruction of Seki et al., 2010. Upper and lower boundaries are shown for the same data. b) Ice volume reconstruction of this study. c) relative strength of NCW at South*

*Atlantic sites 704 and 1090, as previously discussed. Hodell & Venz-Curtis (2006). d) $\delta^{18}O_{sw}$ gradient across the Panama isthmus. Increasing gradient indicates increasingly saline Caribbean waters/fresher Pacific waters (Steph et al., 2010) b), c), and d) data smoothed with a ~100kyr weighted mean.*

Modelling and data studies have investigated the possibility of long-term tectonic changes (aside from ocean gateways) forcing changes in climate. Increased rates of uplift and subsequent weathering of the Himalayas and Andes over the past 5 million years were once thought to have exerted a control on $pCO_2$ (Raymo et al. 1988), however the lack of evidence for long term decreases in $pCO_2$ over the past 15 Ma casts doubt on this (Seki et al. 2010; Badger et al. 2013; Pagani et al. 2005; Pearson & Palmer 2000). Other forcings induced as a result of tectonic uplift include changes in global wind and rainfall patterns; for example, the uplift of the Tibetan plateau at 3600 ka resulted in major aridification in central China and a subsequent increase in Northern Hemisphere atmospheric dust loading in the climatically sensitive mid-northern hemisphere latitudes from 3600 ka (Rea et al. 1998).

The sensitivity of the climate to changes in orography is also seen in climate models simulating both the late Pliocene and the Miocene (Hill et al. 2011; Foster et al. 2010). In both cases, the introduction of increased topography – either as a result of an improved dataset (PRISM3D orography for the MPWP), or as a result of simulating uplift of the Rocky Mountains during the Miocene (Foster et al. 2010) temperature, precipitation and wind patterns differ significantly from the baseline mode. Therefore, periods of tectonic uplift, particularly at a time of inherent climatic sensitivity due to the orbital configuration, can have very significant impacts

### 6.6.3 Summary of potential long term causes of ice sheet growth at 3500 ka

Based on comparisons of global ice volume, high resolution SST and $\delta^{18}O_b$ records (Lawrence et al. 2009; L. E. Lisiecki & Raymo 2005), $\overline{SS}$ bottom water flow speed reconstructions, and the previously discussed tectonic changes, the underlying causes of the increase in global ice volume seen at 3500 ka are interpreted to be:

- Progressive closure of the Central American Seaway from 4200 ka intensified North Atlantic circulation, increasing moisture transport to the high latitudes.

At this point, high latitude Northern Hemisphere climate and deep water formation was dominated by a rapid response to orbital forcing.

- Uplift of the Tibetan plateau caused aridification and erosion in central Asia. The altered wind patterns and increased dust deposition from 3600 ka also increased the sensitivity of the mid-latitudes to cooling.
- An orbital configuration favourable to the initiation of ice sheet growth began at 3500 ka. Low seasonality in both obliquity and eccentricity periods meant that ice that formed in winter was more likely to survive the subsequent summer.
- The presence of larger ice sheets caused a delay in the response of the high latitude Northern Hemisphere to orbital forcing, and increased the sensitivity of the high latitudes to orbital forcing, causing longer term (100 kyr) variability in the North Atlantic climate. Sortable silt records from this study indicate that Northern Hemisphere ice sheets may have also increased the formation of North Atlantic Deep Water, by muting the thermal input of northward surface water transport.
- This variability was inherently unstable, and once this ice had increased to a certain level, a threshold was crossed at 2700 ka, and the global climate shifted into a more strongly orbitally controlled mode. Increases in ocean stratification in the North Pacific and Southern Ocean caused drawdown of $pCO_2$, and increased the proportion of SCW in the Atlantic basin.
- The threshold response may have included a loss of significant continental ice, contributing to the previously discussed decrease in $\delta^{18}O_{sw}$. As at present there is no evidence for such a deglaciation in the Northern Hemisphere it is hypothesised that any ice loss must have occurred in the Antarctic.

# 7 Conclusions and Future Work

Palaeoceanographic records of bottom water temperature, saturation state, ventilation and bottom water flow speed were generated for the North Atlantic ODP Site 982 (1135m water depth). The aim of the project was to reconstruct changes in the behaviour and properties of the intermediate depth North Atlantic water mass and relate them to changes in global climate across the Plio-Pleistocene boundary (5200-1900 ka) during the initiation of Northern Hemisphere Glaciation (3600-2500 ka).

A newly defined morphotype (Rae et al. 2011) 'C *mundulus var*' of a well-known benthic foraminifera *C. mundulus* was described, and its trace metal ratios were compared to other epifaunal and infaunal benthic foraminifera (*C. mundulus, C. wuellerstorfi, M. barleeanum, O. umbonatus*), and to the previous study of this morphotype (Rae et al. 2011). It is found to be similar in many respects to its parent species *C. mundulus*, with a consistent offset in Mg/Ca and B/Ca ratios between the two species.

In Chapter 4, a new, region-specific temperature calibration was constructed for ODP Site 982 using the Pliocene $\delta^{18}O_b$ gradient between intermediate and deep sites (ODP Sites 982 and 607 respectively) to construct a temperature gradient between the two sites, which was then compared with the Mg/Ca offset between the two sites. The calibration produced has a similar temperature sensitivity to other previously published calibrations (e.g., Elderfield et al. 2006; Lear et al. 2002). Variations in the carbonate saturation state of the water mass were reconstructed using benthic B/Ca measurements from this study and the calibration of Yu and Elderfield (2007) to determine if Mg/Ca was influenced by changing $\Delta[CO_3^{2-}]$. Minimal influence was found.

Mg/Ca derived bottom water temperature records showed a relatively warm (~5 °C) water mass persistent at ODP Site 982 prior to 2800 ka. This cooled abruptly (<100 kyr) by approximately 2 °C at 2800-2700 ka, and remained at this average temperature for the rest of the record. The timing and magnitude of bottom water cooling is similar to

records from other sites in the North Atlantic (Bartoli et al, 2005; Sosdian & Rosenthal, 2009).

In Chapter 5, the BWT record was combined with previously published $\delta^{18}O_b$ records (Venz & Hodell 2002; L. Lisiecki & Raymo 2005) from ODP Site 982 to produce a record of $\delta^{18}O_{sw}$ spanning the initiation of Northern Hemisphere Glaciation. This record is the first $\delta^{18}O_{sw}$ record to extend Plio-Pleistocene $\delta^{18}O_{sw}$ reconstructions back into the early Pliocene. The ODP Site 982 $\delta^{18}O_b$ record is believed to be more representative of the global signal than the ODP Site 607 record used in previously published records (Sosdian & Rosenthal 2009), which was affected by local changes in $\delta^{18}O_{sw}$. The likelihood of the Site 982 $\delta^{18}O_{sw}$ record representing global trends accurately was assessed, and it was determined that global ice volume significantly increased from 3500 ka – approximately 900 kyr prior to the onset of significant IRD deposits in the Northern Hemisphere, and 600 kyr prior to significant bottom water cooling. The total increase from 3500 ka to 2900 ka was approximately -0.6 ‰ – equivalent to a sea level decrease of 55m. Based on estimates of the potential 'carrying capacity' of the northern and southern hemisphere polar regions, the potential 55m sea level equivalent increase in ice volume was most likely accommodated partly by formation/expansion of continental ice sheets in the Northern Hemisphere, and partly by expansion of the Antarctic ice sheet.

The global ice volume increased contemporaneously with surface water cooling in the North Atlantic (Lawrence et al. 2009; Naafs et al. 2010), and an expansion in glacial conditions at sites surrounding Antarctica (Naish et al. 2009; Cook et al. 2013; S Passchier 2011). This ice volume increase was then followed by a deglaciation immediately prior to the onset of Pleistocene major ice sheet expansion with IRD deposits in the North Atlantic, at 2700 ka.

The Northern Hemisphere paradox of increased ice volume without concomitant IRD deposits, and at a time of global warmth (Harry J Dowsett, Chandler, et al. 2009; Robinson et al. 2008; Salzmann et al. 2011) was interpreted to be the result of a variable climate with ice sheets repeatedly expanding and retreating, even in the

warmer climate of the Pliocene. This study assumes continental ice sheets in the north prior to 2700 ka never reached the lateral extent of the Pleistocene glaciations, and so were unable to form major IRD belts until ~2700 ka, when major ice sheets reached the continental margin.

A sudden decrease in $\delta^{18}O_{sw}$ at Site 982 contemporaneous with bottom water cooling is interpreted as either potentially major decrease in global ice volume or as a reorganisation of bottom water masses in the North Atlantic. There is evidence to support both explanations, and at present it is not possible to distinguish between them. This study shows that there is no evidence for regional warming or other climatic responses consistent with a return to minimal-ice conditions in the Northern Hemisphere, and that if ice volume did decrease, then this must have occurred predominately in Antarctica.

In Chapter 6, a new Sortable Silt bottom water flow speed record ($\overline{SS}$) for Site 982 was compared to region and global changes in circulation, showing for the first time that physical flow speeds in the North Atlantic deep ocean were persistent throughout major climatic transitions, and independent of major climatic changes. A change in the relationships between previously published orbital scale records of SST (Lawrence et al. 2009), $\delta^{18}O_b$ (Venz & Hodell 2002; L. Lisiecki & Raymo 2005), and new $\overline{SS}$ records from ODP Site 982 after 3500 ka demonstrated the increasing sensitivity of the Northern Hemisphere climate to orbital forcing on both the eccentricity (100 kyr) and obliquity (41kyr) periods. An increased lag of $\delta^{18}O_b$ with respect to SST and obliquity forced changes in insolation coincided with the expansion of ice sheets in the Northern Hemisphere (from 3500 ka), and was interpreted as the increasingly large ice sheets responding less rapidly to changes in orbital forcing than SST. While this is not a novel observation (Lawrence et al. 2009), this study ties it to direct evidence (in the form of the $\delta^{18}O_{sw}$ record) for contemporaneous increasing continental ice volume. The loss of the obliquity signal in the sortable silt record also indicates that the growing ice sheets directly increased the volume of deep water formation in the Northern Hemisphere from 3500 ka, by muting obliquity driven increases in SST and enhancing surface water cooling.

Analysis in this study of the changing $\delta^{18}O_b$ response to orbital forcing to the obliquity and eccentricity orbital solutions of Laskar et al (2004) showed that initial ice volume increase at 3500 ka began at a period of minimal summer insolation and low seasonality, suggesting that this was the immediate trigger for initial ice sheet growth. Increases in the strength of the NAC due to the closure of the Central American Seaway (M Sarnthein et al. 2009) may have increased moisture transport to the high latitiudes (Bartoli, Sarnthein & Weinelt 2005), assisting ice sheet growth at the same time as tectonic uplift altered wind patterns and increased the sensitivity of the high latitudes to orbital forcing.

Reviewing previously published potential climatic influences around the key period at 3500 ka suggested the *underlying* cause of the intensification of glaciation in the late-Pliocene/early-Pleistocene was a series of tectonic shifts changing heat and moisture transport patterns to the high latitudes. This, coincident with orbital conditions favourable to the inception of ice sheets, caused a gradual build-up of continental ice until a threshold was reached at 2700 ka, when the previous energetic transfer of heat/moisture to the high latitudes decreased, and the climate took on the more variable glacial/interglacial nature seen in the Pleistocene. No evidence for $pCO_2$ decline across the key interval 3500-3000 ka was seen, suggesting that the $pCO_2$ decline at 2700 ka may have been a response to cooling climate, rather than a cause.

### 7.1 Future work

New trace metal records are needed from locations outside the North Atlantic region to confirm the global nature of the BWT cooling seen at ODP Sites 982, 609, 607 and 548 at 2800-2700 ka. Given the assumption made in this study that the intermediate depth North Atlantic ODP Site 982 and deep Pacific ODP Site 846 accurately reflect global trends in $\delta^{18}O_b$, BWT records from Site 846 should show an abrupt cooling at 2800-2700 ka, similar to ODP Site 982.

More generally, further research is required into the likely location of the 'hidden' ice sheets of the Late Pliocene. This would include detailed reconstruction of the behaviour of the West and East Antarctic ice sheets, as well as linking them to changes in ocean circulation/ventilation. It is possible that SST records, deep water trace metal records and flow speed records from the Pacific would show different relationships between $\delta^{18}O_{b,}$ SST and flow speed to those seen at Site 982, relating to the evolution of Antarctic ice volumes instead of Arctic.

Within the North Atlantic region, the production of planktonic stable isotope records spanning the period of this study would allow the evaluation of the surface water salinity changes, and the surface to deep $\delta^{13}C$ gradient. This would give further insight into productivity and stratification changes in the North Atlantic surface waters, potentially reinforcing the link between surface water conditions and deep water formation. Much of the current discussion of the North Altantic region is based on relatively few or even single sites. Data from a wide geographical range would allow the establishment of different end-members for NADW formation and the assessment of intra-basinal variability in deep water production.

# 8 References


Adkins, J.F., McIntyre, K. & Schrag, D.P., 2002. The Salinity, Temperature, and δ18O of the Glacial Deep Ocean. *Science* , 298 (5599 ), pp.1769–1773.

Anand, P., Elderfield, H. & Conte, M.H., 2003. Calibration of Mg/Ca thermometry in planktonic foraminifera from a sediment trap time series. *Paleoceanography*, 18(2), p.n/a–n/a.

Badger, M.P.S. et al., 2013. CO2 drawdown following the middle Miocene expansion of the Antarctic Ice Sheet. *Paleoceanography*, pp.1–12.

Bailey, I. et al., 2010. A low threshold for North Atlantic ice rafting from "low-slung slippery" late Pliocene ice sheets. *Atlantic*, 25(1), pp.1–14.

Bailey, I. et al., 2013. An alternative suggestion for the Pliocene onset of major northern hemisphere glaciation based on the geochemical provenance of North Atlantic Ocean ice-rafted debris. *Quaternary Science Reviews*, 75(0), pp.181–194.

Barker, S., Greaves, M. & Elderfield, H., 2003. A study of cleaning procedures used for foraminiferal Mg/Ca paleothermometry. *Geochemistry Geophysics Geosystems*, 4(9), pp.1–20.

Bartoli, G., Sarnthein, M., Weinelt, M., et al., 2005. Final closure of Panama and the onset of northern hemisphere glaciation. *Earth and Planetary Science Letters*, 237, pp.33 – 44.

Bartoli, G., Hönisch, B. & Zeebe, R.E., 2011. Atmospheric CO2 decline during the Pliocene intensification of Northern Hemisphere glaciations. *Paleoceanography*, 26(4), p.PA4213.

Bartoli, G., Sarnthein, M. & Weinelt, M., 2005. Final closure of Panama and the onset of Northern Hemisphere glaciation, Earth Planet. *Sci. Lett*, 237, p.101016/jepsl200506020.

Bartoli, G., Sarnthein, M. & Weinelt, M., 2006. Late Pliocene millennial-scale climate variability in the northern North Atlantic prior to and after the onset of Northern Hemisphere glaciation. *Paleoceanography*, 21(4), pp.1–15.

Bentley, M.J., 1999. Volume of Antarctic Ice at the Last Glacial Maximum, and its impact on global sea level change. *Quaternary Science Reviews*, 18(14), pp.1569–1595.

Bianchi, G.G., 2001. Deep flow variability under apparently stable North Atlantic Deep Water production during the last interglacial of the subtropical NW Atlantic Atlantic Deep Water ( LNADW ). Proxies for both bottom water flow vigor. , 16(3), pp.306–316.

Billups, K., Ravelo, A.C. & Zachos, J.C., 1998. Early Pliocene Deep Water Circulation in the Western Equatorial Atlantic: Implications for High-Latitude Climate Change. *Paleoceanography*, 13(1), pp.84–95.

Billups, K. & Schrag, D.P., 2003. Application of benthic foraminiferal Mg/Ca ratios to questions of Cenozoic climate change. *Earth and Planetary Science Letters*, 209(1-2), pp.181–195.

De Boer, B. et al., 2010. Cenozoic global ice-volume and temperature simulations with 1-D ice-sheet models forced by benthic 18O records. *Annals of Glaciology*, 51(55), pp.23–33.

Boiteau, R., Greaves, M. & Elderfield, H., 2012. Authigenic uranium in foraminiferal coatings: A proxy for ocean redox chemistry. *Paleoceanography*, 27(3), p.PA3227.

Boyle, E. a, 1986. Paired carbon isotope and cadmium data from benthic foraminifera: Implications for changes in oceanic phosphorus, oceanic circulation, and

atmospheric carbon dioxide. *Geochimica et Cosmochimica Acta*, 50(2), pp.265–276.

Boyle, E.A., 1983. Manganese carbonate overgrowths on foraminifera tests. *Geochimica et Cosmochimica Acta*, 47(10), pp.1815–1819.

Boyle, E.A. & Keigwin, L.D., 1985. Comparison of Atlantic and Pacific paleochemical records for the last 215,000 years: Changes in deep ocean circulation and chemical inventories. *Earth and Planetary Science Letters*, 76(1), pp.135–150.

Boyle, E.A. & Keigwin, L.D., 1982. Deep circulation of the North Atlantic over the last 200,000 years: Geochemical evidence. *Science*, 218(4574), pp.784–787.

Brigham-Grette, J. et al., 2013. Pliocene warmth, polar amplification, and stepped Pleistocene cooling recorded in NE Arctic Russia. *Science (New York, N.Y.)*, 340(6139), pp.1421–7.

Broecker, W.S. & Denton, G.H., 1989. The role of ocean-atmosphere reorganizations in glacial cycles. *Geochimica et Cosmochimica Acta*, 53(10), pp.2465–2501.

Cane, M.A., 1998. A Role for the Tropical Pacific. *Science* , 282 (5386 ), pp.59–61.

Cane, M.A. & Molnar, P., 2001. Closing of the Indonesian seaway as a precursor to east African aridi ® cation around 3 ± 4 million years ago. , 411(May), pp.157–162.

Coates, A.G. et al., 1992. Closure of the Isthmus of Panama - the near-Shore Marine Record of Costa-Rica and Western Panama. *Geological Society of America Bulletin*, 104(7), pp.814–828.

Coates, A.G. et al., 2004. The geology of the Darien, Panama, and the late Miocene-Pliocene collision of the Panama arc with northwestern South America. *Geological Society of …*, 116(October 2009), pp.1327–1344.

Coggon, R.M. et al., 2010. Reconstructing Past Seawater Mg/Ca and Sr/Ca from Mid-Ocean Ridge Flank Calcium Carbonate Veins. *Science*, 327(5969), pp.1114–1117.

Cook, C.P. et al., 2013. Dynamic behaviour of the East Antarctic ice sheet during Pliocene warmth. *Nature Geosci*, advance on.

Corliss, B.H. & Honjo, S., 1981. Dissolution of deep-sea benthonic foraminifera. *Micropaleontology*, pp.356–378.

Cramer, B.S. et al., 2011. Late Cretaceous–Neogene trends in deep ocean temperature and continental ice volume: Reconciling records of benthic foraminiferal geochemistry ( δ 18 O and Mg/Ca) with sea level history. *Journal of Geophysical Research*, 116(C12), p.C12023.

Cronin, T.M. et al., 2005. Mid-Pliocene deep-sea bottom-water temperatures based on ostracode Mg/Ca ratios. *Marine Micropaleontology*, 54(3-4), pp.249–261.

Cronin, T.M. et al., 2005. Mid-Pliocene deep-sea bottom-water temperatures based on ostracode Mg/Ca ratios. *Marine Micropaleontology*, 54(3-4), pp.249–261.

Davies, R. et al., 2001. Early Oligocene initiation of North Atlantic Deep Water formation. *Nature*, 410(6831), pp.917–920.

DeConto, R.M. et al., 2008. Thresholds for Cenozoic bipolar glaciation. *Nature*, 455(7213), pp.652–656.

Diester-Haass, L. et al., 2009. Mid-Miocene paleoproductivity in the Atlantic Ocean and implications for the global carbon cycle. *Paleoceanography*, 24.

Dowsett, H.J. et al., 2011. Sea surface temperatures of the mid-Piacenzian Warm Period: A comparison of PRISM3 and HadCM3. *Palaeogeography, Palaeoclimatology, Palaeoecology*, 309(1-2), pp.83–91.

Dowsett, H.J., Chandler, M.A. & Robinson, M.M., 2009. Surface temperatures of the Mid-Pliocene North Atlantic Ocean: implications for future climate. *Philosophical Transactions of the Royal Society A: Mathematical, Physical and Engineering Sciences*, 367(1886), pp.69–84.

Dowsett, H.J., Robinson, M.M. & A, P.T.R.S., 2009. Mid-Pliocene equatorial Pacific sea surface temperature reconstruction : a multi-proxy perspective.

Dowsett, H.J., Robinson, M.M. & Foley, K.M., 2009. Pliocene three-dimensional global ocean temperature reconstruction. *Climate of the Past*, 5(4), pp.769–783.

Driscoll, N.W. & Haug, G.H., 1998. A short circuit in thermohaline circulation: A cause for northern hemisphere glaciation? *Science*, 282(5388), pp.436–438.

Duque-Caro, H., 1990. Neogene stratigraphy, paleoceanography and paleobiogeography in northwest South America and the evolution of the Panama seaway. *Palaeogeography, Palaeoclimatology, Palaeoecology*, 77(3-4), pp.203–234.

Dwyer, G.S. et al., 1995. North Atlantic Deepwater Temperature Change During Late Pliocene and Late Quaternary Climatic Cycles. *Science*, 270(5240), pp.1347–1351.

Dwyer, G.S. & Chandler, M. a, 2009. Mid-Pliocene sea level and continental ice volume based on coupled benthic Mg/Ca palaeotemperatures and oxygen isotopes. *Philosophical transactions. Series A, Mathematical, physical, and engineering sciences*, 367(1886), pp.157–68.

Dwyer, G.S. & Chandler, M.A., 2009. Mid-Pliocene sea level and continental ice volume based on coupled benthic Mg/Ca palaeotemperatures and oxygen isotopes. *Philosophical Transactions of the Royal Society A: Mathematical, Physical and Engineering Sciences*, 367(1886), pp.157–168.

Elderfield, H. et al., 2006. Calibrations for benthic foraminiferal Mg/Ca paleothermometry and the carbonate ion hypothesis. *Earth and Planetary Science Letters*, 250(3-4), pp.633–649.

Elderfield, H., Ferretti, P. & Greaves, M., 2012. Evolution of ocean temperature and ice volume through the Mid-Pleistocene climate transition. *Science*, 704(2012).

Elderfield, H. & Ganssen, G., 2000. Past temperature and delta18O of surface ocean waters inferred from foraminiferal Mg/Ca ratios. *Nature*, 405(6785), pp.442–5.

Evans, D. & Müller, W., 2012. Deep time foraminifera Mg/Ca paleothermometry: Nonlinear correction for secular change in seawater Mg/Ca. *Paleoceanography*, 27(4), p.PA4205.

Fairbanks, R.G., 1989. A 17,000-year glacio-eustatic sea level record: influence of glacial melting rates on the Younger Dryas event and deep-ocean circulation. *Nature*, 342(6250), pp.637–642.

Fauquette, S., Guiot, J. & Suc, J.-P., 1998. A method for climatic reconstruction of the Mediterranean Pliocene using pollen data. *Palaeogeography, Palaeoclimatology, Palaeoecology*, 144(1-2), pp.183–201.

Fedorov, A. V, Brierley, C.M. & Emanuel, K., 2010. Tropical cyclones and permanent El Niño in the early Pliocene epoch. *Nature*, 463(7284), pp.1066–70.

Flesche Kleiven, H. et al., 2002. Intensification of Northern Hemisphere glaciations in the circum Atlantic region (3.5-2.4 Ma) - ice-rafted detritus evidence. *Palaeogeography, Palaeoclimatology, Palaeoecology*, 184(3-4), pp.213–223.

Foster, G.L., Lear, C.H. & Rae, J.W.B., 2012. The evolution of pCO< sub> 2</sub>, ice volume and climate during the middle Miocene. *Earth and Planetary Science Letters*, 341, pp.243–254.

Foster, G.L., Lunt, D.J. & Parrish, R.R., 2010. Mountain uplift and the glaciation of North America – a sensitivity study. *Climate of the Past*, 6(5), pp.707–717.

Francis, J. et al., 2007. Tundra environments in the Neogene Sirius Group, Antarctica: evidence from the geological record and coupled atmosphere–vegetation models. *Journal of the Geological Society*, 164, pp.317–322.

Francis, J.E., 1988. A 50-million-year-old fossil forest from Strathcona Fiord, Ellesmere Island, Arctic Canada: evidence for a warm polar climate. *Arctic*, pp.314–318.

Frank, M. et al., 2002. North Atlantic Deep Water export to the Southern Ocean over the past 14 Myr: evidence from Nd and Pb isotopes in ferromanganese crusts. *Paleoceanography*, 17, p.101029/.

Frank, M., Reynolds, B.C. & Nions, R.K.O., 1999. Nd and Pb isotopes in Atlantic and Pacific water masses before and after closure of the Panama gateway. *Hemisphere*, (October 2009).

Gao, C. et al., 2012. Glaciation of North America in the James Bay Lowland, Canada, 3.5 Ma. *Geology*, 40(11), pp.975–978.

Gibbard, P.L., Head, M.J. & Walker, M.J.C., 2010. Rapid Communication Formal ratification of the Quaternary System / Period and the Pleistocene Series / Epoch with a base at 2 . 58 Ma. , 25(September 2009), pp.96–102.

Glock, N. et al., 2012. EMP and SIMS studies on Mn/Ca and Fe/Ca systematics in benthic foraminifera from the Peruvian OMZ: a contribution to the identification of potential redox proxies and the impact of cleaning protocols. *Biogeosciences*, 9(1), pp.341–359.

Groeneveld, J., 2005. *Effect of the Pliocene closure of the Panamaian gateway on Caribbean and east Pacific sea surface temperatures and salinities by applying combined Mg/Ca and δ18O measure- ments (5.6–2.2 Ma).* University of Kiel.

Hall, I.R. et al., 1998. Coherent deep flow variation in the Iceland and American basins during the last interglacial. *Earth and Planetary Science Letters*, 164(1), pp.15–21.

Hambrey, M.J. et al., 2003. Neogene glacial record from the Sirius Group of the Shackleton Glacier region, central Transantarctic Mountains, Antarctica. *Geological Society of America Bulletin*, 115(8), pp.994–1015.

Hanna, E. et al., 2008. Increased Runoff from Melt from the Greenland Ice Sheet: A Response to Global Warming. *Journal of Climate*, 21(2), pp.331–341.

Haug, G.H. et al., 2005. North Pacific seasonality and the glaciation of North America 2.7 million years ago. *Nature*, 433(7028), pp.821–825.

Haug, G.H. et al., 1999. Onset of permanent stratification in the subarctic Pacific Ocean. *Nature*, 401(6755), pp.779–782.

Haug, G.H. et al., 2001. Role of Panama uplift on oceanic freshwater balance. , (September 2009).

Haug, G.H. & Tiedemann, R., 1998. Effect of the formation of the Isthmus of Panama on Atlantic Ocean thermohaline circulation. *Nature*, 393(6686), pp.673–676.

Haywood, A.M., Valdes, P.J. & Sellwood, B.W., 2000. Global scale palaeoclimate reconstruction of the middle Pliocene climate using the UKMO GCM: initial results. *PRism*.

Healey, S.L., Thunell, R.C. & Corliss, B.H., 2008. The Mg/Ca-temperature relationship of benthic foraminiferal calcite: New core-top calibrations in the < 4 degrees C temperature range. *Earth and Planetary Science Letters*, 272(3-4), pp.523–530.

Heydt, A. von der & Dijkstra, H., 2008. The effect of gateways on ocean circulation patterns in the Cenozoic. *Global and Planetary Change*, 62, pp.132 – 146.

Hill, D.J. et al., 2011. Pliocene climate variability: Northern Annular Mode in models and tree-ring data. *Palaeogeography, Palaeoclimatology, Palaeoecology*, 309(1-2), pp.118–127.

Hodell, D. a. et al., 2009. Surface and deep-water hydrography on Gardar Drift (Iceland Basin) during the last interglacial period. *Earth and Planetary Science Letters*, 288(1-2), pp.10–19.

Hodell, D.A. & Venz-Curtis, K.A., 2006. Late Neogene history of deepwater ventilation in the Southern Ocean. *Geochemistry Geophysics Geosystems*, 7(9).

Holbourn, A. et al., 2013. Changes in Pacific Ocean circulation following the Miocene onset of permanent Antarctic ice cover. *Earth and Planetary Science Letters*, 365, pp.38–50.

Holbourn, A. et al., 2005. Impacts of orbital forcing and atmospheric carbon dioxide on Miocene ice-sheet expansion. , 438(November).

Holbourn, A.E. & Henderson, A.S., 2002. Re-illustration and revised taxonomy for selected deep sea benthic foraminifers. , 4(2), pp.1–36.

Jain, S. & Collins, L.S., 2007. Trends in Caribbean Paleoproductivity related to the Neogene closure of the Central American Seaway. *Marine Micropaleontology*, 63, pp.57 – 74.

Jansen, E. et al., 2000. Pliocene-Pleistocene ice rafting history and cyclicity in the Nordic Seas during the last 3.5 Myr. *Paleoceanography*, 15(6), pp.709–721.

Jansen, E. & Sjøholm, J., 1991. Reconstruction of glaciation over the past 6 Myr from ice-borne deposits in the Norwegian Sea. *Nature*.

Jones, S.M., White, N. & Maclennan, J., 2002. V-shaped ridges around Iceland: Implications for spatial and temporal patterns of mantle convection. *Geochemistry, Geophysics, Geosystems*, 3(10), p.1059.

Kanfoush, S.L., 2000. Millennial-Scale Instability of the Antarctic Ice Sheet During the Last Glaciation. *Science*, 288(5472), pp.1815–1819.

Katz, A., 1973. The interaction of magnesium with calcite during crystal growth at 25–90 C and one atmosphere. *Geochimica et Cosmochimica Acta*, 37(6), pp.1563–1586.

Keigwin, L., 1982. Isotopic Paleoceanography of the Caribbean and East Pacific: Role of Panama Uplift in Late Neogene Time. *Science*, 217(4557), pp.350–353.

Khelifi, N. et al., 2009. A major and long-term Pliocene intensification of the Mediterranean outflow, 3.5-3.3 Ma ago. *Geology*, 37(9), pp.811–814.

Khélifi, N. et al., 2014. Late Pliocene variations of the Mediterranean outflow. *Marine Geology*, 357, pp.182–194.

Khélifi, N., 2010. *Variations in Mediterranean Outflow Water and its salt discharge versus Pliocene changes in North Atlantic thermohaline circulation prior and during the onset of major Northern Hemisphere Glaciation, 3.7 – 2.6 Ma*. University of Kiel.

Khélifi, N., Sarnthein, M. & Naafs, B.D. a., 2012. Technical note: Late Pliocene age control and composite depths at ODP Site 982, revisited. *Climate of the Past*, 8(1), pp.79–87.

Kleiven, H.F. et al., 2002. Intensification of Northern Hemisphere glaciations in the circum Atlantic region (3.5^2.4 Ma) ^ ice-rafted detritus evidence. *Science*, 184.

Kouwenhoven, T.J. & van der Zwaan, G.J., 2006. A reconstruction of late Miocene Mediterranean circulation patterns using benthic foraminifera. *Palaeogeography Palaeoclimatology Palaeoecology*, 238(1-4), pp.373–385.

Kroopnick, P.M., 1985. The distribution of d13C of ΣCO2 in the worlds ocean. *Deep Sea Research Part A. Oceanographic Research Papers*, 32(1), pp.57–84.

Kwiek, P.B.B. & Ravelo, A.C.C., 1999. Pacific Ocean intermediate and deep water circulation during the Pliocene. *Palaeogeography, Palaeoclimatology, Palaeoecology*, 154(3), pp.191–217.

Lambeck, K. et al., 2000. Global ice volumes at the Last Glacial Maximum and early Lateglacial. , 181, pp.513–527.

Lawrence, K.T. et al., 2009. High-amplitude variations in North Atlantic sea surface temperature during the early Pliocene warm period. *Arctic*, 24, pp.1–15.

Lawrence, K.T., Bailey, I. & Raymo, M.E., 2013. Re-evaluation of the age model for North Atlantic Ocean Site 982 – arguments for a return to the original chronology. *Clim. Past Discuss.*, 9(2), pp.2217–2233.

Lea, D.W., Mashiotta, T.A. & Spero, H.J., 1999. Controls on magnesium and strontium uptake in planktonic foraminifera determined by live culturing. *Geochimica Et Cosmochimica Acta*, 63(16), pp.2369–2379.

Lear, C. & Rosenthal, Y., 2004. Late Eocene to early Miocene ice sheet dynamics and the global carbon cycle. *Paleoceanography*, 19(April), pp.1–11.

Lear, C.H., Elderfield, H. & Wilson, P.A., 2000. Cenozoic Deep-Sea Temperatures and Global Ice Volumes from Mg/Ca in Benthic Foraminiferal Calcite. *Science*, 287(5451), pp.269–272.

Lear, C.H., Mawbey, E.M. & Rosenthal, Y., 2010. Cenozoic benthic foraminiferal Mg/Ca and Li/Ca records: Toward unlocking temperatures and saturation states. *Paleoceanography*, 25(4), pp.1–11.

Lear, C.H., Rosenthal, Y. & Slowey, N., 2002. Benthic foraminiferal Mg/Ca-paleothermometry: a revised core-top calibration. *Geochimica et Cosmochimica Acta*, 66(19), pp.3375–3387.

Lear, C.H., Rosenthal, Y. & Wright, J.D., 2003. The closing of a seaway: ocean water masses and global climate change. *Earth and Planetary Science Letters*, 210, pp.425–436.

Lisiecki, L. & Raymo, M., 2005. A Pliocene-Pleistocene stack of 57 globally distributed benthic δ18O records. *Paleoceanography*, doi, p.101029/.

Lisiecki, L.E. & Raymo, M.E., 2005. A Pliocene-Pleistocene stack of 57 globally distributed benthic 18 O records. *Paleoceanography, 20, PA1003*, doi, p.101029/.

Lunt, D.J. et al., 2008. Closure of the Panama Seaway during the Pliocene: implications for climate and Northern Hemisphere glaciation. *Climate Dynamics*, 30(1), pp.1–18.

Mackensen, A. et al., 1993. The δ13C in benthic foraminiferal tests of Fontbotia wuellerstorfi (Schwager) relative to the δ13C of dissolved inorganic carbon in southern ocean deep water: implications for glacial ocean circulation models. *Paleoceanography*, 8(5), pp.587–610.

Maier-Reimer, E., Mikolajewicz, U. & Crowley, T., 1990. Ocean General Circulation Model Sensitivity Experiment with an Open Central American Isthmus. *Paleoceanography*, 5(3), pp.349–366.

Marchitto, T.M. et al., 2007. Mg/Ca temperature calibration for the benthic foraminifer Cibicidoides pachyderma. *Paleoceanography*, 22(1), pp.1–9.

Marchitto, T.M. & Broecker, W.S., 2006. Deep water mass geometry in the glacial Atlantic Ocean: A review of constraints from the paleonutrient proxy Cd/Ca. *Geochemistry, Geophysics, Geosystems*, 7(12), p.Q12003.

Marchitto, T.M., Oppo, D.W. & Curry, W.B., 2002. Paired benthic foraminiferal Cd / Ca and Zn / Ca evidence for a greatly increased presence of Southern Ocean Water in the glacial North Atlantic. , 17(3), pp.1–16.

Marshall, L.G. et al., 1982. Mammalian Evolution and the Great American Interchange. *Science*, 215(4538), pp.1351–1357.

Martin, P.A. et al., 2002. Quaternary deep sea temperature histories derived from benthic foraminiferal Mg/Ca. *Earth and Planetary Science Letters*, 198(1), pp.193–209.

Martin, P.A. & Lea, D.W., 2002. A simple evaluation of cleaning procedures on fossil benthic foraminiferal Mg/Ca. *Geochemistry, Geophysics, Geosystems*, 3(10), pp.1–8.

Martínez-Méndez, G. et al., 2008. 345,000-year-long multi-proxy records off South Africa document variable contributions of Northern versus Southern Component Water to the Deep South Atlantic. *Earth and Planetary Science Letters*, 267(1–2), pp.309–321.

Mawbey, E.M. & Lear, C.H., 2013. Carbon cycle feedbacks during the Oligocene-Miocene transient glaciation. *Geology*, 41(9), pp.963–966.

McCave, I. & Hall, I., 2006. Size sorting in marine muds: Processes, pitfalls, and prospects for paleoflow-speed proxies. *Geochemistry, Geophysics, Geosystems*.

McCave, I., Manighetti, B. & Beveridge, N., 1995. Circulation in the glacial North Atlantic inferred from grain-size measurements. *Nature*.

Mccave, I.N., Manighetti, B. & Robinson, S.G., 1995. Sortable silt and fine sediment size composition slicing - parameters for palaeocurrent speed and palaeoceanography. *Paleoceanography*, 10(3), pp.593–610.

Menzies, J., Gao, C. & Kodors, C., 2013. Microstructural analyses of a Middle Pliocene till from the James Bay Lowlands, Canada—evidence of “potential” fast ice streaming. *Proceedings of the Geologists’ Association*, 124(5), pp.790–801.

Miller, K.G. et al., 2005. The Phanerozoic record of global sea-level change. *Science (New York, N.Y.)*, 310(5752), pp.1293–8.

Mix, A.C. et al., 1995. Benthic foraminifer stable isotope record from Site 849 (0-5 Ma): local and global climate changes. In Proceedings of the Ocean Drilling Program, Scientific Results.

Mortlock, R.A. & Froelich, P.N., 1989. A simple method for the rapid determination of biogenic opal in pelagic marine sediments. *Deep Sea Research Part A. Oceanographic Research Papers*, 36(9), pp.1415–1426.

Mudelsee, M., 1999. RAMPFIT—a Fortran 77 program for ramp function regression. *manfredmudelsee.com*.

Mudelsee, M. & Raymo, M.E., 2005. Slow dynamics of the Northern Hemisphere glaciation. *Paleoceanography, 20, PA4022*, doi, p.101029/.

Murphy, L. et al., 2002. History of ice rafting at South Atlantic ODP Site 177-1092 during the Gauss and Late Gilbert Chrons. *Palaeogeography, Palaeoclimatology, Palaeoecology*, 182(3-4), pp.183–196.

Naafs, B.D. a. et al., 2010. Late Pliocene changes in the North Atlantic Current. *Earth and Planetary Science Letters*, 298(3-4), pp.434–442.

Naafs, B.D.A. et al., 2012. Strengthening of North American dust sources during the late Pliocene (2.7 Ma). *Earth and Planetary Science Letters*, 317–318(0), pp.8–19.

Naish, T. et al., 2009. Obliquity-paced Pliocene West Antarctic ice sheet oscillations. *Nature*, 458(7236), pp.322–8.

Negre, C. et al., 2010. Reversed flow of Atlantic deep water during the Last Glacial Maximum. *Nature*, 468(7320), pp.84–88.

Negre, C. et al., 2010. Reversed flow of Atlantic deep water during the Last Glacial Maximum. *Nature*, 468(7320), pp.84–8.

Nisancioglu, K.H., Raymo, M.E. & Stone, P.H., 2003. Reorganization of Miocene deep water circulation in response to the shoaling of the Central American Seaway. *Paleoceanography*, 18(1), pp.1–12.

Nürnberg, D., Bijma, J. & Hemleben, C., 1996. Assessing the reliability of magnesium in foraminiferal calcite as a proxy for water mass temperatures. *Geochimica et Cosmochimica Acta*, 60(5), pp.803–814.

Oppo, D.W. et al., 1990. Late Pleistocene southern ocean δ13C variability. *Paleoceanography*, 5(1), pp.43–54.

Oppo, D.W. & Fairbanks, R.G., 1987. Variability in the deep and intermediate water circulation of the Atlantic Ocean during the past 25,000 years: Northern Hemisphere modulation of the Southern Ocean. *Earth and Planetary Science Letters*, 86(1), pp.1–15.

Orsi, A.H., Johnson, G.C. & Bullister, J.L., 1999. Circulation, mixing, and production of Antarctic Bottom Water. *Progress in Oceanography*, 43(1), pp.55–109.

Pagani, M. et al., 2009. High Earth-system climate sensitivity determined from Pliocene carbon dioxide concentrations. *Nature Geoscience*, 3(1), pp.27–30.

Pagani, M. et al., 2005. Marked decline in atmospheric carbon dioxide concentrations during the Paleogene. *Science (New York, N.Y.)*, 309(5734), pp.600–3.

Paillard, D., Labeyrie, L. & Yiou, P., 1996. Macintosh Program performs time-series analysis. *Eos, Transactions American Geophysical Union*, 77(39), p.379.

Passchier, S., 2011. Linkages between East Antarctic Ice Sheet extent and Southern Ocean temperatures based on a Pliocene high-resolution record of ice-rafted debris off Prydz Bay, East Antarctica. *Paleoceanography*, 26(4), p.n/a–n/a.

Passchier, S., 2011. Linkages between East Antarctic Ice Sheet extent and Southern Ocean temperatures based on a Pliocene high-resolution record of ice-rafted debris off Prydz Bay, East Antarctica. *Paleoceanography*, 26(4), p.PA4204.

Pearson, P., 2012. Oxygen isotopes in foraminifera: Overview and Historical review. *Paleontological Society Papers*, 18, pp.1–38.

Pearson, P.N. & Palmer, M.R., 2000. Atmospheric carbon dioxide concentrations over the past 60 million years. *Nature*, 406(6797), pp.695–9.

Pollard, D. & DeConto, R.M., 2005. Hysteresis in Cenozoic Antarctic ice-sheet variations. *Global and Planetary Change*, 45(1–3), pp.9–21.

Pollard, D. & DeConto, R.M., 2009. Modelling West Antarctic ice sheet growth and collapse through the past five million years. *Nature*, 458(7236), pp.329–32.

Poore, H.R. et al., 2006. Neogene overflow of Northern Component Water at the Greenland-Scotland Ridge. *Oceans*.

Praetorius, S.K. et al., 2008. Episodic reductions in bottom-water currents since the last ice age. *Nature Geosci*, 1(7), pp.449–452.

Rae, J.W.B.B. et al., 2011. Boron isotopes and B/Ca in benthic foraminifera: Proxies for the deep ocean carbonate system. *Earth and Planetary Science Letters*, 302(3-4), pp.403–413.

Raitzsch, M. et al., 2011. Modern and late Pleistocene B/Ca ratios of the benthic foraminifer Planulina wuellerstorfi determined with laser ablation ICP-MS. *Geology*, 39(11), pp.1039–1042.

Ravelo, A.C. et al., 2004. Regional climate shifts caused by gradual global cooling in the Pliocene epoch. *Nature*, 429, p.101038/nature02567.

Raymo, M.E. et al., 1990. Evolution of Atlantic-Pacific δ13C gradients over the last 2.5 m.y. *Earth and Planetary Science Letters*, 97(3–4), pp.353–368.

Raymo, M.E. et al., 1996. Mid-Pliocene warmth : stronger greenhouse and stronger conveyor. , 27(1987).

Raymo, M.E. et al., 2004. Stability of North Atlantic water masses in face of pronounced climate variability during the Pleistocene. *Paleoceanography*, 19(2), pp.1–13.

Raymo, M.E., 1994. The initiation of northern-hemisphere glaciation. *Annual Review of Earth and Planetary Sciences*, 22, pp.353–383.

Raymo, M.E., 1997. The timing of major climate terminations. *Paleoceanography*, 12(4), pp.577–585.

Raymo, M.E., Hodell, D. & Jansen, E., 1992. Response of Deep Ocean Circulation to Initiation of Northern Hemisphere Glaciation (3-2 MA). *Paleoceanography*, 7.

Raymo, M.E., Ruddiman, F. & Froelich, N., 1988. Influence of late Cenozoic mountain building on ocean geochemical cycles: *Geology*, v, pp.16p649–653.

Raymo, M.E. & Ruddiman, W.F., 1992. Tectonic Forcing of Late Cenozoic Climate. *Nature*, 359(6391), pp.117–122.

Rea, D.K., Snoeckx, H. & Joseph, L.H., 1998. Late Cenozoic eolian deposition in the North Pacific: Asian drying, Tibetan uplift, and cooling of the northern hemisphere. *Paleoceanography*, 13(3), pp.215–224.

Reid, J.L., 1979. On the contribution of the Mediterranean Sea outflow to the Norwegian-Greenland Sea. *Deep Sea Research Part A. Oceanographic Research Papers*, 26(11), pp.1199–1223.

Rhein, M., Stramma, L. & Krahmann, G., 1998. The spreading of Antarctic bottom water in the tropical Atlantic. *Deep Sea Research Part I: Oceanographic Research Papers*, 45(4–5), pp.507–527.

Rickaby, R.E.M. & Elderfield, H., 1999. Planktonic foraminiferal Cd/Ca: Paleonutrients or paleotemperature? *Paleoceanography*, 14(3), pp.293–303.

Ridgwell, A.J., Watson, A.J. & Raymo, M.E., 1999. Is the spectral signature of the 100 kyr glacial cycle consistent with a Milankovitch origin? *Paleoceanography*, 14(4), pp.437–440.

Robinson, M.M. et al., 2011. Bathymetric controls on Pliocene North Atlantic and Arctic sea surface temperature and deepwater production. *Palaeogeography, Palaeoclimatology, Palaeoecology*, 309(1-2), pp.92–97.

Robinson, M.M. et al., 2008. Reevaluation of mid-Pliocene North Atlantic sea surface temperatures. *Paleoceanography*, 23(3), pp.1–9.

Roden, G.I., 1987. Effect of seamounts and seamount chains on ocean circulation and thermohaline structure. *Seamounts, islands, and atolls*, pp.335–354.

Rodríguez-Sanz, L. et al., 2012. Glacial Southern Ocean freshening at the onset of the Middle Pleistocene Climate Transition. *Earth and Planetary Science Letters*, 345, pp.194–202.

Rosenthal, Y., Field, M.P. & Sherrell, R.M., 1999. Precise determination of element/calcium ratios in calcareous samples using sector field inductively coupled plasma mass spectrometry. *Analytical chemistry*, 71(15), pp.3248–53.

Ruddiman, W.F., 1977. LATE QUATERNARY DEPOSITION OF ICE-RAFTED SAND IN SUBPOLAR NORTH-ATLANTIC (LAT 40-DEGREES TO 65-DEGREES-N). *Geological Society of America Bulletin*, 88(12), pp.1813–1827.

Salzmann, U. et al., 2008. A new global biome reconstruction and data-model comparison for the Middle Pliocene. *Global Ecology and Biogeography*, 17(3), pp.432–447.

Salzmann, U. et al., 2011. Climate and environment of a Pliocene warm world. *Palaeogeography, Palaeoclimatology, Palaeoecology*, 309(1-2), pp.1–8.

Sarnthein, M. et al., 2009. Mid-Pliocene shifts in ocean overturning circulation and the onset of Quaternary-style climates. *Climate of the Past*, 5(2), pp.269–283.

Sarnthein, M. et al., 2009. Mid-Pliocene shifts in ocean overturning circulation and the onset of Quaternary-style climates. *Climate of the Past*, 5(2), pp.269–283.

Schlitzer, R., 2013. Ocean Data View.

Schneider, B. & Schmittner, A., 2006. Simulating the impact of the Panamanian seaway closure on ocean circulation, marine productivity and nutrient cycling. *Earth and Planetary Science Letters*, 246, pp.367–380.

Seki, O., Foster, G.L., et al., 2010. Alkenone and boron-based Pliocene pCO2 records. *Earth and Planetary Science Letters*, 292(1-2), pp.201–211.

Seki, O., Foster, G.L., et al., 2010. Earth and Planetary Science Letters. *Earth*, 292, pp.201–211.

Shackleton, N. & Kennett, J., 1975. Paleotemperature history of the Cenozoic and the initiation of Antarctic glaciation: oxygen and carbon isotope analyses in DSDP Sites 277, 279, and 281. In *Init. Repts. Deep Sea Drilling Project*. pp. 743–755.

Shackleton, N.J., 1974. Attainment of isotopic equilibrium between ocean water and the benthonic foraminifera genus Uvigerina: Isotopic changes in the ocean during the last glacial.

Shackleton, N.J. et al., 1984. Oxygen isotope calibration of the onset of ice-rafting and history of glaciation in the North-Atlantic region. *Nature*, 307(5952), pp.620–623.

Shackleton, N.J., 1987. Oxygen isotopes, ice volume and sea-level. *Quaternary Science Reviews*, 6(3-4), pp.183–190.

Shackleton, N.J., 2000. The 100,000-Year Ice-Age Cycle Identified and Found to Lag Temperature, Carbon Dioxide, and Orbital Eccentricity. *Science* , 289 (5486 ), pp.1897–1902.

Shackleton, N.J. et al., 1988. The Evolution of Oceanic Oxygen-Isotope Variability in the North Atlantic Over the Past Three Million Years [and Discussion].

Sigman, D.M., Hain, M.P. & Haug, G.H., 2010. The polar ocean and glacial cycles in atmospheric CO2 concentration. *Nature*, 466(7302), pp.47–55.

Sigman, D.M., Jaccard, S.L. & Haug, G.H., 2004. Polar ocean stratification in a cold climate. *Nature*, 428(6978), pp.59–63.

Sosdian, S. & Rosenthal, Y., 2009. Deep-Sea Temperature and Ice Volume Changes Across the Pliocene-Pleistocene Climate Transitions. *Science*, 325(5938), pp.306–310.

Steph, S., Tiedemann, R., Prange, M., Groeneveld, J., Schulz, M., Timmermann, A., Nürnberg, D., Rühlemann, C., Saukel, C., Haug, G.H., et al., 2010. Early Pliocene increase in thermohaline overturning: A precondition for the development of the modern equatorial Pacific cold tongue. *Paleoceanography*, 25(2), p.PA2202.

Steph, S., Tiedemann, R., Prange, M., Groeneveld, J., Schulz, M., Timmermann, A., Nürnberg, D., Rühlemann, C., Saukel, C. & Haug, G.H., 2010. Early Pliocene increase in thermohaline overturning: A precondition for the development of the modern equatorial Pacific cold tongue. *Paleoceanography*, 25(2), p.PA2202.

Sykes, L.R., McCann, W.R. & Kafka, A.L., 1982. Motion of caribbean plate during last 7 million years and implications for earlier Cenozic movements. *Journal of Geophysical Research*, 87(NB13), pp.656–676.

Tiedemann, R., Sarnthein, M. & Shackleton, N.J., 1994. Astronomic timescale for the Pliocene Atlantic delta-18-O and dust flux records of Ocean Drilling Program Site 659. *Paleoceanography*, 9(4), pp.619–638.

Tisserand, A. a. et al., 2013. Refining benthic foraminiferal Mg/Ca-temperature calibrations using core-tops from the western tropical Atlantic: Implication for paleotemperature estimation. *Geochemistry, Geophysics, Geosystems*, 14(4), pp.1–17.

Tripati, A.K., Roberts, C.D. & Eagle, R. a, 2009. Coupling of CO2 and ice sheet stability over major climate transitions of the last 20 million years. *Science (New York, N.Y.)*, 326(5958), pp.1394–7.

Venz, K. & Hodell, D., 2002. New evidence for changes in Plio–Pleistocene deep water circulation from Southern Ocean ODP Leg 177 Site 1090. *Palaeogeography, Palaeoclimatology, …*, 182, p.10.

Venz, K.A. et al., 2000a. A 1 . 0 Myr record of Glacial North Atlantic Intermediate Water variability from ODP site 982 in the northeast Atlantic of the resumed under full interglacial The magnitude of benthic. , 14(1), pp.42–52.

Venz, K.A. et al., 2000b. A 1.0 Myr record of Glacial North Atlantic Intermediate Water variability from ODP site 982 in the northeast. *Atlantic*, 14(1), pp.42–52.

Wara, M.W., Ravelo, A.C. & Delaney, M.L., 2005. Permanent El Niño-like conditions during the Pliocene warm period. *Science (New York, N.Y.)*, 309(5735), pp.758–61.

Webb, P. & Harwood, D., 1996. A marine and terrestrial Sirius Group succession, middle Beardmore Glacier-Queen Alexandra Range, Transantarctic Mountains, Antarctica. *Marine …*, 27(95), pp.273–297.

Williams, T. et al., 2010. Evidence for iceberg armadas from East Antarctica in the Southern Ocean during the late Miocene and early Pliocene. *Earth and Planetary Science Letters*, 290(3-4), pp.351–361.

Woodruff, F. & Savin, S.M., 1989. Miocene Deepwater Oceanography. *Paleoceanography*, 4.

Wright, D. & Miller, G., 1996. Control of North Atlantic Deep Water circulation by the Greenland-Scotland Ridge A“ o ‘“’•”:’•‘/•’’•‘•’’•’"• - • i Straits Iceland-Faeroe.” , 11(2), pp.157–170.

Yu, J. et al., 2007. Preferential dissolution of benthic foraminiferal calcite during laboratory reductive cleaning. *Geochemistry Geophysics Geosystems*, 8(6).

Yu, J. & Elderfield, H., 2007. Benthic foraminiferal B/Ca ratios reflect deep water carbonate saturation state. *Earth and Planetary Science Letters*, 258(1-2), pp.73–86.

Yu, J. & Elderfield, H., 2007. Benthic foraminiferal B/Ca ratios reflect deep water carbonate saturation state. *Earth and Planetary Science Letters*, 258(1-2), pp.73–86.

Yu, J. & Elderfield, H., 2008. Mg/Ca in the benthic foraminifera Cibicidoides wuellerstorfi and Cibicidoides mundulus: Temperature versus carbonate ion saturation. *Earth and Planetary Science Letters*, 276(1-2), pp.129–139.

Yu, J., Elderfield, H. & Piotrowski, A.M., 2008. Seawater carbonate ion-δ13C systematics and application to glacial–interglacial North Atlantic ocean circulation. *Earth and Planetary Science Letters*, 271(1-4), pp.209–220.

Yu, J.M., Elderfield, H. & Piotrowski, A.M., 2008. Seawater carbonate ion-delta C-13 systematics and application to glacial-interglacial North Atlantic ocean circulation. *Earth and Planetary Science Letters*, 271(1-4), pp.209–220.

Zachos, J. et al., 2001. Trends, rhythms, and aberrations in global climate 65 Ma to present. *Science (New York, N.Y.)*, 292(5517), pp.686–93.

Zachos, J.C., Dickens, G.R. & Zeebe, R.E., 2008. An early Cenozoic perspective on greenhouse warming and carbon-cycle dynamics. *Nature*, 451(7176), pp.279–83.

Zhisheng, a et al., 2001. Evolution of Asian monsoons and phased uplift of the Himalaya-Tibetan plateau since Late Miocene times. *Nature*, 411(6833), pp.62–6.

# 9 Appendices

## 9.1 Cardiff University foraminifera cleaning and dissolving procedures for trace metal analysis

### Foraminifera cleaning procedure

J. Riker, September 2008

*This description is modified from the "Foram Procedure for Cadmium" recorded by Paula Rosener (1988), as updated to reverse the redox steps (1994). Our procedure differs in that the sample transfer is performed between reduction and oxidation. Our procedure is also expanded to include instructions specific to our lab. It is not necessary to perform Step III in all cases; please confirm the appropriate cleaning process before starting.*

**I. Before You Start**

• Set your tubes of crushed forams in a clean, perspex rack. Ensure samples are clearly labelled with permanent ink and record a list or diagram of samples before starting. Randomize your samples prior to cleaning.

• Locate your reagents (remake or refill as necessary). All reagents should be prepared and stored in new, acid-leached PE bottles.

You will need:

10% HCl or HNO3 for rinsing pipette tips (250 mL; top up bottle from labelled dewars in the flow bench each day you clean)

DI H2O for rinsing pipette tips (250 mL; rinse and refill bottle with fresh water each day you clean)

DI H2O for foram cleaning (500 mL wash bottle; rinse and refill with fresh water each day you clean)

Trace grade methanol for foram cleaning (store in a 250 mL bottle; pour off a small amount into a 125 mL spray bottle just before use)

Empty 60 mL bottle for reducing reagent

Empty 60 mL bottle for rinsing reducing reagent

Empty 60 mL bottle for oxidizing reagent

DI H2O for sample transfers (250 mL; rinse and refill bottle with fresh water each day you clean)

0.002 M HNO3 for foram leaching (0.001 M for small samples) (250 mL; make fresh if old or contaminated)

• Turn on flow bench and allow to run for at least 15 minutes before using.

• Wipe down all work surfaces with DI water before starting (counter surfaces, interior of flow benches and fume cupboard, equipment surfaces).

• If floor has not been mopped recently, mop floor using DI water from the reservoir in Room 2.12.

**II. Removal of Fine Clays**

1. Drain the ultrasonic bath in the flow bench and refill with fresh DI H H2O. Fill to the base of your perspex rack. Use the prop provided and never fill below the minimum fill line.

2. Tap your sample rack firmly on the bench to shake forams to the base of tubes.

3. Open tube tops slowly in case forams are stuck to the sides or lids.

4. Using your DI H2O for foram cleaning, gently fill each tube most of the way.

5. If forams are visible in the tube lids, add a small amount of water to the lids as well. Close tubes.

6. Tap rack firmly on the bench to settle forams and get rid of any air bubbles. CHL: If forams will not settle or bubbles won‟t rise, tap the side or corners of the rack firmly on the edge of the flow bench.

7. Turn on siphon (switch is on the rear of the pump, on the right-hand side). Always make sure the siphon tip is in the flow bench when the pump is on.

8. If siphon waste beaker is full, empty into the labelled waste container beneath the water purifier. Check the waste level throughout the cleaning process and don‟t let it rise above the “max fill” line.

9. Rinse siphon tip in 10% HCl (3x) and then DI H2O (3x) tip rinses. Don‟t siphon up too much tip rinse at once, as this can cause siphon waste to splash and contaminate the pump tubing.

10. Siphon off as much water as possible from the tubes. This works best if you avoid putting the siphon tip directly in the sample. Instead, rest the tip against the front of the tube, above water level, and siphon down gradually.

11. Open all tubes and fill ~1/3 full with water (not quite up to the rack base). Close tubes. CHL: The forams will agitate best in minimal H2O.

12. Tap rack as necessary to remove air bubbles.

13. Ultrasonicate for 1 minute (set the bath to “hold”). Fine clays should now be dislodged and held in suspension.

14. Turn off bath and remove rack. Open all tubes and vigorously squirt DI H2O for foram cleaning into each tube so as to agitate the sample and mix clays throughout. Close tubes.

15. Tap rack firmly on the bench, invert and shake, then wait for forams to settle. Don‟t wait too long, or suspended clays will also settle. If necessary, tap the rack again to encourage forams to settle.

16. Clean siphon tip (3x 10% HCl and 3x DI H2O) while waiting for forams to settle.

17. Siphon off as much water as possible. Don‟t siphon off your forams.

18. Repeat steps 11-17 a total of 3x with DI H2O. To avoid systematic variations in the effectiveness of clay removal: Begin siphoning at a different row and (or) side of the rack

during each rinse step. Change the orientation of the rack in the sonic bath during each sonication.

19. Fill 125 mL spray bottle ~1/5 full with trace grade methanol. Loosen cap of spray bottle when not in use to keep methanol from dripping from the tip.

20. Repeat steps 11-17 1-2x with trace grade methanol, depending on the degree of clay contamination in your samples. Special instructions for methanol:

• Always wear goggles when working with methanol

• Fill tubes to the top of the rack with methanol (rather than just 1/3 full)

• Do not add additional methanol after ultrasonicating; simply siphon off existing methanol

• Methanol is less viscous than water, so take special care when siphoning; don‟t go to quite to the bottom of the tube

• When siphoning methanol, it may work better to press siphon tip against the rear of the tube (rather than the front)

• Dispose of any leftover methanol in the labelled waste container

21. Repeat steps 11-17 an additional 2x with DI $H_2O$.

22. Pipette off all remaining water using a clean (3x 10% HCl and 3x DI $H_2O$), 100 µL (yellow) pipette tip. It is not necessary to rinse the tip between samples.

**III. Removal of Metal Oxides (Reducing Step)**

1. Turn on power source for hotplate in the fume cupboard and set to 300 °C.

2. Rinse and fill the glass evaporating dish in the fume cupboard with DI $H_2O$ from the ELGA tap. Fill to the base of your perspex rack. Set on hotplate.

3. Rinse and fill tall form beaker containing thermometer with DI $H_2O$ from the ELGA tap. Set on hot plate. Use this to top up the evaporating dish as water evaporates.

4. Drain the ultrasonic bath in the fume cupboard and refill with fresh DI H2O. Fill to the base of your perspex rack. Use the prop provided and never fill below the minimum fill line.

5. Prepare your reducing reagent in the labelled, empty 60 mL bottle. Please note that hydrous hydrazine is volatile, carcinogenic, and explosive. Always work in the fume cupboard and take care to minimize exposure. Dispose of all related waste (pipette tips, parafilm, gloves) in a plastic bag and seal bag before removing from fume cupboard.

• Pour 10 mLs ammonia solution and 10 mLs citric acid/ammonia solution (both stored in the fridge) into the empty bottle; pour these reagents directly from the bottles (no pipettes) and take care not to touch the lids of reagent bottles to any other surfaces.

• Prepare a waste bag, a fresh strip of parafilm, and a clean (3x 10% HCl and 3x DI H2O) 1000 µL (blue) pipette tip

• Remove hydrous hydrazine from fridge

• Pipette 1200 µL hydrous hydrazine into the reducing reagent

• Dispose of pipette tip

• Cap reducing reagent and invert to mix

• Re-parafilm hydrous hydrazine and return to fridge

6. Before proceeding, ensure hot water bath is hot (on verge of boiling, 80-90 °C). This can take about 30 minutes.

7. Open tubes. Using a clean (3x 10% HCl and 3x DI H2O) 100 µL pipette tip, add 100 µL reducing reagent to each tube. Be aware that the reagent has a low viscosity and tends to drip. Close tubes firmly.

8. Because ammonia has a high vapor pressure, tube caps will tend to blow open in the hot water both. To prevent this, clamp tubes shut by screwing a perspex plate to the top of your rack. Ensure your tubes are firmly closed and that they are in good contact with the plate surface.

9. Place racks in the hot water bath for a total of 30 minutes. Calcium carbonate is slightly soluble in ammonia, so avoid letting your foram fragments sit in the reducing agent for longer than the necessary 30 minutes. Every 2 minutes:

• Remove rack

• Tighten screws on perspex clamp

• Invert, shake, and tap rack to settle forams and remove bubbles

• Ultrasonicate rack for a few seconds (this will agitate the reagent into all parts of the sample and discourage dissolved oxides from re-precipitating)

• Tap rack firmly and return to hot water bath

• Top off the water bath as necessary using hot water from the beaker

10. After 30 minutes, remove rack and clamp and carefully open and close all tubes to release gas. Keep one finger on the top of the tube and use your thumb to open the tube in a peeling motion.

11. Pipette off as much reducing reagent as possible using a clean (3x 10% HCl and 3x DI $H_2O$) 100 µL pipette tip. Do not use siphon. Eject waste into the reducing reagent bottle. Eject tip into waste bag.

12. Fill tube caps and tubes (to top of rack or higher) with DI $H_2O$ for foram cleaning. Close tubes. Tap rack firmly to settle forams.

13. Turn on the siphon in the fume cupboard using the labelled control knob on the left-hand panel. Rinse the siphon tip (3x 10% HCl and 3x DI $H_2O$). Siphon caps and then siphon off as much water as possible from tubes.

14. Repeat steps 12 and 13 two more times.

15. Fill tubes half full with DI $H_2O$ for foram cleaning, close tubes, then set in the hot water bath for 5 minutes.

16. In the meantime, prepare a fresh strip of parafilm.

17. Remove hydrazine waste container (brown bottle) from fridge and place in fume cupboard.

18. Dump leftover reducing reagent into waste container.

19. Fill the empty 60 mL bottle for rinsing reducing reagent with DI H2O from the ELGA tap.

20. Rinse the reducing reagent bottle 2-3x with DI H2O, dumping rinse water into the waste container.

21. Re-parafilm waste container and return to fridge.

22. If 5 minutes have passed, remove rack from hot water bath, clean siphon tip (3x 10% HCl and 3x DI H2O), siphon caps, and then siphon off as much water as possible from tubes.

23. Repeat steps 12 and 13 two more times.

24. Repeat step 15.

25. Repeat step 22. It is now safe to remove the rack from the fume hood.

26. Turn hotplate off or down as appropriate (you will need it again in Section V). Please remember to turn off the power source as well.

**IV. Sample Transfer**

1. In the flow bench, label a new set of acid-leached tubes for your samples.

2. Using a disposable scalpel, cut off ~1/4 of a 100 µL pipette tip.

3. Set the pipettor to 70 µL and thoroughly clean the pipette tip (6x 10% HCl and 6x DI H2O).

4. If you haven‟t already, rinse and refill your DI H2O for sample transfers.

5. Open an old tube. Hold pipette tip directly over foram fragments and pipette and expel fragments (±H2O) into the new tube of the same sample number.

6. Add a small amount of DI H2O for sample transfers to the old tube. Repeat transfer until no foram fragments are visible in the old tube and then again once more (usually 2-3x).

7. Between samples, rinse the pipette tip 2-3x in your DI H2O for sample transfers.

8. Once all samples have been transferred into new tubes, turn on the siphon, clean the siphon tip (3x 10% HCl and 3x DI H2O), and siphon off as much water as possible.

**V. Removal of Organic Matter (Oxidizing Step)**

1. In the fume cupboard, ensure hot water bath is hot (on verge of boiling, 80-90 °C) and filled to the base of your perspex rack.

2. Prepare your oxidizing reagent in the labelled, empty 60 mL bottle.

• Pour 15 mL 0.1 N NaOH (stored in the fridge) into the empty bottle; pour this reagent directly from the bottle (no pipettes) and take care not to touch the lid of the reagent bottle to any other surface

• Using a clean (3x 10% HCl and 3x DI H2O) 100 µL pipette tip, add 50 µL H2O2; SB: please pour a small quantity of H2O2 into the H2O2 bottle cap, pipette from the cap, and dispose of cap contents before re-capping the bottle

• Cap reagent bottle and invert to mix

3. Open tubes and add 250 µL oxidizing reagent to each sample. Close tubes.

4. Set rack in hot water bath for 5 minutes.

5. Remove rack and invert, shake, and tap the rack to settle forams and remove bubbles. Ultrasonicate rack for a few seconds, then tap rack firmly and return to hot water bath.

6. Repeat steps 4 and 5.

7. Open tubes and top them off with DI H2O for foram cleaning.

8. Turn on siphon, clean siphon tip (3x 10% HCl and 3x DI H2O), and siphon off oxidizing reagent.

9. Repeat steps 7 and 8 two more times.

**VI. Dilute Acid Leach**

1. In the flow bench, clean a 1000 µL pipette tip (3x 10% HCl and 3x DI H2O).

2. dd 250 µL 0.002 N $HNO_3$ to each tube. Because $HNO_3$ will dissolve carbonate, you may wish to use 0.001 N $HNO_3$ for small samples. You may also wish to skip ultrasonication and do fewer (or no) repetitions of the leach.

3. Tap the rack firmly and check for air bubbles. If necessary, tap some more.

4. Ultrasonicate the rack for 30 seconds.

5. Remove rack from bath. Invert, shake, and tap rack firmly to settle forams.

6. Open tubes. While waiting for forams to settle, turn on siphon and clean siphon tip (3x 10% HCl and 3x DI $H_2O$).

7. Once forams have settled, siphon off as much acid as possible.

8. Repeat steps 2-7 4x as quickly as possible to avoid dissolving your samples. To avoid systematic variations in the effectiveness of the acid leach: Begin siphoning at a different row and (or) side of the rack during each rinse step. Change the orientation of the rack in the sonic bath during each sonication.

9. Fill tubes and caps with DI $H_2O$ for foram cleaning. Close tubes.

10. Tap rack firmly, check for bubbles, and ultrasonicate for a few seconds.

11. Remove rack from bath. Invert, shake, and tap rack firmly to settle forams.

12. Turn on siphon and clean siphon tip (3x 10% HCl and 3x DI $H_2O$). Once forams have settled, siphon caps and then siphon off as much water as possible from tubes.

13. Repeat steps 10-13.

14. Pipette off all remaining water using a clean (3x 10% HCl and 3x DI $H_2O$), 100 µL pipette tip. It is important to remove as much water as possible. Use a new, freshly-cleaned tip for each sample.

Your samples may be stored indefinitely at this point.

# Dissolving and Diluting Benthic Forams for Trace Metal Analysis

*J. Riker, May 2008*

The following protocol describes how to dissolve and dilute cleaned benthic forams for trace metal analysis on the Element (using the FULL_FORAM_LMR method). This protocol assumes you have ~20 small tests per sample. If you have large or bulky samples, or if you are analyzing a different species, please consult with a lab manager to ensure that your final sample concentrations fall within the working range of the instrument.

Dissolving Cleaned Forams

1. Before starting, check to see that fluid was successfully siphoned from all tubes following the weak acid leach. Remove any excess fluid with a clean pipette tip (6x HNO3 tip rinse, 6x H2O tip rinse).

2. Add 120 mL 0.065 M Optima HNO3 (see " eagents," below) to each tube with a clean pipette tip (6x HNO3 tip rinse, 6x H2O tip rinse). Be aware that static may draw dry forams up the sides of the tubes; open tubes gently, one at a time, with the cleaned and acid-filled pipette tip ready to dispense.

3. After filling, close caps, invert each sample, and mix for a few seconds on the vortex tube stirrer. Centrifuge each tube for 3 minutes.

4. Leave overnight to dissolve. If samples do not dissolve overnight, try the following (in order):

a. Release any built up CO2 by gently opening and closing tube (trapped CO2 will buffer the dissolution reaction).

b. Invert and rotate tube (this should expose more of the foram surface area to the dissolution acid and disturb any buffered environment that may exist at the tube base). Watch to see if forams dissolve.

c. Ultrasonicate tubes (same effect as above). Check to see if forams have dissolved.

d. Place tubes in the fridge overnight (carbonate is more soluble at low temperature). Check to see if forams have dissolved.

e. As a last resort (if 10-20 forams remain undissolved), add an additional 50-100 mL 0.065 M HNO3 to the tube. ***Transfer forams plus acid to a new, clean centrifuge tube before adding more acid.*** Never fill tubes used during the cleaning process above the 120 mL mark, as microfractures often form in these tubes during cleaning.

# Splitting Dissolved Samples for Ratio and Ca Concentration Analysis

1. If your samples have been refrigerated, allow them to warm to room temperature before proceeding.

2. Once you have confirmed that samples are dissolved, label two sets of clean tubes with the appropriate sample numbers. Label one set of tubes with the letters “CC” (for Ca concentration analysis) and the other set with “TM” (for trace metal ratio analysis).

3. Invert, vortex, and centrifuge all samples.

4. Set pipettor to 100 mL and clean a pipette tip (6x HNO3 tip rinse, 6x H2O tip rinse). Open the first trace metal ratio tube you wish to fill.

5. Gently remove the corresponding sample tube from the centrifuge (always double check the sample number), taking care not to disturb the sediment pack at the tube base. Keep the tube in the same orientation it was sitting at in the centrifuge and walk slowly to the flow bench.

6. Gently open the tube and withdraw 100 mL of dissolved sample. Keep the pipette tip as close to the fluid surface as possible, moving the tip down as you pipette. This will help you to avoid sucking up solid contaminants at the tube base. Pipette the fluid into the opened empty tube.

7. Repeat with all tubes for trace metal analysis, using a new, cleaned pipette tip for each sample.

8. Re-centrifuge remaining dissolved samples.

9. Set pipettor to 10 mL and clean a pipette tip (3x HNO3 tip rinse, 3x H2O tip rinse). Open the first Ca concentration tube you wish to fill.

10. Using the same technique described above, pipette 10 mL of dissolved sample into each tube for Ca concentration analysis.

11. ***As a rule, always pipette off 100*** m***L of each dissolved sample for ratio analyses before pipetting off 10*** m***L for Ca analyses.*** This will help to minimize contamination of your ratio samples, which require more accurate analysis than your Ca samples, with particles or leachants concentrated at the tube base.

12. Discard (or label and store, if you prefer) the original dissolved sample tubes.

# Diluting Dissolved Samples for Ca Concentration Analyses

1. ***On the day you plan to run your Ca concentration analyses,*** add 190 mL 0.5 M Optima HNO3 (see " eagents") to each Ca concentration sample tube using a clean pipette tip (6x HNO3 tip rinse, 6x H2O tip rinse), for a total sample volume of 200 mL.

2. Invert, vortex, and centrifuge sample tubes immediately prior to analysis.

Diluting Dissolved Samples for Ratio Analysis and Matrix-Matching Standards

1. Run Ca concentration analyses to determine the appropriate dilution of a matrix-matched standard (a standard of roughly equivalent Ca concentration) for each trace metal ratio sample. To calculate volumes of acid and standard to pipette, use the template spreadsheets provided by the lab manager.

2. Label a set of clean centrifuge tubes with the appropriate sample numbers and the letter "S" for standard. If you are planning to run your blanks in tubes (rather than in a vial), prepare an additional set of tubes for the blanks.

3. ***On the day you plan to run your ratio analyses,*** add 250 mL 0.5M Optima HNO3 to each trace metal ratio sample tube using a clean pipette tip (6x HNO3 tip rinse, 6x H2O tip rinse), for a total sample volume of 350 mL.

4. Pipette each matrix-matched standard using your calculated volumes of standard and 0.5 M Optima HNO3, for a total standard volume of 350 mL (same as your samples).

5. If necessary, pipette tube blanks (350 mL 0.5M Optima HNO3).

6. Invert, vortex, and centrifuge sample tubes immediately prior to analysis. Stir standard tubes on the vortex, but it is not necessary to centrifuge them.

Reagents

Before preparing reagents, have a lab manager pour an aliquot of concentrated Optima HNO3 into an acid-cleaned 60 mL Nalgene bottle. Pipette only out of this small bottle. ***Never handle***

***the large Optima HNO3 bottle stored in the fridge unless you have been given explicit permission.*** Your aliquot can be stored at room temperature in a plastic bag.

**0.065 Molar Optima HNO3:** Weigh out 249.35 g DI H2O from the ELGA system in an acid-cleaned 250 mL Nalgene bottle (don‟t forget to zero the scale with the empty bottle first). Using a clean pipette tip, add 1036 mL 16 M Optima HNO3.

**0.5 Molar Optima HNO3:** Weigh out 242.5 g DI H2O from the ELGA system in an acid-cleaned 250 mL Nalgene bottle. Using a clean pipette tip, add 7750 mL 16 M Optima HNO3.

## 9.2 Cardiff University biogenic material removal procedure for Sortable Silt analysis

1 Weigh out 2-4g of fine fraction (more if sample is very carbonate rich) into 500ml glass jars and fill ¾ full with 2mol acetic acid.

2 Leave sediment to settle, then siphon off excess acid and replace

3 When settled, sipon off the second acid and replace with deionised water and leave to settle

4 Siphon off water and add 0.0002M sodium carbonate ($Na_2CO_3$) to the sample in a conical flask. Place flasks in hot water bath at 85°C for 5 hours, stirring every 2 hours.

5 Remove samples and cool

6 Siphon off sodium carbonate and rinse with deionised water twice.

7 When settled, wash the sample into a 60ml white plastic pot with 0.002M calgon.

8 Samples are now ready to put through Coulter Counter or Sedigraph.

## 9.3 Data from this study.

### 9.3.1 Trace metal data

Grey highlight = data from sample not included in analysis due to probable contamination by the highlighted element.

#### *9.3.1.1 C. wuellerstorfi*

| Site | H | Cor | T | Sc | Top (cm) | Bot (cm) | Depth (mcd) | Age (Ka) | Li7/Ca43 | B11/Ca43 | Mg25/Ca43 | Al27/Ca43 | Mn55/Ca43 | Cd111/Ca43 | U238/Ca43 | Fe56/Ca43 | Ca v. Ca (matrix matching) | Fe/Mg ratio |
|---|---|---|---|---|---|---|---|---|---|---|---|---|---|---|---|---|---|---|
| | | | | | | | | | umol/mol | umol/mol | mmol/mol | umol/mol | umol/mol | umol/mol | nmol/mol | umol/mol | | |
| 982 | B | 7.00 | H | 2 | 110 | 112 | 61.37 | 2830.25 | 10.69 | 231.09 | 1.90 | 7.60 | 144.51 | 0.01 | 137.42 | 65.57 | 0.00 | 0.03 |
| 982 | B | 7.00 | H | 3 | 40 | 42 | 62.17 | 2874.91 | 10.74 | 231.50 | 1.87 | 2.47 | 96.69 | 0.01 | 36.43 | 55.20 | 0.96 | 0.03 |
| 982 | B | 7.00 | H | 3 | 61.5 | 65.5 | 62.385 | 2885.05 | 10.75 | 238.99 | 1.96 | 2.32 | 126.50 | 0.01 | 47.62 | 65.22 | 0.00 | 0.03 |
| 982 | B | 7.00 | H | 3 | 99.5 | 103.5 | 62.765 | 2902.59 | 10.77 | 249.74 | 2.07 | 5.42 | 90.55 | 0.00 | 42.07 | 54.83 | 0.92 | 0.03 |
| 982 | B | 8.00 | H | 2 | 57 | 59.5 | 71.18 | 3254.62 | 10.24 | 240.37 | 1.83 | 16.64 | 64.68 | 0.00 | 33.52 | 46.04 | 0.96 | 0.03 |
| 982 | B | 8.00 | H | 2 | 132.5 | 135 | 71.805 | 3269.84 | 10.63 | 243.74 | 1.94 | 8.61 | 69.40 | 0.00 | 28.79 | 42.87 | 0.91 | 0.02 |

| | | | | | | | | | | | | | | | | | | |
|---|---|---|---|---|---|---|---|---|---|---|---|---|---|---|---|---|---|---|
| 982 | B | 8.00 | H | 2 | 138 | 140 | 71.86 | 3271.06 | 11.07 | 255.96 | 2.00 | 21.02 | 73.03 | 0.01 | 30.56 | 43.25 | 0.99 | 0.02 |
| 982 | B | 8.00 | H | 3 | 24 | 26.5 | 72.22 | 3280.35 | 11.08 | 237.95 | 2.03 | 6.73 | 103.60 | 0.01 | 48.80 | 45.43 | 0.89 | 0.02 |
| 982 | B | 8.00 | H | 4 | 48 | 50 | 74.87 | 3335.12 | 11.72 | 227.39 | 2.01 | 93.90 | 82.64 | 0.00 | 41.68 | 97.98 | 1.01 | 0.05 |
| 982 | B | 8.00 | H | 5 | 82 | 84.5 | 76.71 | 3393.73 | 10.42 | 243.90 | 1.83 | 21.77 | 65.25 | 0.01 | 35.45 | 29.87 | 0.93 | 0.02 |
| 982 | B | 9.00 | H | 7 | 30 | 32.5 | 89.24 | 3769.96 | 10.19 | 237.34 | 1.99 | 10.85 | 69.06 | 0.01 | 55.18 | 25.27 | 0.92 | 0.01 |
| 982 | B | 10.00 | H | 2 | 130 | 132.5 | 93.51 | 3887.00 | 10.54 | 181.08 | 2.10 | 14.41 | 63.07 | 0.11 | 85.05 | 6.73 | 0.91 | 0.00 |
| 982 | B | 10.00 | H | 3 | 60 | 62.5 | 94.31 | 3903.02 | 10.59 | 229.00 | 1.74 | 15.75 | 46.85 | 0.00 | 28.82 | 15.83 | 0.96 | 0.01 |
| 982 | B | 10.00 | H | 5 | 1 | 3.5 | 96.72 | 3959.07 | 10.41 | 220.44 | 1.92 | 4.92 | 53.86 | 0.09 | 36.25 | 8.44 | 1.01 | 0.00 |
| 982 | B | 10.00 | H | 6 | 9.5 | 12 | 98.305 | 3996.56 | 10.28 | 210.92 | 1.96 | 12.60 | 55.54 | 0.14 | 55.73 | 14.50 | 0.97 | 0.01 |
| 982 | B | 10.00 | H | 7 | 21 | 23.5 | 99.92 | 4032.11 | 9.33 | 199.31 | 1.99 | 7.74 | 62.75 | 0.16 | 19.48 | 12.52 | 1.12 | 0.01 |
| 982 | B | 11.00 | H | 3 | 60 | 62.5 | 104.67 | 4155.12 | 10.59 | 220.22 | 2.25 | 7.58 | 84.39 | 0.00 | 69.87 | 24.31 | 0.97 | 0.01 |
| 982 | B | 11.00 | H | 3 | 140 | 142.5 | 105.47 | 4185.89 | 10.27 | 222.11 | 1.86 | 19.60 | 54.10 | 0.07 | 27.77 | -9.50 | 0.98 | -0.01 |
| 982 | B | 11.00 | H | 5 | 0 | 2.5 | 107.07 | 4224.34 | | 218.97 | 1.83 | 13.31 | 73.63 | 0.11 | 36.72 | 3.80 | 1.02 | 0.00 |
| 982 | B | 11.00 | H | 5 | 80 | 82.5 | 107.87 | 4238.07 | 10.13 | 215.19 | 1.92 | 8.74 | 65.39 | 0.00 | 41.92 | 17.57 | 0.93 | 0.01 |
| 982 | B | 11.00 | H | 6 | 97 | 99.5 | 109.54 | 4283.98 | 9.96 | 222.26 | 1.67 | 6.93 | 53.81 | 0.00 | 20.58 | 12.94 | 0.93 | 0.01 |

| | | | | | | | | | | | | | | | | | | |
|---|---|---|---|---|---|---|---|---|---|---|---|---|---|---|---|---|---|---|
| 982 | B | 11.00 | H | 7 | 21 | 23.5 | 110.28 | 4303.87 | 10.30 | 228.51 | 1.91 | 7.40 | 56.54 | 0.13 | 63.49 | 7.59 | 0.90 | 0.00 |
| 982 | B | 12.00 | H | 1 | 60 | 62.5 | 111.59 | 4337.35 | 9.56 | 189.85 | 2.27 | 13.68 | 46.00 | 0.11 | 30.77 | 5.05 | 1.02 | 0.00 |
| 982 | B | 12.00 | H | 3 | 0 | 3 | 113.99 | 4396.61 | 10.77 | 224.95 | 1.92 | 27.16 | 40.00 | 0.06 | 15.64 | -4.23 | 1.00 | 0.00 |
| 982 | B | 12.00 | H | 5 | 20 | 22.5 | 117.19 | 4471.82 | 10.29 | 233.86 | 2.06 | 16.86 | 36.80 | 0.12 | 46.95 | -7.39 | 1.01 | 0.00 |
| 982 | B | 12.00 | H | 5 | 99.5 | 102 | 117.985 | 4493.29 | 40.07 | 230.89 | 1.81 | 587.16 | 73.37 | 0.01 | 104.32 | 57.20 | 0.90 | 0.03 |
| 982 | B | 12.00 | H | 6 | 30 | 32.5 | 118.79 | 4514.87 | 10.30 | 234.45 | 1.70 | 5.88 | 58.20 | 0.10 | 33.84 | 7.53 | 1.07 | 0.00 |
| 982 | B | 12.00 | H | 6 | 110 | 112.5 | 119.59 | 4534.45 | 10.05 | 217.77 | 1.77 | 25.47 | 50.51 | 0.00 | 47.19 | 20.29 | 1.05 | 0.01 |
| 982 | B | 13.00 | H | 1 | 60 | 62.5 | 122.14 | 4577.88 | 10.11 | 239.75 | 1.77 | 8.42 | 34.68 | 0.00 | 33.18 | 11.88 | 0.96 | 0.01 |
| 982 | B | 13.00 | H | 1 | 140 | 142.5 | 122.94 | 4593.97 | 9.77 | 244.64 | 1.92 | 14.35 | 46.45 | 0.08 | 26.02 | 0.94 | 0.93 | 0.00 |
| 982 | B | 13.00 | H | 3 | 0 | 3 | 124.54 | 4628.18 | 9.26 | 199.10 | 1.84 | 4.36 | 54.36 | 0.10 | 20.94 | 9.30 | 1.14 | 0.01 |
| 982 | B | 13.00 | H | 3 | 80 | 82.5 | 125.34 | 4645.31 | 10.21 | 214.87 | 1.68 | 8.59 | 57.21 | 0.01 | 82.02 | 17.34 | 0.95 | 0.01 |
| 982 | B | 13.00 | H | 4 | 10 | 12.5 | 126.14 | 4659.32 | 12.37 | 228.74 | 1.93 | 33.18 | 28.17 | 0.00 | 43.31 | 12.16 | 1.01 | 0.01 |
| 982 | B | 13.00 | H | 5 | 20 | 22.5 | 127.74 | 4687.50 | 10.01 | 219.00 | 1.81 | 5.50 | 86.38 | 0.17 | 59.33 | 17.80 | 0.99 | 0.01 |
| 982 | B | 13.00 | H | 6 | 30 | 32.5 | 129.34 | 4722.00 | 9.24 | 202.63 | 1.81 | 7.05 | 64.72 | 0.08 | 42.59 | 13.42 | 1.08 | 0.01 |
| 982 | B | 13.00 | H | 6 | 110 | 112.5 | 130.14 | 4736.22 | 9.97 | 221.92 | 1.84 | 8.14 | 75.69 | 0.00 | 95.13 | 21.17 | 0.93 | 0.01 |

| | | | | | | | | | | | | | | | | | | |
|---|---|---|---|---|---|---|---|---|---|---|---|---|---|---|---|---|---|---|
| 982 | B | 14.00 | H | 3 | 59 | 61.5 | 136.1 | 4845.07 | 9.80 | 219.98 | 1.99 | 6.02 | 55.10 | 0.01 | 56.21 | 13.51 | 0.93 | 0.01 |
| 982 | B | 14.00 | H | 3 | 140 | 142.5 | 136.9 | 4856.43 | 9.53 | 223.83 | 1.77 | 7.15 | 65.51 | 0.11 | 57.24 | 10.31 | 0.99 | 0.01 |
| 982 | B | 14.00 | H | 4 | 70 | 72.5 | 137.7 | 4870.07 | 9.47 | 237.92 | 1.68 | 6.44 | 63.61 | 0.00 | 43.09 | 12.22 | 0.96 | 0.01 |
| 982 | B | 14.00 | H | 5 | 0 | 3 | 138.495 | 4885.90 | 9.60 | 233.32 | 1.87 | 15.92 | 99.09 | 0.07 | 19.04 | 26.39 | 1.04 | 0.01 |
| 982 | B | 14.00 | H | 5 | 80 | 82.5 | 139.3 | 4896.65 | 9.97 | 249.40 | 1.67 | 12.15 | 54.00 | 0.00 | 39.18 | 12.52 | 0.98 | 0.01 |
| 982 | B | 14.00 | H | 7 | 61 | 63.5 | 141.7 | 4920.98 | 12.55 | 195.49 | 2.71 | 49.36 | 102.26 | 0.04 | 6.60 | 27.02 | 0.93 | 0.01 |
| 982 | B | 15.00 | H | 2 | 40 | 42.5 | 145.36 | 5008.96 | 9.69 | 231.79 | 1.78 | 6.26 | 50.17 | 0.00 | 36.71 | 9.92 | 0.93 | 0.01 |
| 982 | B | 15.00 | H | 2 | 120 | 122.5 | 146.16 | 5024.56 | 9.08 | 207.42 | 1.81 | 6.01 | 65.45 | 0.08 | 25.79 | 3.79 | 1.00 | 0.00 |
| 982 | B | 15.00 | H | 3 | 130 | 132.5 | 147.76 | 5054.75 | 9.54 | 216.72 | 1.61 | 15.19 | 52.44 | 0.07 | 41.35 | 2.84 | 1.08 | 0.00 |
| 982 | B | 15.00 | H | 4 | 60 | 62.5 | 148.56 | 5069.81 | 9.48 | 227.75 | 1.65 | 5.17 | 60.72 | 0.00 | 38.30 | 13.13 | 0.92 | 0.01 |

### *9.3.1.2 C. mundulus*

| Site | H | Cor | T | Sc | Top (cm) | Bot (cm) | Depth (mcd) | Age (Ka) | Li7/Ca43 | B11/Ca43 | Mg25/Ca43 | Al27/Ca43 | Mn55/Ca43 | Cd111/Ca43 | U238/Ca43 | Fe56/Ca43 | Ca v. Ca (matrix matching) | Fe/Mg ratio |
|---|---|---|---|---|---|---|---|---|---|---|---|---|---|---|---|---|---|---|
| | | | | | | | | | umol/mol | umol/mol | mmol/mol | umol/mol | umol/mol | umol/mol | nmol/mol | umol/mol | | |
| 982 | B | 5.00 | H | 4 | 50 | 54 | 43.08 | 1912.94 | 9.11 | 150.06 | 2.10 | 19.90 | 121.22 | 0.01 | 33.44 | 197.75 | | 0.09 |
| 982 | B | 5.00 | H | 4 | 68 | 70 | 43.26 | 1926.78 | 12.66 | 209.58 | 2.36 | 97.18 | 86.46 | 0.64 | 2.59 | 313.13 | | 0.13 |
| 982 | B | 5.00 | H | 5 | 77.5 | 79.5 | 44.855 | 2036.59 | 10.85 | 170.66 | 2.05 | 39.01 | 89.03 | 0.00 | 17.41 | 152.49 | 0.96 | 0.07 |
| 982 | B | 5.00 | H | 6 | 7.5 | 9.5 | 45.655 | 2064.28 | 10.26 | 173.05 | 1.79 | 59.15 | 87.47 | 0.00 | 15.19 | 133.20 | 0.00 | 0.07 |
| 982 | B | 5.00 | H | 7 | 40 | 42.5 | 47.48 | 2136.76 | 9.44 | 159.40 | 2.19 | 14.84 | 105.02 | 0.00 | 33.82 | 135.28 | 0.00 | 0.06 |
| 982 | B | 5.00 | H | 7 | 59.5 | 61.5 | 47.675 | 2146.20 | 9.65 | 169.20 | 1.75 | 50.74 | 84.62 | 0.00 | 20.17 | 143.21 | 0.00 | 0.08 |
| 982 | B | 6.00 | H | 1 | 10 | 12 | 49.11 | 2220.40 | 9.57 | 161.33 | 2.08 | 16.80 | 88.73 | 0.00 | 16.47 | 163.98 | 0.00 | 0.08 |
| 982 | B | 6.00 | H | 1 | 50 | 52 | 49.51 | 2245.01 | 9.69 | 166.22 | 2.22 | 16.44 | 95.47 | 0.00 | 19.73 | 184.31 | 0.00 | 0.08 |
| 982 | B | 6.00 | H | 1 | 90 | 92 | 49.91 | 2269.61 | 9.83 | 160.26 | 2.11 | 35.41 | 88.09 | 0.00 | 7.92 | 178.16 | 0.00 | 0.08 |
| 982 | B | 6.00 | H | 3 | 68 | 70 | 52.69 | 2458.40 | 9.48 | 154.45 | 2.07 | 40.96 | 100.18 | 0.01 | 51.16 | 133.34 | 0.98 | 0.06 |
| 982 | B | 6.00 | H | 4 | 32 | 36 | 53.83 | 2506.68 | 10.33 | 181.97 | 1.76 | 43.48 | 90.25 | 0.01 | 41.48 | 117.47 | 0.00 | 0.07 |

| | | | | | | | | | | | | | | | | | | |
|---|---|---|---|---|---|---|---|---|---|---|---|---|---|---|---|---|---|---|
| 982 | B | 6.00 | H | 5 | 39.5 | 43.5 | 55.405 | 2550.41 | 10.88 | 183.91 | 1.86 | 27.72 | 72.92 | 0.00 | 28.09 | 101.47 | 0.87 | 0.05 |
| 982 | B | 6.00 | H | 6 | 48 | 52 | 56.99 | 2580.90 | 9.61 | 162.49 | 1.92 | 28.87 | 57.64 | 0.00 | 22.00 | 83.26 | 0.00 | 0.04 |
| 982 | B | 6.00 | H | 6 | 57.5 | 59.5 | 57.085 | 2583.68 | 10.41 | 162.33 | 1.77 | 17.47 | 58.16 | 0.00 | 18.28 | 80.52 | | 0.05 |
| 982 | B | 6.00 | H | 6 | 140 | 142 | 57.91 | 2628.06 | 9.96 | 153.90 | 1.97 | 48.78 | 78.81 | 0.01 | 96.94 | 85.75 | 0.00 | 0.04 |
| 982 | B | 6.00 | H | 7 | 30 | 32 | 58.31 | 2647.78 | 9.85 | 148.93 | 1.97 | 27.84 | 90.76 | 0.00 | 69.23 | 78.71 | 0.98 | 0.04 |
| 982 | B | 7.00 | H | 1 | 20 | 22 | 58.97 | 2674.77 | 10.72 | 181.04 | 1.57 | 101.72 | 87.11 | 0.00 | 66.76 | 83.93 | 0.98 | 0.05 |
| 982 | B | 7.00 | H | 1 | 100 | 102 | 59.77 | 2721.14 | 10.47 | 160.14 | 1.73 | 31.06 | 77.34 | 0.00 | 121.66 | 59.00 | 0.98 | 0.03 |
| 982 | B | 7.00 | H | 1 | 140 | 142 | 60.17 | 2745.74 | 9.74 | 160.92 | 2.24 | 25.71 | 84.81 | 0.00 | 54.16 | 68.29 | 1.00 | 0.03 |
| 982 | B | 7.00 | H | 2 | 110 | 112 | 61.37 | 2830.25 | 10.20 | 167.25 | 2.44 | 13.30 | 120.21 | 0.01 | 100.09 | 65.63 | 0.00 | 0.03 |
| 982 | B | 7.00 | H | 3 | 18 | 22 | 61.95 | 2864.76 | 10.06 | 153.49 | 2.19 | 24.44 | 118.43 | 0.01 | 55.17 | 55.71 | 0.92 | 0.03 |
| 982 | B | 7.00 | H | 4 | 10 | 12 | 63.37 | 2930.27 | 10.00 | 166.14 | 2.42 | 46.87 | 84.45 | 0.00 | 49.25 | 47.78 | 0.95 | 0.02 |
| 982 | B | 7.00 | H | 5 | 39.5 | 43.5 | 65.165 | 3003.24 | 9.68 | 151.17 | 2.23 | 11.82 | 92.12 | 0.01 | 42.50 | 43.43 | 0.91 | 0.02 |
| 982 | B | 7.00 | H | 6 | 12 | 14.5 | 66.39 | 3052.44 | 12.43 | 203.69 | 2.31 | 102.93 | 85.43 | 0.63 | 2.60 | 309.07 | | 0.13 |
| 982 | B | 7.00 | H | 6 | 68 | 70 | 66.95 | 3083.12 | 10.09 | 159.32 | 2.15 | 12.55 | 102.77 | 0.00 | 22.10 | 52.22 | | 0.02 |
| 982 | B | 7.00 | H | 6 | 108 | 110 | 67.35 | 3105.87 | 9.78 | 162.04 | 2.30 | 8.34 | 79.39 | 0.00 | 54.46 | 31.68 | 0.95 | 0.01 |

| | | | | | | | | | | | | | | | | | | |
|---|---|---|---|---|---|---|---|---|---|---|---|---|---|---|---|---|---|---|
| 982 | B | 7.00 | H | 7 | 40 | 42 | 68.17 | 3141.00 | 10.12 | 167.59 | 2.23 | 24.18 | 62.12 | 0.00 | 30.13 | 48.68 | 0.98 | 0.02 |
| 982 | B | 8.00 | H | 1 | 18 | 20 | 70.08 | 3182.28 | 10.27 | 150.16 | 2.60 | 14.87 | 102.07 | 0.00 | 26.90 | 54.81 | 0.95 | 0.02 |
| 982 | B | 8.00 | H | 1 | 124 | 126.5 | | 3225.57 | 164.36 | 2.35 | 28.98 | 79.74 | 0.00 | 25.67 | 52.96 | 0.80 | 0.02 | 0.00 |
| 982 | B | 8.00 | H | 2 | 57 | 59.5 | 71.18 | 3254.62 | 178.68 | 2.26 | 15.73 | 68.32 | 0.00 | 34.74 | 47.25 | 0.91 | 0.02 | 0.00 |
| 982 | B | 8.00 | H | 2 | 132.5 | 135 | 71.805 | 3269.84 | 159.26 | 2.47 | 19.74 | 66.70 | 0.00 | 31.65 | 51.48 | 0.96 | 0.02 | 0.00 |
| 982 | B | 8.00 | H | 2 | 138 | 140 | 71.86 | 3271.06 | 169.10 | 2.62 | 23.12 | 75.08 | 0.00 | 27.28 | 49.68 | 0.97 | 0.02 | 0.00 |
| 982 | B | 8.00 | H | 3 | 24 | 26.5 | 72.22 | 3280.35 | 154.56 | 2.70 | 20.73 | 78.28 | 0.01 | 38.83 | 46.38 | 0.95 | 0.02 | 0.00 |
| 982 | B | 8.00 | H | 3 | 42 | 44 | 73.31 | 3285.51 | 154.45 | 2.18 | 38.78 | 77.82 | 0.01 | 47.61 | 50.26 | 1.01 | 0.02 | 0.00 |
| 982 | B | 8.00 | H | 6 | 148 | 150 | 78.87 | 3466.46 | 159.36 | 2.31 | 14.46 | 56.33 | 0.00 | 20.81 | 24.53 | 0.93 | 0.01 | 0.00 |
| 982 | B | 9.00 | H | 3 | 8 | 10 | 83.58 | 3621.47 | 166.86 | 2.31 | 9.22 | 57.72 | 0.00 | 19.93 | 22.06 | 0.90 | 0.01 | 0.00 |
| 982 | B | 9.00 | H | 4 | 0 | 3 | 85 | 3643.69 | 170.64 | 2.11 | 12.34 | 34.99 | 0.00 | 15.65 | 17.73 | | 0.01 | 0.00 |
| 982 | B | 9.00 | H | 5 | 28 | 30 | 86.78 | 3696.79 | 142.74 | 2.16 | 21.50 | 50.71 | 0.01 | 32.63 | 43.20 | 0.98 | 0.02 | 0.00 |
| 982 | B | 9.00 | H | 6 | 20.5 | 23 | 87.645 | 3728.25 | 173.47 | 2.34 | 29.05 | 44.76 | 0.00 | 28.42 | 23.78 | 0.91 | 0.01 | 0.00 |
| 982 | B | 10.00 | H | 1 | 40 | 42.5 | 91.11 | 3831.78 | 150.37 | 2.26 | 16.67 | 66.61 | 0.00 | 20.34 | 40.23 | 0.94 | 0.02 | 0.00 |
| 982 | B | 10.00 | H | 1 | 120 | 122.5 | 91.91 | 3855.16 | 164.88 | 2.53 | 12.04 | 53.46 | 0.00 | 64.11 | 25.66 | 0.88 | 0.01 | 0.00 |

| | | | | | | | | | | | | | | | | | | |
|---|---|---|---|---|---|---|---|---|---|---|---|---|---|---|---|---|---|---|
| 982 | B | 10.00 | H | 2 | 50 | 52.5 | 92.71 | 3872.24 | 160.07 | 2.33 | 15.95 | 44.46 | 0.00 | 40.73 | 24.82 | 0.93 | 0.01 | 0.00 |
| 982 | B | 10.00 | H | 2 | 130 | 132.5 | 93.51 | 3887.00 | 171.39 | 2.58 | 19.66 | 45.76 | 0.08 | 27.08 | 8.74 | 0.97 | 0.00 | 0.00 |
| 982 | B | 10.00 | H | 3 | 60 | 62.5 | 94.31 | 3903.02 | 158.07 | 2.57 | 15.04 | 44.92 | 0.00 | 39.05 | 21.26 | 0.92 | 0.01 | 0.00 |
| 982 | B | 10.00 | H | 3 | 140 | 142.5 | 95.11 | 3920.42 | 171.41 | 2.52 | 9.01 | 27.99 | 0.09 | 28.82 | 4.70 | 0.94 | 0.00 | 0.00 |
| 982 | B | 10.00 | H | 4 | 70 | 72.5 | 95.91 | 3940.04 | 160.19 | 2.40 | 15.61 | 48.90 | 0.00 | 56.72 | 18.68 | 0.98 | 0.01 | 0.00 |
| 982 | B | 10.00 | H | 5 | 80 | 82.5 | 97.51 | 3976.65 | 149.33 | 2.47 | 22.32 | 36.90 | 0.01 | 31.05 | 19.04 | 0.91 | 0.01 | 0.00 |
| 982 | B | 11.00 | H | 1 | 40 | 42.5 | 101.47 | 4088.77 | 162.78 | 2.36 | 13.98 | 42.58 | 0.00 | 30.25 | 20.13 | 0.90 | 0.01 | 0.00 |
| 982 | B | 11.00 | H | 2 | 51 | 53.5 | 103.08 | 4117.30 | 153.17 | 2.40 | 10.72 | 42.25 | 0.00 | 42.89 | 20.09 | 0.95 | 0.01 | 0.00 |
| 982 | B | 11.00 | H | 3 | 60 | 62.5 | 104.67 | 4155.12 | 158.41 | 2.39 | 9.87 | 45.47 | 0.00 | 47.85 | 18.70 | 1.04 | 0.01 | 0.00 |
| 982 | B | 11.00 | H | 4 | 71.5 | 74 | 106.285 | 4211.71 | 152.03 | 2.23 | 23.44 | 44.95 | 0.00 | 31.68 | 22.55 | 0.96 | 0.01 | 0.00 |
| 982 | B | 11.00 | H | 5 | 80 | 82.5 | 107.87 | 4238.07 | 166.08 | 2.28 | 43.27 | 49.38 | 0.00 | 39.04 | 31.96 | 0.97 | 0.01 | 0.00 |
| 982 | B | 11.00 | H | 6 | 97 | 99.5 | 109.54 | 4283.98 | 163.92 | 2.58 | 15.21 | 56.29 | 0.00 | 24.71 | 20.49 | 0.96 | 0.01 | 0.00 |
| 982 | B | 11.00 | H | 7 | 21 | 23.5 | 110.28 | 4303.87 | 174.79 | 2.51 | 7.57 | 48.32 | 0.12 | 43.87 | 7.09 | 1.06 | 0.00 | 0.00 |
| 982 | B | 12.00 | H | 2 | 70 | 72.5 | 113.19 | 4376.54 | 169.04 | 2.28 | 13.21 | 44.67 | 0.00 | 37.34 | 17.52 | 1.01 | 0.01 | 0.00 |
| 982 | B | 12.00 | H | 3 | 0 | 3 | 113.99 | 4396.61 | 168.88 | 2.18 | 14.31 | 35.45 | 0.08 | 20.36 | -7.30 | 0.95 | 0.00 | 0.00 |

| | | | | | | | | | | | | | | | | | | |
|---|---|---|---|---|---|---|---|---|---|---|---|---|---|---|---|---|---|---|
| 982 | B | 12.00 | H | 3 | 80 | 82.5 | 114.79 | 4418.83 | 150.58 | 2.16 | 15.17 | 51.65 | 0.00 | 48.69 | 25.49 | 1.04 | 0.01 | 0.00 |
| 982 | B | 12.00 | H | 4 | 10 | 12.5 | 115.59 | 4436.20 | 152.18 | 2.36 | 10.81 | 32.59 | 0.09 | 32.14 | 8.08 | 1.07 | 0.00 | 0.00 |
| 982 | B | 12.00 | H | 5 | 20 | 22.5 | 117.19 | 4471.82 | 171.67 | 2.11 | 22.61 | 33.13 | 0.09 | 52.96 | 2.95 | 0.94 | 0.00 | 0.00 |
| 982 | B | 12.00 | H | 6 | 30 | 32.5 | 118.79 | 4514.87 | 171.95 | 2.37 | 20.08 | 29.67 | 0.08 | 28.83 | 4.87 | 0.95 | 0.00 | 0.00 |
| 982 | B | 12.00 | H | 7 | 50 | 52.5 | 120.49 | 4552.91 | 171.41 | 2.52 | 9.01 | 27.99 | 0.09 | 28.82 | 4.70 | | 0.00 | 0.00 |
| 982 | B | 13.00 | H | 1 | 140 | 142.5 | 122.94 | 4593.97 | 173.22 | 2.09 | 15.17 | 42.06 | 0.11 | 23.38 | -15.75 | 0.96 | -0.01 | 0.00 |
| 982 | B | 13.00 | H | 4 | 10 | 12.5 | 126.14 | 4659.32 | 161.34 | 2.04 | 27.74 | 42.13 | 0.10 | 45.68 | 11.17 | 1.09 | 0.01 | 0.00 |
| 982 | B | 13.00 | H | 4 | 90 | 92.5 | 126.94 | 4671.93 | 143.26 | 2.20 | 23.25 | 43.85 | 0.01 | 60.19 | 27.89 | 0.96 | 0.01 | 0.00 |
| 982 | B | 13.00 | H | 5 | 100 | 102.5 | 128.54 | 4706.41 | 153.06 | 2.33 | 14.66 | 64.46 | 0.01 | 79.13 | 28.05 | 0.94 | 0.01 | 0.00 |
| 982 | B | 13.00 | H | 6 | 110 | 112.5 | 130.14 | 4736.22 | 146.40 | 2.10 | 13.58 | 48.04 | 0.00 | 54.98 | 19.84 | 0.93 | 0.01 | 0.00 |
| 982 | B | 14.00 | H | 1 | 40 | 42.5 | 132.5 | 4773.15 | 146.73 | 1.96 | 20.16 | 54.64 | 0.00 | 45.67 | 35.55 | 0.98 | 0.02 | 0.00 |
| 982 | B | 14.00 | H | 2 | 50 | 52.5 | 134.5 | 4808.43 | 147.91 | 2.07 | 18.44 | 44.42 | 0.00 | 32.56 | 14.54 | 1.02 | 0.01 | 0.00 |
| 982 | B | 14.00 | H | 2 | 130 | 132.5 | 135.3 | 4828.27 | 178.61 | 2.01 | 39.74 | 45.39 | 0.07 | 45.94 | 2.53 | 0.93 | 0.00 | 0.00 |
| 982 | B | 14.00 | H | 3 | 59 | 61.5 | 136.1 | 4845.07 | 176.54 | 2.11 | 11.22 | 42.31 | 0.00 | 46.87 | 14.57 | 1.13 | 0.01 | 0.00 |
| 982 | B | 14.00 | H | 4 | 70 | 72.5 | 137.7 | 4870.07 | 159.49 | 2.06 | 32.07 | 53.56 | 0.00 | 45.96 | 23.39 | 0.92 | 0.01 | 0.00 |

| | | | | | | | | | | | | | | | | | | |
|---|---|---|---|---|---|---|---|---|---|---|---|---|---|---|---|---|---|---|
| 982 | B | 14.00 | H | 5 | 0 | 3 | 138.495 | 4885.90 | 181.06 | 2.23 | 8.88 | 88.15 | 0.10 | 19.42 | 11.64 | 1.06 | 0.01 | 0.00 |
| 982 | B | 14.00 | H | 6 | 90 | 92.5 | 140.92 | 4913.09 | 166.85 | 2.44 | 28.97 | 47.82 | 0.00 | 28.76 | 6.72 | 0.95 | 0.00 | 0.00 |
| 982 | B | 14.00 | H | 7 | 61 | 63.5 | 141.7 | 4920.98 | 167.32 | 2.29 | 5.72 | 56.03 | 0.07 | 24.79 | 14.07 | 1.08 | 0.01 | 0.00 |
| 982 | B | 15.00 | H | 1 | 30.5 | 33 | 143.76 | 4963.88 | | 2.20 | 54.52 | 56.16 | 0.00 | 51.66 | 25.26 | 0.97 | 0.01 | 0.00 |
| 982 | B | 15.00 | H | 1 | 111 | 113.5 | 144.56 | 4988.99 | 160.98 | 2.35 | 13.70 | 79.04 | 0.09 | 55.37 | 5.01 | 1.00 | 0.00 | 0.00 |
| 982 | B | 15.00 | H | 2 | 40 | 42.5 | 145.36 | 5008.96 | 157.63 | 2.41 | 11.24 | 51.97 | 0.00 | 44.19 | 14.36 | 0.92 | 0.01 | 0.00 |
| 982 | B | 15.00 | H | 2 | 120 | 122.5 | 146.16 | 5024.56 | 155.35 | 2.30 | 12.84 | 62.14 | 0.00 | 34.83 | 19.03 | 1.00 | 0.01 | 0.00 |
| 982 | B | 15.00 | H | 3 | 50 | 52.5 | 146.96 | 5039.79 | 160.81 | 2.25 | 9.85 | 54.83 | 0.00 | 30.21 | 17.80 | 0.93 | 0.01 | 0.00 |
| 982 | B | 15.00 | H | 4 | 60 | 62.5 | 148.56 | 5069.81 | 167.48 | 2.15 | 20.81 | 38.16 | 0.00 | 32.10 | 21.47 | 0.93 | 0.01 | 0.00 |
| 982 | B | 15.00 | H | 4 | 140 | 142.5 | 149.36 | 5081.01 | 152.57 | 2.43 | 5.69 | 81.09 | 0.08 | 58.40 | 7.02 | 1.12 | 0.00 | 0.00 |

### *9.3.1.3 C. mundulus var*

| Site | H | Cor | T | Sc | Top (cm) | Bot (cm) | Depth (mcd) | Age (Ka) | Li7/Ca43 | B11/Ca43 | Mg25/Ca43 | Al27/Ca43 | Mn55/Ca43 | Cd111/Ca43 | U238/Ca43 | Fe56/Ca43 | Ca v. Ca | Fe/Mg ratio |
|---|---|---|---|---|---|---|---|---|---|---|---|---|---|---|---|---|---|---|
| | | | | | | | | | umol/mol | umol/mol | mmol/mol | umol/mol | umol/mol | umol/mol | nmol/mol | umol/mol | | |
| 982 | B | 5.00 | H | 4 | 50 | 54 | 43.08 | 1912.94 | 11.39 | 188.65 | 1.55 | 58.92 | 82.79 | 0.00 | 23.19 | 141.37 | 0.00 | 0.09 |
| 982 | B | 5.00 | H | 4 | 68 | 70 | 43.26 | 1926.78 | 11.59 | 195.92 | 1.64 | 33.34 | 78.65 | 0.00 | 13.54 | 124.42 | 0.96 | 0.08 |
| 982 | B | 5.00 | H | 4 | 147 | 149 | 44.05 | 1997.79 | 11.20 | 188.77 | 1.66 | 65.11 | 87.48 | 0.00 | 15.23 | 153.02 | 0.00 | 0.09 |
| 982 | B | 5.00 | H | 5 | 140 | 144 | 45.48 | 2058.04 | 11.72 | 208.81 | 1.59 | 63.06 | 115.75 | 0.01 | 37.69 | 159.53 | 0.88 | 0.10 |
| 982 | B | 5.00 | H | 7 | 1 | 3.5 | 47.09 | 2118.76 | 11.80 | 196.04 | 1.72 | 58.04 | 91.45 | 0.01 | 66.95 | 155.93 | 1.00 | 0.09 |
| 982 | B | 5.00 | H | 7 | 40 | 42.5 | 47.48 | 2136.76 | 10.96 | 194.28 | 1.65 | 60.46 | 88.23 | 0.00 | 40.14 | 132.38 | 0.00 | 0.08 |
| 982 | B | 5.00 | H | 7 | 59.5 | 61.5 | 47.675 | 2146.20 | 10.36 | 176.86 | 1.59 | 67.13 | 81.27 | 0.00 | 34.23 | 142.01 | 0.00 | 0.09 |
| 982 | B | 6.00 | H | 1 | 50 | 52 | 49.51 | 2245.01 | 11.72 | 188.24 | 1.61 | 58.66 | 126.76 | 0.01 | 49.57 | 165.90 | 0.00 | 0.10 |
| 982 | B | 6.00 | H | 1 | 90 | 92 | 49.91 | 2269.61 | 11.27 | 183.32 | 1.55 | 143.39 | 72.69 | 0.00 | 8.84 | 161.70 | 1.07 | 0.10 |
| 982 | B | 6.00 | H | 2 | 130 | 134 | 51.81 | 2393.52 | 10.87 | 181.82 | 1.52 | 81.60 | 72.82 | 0.00 | 11.54 | 136.79 | 1.00 | 0.09 |
| 982 | B | 6.00 | H | 3 | 28 | 30 | 52.29 | 2435.28 | 13.51 | 187.55 | 1.63 | 70.94 | 77.88 | 0.00 | 26.30 | 112.74 | 0.00 | 0.07 |

| | | | | | | | | | | | | | | | | | | |
|---|---|---|---|---|---|---|---|---|---|---|---|---|---|---|---|---|---|---|
| 982 | B | 6.00 | H | 3 | 68 | 70 | 52.69 | 2458.40 | 11.11 | 188.49 | 1.62 | 133.97 | 93.71 | 0.01 | 88.77 | 142.95 | 0.00 | 0.09 |
| 982 | B | 6.00 | H | 3 | 100 | 104 | 53.01 | 2476.35 | 12.11 | 206.45 | 1.96 | 181.58 | 87.40 | 0.00 | 120.11 | 175.99 | 1.04 | 0.09 |
| 982 | B | 6.00 | H | 4 | 32 | 36 | 53.83 | 2506.68 | 11.56 | 201.41 | 1.69 | 70.19 | 86.22 | 0.01 | 54.39 | 146.71 | 1.87 | 0.09 |
| 982 | B | 6.00 | H | 5 | 39.5 | 43.5 | 55.405 | 2550.41 | 10.58 | 187.18 | 1.63 | 38.17 | 64.90 | 0.00 | | 82.80 | 0.00 | 0.05 |
| 982 | B | 6.00 | H | 5 | 50 | 52 | 55.51 | 2552.98 | 11.51 | 189.85 | 1.80 | 29.47 | 82.73 | 0.01 | 33.72 | 108.16 | 1.03 | 0.06 |
| 982 | B | 6.00 | H | 5 | 122 | 126 | 56.23 | 2566.52 | 11.00 | 177.23 | 1.65 | 109.68 | 51.48 | 0.00 | 47.46 | 80.79 | 0.92 | 0.05 |
| 982 | B | 6.00 | H | 6 | 48 | 52 | 56.99 | 2580.90 | | 177.86 | 1.67 | 53.97 | 56.45 | 0.01 | 35.67 | 76.94 | 0.00 | 0.05 |
| 982 | B | 6.00 | H | 6 | 57.5 | 59.5 | 57.085 | 2583.68 | 11.50 | 184.79 | 1.74 | 96.00 | 58.58 | 0.00 | 40.90 | 96.19 | 1.10 | 0.06 |
| 982 | B | 6.00 | H | 6 | 140 | 142 | 57.91 | 2628.06 | 11.47 | 181.27 | 1.69 | 124.42 | 66.00 | 0.00 | 87.73 | 71.26 | 0.96 | 0.04 |
| 982 | B | 7.00 | H | 1 | 100 | 102 | 59.77 | 2721.14 | 11.83 | 184.04 | 1.65 | 115.31 | 90.54 | 0.00 | 124.68 | 64.91 | 0.98 | 0.04 |
| 982 | B | 7.00 | H | 2 | 28 | 30 | 60.55 | 2769.12 | 11.54 | 180.67 | 2.10 | 130.69 | 77.92 | 0.01 | 29.00 | 77.87 | 0.00 | 0.04 |
| 982 | B | 7.00 | H | 2 | 110 | 112 | 61.37 | 2830.25 | 10.92 | 205.69 | 2.00 | 65.41 | 126.91 | 0.01 | 152.87 | 63.57 | 0.00 | 0.03 |
| 982 | B | 7.00 | H | 2 | 147 | 149 | 61.74 | 2852.92 | 11.08 | 184.03 | 1.88 | 213.57 | 141.36 | 0.01 | 107.44 | 146.85 | 0.00 | 0.08 |
| 982 | B | 7.00 | H | 3 | 40 | 42 | 62.17 | 2874.91 | 11.07 | 179.33 | 2.04 | 87.81 | 90.48 | 0.01 | 47.43 | 62.12 | 1.07 | 0.03 |
| 982 | B | 7.00 | H | 3 | 99.5 | 103.5 | 62.765 | 2902.59 | 11.37 | 191.04 | 2.16 | 106.64 | 88.03 | 0.00 | 71.64 | 69.23 | 0.00 | 0.03 |

| | | | | | | | | | | | | | | | | | | |
|---|---|---|---|---|---|---|---|---|---|---|---|---|---|---|---|---|---|---|
| 982 | B | 7.00 | H | 4 | 10 | 12 | 63.37 | 2930.27 | 10.81 | 171.10 | 2.06 | 63.83 | 87.23 | 0.01 | 63.68 | 53.97 | 0.89 | 0.03 |
| 982 | B | 7.00 | H | 4 | 108 | 112 | 64.35 | 2972.98 | 11.22 | 185.19 | 1.73 | 106.03 | 77.93 | 0.00 | 32.81 | 65.08 | 1.05 | 0.04 |
| 982 | B | 7.00 | H | 5 | 39.5 | 43.5 | 65.165 | 3003.24 | | | 1.99 | 114.09 | 88.49 | 0.01 | 62.16 | 64.98 | 0.00 | 0.03 |
| 982 | B | 7.00 | H | 5 | 58 | 60 | 65.35 | 3009.88 | 11.50 | 174.56 | 1.77 | 122.30 | 106.33 | 0.01 | 92.41 | 75.44 | 1.00 | 0.04 |
| 982 | B | 7.00 | H | 6 | 12 | 14.5 | 66.39 | 3052.44 | 10.65 | 174.59 | 2.03 | 70.93 | 97.51 | 0.00 | 49.17 | 67.32 | 1.02 | 0.03 |
| 982 | B | 7.00 | H | 6 | 52 | 54.5 | 66.79 | 3073.89 | 10.93 | 181.19 | 1.78 | 62.07 | 81.66 | 0.01 | 37.24 | 59.08 | 0.00 | 0.03 |
| 982 | B | 7.00 | H | 6 | 68 | 70 | 66.95 | 3083.12 | 10.91 | 172.26 | 1.71 | 34.03 | 91.79 | 0.00 | | 53.30 | 0.00 | 0.03 |
| 982 | B | 7.00 | H | 6 | 108 | 110 | 67.35 | 3105.87 | | 187.54 | 1.63 | 47.81 | 82.11 | 0.01 | | 48.28 | 0.00 | 0.03 |
| 982 | B | 7.00 | H | 6 | 132 | 134.5 | 67.59 | 3116.93 | 11.40 | 190.81 | 1.86 | 218.63 | 103.42 | 0.00 | 43.65 | 78.83 | 1.04 | 0.04 |
| 982 | B | 7.00 | H | 6 | 148 | 150 | 67.75 | 3124.31 | 10.33 | 159.72 | 2.10 | 116.83 | 84.32 | 0.00 | 42.98 | 89.61 | 0.00 | 0.04 |
| 982 | B | 8.00 | H | 1 | 42 | 44.5 | 70.32 | 3189.55 | 10.94 | 186.55 | 1.77 | 27.50 | 68.35 | 0.00 | 23.25 | 50.57 | 0.94 | 0.03 |
| 982 | B | 8.00 | H | 1 | 84 | 86.5 | 70.74 | 3204.66 | 10.53 | 184.97 | 1.86 | 26.62 | 68.68 | 0.00 | 23.39 | 52.41 | 17.43 | 0.03 |
| 982 | B | 8.00 | H | 2 | 28 | 30 | | 3247.09 | 11.17 | 189.33 | 1.62 | 97.61 | 74.12 | 0.00 | 33.21 | 55.34 | 1.03 | 0.03 |
| 982 | B | 8.00 | H | 2 | 57 | 59.5 | 71.18 | 3254.62 | 11.12 | 194.03 | 1.62 | 29.05 | 55.50 | 0.00 | 49.24 | 37.85 | 0.92 | 0.02 |

| | | | | | | | | | | | | | | | | | | |
|---|---|---|---|---|---|---|---|---|---|---|---|---|---|---|---|---|---|---|
| 982 | B | 8.00 | H | 2 | 132.5 | 135 | 71.805 | 3269.84 | 11.11 | 187.33 | 1.81 | 49.82 | 71.00 | 0.01 | 43.04 | 49.01 | 0.98 | 0.03 |
| 982 | B | 8.00 | H | 2 | 138 | 140 | 71.86 | 3271.06 | 10.95 | 186.04 | 1.68 | 47.01 | 65.10 | 0.00 | 38.88 | 45.94 | 1.01 | 0.03 |
| 982 | B | 8.00 | H | 3 | 24 | 26.5 | 72.22 | 3280.35 | 11.27 | 194.92 | 1.81 | 85.84 | 71.48 | 0.00 | 57.07 | 59.30 | 1.03 | 0.03 |
| 982 | B | 8.00 | H | 3 | 42 | 44 | 73.31 | 3285.51 | 11.10 | 174.29 | 1.80 | 89.05 | 87.83 | 0.01 | 70.04 | 67.81 | 1.01 | 0.04 |
| 982 | B | 8.00 | H | 3 | 102 | 104.5 | 73.91 | 3305.17 | 11.94 | 189.20 | 1.85 | 68.11 | 78.52 | 0.00 | 65.91 | 71.20 | 1.03 | 0.04 |
| 982 | B | 8.00 | H | 4 | 12 | 14 | 74.51 | 3323.65 | 11.03 | 185.37 | 1.56 | 41.54 | 51.03 | 0.00 | 36.40 | 29.88 | 1.09 | 0.02 |
| 982 | B | 8.00 | H | 5 | 122 | 124.5 | 77.11 | 3404.72 | 11.30 | 192.45 | 1.84 | 28.17 | 65.25 | 0.00 | 37.91 | 31.71 | 0.91 | 0.02 |
| 982 | B | 8.00 | H | 6 | 92 | 94.5 | 78.31 | 3444.40 | 10.25 | 165.44 | 1.63 | 8.63 | 79.01 | 0.01 | 38.02 | 29.68 | | 0.02 |
| 982 | B | 8.00 | H | 6 | 132 | 134.5 | 78.71 | 3459.87 | | 199.24 | 1.63 | 37.55 | 68.48 | 0.00 | 35.58 | 29.34 | 0.93 | 0.02 |
| 982 | B | 8.00 | H | 6 | 148 | 150 | 78.87 | 3466.46 | | 166.26 | 1.66 | 23.17 | 87.95 | 0.01 | | 39.49 | 0.00 | 0.02 |
| 982 | B | 9.00 | H | 1 | 10 | 12.5 | 80.6 | 3544.59 | 10.42 | 170.16 | 1.69 | 16.20 | 70.57 | 0.00 | 34.88 | 36.36 | 0.00 | 0.02 |
| 982 | B | 9.00 | H | 1 | 30 | 32 | 80.8 | 3552.98 | 11.13 | 187.65 | 1.62 | 22.58 | 45.33 | 0.01 | 38.85 | 31.95 | 0.95 | 0.02 |
| 982 | B | 9.00 | H | 2 | 100 | 102.5 | 83 | 3610.22 | 11.59 | 194.15 | 1.67 | 49.87 | 57.80 | 0.00 | 59.75 | 33.72 | 0.97 | 0.02 |
| 982 | B | 9.00 | H | 3 | 8 | 10 | 83.58 | 3621.47 | 10.40 | 174.56 | 1.78 | 34.21 | 63.55 | 0.01 | 28.85 | 26.29 | 0.00 | 0.01 |
| 982 | B | 9.00 | H | 3 | 30 | 32.5 | 83.8 | 3624.74 | 10.83 | 175.27 | 1.72 | 107.92 | 55.50 | 0.00 | 35.11 | 47.62 | 0.96 | 0.03 |

| | | | | | | | | | | | | | | | | | | |
|---|---|---|---|---|---|---|---|---|---|---|---|---|---|---|---|---|---|---|
| 982 | B | 9.00 | H | 4 | 0 | 3 | 85 | 3643.69 | 11.25 | 183.67 | 1.82 | 29.82 | 55.13 | 0.00 | 42.76 | 28.20 | 0.99 | 0.02 |
| 982 | B | 9.00 | H | 4 | 58 | 60 | 85.58 | 3657.45 | 11.55 | 181.07 | 1.55 | 38.32 | 39.54 | 0.00 | 39.00 | 26.57 | 0.95 | 0.02 |
| 982 | B | 9.00 | H | 6 | 100 | 102.5 | 88.44 | 3743.89 | 10.68 | 165.47 | 1.78 | 33.53 | 60.37 | 0.00 | 62.07 | 50.91 | 0.95 | 0.03 |
| 982 | B | 10.00 | H | 3 | 140 | 142.5 | 95.11 | 3920.42 | 11.13 | 170.12 | 1.74 | 26.33 | 64.74 | 0.01 | 78.37 | 34.34 | 0.00 | 0.02 |
| 982 | B | 10.00 | H | 4 | 70 | 72.5 | 95.91 | 3940.04 | 10.69 | 166.65 | 1.84 | 29.00 | 56.28 | 0.01 | 100.49 | 35.29 | 0.00 | 0.02 |
| 982 | B | 10.00 | H | 6 | 9.5 | 12 | 98.305 | 3996.56 | 10.90 | 185.59 | 1.76 | 26.98 | 53.61 | 0.01 | 85.94 | 33.22 | 1.00 | 0.02 |
| 982 | B | 11.00 | H | 1 | 40 | 42.5 | 101.47 | 4088.77 | 11.33 | 178.39 | 2.11 | 10.71 | 67.53 | 0.00 | 47.65 | 23.01 | 0.00 | 0.01 |
| 982 | B | 11.00 | H | 2 | 129 | 131.5 | 103.86 | 4131.00 | 10.75 | 188.74 | 1.75 | 12.50 | 42.61 | 0.00 | 43.10 | 16.62 | 1.04 | 0.01 |
| 982 | B | 11.00 | H | 3 | 60 | 62.5 | 104.67 | 4155.12 | 10.69 | 179.00 | 1.68 | 27.81 | 40.06 | 0.00 | 65.91 | 34.84 | 0.00 | 0.02 |
| 982 | B | 11.00 | H | 3 | 140 | 142.5 | 105.47 | 4185.89 | 10.72 | 178.17 | 1.80 | 15.76 | 51.82 | 0.01 | 82.25 | 25.57 | 1.06 | 0.01 |
| 982 | B | 11.00 | H | 5 | 80 | 82.5 | 107.87 | 4238.07 | 9.75 | 157.94 | 2.09 | 15.89 | 64.75 | 0.00 | 92.10 | 29.05 | 0.00 | 0.01 |
| 982 | B | 11.00 | H | 6 | 97 | 99.5 | 109.54 | 4283.98 | 10.89 | 186.68 | 1.80 | 14.91 | 57.33 | 0.00 | 37.47 | 16.44 | 0.00 | 0.01 |
| 982 | B | 11.00 | H | 7 | 21 | 23.5 | 110.28 | 4303.87 | 10.54 | 181.08 | 2.10 | 14.41 | 63.07 | 0.11 | | 6.73 | | 0.00 |
| 982 | B | 12.00 | H | 1 | 60 | 62.5 | 111.59 | 4337.35 | 10.74 | 178.33 | 1.81 | 8.89 | 51.76 | 0.01 | 62.42 | 24.17 | 1.07 | 0.01 |
| 982 | B | 12.00 | H | 2 | 70 | 72.5 | 113.19 | 4376.54 | 10.88 | 165.53 | 2.18 | 18.65 | 63.81 | 0.00 | 67.54 | 18.38 | 1.06 | 0.01 |

| | | | | | | | | | | | | | | | | | | |
|---|---|---|---|---|---|---|---|---|---|---|---|---|---|---|---|---|---|---|
| 982 | B | 12.00 | H | 3 | 0 | 3 | 113.99 | 4396.61 | 11.42 | 191.51 | 1.72 | 11.22 | 30.91 | 0.05 | | -2.17 | 0.94 | 0.00 |
| 982 | B | 12.00 | H | 3 | 80 | 82.5 | 114.79 | 4418.83 | 10.66 | 178.92 | 1.70 | 40.61 | 40.45 | 0.00 | 53.06 | 49.40 | 0.00 | 0.03 |
| 982 | B | 12.00 | H | 4 | 10 | 12.5 | 115.59 | 4436.20 | 10.93 | 186.63 | 1.64 | 17.24 | 25.58 | 0.11 | 69.35 | -9.56 | 0.95 | -0.01 |
| 982 | B | 12.00 | H | 5 | 99.5 | 102 | 117.985 | 4493.29 | 10.48 | 171.68 | 1.63 | 44.90 | 64.80 | 0.00 | 142.19 | 39.75 | 0.00 | 0.02 |
| 982 | B | 12.00 | H | 6 | 30 | 32.5 | 118.79 | 4514.87 | 10.55 | 191.61 | 1.86 | 12.01 | 36.21 | 0.08 | 46.64 | 2.46 | 0.99 | 0.00 |
| 982 | B | 12.00 | H | 6 | 110 | 112.5 | 119.59 | 4534.45 | 10.26 | 163.70 | 1.77 | 39.79 | 58.83 | 0.00 | 82.91 | 27.51 | 1.13 | 0.02 |
| 982 | B | 12.00 | H | 7 | 50 | 52.5 | 120.49 | 4552.91 | | 199.15 | 1.94 | 24.68 | 30.23 | 0.08 | | -13.41 | 0.97 | -0.01 |
| 982 | B | 13.00 | H | 1 | 60 | 62.5 | 122.14 | 4577.88 | 10.63 | 173.02 | 1.91 | 20.14 | 26.35 | 0.00 | 39.72 | 21.78 | 0.99 | 0.01 |
| 982 | B | 13.00 | H | 2 | 70 | 72.5 | 123.74 | 4610.00 | 10.56 | 163.66 | 1.87 | 39.92 | 52.40 | 0.00 | 56.69 | 38.98 | 0.00 | 0.02 |
| 982 | B | 13.00 | H | 3 | 0 | 3 | 124.54 | 4628.18 | 11.57 | 174.73 | 1.72 | 106.88 | 90.85 | 0.01 | 161.08 | 84.89 | 0.00 | 0.05 |
| 982 | B | 13.00 | H | 3 | 80 | 82.5 | 125.34 | 4645.31 | 10.30 | 166.87 | 1.78 | 50.86 | 48.14 | 0.01 | 94.75 | 44.09 | 1.10 | 0.02 |
| 982 | B | 13.00 | H | 4 | 10 | 12.5 | 126.14 | 4659.32 | 11.34 | 183.29 | 1.67 | 17.96 | 34.86 | 0.00 | 66.60 | 15.58 | 1.01 | 0.01 |
| 982 | B | 13.00 | H | 4 | 90 | 92.5 | 126.94 | 4671.93 | 10.27 | 173.61 | 1.64 | 35.85 | 63.19 | 0.00 | 137.54 | 26.11 | 0.00 | 0.02 |
| 982 | B | 13.00 | H | 5 | 100 | 102.5 | 128.54 | 4706.41 | 10.32 | 172.99 | 1.87 | 34.07 | 70.36 | 0.00 | 113.76 | 34.46 | 1.15 | 0.02 |

| | | | | | | | | | | | | | | | | | | |
|---|---|---|---|---|---|---|---|---|---|---|---|---|---|---|---|---|---|---|
| 982 | B | 13.00 | H | 6 | 110 | 112.5 | 130.14 | 4736.22 | 9.95 | 174.58 | 1.67 | 21.39 | 48.29 | 0.00 | 94.13 | 16.30 | 1.01 | 0.01 |
| 982 | B | 14.00 | H | 1 | 40 | 42.5 | 132.5 | 4773.15 | 10.19 | 169.39 | 1.59 | 34.08 | 67.24 | 0.00 | 78.53 | 45.15 | 0.00 | 0.03 |
| 982 | B | 14.00 | H | 2 | 50 | 52.5 | 134.5 | 4808.43 | 10.34 | 180.10 | 2.03 | 14.92 | 51.66 | 0.00 | 49.21 | 12.94 | 0.00 | 0.01 |
| 982 | B | 14.00 | H | 2 | 130 | 132.5 | 135.3 | 4828.27 | 9.84 | 165.57 | 1.78 | 26.31 | 64.89 | 0.00 | 109.70 | 27.26 | 0.00 | 0.02 |
| 982 | B | 14.00 | H | 3 | 140 | 142.5 | 136.9 | 4856.43 | 10.83 | 188.50 | 1.49 | 22.12 | 47.23 | 0.00 | 76.68 | 34.71 | 0.96 | 0.02 |
| 982 | B | 14.00 | H | 4 | 70 | 72.5 | 137.7 | 4870.07 | 10.53 | 191.52 | 1.73 | 20.04 | 47.54 | 0.00 | 62.64 | 18.90 | 1.02 | 0.01 |
| 982 | B | 14.00 | H | 5 | 0 | 3 | 138.495 | 4885.90 | 10.67 | 189.14 | 1.95 | 8.99 | 83.70 | 0.09 | 31.02 | 15.98 | 0.99 | 0.01 |
| 982 | B | 14.00 | H | 5 | 80 | 82.5 | 139.3 | 4896.65 | 10.97 | 190.97 | 1.48 | 39.63 | 43.62 | 0.00 | 41.24 | 42.15 | 0.97 | 0.03 |
| 982 | B | 14.00 | H | 6 | 90 | 92.5 | 140.92 | 4913.09 | 10.32 | 177.99 | 1.89 | 19.27 | 68.87 | 0.00 | 69.14 | 21.38 | 0.00 | 0.01 |
| 982 | B | 15.00 | H | 1 | 30.5 | 33 | 143.76 | 4963.88 | 10.61 | 183.38 | 1.83 | 31.67 | 70.08 | 0.00 | 95.22 | 30.15 | 1.03 | 0.02 |
| 982 | B | 15.00 | H | 1 | 111 | 113.5 | 144.56 | 4988.99 | 9.50 | 170.53 | 1.85 | 18.16 | 101.42 | 0.10 | 118.27 | 27.61 | 1.03 | 0.01 |
| 982 | B | 15.00 | H | 2 | 40 | 42.5 | 145.36 | 5008.96 | 10.44 | 183.35 | 1.90 | 13.97 | 49.01 | 0.00 | 61.41 | 14.61 | 0.95 | 0.01 |
| 982 | B | 15.00 | H | 2 | 120 | 122.5 | 146.16 | 5024.56 | 10.46 | 192.19 | 1.83 | 18.43 | 52.29 | 0.00 | 46.53 | 16.74 | 0.96 | 0.01 |
| 982 | B | 15.00 | H | 3 | 50 | 52.5 | 146.96 | 5039.79 | 10.42 | 181.93 | 1.76 | 14.93 | 50.78 | 0.00 | 40.20 | 18.50 | 0.00 | 0.01 |

| | | | | | | | | | | | | | | | | | | |
|---|---|---|---|---|---|---|---|---|---|---|---|---|---|---|---|---|---|---|
| 982 | B | 15.00 | H | 4 | 60 | 62.5 | 148.56 | 5069.81 | 9.95 | 174.46 | 1.69 | 23.26 | 57.61 | 0.00 | 53.71 | 21.74 | 0.00 | 0.01 |
| 982 | B | 15.00 | H | 4 | 140 | 142.5 | 149.36 | 5081.01 | 10.57 | 194.92 | 1.71 | 20.57 | 54.02 | 0.00 | 58.93 | 13.97 | 0.91 | 0.01 |

### *9.3.1.4 M. barleeanum*

| Site | H | Cor | T | Sc | Top (cm) | Bot (cm) | Depth (mcd) | Age (Ka) | Li7/Ca43 | B11/Ca43 | Mg25/Ca43 | Al27/Ca43 | Mn55/Ca43 | Cd111/Ca43 | U238/Ca43 | Fe56/Ca43 | Ca v. Ca (matrix matching) | Fe/Mg ratio |
|---|---|---|---|---|---|---|---|---|---|---|---|---|---|---|---|---|---|---|
| | | | | | | | | | umol/mol | umol/mol | mmol/mol | umol/mol | umol/mol | umol/mol | nmol/mol | umol/mol | | |
| 982 | B | 5.00 | H | 5 | 140 | 144 | 45.48 | 2058.04 | 2.46 | 92.86 | 1.30 | 190.51 | 63.93 | 0.01 | 20.53 | 146.74 | | 0.11 |
| 982 | B | 5.00 | H | 6 | 7.5 | 9.5 | 45.655 | 2064.28 | 9.32 | 96.17 | 1.42 | 88.34 | 93.38 | 0.00 | 20.71 | 163.11 | 0.93 | 0.11 |
| 982 | B | 5.00 | H | 7 | 1 | 3.5 | 47.09 | 2118.76 | 8.60 | 87.86 | 1.50 | 75.74 | 88.05 | 0.01 | 41.21 | 155.72 | 0.93 | 0.10 |
| 982 | B | 5.00 | H | 7 | 40 | 42.5 | 47.48 | 2136.76 | 8.63 | 98.67 | 1.44 | 143.12 | 95.98 | 0.01 | 39.09 | | | |
| 982 | B | 6.00 | H | 1 | 10 | 12 | 49.11 | 2220.40 | 11.04 | 119.64 | 1.60 | 179.83 | 93.13 | 0.01 | 64.49 | 155.72 | | 0.10 |
| 982 | B | 6.00 | H | 1 | 80 | 84 | 49.81 | 2263.46 | 9.12 | 85.70 | 1.46 | 103.34 | 72.88 | 0.01 | 11.32 | 161.93 | 0.92 | 0.11 |
| 982 | B | 6.00 | H | 2 | 18 | 20 | 50.69 | 2312.23 | 9.05 | 88.90 | 1.55 | 87.70 | 84.83 | 0.01 | 12.46 | 198.03 | 0.96 | 0.13 |
| 982 | B | 6.00 | H | 2 | 130 | 134 | 51.81 | 2393.52 | 8.56 | 86.41 | 1.37 | 113.05 | 79.26 | 0.01 | 13.83 | 140.21 | 0.89 | 0.10 |
| 982 | B | 6.00 | H | 3 | 60 | 64 | 52.61 | 2453.79 | 9.04 | 81.31 | 1.47 | 136.41 | 116.54 | 0.01 | 72.16 | 138.48 | | 0.09 |
| 982 | B | 6.00 | H | 4 | 108 | 112 | 54.59 | 2527.72 | 7.31 | 72.88 | 1.03 | 112.14 | 84.73 | 0.01 | 21.12 | 76.10 | 0.00 | 0.07 |
| 982 | B | 6.00 | H | 5 | 122 | 126 | 56.23 | 2566.52 | 9.93 | 85.12 | 2.13 | 408.18 | 56.27 | 0.01 | 32.86 | 113.80 | 1.00 | 0.05 |

| | | | | | | | | | | | | | | | | | | |
|---|---|---|---|---|---|---|---|---|---|---|---|---|---|---|---|---|---|---|
| 982 | B | 6.00 | H | 6 | 100 | 102 | 57.51 | 2603.46 | 6.56 | 79.37 | 1.28 | 140.51 | 69.46 | 0.01 | 71.43 | 67.35 | | 0.05 |
| 982 | B | 7.00 | H | 1 | 78.5 | 82.5 | 59.555 | 2708.23 | 9.28 | 51.94 | 1.30 | 86.64 | 65.62 | 0.01 | 50.92 | 51.22 | 0.00 | 0.04 |
| 982 | B | 7.00 | H | 1 | 100 | 102 | 59.77 | 2721.14 | 8.56 | 70.79 | 1.28 | 157.24 | 76.99 | 0.01 | 98.77 | 70.84 | | 0.06 |
| 982 | B | 7.00 | H | 2 | 28 | 30 | 60.55 | 2769.12 | | | 1.77 | 157.65 | 58.42 | 0.01 | 28.18 | 303.36 | 0.96 | 0.17 |
| 982 | B | 7.00 | H | 2 | 110 | 112 | 61.37 | 2830.25 | 8.14 | 86.84 | 1.42 | 124.19 | 70.71 | 0.01 | 68.47 | 57.81 | | 0.04 |
| 982 | B | 7.00 | H | 3 | 99.5 | 103.5 | 62.765 | 2902.59 | | 100.40 | 1.74 | 70.39 | 56.85 | 0.01 | 37.40 | 55.15 | | 0.03 |
| 982 | B | 7.00 | H | 5 | 39.5 | 43.5 | 65.165 | 3003.24 | 7.16 | 74.75 | 1.63 | 223.27 | 72.76 | 0.01 | 26.77 | 112.86 | 1.00 | 0.07 |
| 982 | B | 7.00 | H | 5 | 58 | 60 | 65.35 | 3009.88 | 9.14 | 113.06 | 1.56 | 94.65 | 101.36 | 0.01 | 61.58 | 57.32 | 0.98 | 0.04 |
| 982 | B | 7.00 | H | 6 | 12 | 14.5 | 66.39 | 3052.44 | 9.84 | 110.02 | 1.68 | 323.15 | 97.68 | 0.01 | 86.46 | 94.91 | 1.00 | 0.06 |
| 982 | B | 7.00 | H | 6 | 52 | 54.5 | 66.79 | 3073.89 | 7.53 | 77.15 | 1.49 | 171.36 | 78.73 | 0.01 | 20.78 | 78.19 | 1.08 | 0.05 |
| 982 | B | 7.00 | H | 7 | 40 | 42 | 68.17 | 3141.00 | 8.25 | 83.12 | 1.46 | 153.02 | 63.22 | 0.01 | 39.26 | 82.19 | 1.04 | 0.06 |
| 982 | B | 8.00 | H | 1 | 18 | 20 | 70.08 | 3182.28 | 7.42 | 79.51 | 1.67 | 90.49 | 73.96 | 0.01 | 24.43 | 48.87 | 1.08 | 0.03 |
| 982 | B | 8.00 | H | 2 | 57 | 59.5 | 71.18 | 3254.62 | 8.45 | | 1.54 | 49.26 | 45.14 | 0.01 | 30.30 | 55.31 | | 0.04 |
| 982 | B | 8.00 | H | 2 | 94 | 96.5 | 71.42 | 3261.44 | 8.38 | | 1.30 | 37.45 | 49.48 | 0.01 | 36.18 | 39.41 | | 0.03 |
| 982 | B | 8.00 | H | 3 | 24 | 26.5 | 72.22 | 3280.35 | 8.28 | 85.44 | 1.58 | 84.16 | 83.15 | 0.01 | 51.32 | 80.31 | 0.98 | 0.05 |

| | | | | | | | | | | | | | | | | | | |
|---|---|---|---|---|---|---|---|---|---|---|---|---|---|---|---|---|---|---|
| 982 | B | 8.00 | H | 3 | 42 | 44 | 73.31 | 3285.51 | 8.67 | 97.91 | 1.59 | 61.72 | 64.30 | 0.01 | 31.91 | 47.90 | | 0.03 |
| 982 | B | 8.00 | H | 4 | 107.5 | 110 | 75.465 | 3354.68 | 8.12 | 75.71 | 1.62 | 97.37 | 71.40 | 0.01 | 49.82 | 78.47 | 0.97 | 0.05 |
| 982 | B | 8.00 | H | 5 | 58 | 60 | 76.47 | 3386.76 | 8.10 | 96.87 | 1.58 | 93.55 | 59.17 | 0.01 | 39.94 | 73.48 | | 0.05 |
| 982 | B | 8.00 | H | 5 | 122 | 124.5 | 77.11 | 3404.72 | 9.12 | 105.83 | 2.16 | 26.47 | 75.84 | 0.00 | 35.98 | 31.98 | | 0.01 |
| 982 | B | 9.00 | H | 2 | 100 | 102.5 | 83 | 3610.22 | 8.51 | 91.94 | 1.76 | 56.35 | 64.33 | 0.01 | 56.85 | 32.30 | 0.94 | 0.02 |
| 982 | B | 9.00 | H | 3 | 8 | 10 | 83.58 | 3621.47 | 8.05 | 90.07 | 1.61 | 102.74 | 56.24 | 0.01 | 23.66 | 29.35 | 0.98 | 0.02 |
| 982 | B | 9.00 | H | 3 | 30 | 32.5 | 83.8 | 3624.74 | 7.41 | 75.65 | 1.55 | 166.56 | 52.42 | 0.01 | 27.66 | 45.03 | 0.97 | 0.03 |
| 982 | B | 9.00 | H | 3 | 48 | 50 | 83.98 | 3627.40 | 7.78 | 81.56 | 1.56 | 169.80 | 54.74 | 0.01 | 32.08 | 36.23 | 0.95 | 0.02 |
| 982 | B | 9.00 | H | 4 | 0 | 3 | 85 | 3643.69 | 7.71 | 82.25 | 1.74 | 77.40 | 41.30 | 0.01 | 20.49 | 23.39 | 0.91 | 0.01 |
| 982 | B | 9.00 | H | 4 | 58 | 60 | 85.58 | 3657.45 | 9.55 | 93.20 | 1.73 | 91.92 | 54.89 | 0.01 | 34.17 | 34.03 | 0.96 | 0.02 |
| 982 | B | 9.00 | H | 4 | 80 | 82.5 | 85.8 | 3663.28 | 7.82 | 75.32 | 1.63 | 159.21 | 63.59 | 0.01 | 52.06 | 56.93 | 1.09 | 0.03 |
| 982 | B | 9.00 | H | 5 | 10 | 12.5 | 86.6 | 3691.53 | | | 1.85 | 102.69 | 41.66 | 0.01 | 19.33 | 31.68 | 0.92 | 0.02 |
| 982 | B | 9.00 | H | 5 | 90 | 92.5 | 86.84 | 3712.91 | 8.40 | 81.10 | 1.75 | 92.33 | 61.34 | 0.01 | 47.60 | 54.21 | 1.01 | 0.03 |
| 982 | B | 9.00 | H | 6 | 20.5 | 23 | 87.645 | 3728.25 | 8.26 | | 1.53 | 63.68 | 28.78 | 0.01 | 17.85 | 22.05 | 0.94 | 0.01 |
| 982 | B | 9.00 | H | 6 | 100 | 102.5 | 88.44 | 3743.89 | 7.75 | 78.96 | 1.57 | 137.38 | 54.23 | 0.01 | 38.19 | 53.45 | 1.03 | 0.03 |

| | | | | | | | | | | | | | | | | | | |
|---|---|---|---|---|---|---|---|---|---|---|---|---|---|---|---|---|---|---|
| 982 | B | 10.00 | H | 1 | 40 | 42.5 | 91.11 | 3831.78 | 8.30 | 68.83 | 1.53 | 39.50 | 94.23 | 0.01 | 101.23 | 45.45 | 0.96 | 0.03 |
| 982 | B | 10.00 | H | 1 | 120 | 122.5 | 91.91 | 3855.16 | 9.06 | 96.73 | 1.77 | 64.87 | 43.44 | 0.01 | 57.61 | 47.96 | 0.00 | 0.03 |
| 982 | B | 10.00 | H | 2 | 50 | 52.5 | 92.71 | 3872.24 | | 100.14 | 1.63 | 69.12 | 37.13 | 0.01 | 41.99 | 30.99 | | 0.02 |
| 982 | B | 10.00 | H | 2 | 130 | 132.5 | 93.51 | 3887.00 | 8.36 | 77.28 | 1.62 | 29.25 | 32.65 | 0.00 | 25.34 | 34.81 | | 0.02 |
| 982 | B | 10.00 | H | 3 | 60 | 62.5 | 94.31 | 3903.02 | 8.28 | 84.04 | 2.02 | 129.24 | 53.36 | 0.01 | 45.60 | 65.20 | 1.01 | 0.03 |
| 982 | B | 10.00 | H | 3 | 140 | 142.5 | 95.11 | 3920.42 | 8.64 | 84.18 | 1.68 | 53.14 | 47.03 | 0.01 | 49.71 | 36.78 | | 0.02 |
| 982 | B | 10.00 | H | 4 | 70 | 72.5 | 95.91 | 3940.04 | 8.24 | 76.99 | 1.80 | 51.46 | 43.10 | 0.01 | 73.86 | 34.19 | 0.99 | 0.02 |
| 982 | B | 10.00 | H | 5 | 1 | 3.5 | 96.72 | 3959.07 | 8.64 | 97.28 | 1.74 | 27.69 | 33.98 | 0.01 | 38.66 | 26.79 | | 0.02 |
| 982 | B | 11.00 | H | 3 | 140 | 142.5 | 105.47 | 4185.89 | 8.41 | | 1.58 | 29.59 | 27.95 | 0.01 | 24.89 | 20.66 | | 0.01 |
| 982 | B | 11.00 | H | 4 | 71.5 | 74 | 106.285 | 4211.71 | 8.22 | | 1.89 | 61.26 | 30.54 | 0.01 | 22.57 | 19.86 | 1.00 | 0.01 |
| 982 | B | 11.00 | H | 5 | 80 | 82.5 | 107.87 | 4238.07 | | | 1.66 | 31.51 | 39.13 | 0.01 | 44.82 | 22.45 | | 0.01 |
| 982 | B | 11.00 | H | 7 | 21 | 23.5 | 110.28 | 4303.87 | 9.37 | 107.35 | 1.66 | 25.94 | 42.94 | 0.01 | 52.37 | 28.72 | | 0.02 |
| 982 | B | 12.00 | H | 3 | 80 | 82.5 | 114.79 | 4418.83 | 9.33 | 108.60 | 1.57 | 52.88 | 28.92 | 0.00 | 28.23 | 54.51 | | 0.03 |
| 982 | B | 14.00 | H | 6 | 10 | 12.5 | 140.095 | 4904.82 | 8.98 | | 1.54 | 124.97 | 47.03 | 0.00 | 75.04 | 43.51 | 0.99 | 0.03 |
| 982 | B | 14.00 | H | 6 | 90 | 92.5 | 140.92 | 4913.09 | 9.23 | 104.17 | 1.59 | 48.11 | 43.08 | 0.00 | 30.96 | 57.75 | | 0.04 |

| | | | | | | | | | | | | | | | | | | |
|---|---|---|---|---|---|---|---|---|---|---|---|---|---|---|---|---|---|---|
| 982 | B | 14.00 | H | 7 | 61 | 63.5 | 141.7 | 4920.98 | 8.70 | 137.29 | 1.57 | 32.19 | 25.19 | 0.00 | 22.06 | 23.88 | | 0.02 |
| 982 | B | 15.00 | H | 1 | 30.5 | 33 | 143.76 | 4963.88 | 8.87 | 111.58 | 1.46 | 60.75 | 62.29 | 0.00 | 78.05 | 40.67 | | 0.03 |
| 982 | B | 15.00 | H | 2 | 120 | 122.5 | 146.16 | 5024.56 | 9.56 | 106.33 | 1.65 | 45.85 | 47.42 | 0.00 | 29.52 | 44.16 | | 0.03 |
| 982 | B | 15.00 | H | 4 | 60 | 62.5 | 148.56 | 5069.81 | 9.60 | | 1.41 | 34.34 | 27.64 | 0.01 | 21.93 | 22.06 | | 0.02 |
| 982 | B | 15.00 | H | 4 | 140 | 142.5 | 149.36 | 5081.01 | | | 1.59 | 35.16 | 45.88 | 0.01 | 49.45 | 25.81 | 0.87 | 0.02 |

### *9.3.1.5 O. umbonatus*

| Site | H | Cor | T | Sc | Top (cm) | Bot (cm) | Depth (mcd) | Age (Ka) | Li7/Ca43 | B11/Ca43 | Mg25/Ca43 | Al27/Ca43 | Mn55/Ca43 | Cd111/Ca43 | U238/Ca43 | Fe56/Ca43 | Ca v. Ca (matrix matching) | Fe/Mg ratio |
|---|---|---|---|---|---|---|---|---|---|---|---|---|---|---|---|---|---|---|
| | | | | | | | | | umol/mol | umol/mol | mmol/mol | umol/mol | umol/mol | umol/mol | nmol/mol | umol/mol | | |
| 982 | B | 5.00 | H | 4 | 50 | 54 | 43.08 | 1912.94 | 12.02 | 49.22 | 2.39 | 12.50 | 95.39 | 0.01 | 32.09 | 150.54 | 0.94 | 0.06 |
| 982 | B | 5.00 | H | 4 | 68 | 70 | 43.26 | 1926.78 | 10.83 | 44.97 | 2.11 | 6.03 | 81.95 | 0.01 | 17.54 | 121.29 | 0.96 | 0.06 |
| 982 | B | 5.00 | H | 5 | 140 | 144 | 45.48 | 2058.04 | 12.34 | 50.00 | 2.33 | 8.80 | 82.15 | 0.00 | 27.24 | 126.66 | 0.97 | 0.05 |
| 982 | B | 5.00 | H | 6 | 87.5 | 89.5 | 46.455 | 2093.78 | 11.97 | 45.23 | 2.02 | 8.12 | 60.16 | 0.00 | 13.36 | 120.40 | 0.95 | 0.06 |
| 982 | B | 5.00 | H | 7 | 1 | 3.5 | 47.09 | 2118.76 | 12.47 | 53.19 | 2.12 | 17.83 | 64.77 | 0.01 | 32.73 | 99.61 | 1.03 | 0.05 |
| 982 | B | 6.00 | H | 1 | 80 | 84 | 49.81 | 2263.46 | 12.19 | 54.14 | 2.19 | 3.43 | 70.23 | 0.00 | 12.25 | 134.96 | 1.05 | 0.06 |
| 982 | B | 6.00 | H | 2 | 130 | 134 | 51.81 | 2393.52 | 11.17 | 45.36 | 2.00 | 7.33 | 67.33 | 0.01 | 11.43 | 110.06 | 0.97 | 0.05 |
| 982 | B | 6.00 | H | 4 | 32 | 36 | 53.83 | 2506.68 | 12.61 | 58.94 | 2.44 | 9.61 | 89.15 | 0.01 | 53.89 | 122.36 | 1.06 | 0.05 |
| 982 | B | 6.00 | H | 4 | 40 | 42 | 53.91 | 2508.89 | 13.08 | | 2.43 | 39.93 | 94.89 | 0.01 | 38.57 | 142.42 | 0.99 | 0.06 |
| 982 | B | 6.00 | H | 5 | 39.5 | 43.5 | 55.405 | 2550.41 | 11.79 | 54.93 | 2.72 | 20.59 | 75.47 | 0.01 | 46.58 | 117.62 | 1.01 | 0.04 |
| 982 | B | 6.00 | H | 6 | 48 | 52 | 56.99 | 2580.90 | 11.42 | 45.01 | 2.08 | 9.93 | 54.60 | 0.01 | 38.39 | 65.60 | 1.01 | 0.03 |

| | | | | | | | | | | | | | | | | | | |
|---|---|---|---|---|---|---|---|---|---|---|---|---|---|---|---|---|---|---|
| 982 | B | 6.00 | H | 6 | 57.5 | 59.5 | 57.085 | 2583.68 | 12.05 | 47.40 | 2.25 | 5.53 | 43.36 | 0.00 | 25.79 | 59.74 | 1.02 | 0.03 |
| 982 | B | 6.00 | H | 6 | 129 | 133 | 57.8 | 2621.29 | 12.34 | 52.03 | 2.20 | 46.37 | 44.73 | 0.01 | 67.04 | 103.08 | 0.00 | 0.05 |
| 982 | B | 7.00 | H | 1 | 140 | 142 | 60.17 | 2745.74 | 13.16 | 55.92 | 2.48 | 6.81 | 90.84 | 0.00 | 58.39 | 61.45 | 1.17 | 0.02 |
| 982 | B | 7.00 | H | 2 | 91.5 | 95.5 | 61.185 | 2816.57 | 12.48 | | 2.10 | 18.35 | 101.92 | 0.01 | 47.42 | 50.96 | 0.98 | 0.02 |
| 982 | B | 7.00 | H | 2 | 110 | 112 | 61.37 | 2830.25 | 11.78 | 44.57 | 2.14 | 12.91 | 98.19 | 0.01 | 96.79 | 53.57 | 1.02 | 0.03 |
| 982 | B | 7.00 | H | 3 | 61.5 | 65.5 | 62.385 | 2885.05 | 11.36 | 50.76 | 2.48 | 4.69 | 82.79 | 0.01 | 45.19 | 51.07 | 0.95 | 0.02 |
| 982 | B | 7.00 | H | 4 | 10 | 12 | 63.37 | 2930.27 | 11.53 | 47.31 | 2.12 | 13.85 | 78.61 | 0.00 | 57.39 | 45.41 | 1.00 | 0.02 |
| 982 | B | 7.00 | H | 4 | 108 | 112 | 64.35 | 2972.98 | 12.24 | | 2.87 | 113.93 | 80.85 | 0.01 | 52.18 | -0.76 | 1.23 | 0.00 |
| 982 | B | 7.00 | H | 5 | 39.5 | 43.5 | 65.165 | 3003.24 | 12.31 | | 2.60 | 15.50 | 77.12 | 0.00 | 50.15 | 50.65 | 1.01 | 0.02 |
| 982 | B | 7.00 | H | 5 | 122 | 126 | 65.99 | 3033.99 | 11.34 | 43.55 | 2.18 | 5.22 | 64.33 | 0.01 | 42.53 | 43.16 | 0.94 | 0.02 |
| 982 | B | 8.00 | H | 1 | 42 | 44.5 | 70.32 | 3189.55 | 10.19 | 39.01 | 2.02 | 8.77 | 49.19 | 0.01 | 19.48 | 34.16 | 0.00 | 0.02 |
| 982 | B | 8.00 | H | 2 | 138 | 140 | 71.86 | 3271.06 | 11.27 | | 2.45 | 15.09 | 43.01 | 0.01 | 27.96 | 27.38 | 1.00 | 0.01 |
| 982 | B | 8.00 | H | 3 | 24 | 26.5 | 72.22 | 3280.35 | 12.54 | 44.19 | 2.16 | 63.33 | 63.69 | 0.01 | 48.47 | 80.36 | 1.02 | 0.04 |
| 982 | B | 8.00 | H | 4 | 107.5 | 110 | 75.465 | 3354.68 | 11.70 | 39.22 | 2.18 | 6.47 | 48.25 | 0.00 | 34.29 | 44.59 | 0.96 | 0.02 |
| 982 | B | 8.00 | H | 5 | 18 | 20 | 76.07 | 3374.11 | 11.49 | 39.21 | 2.20 | 12.24 | 104.61 | 0.01 | 68.83 | 54.25 | 0.95 | 0.02 |

| | | | | | | | | | | | | | | | | | | |
|---|---|---|---|---|---|---|---|---|---|---|---|---|---|---|---|---|---|---|
| 982 | B | 8.00 | H | 5 | 58 | 60 | 76.47 | 3386.76 | 12.05 | 44.26 | 2.26 | 10.62 | 88.92 | 0.01 | 43.76 | 42.36 | 0.96 | 0.02 |
| 982 | B | 8.00 | H | 5 | 82 | 84.5 | 76.71 | 3393.73 | 10.92 | 46.00 | 2.06 | 8.73 | 50.04 | 0.01 | 38.48 | 25.00 | 0.94 | 0.01 |
| 982 | B | 8.00 | H | 5 | 122 | 124.5 | 77.11 | 3404.72 | 11.66 | 48.16 | 2.42 | 9.57 | 61.61 | 0.01 | 39.40 | 29.10 | 0.95 | 0.01 |
| 982 | B | 8.00 | H | 6 | 148 | 150 | 78.87 | 3466.46 | 10.38 | 37.98 | 1.71 | 15.54 | 56.81 | 0.03 | 36.73 | 40.40 | 32.96 | 0.02 |
| 982 | B | 9.00 | H | 5 | 10 | 12.5 | 86.6 | 3691.53 | 10.68 | 42.23 | 2.23 | 7.07 | 48.08 | 0.01 | 34.40 | 19.03 | 0.90 | 0.01 |
| 982 | B | 10.00 | H | 3 | 140 | 142.5 | 95.11 | 3920.42 | 11.24 | 37.64 | 2.18 | 8.35 | 60.12 | 0.01 | 54.33 | 31.70 | 0.92 | 0.01 |
| 982 | B | 10.00 | H | 5 | 1 | 3.5 | 96.72 | 3959.07 | 12.13 | 46.87 | 2.10 | 25.43 | 43.30 | 0.01 | 53.43 | 20.84 | 0.96 | 0.01 |
| 982 | B | 11.00 | H | 5 | 80 | 82.5 | 107.87 | 4238.07 | 11.79 | 39.04 | 2.27 | 16.83 | 47.50 | 0.01 | 78.23 | 35.07 | 1.05 | 0.02 |
| 982 | B | 12.00 | H | 3 | 0 | 3 | 113.99 | 4396.61 | 12.20 | 45.94 | 2.53 | 13.90 | 37.66 | 0.01 | 39.75 | 17.63 | 0.95 | 0.01 |
| 982 | B | 12.00 | H | 6 | 30 | 32.5 | 118.79 | 4514.87 | 10.55 |  | 2.23 | 18.23 | 28.43 | 0.01 | 34.63 | 11.80 | 1.05 | 0.01 |
| 982 | B | 12.00 | H | 7 | 50 | 52.5 | 120.49 | 4552.91 | 11.12 | 39.63 | 2.21 | 11.96 | 29.41 | 0.01 | 35.40 | 16.02 | 0.92 | 0.01 |
| 982 | B | 13.00 | H | 7 | 40 | 42.5 | 130.94 | 4751.38 | 11.43 | 42.02 | 2.17 | 25.47 | 71.81 | 0.01 | 36.15 | 46.41 | 0.94 | 0.02 |
| 982 | B | 14.00 | H | 1 | 120 | 122.5 | 133.7 | 4790.01 | 11.11 | 41.14 | 2.19 | 8.14 | 35.92 | 0.00 | 39.59 | 10.88 | 0.98 | 0.00 |
| 982 | B | 14.00 | H | 2 | 50 | 52.5 | 134.5 | 4808.43 | 11.18 | 42.47 | 2.26 | 15.75 | 31.34 | 0.00 | 34.61 | 9.99 | 0.96 | 0.00 |
| 982 | B | 14.00 | H | 3 | 140 | 142.5 | 136.9 | 4856.43 | 10.86 | 37.33 | 2.14 | 14.01 | 44.76 | 0.00 | 66.90 | 12.61 | 0.90 | 0.01 |

| | | | | | | | | | | | | | | | | | | |
|---|---|---|---|---|---|---|---|---|---|---|---|---|---|---|---|---|---|---|
| 982 | B | 14.00 | H | 5 | 0 | 3 | 138.495 | 4885.90 | 10.83 | 40.25 | 2.36 | 10.80 | 55.37 | 0.00 | 30.17 | 16.81 | 1.02 | 0.01 |
| 982 | B | 14.00 | H | 6 | 10 | 12.5 | 140.095 | 4904.82 | 11.61 | | 2.16 | 9.85 | 53.93 | 0.00 | 67.18 | 14.76 | 0.93 | 0.01 |
| 982 | B | 14.00 | H | 7 | 61 | 63.5 | 141.7 | 4920.98 | 11.50 | 39.85 | 2.13 | 16.76 | 35.74 | 0.01 | 37.94 | 17.39 | 0.94 | 0.01 |
| 982 | B | 15.00 | H | 1 | 111 | 113.5 | 144.56 | 4988.99 | 10.94 | 36.82 | 2.11 | 16.85 | 61.29 | 0.01 | 89.79 | 21.36 | 0.99 | 0.01 |

### *9.3.1.6 G bulloides*

| Site | H | Cor | T | Sc | Top(cm) | Bot(cm) | Age (ka) | Li7/Ca43 | B11/Ca43 | Mg25/Ca43 | Al27/Ca43 | Mn55/Ca43 | Cd111/Ca43 | U238/Ca43 | Fe56/Ca43 | Ca v. Ca (matrix matching) | Fe/Mg ratio |
|---|---|---|---|---|---|---|---|---|---|---|---|---|---|---|---|---|---|
| | | | | | | | | umol/mol | umol/mol | mmol/mol | umol/mol | umol/mol | umol/mol | nmol/mol | umol/mol | | |
| 982 | B | 6 | H | 5 | 39.5 | 43.5 | 2550.41 | 9.51 | 37.01 | 1.58 | 6.18 | 88.07 | 0.12 | 44.45 | 36.19 | 1.17 | 0.02 |
| 982 | B | 6 | H | 5 | 50 | 52 | 2552.98 | 10.59 | 44.17 | 1.27 | 14.97 | 64.20 | 0.06 | 28.64 | 66.69 | 0.00 | 0.05 |
| 982 | B | 6 | H | 5 | 122 | 126 | 2566.52 | 10.30 | 43.86 | 1.62 | 11.77 | 61.25 | 0.06 | 65.88 | 50.71 | 0.00 | 0.03 |
| 982 | B | 6 | H | 6 | 48 | 52 | 2580.90 | 10.78 | 39.16 | 1.73 | 8.03 | 57.49 | 0.06 | 45.76 | 49.04 | 0.00 | 0.03 |
| 982 | B | 6 | H | 6 | 57.5 | 59.5 | 2583.68 | 10.27 | 41.44 | 1.65 | 16.85 | 68.02 | 0.07 | 50.32 | 60.50 | 0.00 | 0.04 |
| 982 | B | 6 | H | 6 | 100 | 102 | 2603.46 | 11.85 | 49.95 | 0.90 | 14.84 | 19.47 | 0.04 | 18.80 | 22.65 | 0.95 | 0.03 |
| 982 | B | 6 | H | 6 | 140 | 142 | 2628.06 | 10.55 | 43.23 | 1.40 | 12.39 | 47.41 | 0.06 | 58.95 | 40.63 | 0.00 | 0.03 |
| 982 | B | 6 | H | 7 | 30 | 32 | 2647.78 | 10.51 | 38.82 | 1.51 | 5.75 | 53.68 | 0.05 | 55.82 | 29.50 | 1.00 | 0.02 |
| 982 | B | 7 | H | 1 | 20 | 22 | 2674.77 | 10.71 | 41.75 | 1.38 | 8.69 | 59.54 | 0.06 | 33.19 | 35.71 | 0.89 | 0.03 |
| 982 | B | 7 | H | 1 | 40 | 44 | 2684.47 | 10.67 | 38.63 | 1.44 | 31.21 | 67.32 | 0.06 | 37.34 | 68.73 | 0.97 | 0.05 |
| 982 | B | 7 | H | 1 | 78.5 | 82.5 | 2708.23 | 11.22 | 40.03 | 1.44 | 113.85 | 30.74 | 0.03 | 147.59 | 66.99 | 0.00 | 0.05 |
| 982 | B | 7 | H | 1 | 100 | 102 | 2721.14 | 10.88 | 45.11 | 1.36 | 43.80 | 45.44 | 0.04 | 59.98 | 47.06 | 1.10 | 0.03 |
| 982 | B | 7 | H | 1 | 122 | 126 | 2734.67 | 10.17 | 39.42 | 1.33 | 6.00 | 67.30 | 0.07 | 93.59 | 32.68 | 0.00 | 0.02 |
| 982 | B | 7 | H | 1 | 140 | 142 | 2745.74 | 9.96 | 38.06 | 1.60 | 28.08 | 76.08 | 0.09 | 58.92 | 65.32 | 1.03 | 0.04 |
| 982 | B | 7 | H | 2 | 28 | 30 | 2769.12 | 10.17 | 32.97 | 1.91 | 21.49 | 79.17 | 0.11 | 30.45 | 49.59 | 0.00 | 0.03 |
| 982 | B | 7 | H | 2 | 91.5 | 95.5 | 2816.57 | 9.91 | 39.67 | 1.43 | 12.23 | 92.38 | 0.13 | 43.74 | 37.63 | 0.00 | 0.03 |
| 982 | B | 7 | H | 2 | 110 | 112 | 2830.25 | 9.87 | 34.47 | 1.67 | 5.35 | 92.85 | 0.17 | 197.97 | 40.98 | 0.97 | 0.02 |
| 982 | B | 7 | H | 3 | 40 | 42 | 2874.91 | 9.85 | 40.31 | 1.54 | 4.08 | 89.55 | 0.15 | 42.95 | 42.06 | 1.01 | 0.03 |
| 982 | B | 7 | H | 3 | 61.5 | 65.5 | 2885.05 | 10.18 | 41.87 | 1.54 | 5.65 | 72.62 | 0.09 | 62.09 | 31.33 | 0.00 | 0.02 |
| 982 | B | 7 | H | 3 | 99.5 | 103.5 | 2902.59 | 9.52 | 44.34 | 1.72 | 7.58 | 98.82 | 0.12 | 107.19 | 69.32 | 0.00 | 0.04 |
| 982 | B | 7 | H | 4 | 10 | 12 | 2930.27 | 10.06 | 32.86 | 1.42 | 10.20 | 46.32 | 0.06 | 68.97 | 47.50 | 0.98 | 0.03 |
| 982 | B | 7 | H | 4 | 108 | 112 | 2972.98 | 9.90 | 34.23 | 1.96 | 10.78 | 81.08 | 0.07 | 29.14 | 37.88 | 1.01 | 0.02 |
| 982 | B | 7 | H | 5 | 39.5 | 43.5 | 3003.24 | 10.81 | 80.69 | 1.49 | 17.56 | 78.86 | 0.13 | 47.92 | 32.92 | 0.90 | 0.02 |
| 982 | B | 7 | H | 5 | 58 | 60 | 3009.88 | 10.21 | 41.01 | 1.74 | 6.36 | 76.97 | 0.09 | 54.08 | 31.79 | 0.94 | 0.02 |
| 982 | B | 7 | H | 5 | 78 | 82 | 3017.27 | 11.18 | 45.60 | 1.35 | 5.73 | 64.32 | 0.08 | 66.03 | 27.67 | 0.98 | 0.02 |
| 982 | B | 7 | H | 5 | 122 | 126 | 3033.99 | 9.51 | 39.57 | 1.54 | 33.92 | 101.75 | 0.12 | 46.36 | 71.07 | 0.00 | 0.05 |
| 982 | B | 7 | H | 6 | 12 | 14.5 | 3052.44 | 10.72 | 43.88 | 2.23 | 8.74 | 69.70 | 0.07 | 27.78 | 31.35 | 1.09 | 0.01 |
| 982 | B | 7 | H | 6 | 52 | 54.5 | 3073.89 | 10.48 | | 1.92 | 23.65 | 74.24 | 0.12 | 31.93 | 42.49 | 1.08 | 0.02 |
| 982 | B | 7 | H | 6 | 68 | 70 | 3083.12 | 11.30 | 48.95 | 1.69 | 34.02 | 59.89 | 0.05 | 29.61 | 43.67 | 0.99 | 0.03 |

| | | | | | | | | | | | | | | | | | | |
|---|---|---|---|---|---|---|---|---|---|---|---|---|---|---|---|---|---|---|
| 982 | B | 7 | H | 6 | 108 | 110 | 3105.87 | 10.21 | 46.85 | 1.42 | 21.60 | 74.92 | 0.08 | 226.84 | 35.59 | 0.00 | 0.03 |
| 982 | B | 7 | H | 7 | 40 | 42 | 3141.00 | 10.47 | 45.41 | 1.85 | 37.69 | 60.07 | 0.09 | 119.54 | 53.57 | 0.95 | 0.03 |
| 982 | B | 8 | H | 1 | 42 | 44.5 | 3189.55 | 9.01 | 39.17 | 1.66 | 9.64 | 77.53 | 0.08 | 27.24 | 38.00 | 0.00 | 0.02 |
| 982 | B | 8 | H | 1 | 58 | 60 | 3194.67 | 10.01 | 41.11 | 1.51 | 54.86 | 72.73 | 0.06 | 21.98 | 84.42 | 1.02 | 0.06 |
| 982 | B | 8 | H | 1 | 84 | 86.5 | 3204.66 | 9.47 | 43.12 | 2.33 | 18.29 | 58.25 | 0.06 | 24.36 | 32.95 | 0.97 | 0.01 |
| 982 | B | 8 | H | 1 | 102 | 104 | 3212.92 | 9.58 | 42.85 | 1.76 | 30.97 | 84.80 | 0.07 | 32.95 | 77.24 | 0.00 | 0.04 |
| 982 | B | 8 | H | 1 | 124 | 126.5 | 3225.57 | 10.13 | 40.42 | 1.91 | 30.76 | 78.74 | 0.06 | 41.65 | 71.69 | 0.98 | 0.04 |
| 982 | B | 8 | H | 2 | 57 | 59.5 | 3254.62 | 9.53 | 44.06 | 1.80 | 11.83 | 72.63 | 0.10 | 51.86 | 42.63 | 1.02 | 0.02 |
| 982 | B | 8 | H | 2 | 94 | 96.5 | 3261.44 | 10.05 | 42.75 | 1.70 | 8.05 | 64.81 | 0.07 | 75.40 | 35.96 | 0.00 | 0.02 |
| 982 | B | 8 | H | 2 | 132.5 | 135 | 3269.84 | 10.75 | 42.98 | 1.90 | 65.44 | 68.29 | 0.09 | 47.76 | 101.81 | 0.00 | 0.05 |
| 982 | B | 8 | H | 3 | 24 | 26.5 | 3280.35 | 10.52 | 35.97 | 1.70 | 20.96 | 48.13 | 0.07 | 71.96 | 41.12 | 0.00 | 0.02 |
| 982 | B | 8 | H | 3 | 42 | 44 | 3285.51 | 10.11 | 33.32 | 1.74 | 27.96 | 39.89 | 0.05 | 73.78 | 46.33 | 1.88 | 0.03 |
| 982 | B | 8 | H | 3 | 118 | 120 | 3310.07 | 10.04 | 31.91 | 1.89 | 7.47 | 47.18 | 0.04 | 58.62 | 20.03 | 1.01 | 0.01 |

### 9.3.2 Physical data – cfwt%, SS, IRD counts.

| Age (ka) | SS | Cfwt% | IRD flux Grains/g |
|---|---|---|---|
| 1912.94 | 22.87 | 27.17 | 57.04179 |
| 1926.78 | 20.82 | 23.89 | 397.6073 |
| 1949.56 | 26.49 | 21.43 | 532.4654 |
| 1970.12 | 23.48 | 23.81 | 322.3798 |
| 1984.71 | 23.56 | 28.54 | 368.205 |
| 1997.79 | 22.89 | 23.49 | 334.2534 |
| 2013.43 | 27.69 | 33.97 | 0 |
| 2022.03 | 24.03 | 32.03 | 86.0326 |
| 2030.15 | 24.08 | 29.51 | 1182.824 |
| 2036.59 | 23.75 | 24.53 | 129.4585 |
| 2044.20 | 23.07 | 27.27 | 54.3714 |
| 2050.44 | 21.94 | 25.85 | 70.14565 |
| 2058.04 | 22.89 | 16.71 | 248.884 |
| 2064.28 | 21.90 | 17.30 | 1100.437 |
| 2072.37 | 22.59 | 14.88 | 3068.978 |
| 2079.02 | 21.49 | 19.13 | 3437.05 |
| 2087.13 | 21.60 | 13.78 | 613.3304 |
| 2093.78 | 23.82 | 11.91 | 160.8899 |
| 2103.01 | 23.78 | 20.98 | 460.4918 |
| 2109.28 | 21.75 | 20.12 | 370.7274 |
| 2118.76 | 21.49 | 13.24 | 163.4418 |
| 2127.54 | 24.16 | 17.86 | 268.2461 |
| 2136.76 | 24.80 | 20.23 | 102.5956 |

| | | | |
|---|---|---|---|
| 2146.20 | 22.96 | 25.92 | 370.8961 |
| 2215.10 | 24.18 | 30.22 | 106.7886 |
| 2220.40 | 23.33 | 34.34 | 104.0094 |
| 2238.86 | 22.83 | 20.10 | 137.4302 |
| 2245.01 | 24.25 | 28.23 | 82.26931 |
| 2263.46 | 21.73 | 23.11 | 122.2666 |
| 2269.61 | 21.73 | 24.40 | 265.4091 |
| 2288.06 | 23.68 | 31.42 | 42.37109 |
| 2295.21 | 23.92 | 30.54 | 100.3503 |
| 2308.55 | 23.60 | 29.02 | 47.80095 |
| 2312.23 | 19.98 | 17.90 | 465.3442 |
| 2327.00 | 20.41 | 18.17 | 23.84069 |
| 2330.68 | 20.76 | 19.11 | 83.77432 |
| 2349.75 | 22.67 | 18.72 | 150.0438 |
| 2356.64 | 21.88 | 19.00 | 256.3563 |
| 2393.52 | 27.44 | 41.11 | 251.8617 |
| 2402.74 | 24.62 | 38.49 | 353.8787 |
| 2430.43 | 26.58 | 26.63 | 772.8112 |
| 2435.28 | 23.49 | 23.64 | 2710.986 |
| 2453.79 | 21.97 | 29.38 | 109.7091 |
| 2458.40 | 23.46 | 29.91 | 54.20746 |
| 2476.35 | 20.48 | 24.42 | 218.1813 |
| 2480.04 | 22.15 | 28.18 | 934.9476 |
| 2493.89 | 21.78 | 29.95 | 271.0347 |
| 2496.73 | 22.91 | 17.35 | 18.28096 |

| | | | |
|---|---|---|---|
| 2506.68 | 21.52 | 9.49 | 137.3999 |
| 2508.89 | 20.86 | 10.05 | 118.9401 |
| 2517.20 | 19.55 | 20.40 | 2099.208 |
| 2519.41 | 21.36 | 15.18 | 3875.568 |
| 2527.72 | 25.43 | 25.01 | 5761.659 |
| 2530.49 | 21.44 | 18.87 | 5608.36 |
| 2539.89 | 21.68 | 9.60 | 155.4454 |
| 2542.11 | 23.40 | 9.55 | 112.8548 |
| 2550.41 | 22.04 | 9.53 | 83.55102 |
| 2552.98 | 20.29 | 10.31 | 77.0796 |
| 2558.58 | 21.46 | 15.65 | 173.2008 |
| 2560.24 | 21.56 | 21.44 | 162.0339 |
| 2566.52 | 20.27 | 21.48 | 203.6185 |
| 2567.99 | 22.67 | 23.52 | 62.8408 |
| 2573.53 | 19.45 | 13.85 | 87.44051 |
| 2575.37 | 20.43 | 14.51 | 95.22259 |
| 2580.90 | 22.01 | 11.78 | 134.9324 |
| 2583.68 | 21.91 | 11.51 | 62.82382 |
| 2598.53 | 20.82 | 28.48 | 4109.883 |
| 2603.46 | 23.02 | 27.64 | 3520.058 |
| 2621.29 | 19.63 | 15.98 | 480.6123 |
| 2628.06 | 21.67 | 17.29 | 744.8689 |
| 2644.09 | 19.86 | 20.16 | 56.34351 |
| 2647.78 | 21.17 | 12.14 | 156.0907 |
| 2659.22 | 19.16 | 9.42 | 17.71617 |

| | | | |
|---|---|---|---|
| 2674.77 | 18.97 | 10.77 | 79.97181 |
| 2684.47 | 20.01 | 16.81 | 128.8139 |
| 2695.31 | | 18.95 | 457.0634 |
| 2708.23 | 21.49 | 28.93 | 4137.155 |
| 2721.14 | 24.39 | 26.72 | 261.9131 |
| 2734.67 | 17.53 | 14.06 | 29.07523 |
| 2745.74 | 22.27 | 12.03 | 82.93217 |
| 2758.05 | 23.75 | 17.12 | 18.51831 |
| 2769.12 | 20.29 | 18.12 | 16.45707 |
| 2782.74 | 19.82 | 17.76 | 10.4131 |
| 2799.65 | 24.48 | 16.42 | 10.0797 |
| 2816.57 | 24.50 | 16.77 | 11.28411 |
| 2830.25 | 23.75 | 14.61 | 11.56843 |
| 2842.28 | 21.55 | 17.56 | 14.65437 |
| 2852.92 | 20.01 | 15.05 | 6.253527 |
| 2864.76 | 19.55 | 18.94 | 0 |
| 2874.91 | 21.44 | 13.19 | 1.671798 |
| 2885.05 | 23.43 | 16.85 | 12.88153 |
| 2893.36 | 22.04 | 14.41 | 0 |
| 2902.59 | 24.73 | 17.24 | 2.1404 |
| 2912.74 | 20.37 | 15.68 | 3.711863 |
| 2920.11 | 23.23 | 21.70 | 4.822142 |
| 2930.27 | 22.09 | 23.48 | 0 |
| 2940.76 | 22.95 | 9.99 | 3.600065 |
| 2950.91 | 21.52 | 11.27 | 4.818494 |

| | | | |
|---|---|---|---|
| 2958.95 | 21.71 | 8.76 | 4.707307 |
| 2967.08 | 21.51 | 9.43 | 4.845761 |
| 2972.98 | 22.10 | 12.42 | 0.488578 |
| 2981.10 | 22.20 | 10.36 | 0.514901 |
| 2989.22 | 21.32 | 17.04 | 0 |
| 2995.86 | 19.72 | 21.83 | 0 |
| 3003.24 | 19.88 | 19.49 | 61.87016 |
| 3009.88 | 21.59 | 19.22 | 0 |
| 3017.27 | 20.27 | 15.35 | 0 |
| 3025.38 | 22.72 | 20.11 | 0 |
| 3033.99 | 22.66 | 17.64 | 0 |
| 3042.30 | 20.16 | 13.74 | 0 |
| 3052.44 | 19.33 | 7.40 | 5.835904 |
| 3060.05 | 22.90 | 10.20 | 0 |
| 3073.89 | 21.72 | 12.62 | 0 |
| 3083.12 | 22.23 | 14.02 | 0 |
| 3096.95 | 21.70 | 14.48 | 0 |
| 3105.87 | 19.98 | 14.87 | 0 |
| 3116.93 | 19.79 | 8.34 | 0 |
| 3124.31 | 20.53 | 8.61 | 0 |
| 3135.38 | 22.77 | 8.15 | 0 |
| 3141.00 | 23.20 | 6.92 | 0 |
| 3144.26 | 20.32 | 8.41 | 0 |
| 3182.28 | 22.99 | 5.78 | 0 |
| 3189.55 | 22.84 | 6.30 | 0 |

| | | | |
|---|---|---|---|
| 3194.67 | 23.19 | 6.43 | 0 |
| 3204.66 | 22.11 | 6.85 | 0 |
| 3212.92 | 22.06 | 5.09 | 529.9075 |
| 3225.57 | 21.31 | 5.13 | 0 |
| 3231.76 | 22.48 | 4.65 | 0 |
| 3242.12 | 23.02 | 10.18 | 0 |
| 3247.09 | 23.80 | 7.39 | 0 |
| 3254.62 | 21.42 | 9.45 | 0 |
| 3257.60 | 22.48 | 8.58 | 0 |
| 3261.44 | 21.72 | 9.74 | 0 |
| 3264.35 | 23.23 | 8.73 | 0 |
| 3269.84 | 21.44 | 8.68 | 0 |
| 3271.06 | 23.79 | 8.25 | 0 |
| 3280.35 | 23.42 | 14.92 | |
| 3285.51 | 22.47 | 14.94 | |
| 3292.52 | 20.95 | 13.46 | |
| 3297.19 | 26.71 | 10.23 | |
| 3305.17 | 20.97 | 9.47 | |
| 3310.07 | 20.29 | 6.60 | |
| 3318.03 | 20.82 | 5.60 | |
| 3323.65 | 21.69 | 6.29 | |
| 3330.74 | 19.26 | 7.29 | |
| 3335.12 | 22.99 | 10.48 | |
| 3342.76 | 21.37 | 8.05 | |
| 3348.75 | 24.44 | 10.57 | |

| | | | | |
|---|---|---|---|---|
| 3354.68 | 19.00 | 10.38 | | |
| 3361.16 | 19.50 | 9.68 | | |
| 3367.64 | 23.23 | 17.45 | | |
| 3374.11 | 25.43 | 14.21 | | |
| 3381.86 | 23.28 | 15.87 | | |
| 3386.76 | 22.28 | 14.67 | | |
| 3393.73 | 22.81 | 10.23 | | |
| 3398.19 | 23.75 | 8.33 | | |
| 3404.72 | 22.50 | 7.30 | | |
| 3409.61 | 21.91 | 6.04 | | |
| 3417.77 | 24.24 | 4.82 | | |
| 3423.54 | 20.86 | 5.87 | | |
| 3431.37 | 19.69 | 4.71 | | |
| 3436.73 | 20.64 | 4.64 | | |
| 3444.40 | 21.85 | 4.01 | | |
| 3450.27 | 20.44 | 3.70 | | |
| 3459.87 | 22.28 | 4.88 | | |
| 3466.46 | 21.49 | 5.89 | | |
| 3478.35 | 23.57 | 4.99 | | |
| 3488.70 | 22.58 | 4.73 | | |
| 3544.59 | 23.76 | 6.05 | | |
| 3552.98 | 22.10 | 5.36 | | |
| 3560.90 | 25.07 | 4.90 | | |
| 3568.70 | 22.78 | 5.84 | | |
| 3575.79 | 22.64 | 7.60 | | |

| | | | | |
|---|---|---|---|---|
| 3581.46 | 22.23 | 5.39 | | |
| 3586.33 | 23.78 | 4.66 | | |
| 3590.22 | 22.33 | 7.44 | | |
| 3594.32 | 24.38 | 7.44 | | |
| 3597.75 | 22.21 | 6.07 | | |
| 3601.95 | 23.79 | 8.77 | | |
| 3605.38 | 21.88 | 6.38 | | |
| 3610.22 | 22.59 | 11.15 | | |
| 3614.15 | 21.48 | 12.28 | | |
| 3618.38 | 20.99 | 11.64 | | |
| 3621.47 | 25.40 | 7.43 | | |
| 3624.74 | 22.02 | 9.34 | | |
| 3627.40 | 24.06 | 9.11 | | |
| 3630.62 | | 8.28 | | |
| 3633.29 | 21.24 | 7.44 | | |
| 3636.60 | 22.80 | 6.92 | | |
| 3639.56 | 25.83 | 7.82 | | |
| 3643.69 | 22.46 | 4.95 | | |
| 3647.69 | 22.65 | 6.25 | | |
| 3652.91 | 22.55 | 4.12 | | |
| 3657.45 | 22.04 | 5.26 | | |
| 3663.28 | 21.36 | 6.25 | | |
| 3668.97 | 20.88 | 6.53 | | |
| 3677.24 | 21.13 | 5.78 | | |
| 3684.10 | 21.35 | 6.39 | | |

| | | | | |
|---|---|---|---|---|
| 3691.53 | 22.62 | 6.74 | | |
| 3696.79 | 23.57 | 6.16 | | |
| 3702.03 | 23.52 | 8.64 | | |
| 3712.91 | 21.38 | 10.52 | | |
| 3721.16 | 23.20 | 7.80 | | |
| 3728.25 | 23.54 | 8.01 | | |
| 3735.12 | 23.36 | 9.64 | | |
| 3743.89 | 20.38 | 9.64 | | |
| 3754.93 | 20.89 | 6.98 | | |
| 3769.96 | 23.65 | 9.79 | | |
| 3788.65 | 20.72 | 8.16 | | |
| 3831.78 | 21.55 | 8.49 | | |
| 3842.96 | 23.33 | 7.14 | | |
| 3855.16 | 22.09 | 5.00 | | |
| 3864.28 | 19.96 | 4.01 | | |
| 3872.24 | 20.65 | 4.98 | | |
| 3879.79 | 20.88 | 7.34 | | |
| 3887.00 | 21.95 | 5.42 | | |
| 3894.70 | 24.33 | 4.43 | | |
| 3903.02 | 21.62 | 5.74 | | |
| 3911.64 | 21.84 | 8.40 | | |
| 3920.42 | 20.30 | 11.75 | | |
| 3930.07 | 24.62 | 6.97 | | |
| 3940.04 | 21.85 | 6.52 | | |
| 3949.93 | 22.89 | 5.47 | | |

| | | | | |
|---|---|---|---|---|
| 3959.07 | 22.29 | 5.55 | | |
| 3967.97 | 23.58 | 5.20 | | |
| 3976.65 | 22.14 | 4.89 | | |
| 3985.57 | 23.76 | 8.52 | | |
| 3996.56 | 22.49 | 6.91 | | |
| 4006.38 | 22.87 | 3.52 | | |
| 4014.71 | 22.30 | 3.80 | | |
| 4022.61 | 21.25 | 4.48 | | |
| 4032.11 | 23.24 | 4.29 | | |
| 4047.66 | 23.65 | 6.18 | | |
| 4088.77 | 21.77 | 4.31 | | |
| 4099.09 | 21.55 | 4.06 | | |
| 4105.69 | | 5.89 | | |
| 4111.62 | 23.11 | 6.52 | | |
| 4117.30 | 23.58 | 8.10 | | |
| 4123.53 | 23.38 | 7.64 | | |
| 4131.00 | 23.98 | 4.93 | | |
| 4140.84 | 22.70 | 8.29 | | |
| 4155.12 | 23.19 | 10.40 | | |
| 4170.92 | | 9.62 | | |
| 4185.89 | 24.95 | 8.84 | | |
| 4200.53 | 22.53 | 7.00 | | |
| 4211.71 | 22.89 | 5.80 | | |
| 4217.97 | 19.74 | 9.45 | | |
| 4224.34 | 23.49 | 6.18 | | |

| | | | | |
|---|---|---|---|---|
| 4230.62 | 21.52 | 4.38 | | |
| 4238.07 | 20.12 | 5.60 | | |
| 4246.98 | 22.36 | 4.43 | | |
| 4256.81 | 21.61 | 8.33 | | |
| 4269.19 | 21.59 | 11.04 | | |
| 4283.98 | 23.41 | 4.86 | | |
| 4293.82 | 20.64 | 5.30 | | |
| 4303.87 | 21.61 | 8.85 | | |
| 4314.68 | 21.26 | 4.93 | | |
| 4328.17 | 21.79 | 5.61 | | |
| 4337.35 | 22.49 | 5.68 | | |
| 4346.19 | 21.19 | 6.14 | | |
| 4355.82 | | 6.60 | | |
| 4366.92 | 22.47 | 3.75 | | |
| 4376.54 | 19.43 | 3.71 | | |
| 4385.75 | 22.51 | 3.60 | | |
| 4396.61 | 16.55 | 3.51 | | |
| 4407.93 | 18.17 | 3.52 | | |
| 4418.83 | 18.13 | 5.14 | | |
| 4427.70 | 23.83 | 5.23 | | |
| 4436.20 | 24.12 | 4.81 | | |
| 4444.70 | 23.43 | 5.85 | | |
| 4453.20 | 22.69 | 8.51 | | |
| 4461.77 | 21.93 | 8.61 | | |
| 4471.82 | 25.26 | 7.07 | | |

| | | | | |
|---|---|---|---|---|
| 4482.45 | 24.11 | 5.26 | | |
| 4493.29 | 19.89 | 8.23 | | |
| 4504.72 | 23.72 | 8.01 | | |
| 4514.87 | 21.72 | 8.07 | | |
| 4525.02 | 22.10 | 5.34 | | |
| 4534.45 | 23.05 | 9.25 | | |
| 4545.18 | 24.49 | 4.97 | | |
| 4552.91 | | 4.61 | | |
| 4571.39 | 22.97 | 2.23 | | |
| 4577.88 | 21.26 | 5.18 | | |
| 4585.31 | 22.26 | 5.41 | | |
| 4593.97 | 24.86 | 3.54 | | |
| 4601.69 | 23.28 | 3.10 | | |
| 4610.00 | 18.97 | 5.97 | | |
| 4619.40 | 23.25 | 4.13 | | |
| 4628.18 | 23.66 | 7.10 | | |
| 4636.87 | 23.73 | 5.36 | | |
| 4645.31 | 23.35 | 7.33 | | |
| 4652.80 | 24.30 | 7.19 | | |
| 4659.32 | 23.52 | 6.06 | | |
| 4665.63 | 24.44 | 6.28 | | |
| 4671.93 | 25.02 | 6.61 | | |
| 4678.72 | 24.38 | 3.91 | | |
| 4687.50 | 23.65 | 4.52 | | |
| 4697.45 | 22.85 | 4.11 | | |

| | | | | |
|---|---|---|---|---|
| 4706.41 | 23.44 | 3.31 | | |
| 4714.78 | 24.18 | 3.19 | | |
| 4722.00 | 22.93 | 3.28 | | |
| 4729.15 | 23.03 | 3.08 | | |
| 4736.22 | 23.50 | 2.25 | | |
| 4744.56 | 23.12 | 3.32 | | |
| 4751.38 | 24.21 | 2.96 | | |
| 4767.97 | 19.01 | 3.62 | | |
| 4773.15 | 20.31 | 5.61 | | |
| 4783.82 | 23.22 | 3.44 | | |
| 4790.01 | 23.45 | 4.51 | | |
| 4799.00 | 22.73 | 3.45 | | |
| 4808.43 | 22.11 | 3.74 | | |
| 4818.02 | 21.14 | 5.80 | | |
| 4828.27 | 22.66 | 3.02 | | |
| 4837.98 | 23.86 | 3.09 | | |
| 4845.07 | 22.99 | 3.48 | | |
| 4850.53 | 20.83 | 3.42 | | |
| 4856.43 | 19.35 | 3.74 | | |
| 4862.78 | 22.01 | 4.08 | | |
| 4870.07 | 22.25 | 3.61 | | |
| 4877.84 | 23.79 | 3.74 | | |
| 4885.90 | 22.57 | 2.27 | | |
| 4891.67 | 22.60 | 2.51 | | |
| 4896.65 | 20.69 | 4.29 | | |

| | | | | |
|---|---|---|---|---|
| 4900.80 | 19.87 | 3.50 | | |
| 4904.82 | 21.33 | 5.44 | | |
| 4908.84 | 19.15 | 6.64 | | |
| 4913.09 | 23.99 | 4.07 | | |
| 4917.04 | 25.93 | 2.81 | | |
| 4920.98 | 24.85 | 3.00 | | |
| 4923.10 | 23.82 | 21.46 | | |
| 4963.88 | 23.90 | 4.65 | | |
| 4977.45 | 22.02 | 4.23 | | |
| 4988.99 | 22.32 | 5.80 | | |
| 5000.03 | 21.93 | 5.99 | | |
| 5008.96 | 23.09 | 3.95 | | |
| 5016.92 | 23.15 | 3.49 | | |
| 5024.56 | | 3.51 | | |
| 5033.41 | 23.00 | 3.32 | | |
| 5039.79 | 22.89 | 3.75 | | |
| 5046.72 | 22.20 | 5.51 | | |
| 5054.75 | 21.15 | 13.35 | | |
| 5062.71 | 18.72 | 5.20 | | |
| 5069.81 | 24.58 | 4.49 | | |
| 5075.93 | 23.43 | 3.86 | | |
| 5081.01 | 23.52 | 3.01 | | |